Synchronization of biological oscillators : modeling, analysis and coupling of the mammalian cell cycle and circadian clock

Sofia José Figueiredo Almeida

UNIVERSITÉ CÔTE D'AZUR

ÉCOLE DOCTORALE
SCIENCES ET TECHNOLOGIES DE L'INFORMATION ET DE LA COMMUNICATION

THÈSE DE DOCTORAT

Synchronisation d'oscillateurs biologiques: modélisation, analyse et couplage du cycle cellulaire et de l'horloge circadienne

Sofia FIGUEIREDO ALMEIDA

INRIA Sophia Antipolis/iBV

Présentée en vue de l'obtention du grade de docteur en Informatique **d'**UniversitéCôte d'Azur
Dirigée par: Madalena Chaves/Franck Delaunay
Soutenue le: 17 décembre 2018

Devant le jury, composé de :
Attila Csikász-Nagy, King's College London, UK
Marc Lefranc, Université de Lille 1, France
Annabelle Ballesta, University of Warwick, UK
Jean-Paul Comet, Université de Nice Sophia Antipolis, France
Rui Dilão, Instituto Superior Técnico, Portugal
Didier Gonze, Université Libre de Bruxelles, Belgium

Doctoral School Sciences et Technologies de l'Information et de la Communication

Research Center Inria Sophia Antipolis - Méditerranée

PhD Thesis

Submitted in partial fulfillment of the requirements for the degree of doctor of the Université Côte d'Azur

Specialized in: Informatics

by

Sofia José Figueiredo Almeida

Synchronization of biological oscillators: modeling, analysis and coupling of the mammalian cell cycle and circadian clock

---

Defended on December 17^{th} 2018 in front of the jury composed by:

Reviewers	Attila Csikász-Nagy	King's College London
	Marc Lefranc	Université de Lille 1, France
Examiners	Annabelle Ballesta	University of Warwick, UK
	Jean-Paul Comet	Université de Nice Sophia Antipolis, France
	Rui Dilão	Instituto Superior Técnico, Portugal
	Didier Gonze	Université Libre de Bruxelles, Belgium
Supervisor	Madalena Chaves	Inria Sophia Antipolis, France
Co-supervisor	Franck Delaunay	Univeristé de Nice Sophia Antipolis, France

École doctorale Sciences et Technologies de l'Information et de la Communication

Centre de Recherche Inria Sophia Antipolis - Méditerranée

Thèse

Présentée en vue de l'obtention du grade de docteur

de l'Université Côte d'Azur

Spécialité : Informatique

par

Sofia José Figueiredo Almeida

Synchronisation d'oscillateurs biologiques: modélisation, analyse et couplage du cycle cellulaire et de l'horloge circadienne

---

Soutenue le 17 Décembre 2018 devant le jury composé de :

Rapporteurs	Attila Csikász-Nagy	King's College London, UK
	Marc Lefranc	Université de Lille 1, France
Examinateurs	Annabelle Ballesta	University of Warwick, UK
	Jean-Paul Comet	Université de Nice Sophia Antipolis, France
	Rui Dilão	Instituto Superior Técnico, Portugal
	Didier Gonze	Université Libre de Bruxelles, Belgium
Directrice	Madalena Chaves	Inria Sophia Antipolis, France
Co-directeur	Franck Delaunay	Université de Nice Sophia Antipolis, France

Abstract

The cell division cycle and the circadian clock are two fundamental processes of cellular control that generate cyclic patterns of gene activation and protein expression, which tend to be synchronous in healthy cells. In mammalian cells, the mechanisms that govern the interactions between cell cycle and clock are still not well identified. In this thesis we analyze these two biological oscillators, both separately and as a coupled system, to understand and reproduce their main dynamical properties, uncover essential cell cycle and clock components, and identify coupling mechanisms. Each biological oscillator is first modeled by a system of non-linear ordinary differential equations and its parameters calibrated against experimental data: the cell cycle model is based on post-translational modifications of the mitosis promoting factor and results in a relaxation oscillator whose dynamics and period are controlled by growth factor; the circadian clock model is transcription-based, recovers antiphasic BMAL1/PER:CRY oscillation and relates clock phases to metabolic states. This model shows how the relative duration of activating and repressing molecular clock states is adjusted in response to two out-of-phase hormonal inputs. Finally, we explore the interactions between the two oscillators by investigating the control of synchronization under uni- or bi-directional coupling schemes. Simulations of experimental protocols replicate the oscillators' period-lock response and recover observed clock to cell cycle period ratios such as 1:1, 3:2 and 5:4. Our analysis suggests mechanisms for slowing down the cell cycle with implications for the design of new chronotherapies.

Keywords: cell cycle, circadian clock, coupled oscillators, dynamical systems, period control, model calibration, model reduction, sensitivity analysis, phase-locking, synchronization;

Résumé

Le cycle de division cellulaire et l'horloge circadienne sont deux processus fondamentaux de la regulation cellulaire qui génèrent une expression rythmique des gènes et des protéines. Dans les cellules mammifères, les mécanismes qui sous-tendent les interactions entre le cycle cellulaire et l'horloge restent très mal connus. Dans cette thèse, nous étudions ces deux oscillateurs biologiques, à la fois individuellement et en tant que système couplé, pour comprendre et reproduire leurs principales propriétés dynamiques, détecter les composants essentiels du cycle cellulaire et de l'horloge, et identifier les mécanismes de couplage. Chaque oscillateur biologique est modélisé par un système d'équations différentielles ordinaires non linéaires et ses paramètres sont calibrés par rapport à des données expérimentales: le modèle du cycle cellulaire se base sur les modifications post-traductionnelles du complexe Cdk1-CycB et mène à un oscillateur de relaxation dont la dynamique et la période sont contrôlés par les facteurs de croissance; le modèle de l'horloge circadienne reproduit l'oscillation antiphasique BMAL1/PER:CRY et l'adaptation de la durée des états d'activation et répression par rapport à deux signaux d'entrée hormonaux déphasés. Pour analyser les interactions entre les deux oscillateurs nous étudions la synchronisation des deux rythmes pour des régimes de couplage uni- ou bi-directionnels. Les simulations numériques reproduisent les ratios entre les périodes de l'horloge et du cycle cellulaire, tels que 1:1, 3:2 et 5:4. Notre étude suggère des mécanismes pour le ralentissement du cycle cellulaire avec des implications pour la conception de nouvelles chronothérapies.

Mots clés: cycle cellulaire, horloge circadienne, oscillateurs couplés, systèmes dynamiques, contrôle de la période, calibration de modèles, réduction de modèles, analyse de sensibilité, verrouillage de phase, synchronisation;

Acknowledgements

I would like to begin by thanking my supervisor Professor Madalena Chaves for permanent guidance and teaching, as well as for always being supportive and encouraging, allowing me independence to pursue my own ideas and, in general, helping me to grow scientifically during the course of these years. Similarly, I would like to thank my co-supervisor Professor Franck Delaunay for his expert guidance, support and sharing of scientific ideas as well as for inviting me to take part in this interesting project.

Secondly, I would like to thank Professors Attila Csikász-Nagy, Marc Lefranc, Annabelle Ballesta, Jean-Paul Comet, Rui Dilão and Didier Gonze for taking the time to review and evaluate my work. My sincere gratitude.

Thirdly, I acknowledge the Labex SIGNALIFE Network for Innovation on signal Transduction Pathways in Life Sciences and the ICycle project, for the funding provided during my PhD.

I also like to show my gratitude to the entire BIOCORE team that has received me during these years. A special thank you for the friends I've made among PhDs and Post-Docs during my thesis: Stefano, Ivan, Carlos, Marjorie, Lucie and Claudia.

A word of thank you also to Marie-Line Meirinho for always being helpful with a variety of issues. And a word of appreciation to Sophie Guerin for patiently teaching me some wet lab techniques, during my first month as a PhD.

To conclude, I would also like to thank the closest people in my life: José Gustavo Elias Rebelo for always being by my side, sharing this journey with me, Catarina Santos and Catarina Viegas, my friends of over 23 years, my parents for their general support and last, but not least, my grandparents, who are my favorite people in the world.

Contents

List of Figures

1

Introduction

The cell division cycle and the circadian clock are two fundamental processes of cellular control that generate cyclic patterns of gene activation and protein expression, which tend to be synchronous in a variety of healthy cell lineages.

The cell cycle is the process of cell growth and division, where the cell undergoes a sequence of observable changes culminating in mitosis. There is an oscillatory nature of this process as, after cell division, daughter cells re-start the cell cycle. In turn, the circadian clock is a biological oscillator conserved across species that results in 24 h rhythms (circadian rhythms). In mammals, peripheral cellular clocks are entrained by a central pacemaker localized in the suprachiasmatic nuclei of the hypothalamus, through internal synchronizers. This central clock also coordinates rest/activity and fast/feeding rhythmic behaviors. At the cellular level, a molecular cell clock generates circadian patterns of gene activation and protein expression. The basic molecular mechanisms of both systems are explained on Section 1.1.

The interconnection between these two systems is a main topic of interest for biologists and modelers alike. Because both systems result in rhythmic behavior they can be interpreted and modeled as oscillators, possibly subjected to some form of coupling. Section 1.2 of this Chapter gives a brief discussion of the state of the art on the relevance of these systems and their connection with a variety of biological processes.

The present work is motivated in large part by observations of Feillet et al., (2014) on phase-locking between the cell cycle and the circadian clock of mammalian cells [1]. Therefore, Section 1.3 describes how these results changed the state of the art on clock/cell cycle coupling. Our work is centered in recovering and understanding these results by the development and analysis of non-linear dynamical models.

Furthermore, our work is part of a larger project – ICycle [2] – concerning the design and building of synthetic biological oscillators. Synthetic biology is an expanding interdisciplinary field that aims at the construction of artificial biological systems. The building of synthetic oscillators has an added layer of difficulty over other types of synthetic designs, in that it requires obtaining robust and regular oscillations. A comparative review of various successful biological oscillators is provided by Purcell et al., (2010), [3] – synthetic oscillators are comprised of a reduced number of variables, generally two. Because of this, there is, in this thesis, a large focus

on achieving reduced models that consistently recover the fundamental mechanisms of the clock and cell cycle systems – a reduced number of variables and interactions allows to better use our models to inform the design of synthetic oscillators. On Section 1.5 we discuss the methodology and goals of our work.

Finally, Section 1.6 of this Chapter presents an overview of the work and main results of this thesis. Generally, on Chapter 2 of this thesis we develop and analyze a mathematical model of the mammalian cell cycle ([4]), on Chapter 3 we develop and study a model for the mammalian circadian cell clock, on Chapter 4 we investigate the coupling between the two oscillators and Chapter 5 presents conclusions and future perspectives. Chapters 2 and 3 of cell cycle and clock modeling are written as articles, with appropriate introduction of background and methods provided for each of them.

1.1 Basic Mechanisms of the Mammalian Cell Cycle and Circadian Cell Clock Systems

In this Section we briefly expose some of the basic molecular mechanisms of the mammalian cell cycle and cellular clock oscillators. Because Chapters 2 and 3 are written as articles, further explanation and schemes are provided there.

1.1.1 Cell Cycle Mechanisms

A cell that has entered the cell cycle will go through several different phases of growth culminating in mitosis (M phase). M phase is the key phase during which two daughter cells are generated. The previous cell cycle stages form the interphase, composed of: the G1 phase of cellular growth, the S phase of DNA replication and the G2 phase of growth and preparation for mitosis [5]. Cell cycle arrest can occur and the cell exits the cell cycle (G0 phase).

Moreover, a characteristic of the eukaryotic cell cycle is that of checkpoints: thresholds of control in the cycle that assess whether a given sequence of events was performed correctly. These are: the G1 checkpoint, where the cell "commits" to divide, the G2/M checkpoint, where possible DNA damage is repaired, and the mitotic spindle checkpoint, that ensures chromosomes are well aligned at the metaphasic plate before releasing the anaphase promoting complex (APC), that promotes cell cycle progression. After each checkpoint the cell cannot revert to its previous cell cycle phase.

The cell cycle phases are characterized at the molecular level by the sequential elevated expression of a family of proteins called Cyclins, each supporting the activity of specific cyclin-dependent kinases (cdks). Cyclin D forms a complex with either cdk4 or cdk6 and is the cyclin of the G1 phase, Cyclin E pairs mostly with cdk2 and controls the passage from G1 to S phase, cyclin A also pairs with cdk2 and is active during S phase and G2, and finally cyclin B forms a complex with cdk1 and controls the G2/M transition. The cyclin B-cdk1 complex is also known

as the mitosis promoting factor (MPF) and is the necessary and sufficient element to carry out the mitotic process [6].

Because MPF is the essential cell cycle component, regulatory loops involving this complex are often considered central to the cell cycle. Important regulators of MPF include the wee1 kinase that inactivates MPF by phosphorylation, the cdc25 phosphatase that activates MPF by dephosphorylation and the APC:cdc20 complex that targets MPF for degradation [7], [8]. MPF in turn also phosphorylates these three components, which leads to activation of cdc25, inactivation of wee1 and allows APC to dimerize with cdc20, forming the APC:cdc20 complex. Therefore, MPF forms positive self-regulatory loops via its action in activating its activator cdc25 and repressing its repressor wee1, and a negative feedback loop by promoting the formation of its repressor APC:cdc20. These regulatory mechanisms are important cell cycle controls and are at the center of a variety of cell cycle models (further discussed on Section 1.4), including ours on Chapter 2 (schemes of these interactions are provided on the same Chapter).

1.1.2 Circadian Clock Mechanisms

The central regulatory clock network of mammalian cells is a transcription/translation feedback loop (TTFL) [9]. Two central elements of this network are the CLOCK:BMAL1 and PER:CRY protein complexes. CLOCK:BMAL1 binds to regions of the genome called E-boxes and promotes transcription of the *Per* and *Cry* genes. PER and CRY proteins in turn form the PER:CRY complex that reenters the nucleus and binds to CLOCK:BMAL1, blocking its promoter activity. This forms the core negative feedback loop of the mammalian circadian clock.

Furthermore, RORs and REV-ERBs are families of transcription factors that are also important for clock regulation. CLOCK:BMAL1 promotes expression of *Ror* and *Rev*. In turn, ROR proteins are activators of the *Clock* and *Bmal1* genes, while REV-ERBs are repressors. ROR and REV-ERBs compete for binding at the BMAL1 promoter, thus a positive feedback loop is formed between ROR and CLOCK:BMAL1. The negative feedback loop between CLOCK:BMAL1 and REV-ERBα is considered an important and fundamental part of the core clock mechanism [10].

Moreover, post-transcriptional mechanisms, including RNA-based mechanisms, are also controls of the mammalian circadian clock. Therefore, processes of mRNA stability, translation and alternative splicing are required for maintaining proper clock function [11]. Furthermore, post-translational mechanisms such as phosphorylations and dephosphorylations allow the rapid incorporation of signals by the clock system and play a role in the generation of the 24 h rhythm by controlling the delay of entrance of clock proteins, such as PER, in the nucleus [12].

1.2 The Cell Cycle and Circadian Clock Systems – a Brief Discussion

Both clock and cell cycle processes are essential for cellular health in mammals and when unregulated can result in disease at the organism level. In particular, cancer is characterized by unregulated growth of mutated cells, while disruptions in circadian rhythms have been linked with insulin resistance and inflammation [13]. Due to the tight interconnection between the

two oscillators, deregulation in one of them often deregulates the other as well, as evidenced by increased risk of circadian clock disturbances in cancer patients [14].

Furthermore, the circadian clock can impact cancer development [14]. Recently, agonists of REV-ERB (a central clock component) demonstrated efficacy in impairing glioblastoma growth in mice [15]. The mechanism behind these observations may involve REV-ERB-induced inhibition of autophagy and *de novo* lipogenesis, processes that are a part of fat metabolism [15]. This discovery highlights the tight control exerted by the clock oscillator in a variety of cellular internal systems and reveals that pharmacological modulation of circadian components is a promising strategy for cancer therapy.

Besides cancer, circadian rhythms control a variety of cellular processes from energy homeostasis, insulin secretion, insulin resistance/sensitivity, DNA repair and inflammation. In particular the interplay between the circadian clock and metabolism is of great relevance for understanding a variety of metabolic diseases. For instance, shift workers have a higher incidence of metabolic disorders [16], that are known to be caused by misalignment between the clock of the organism and the external light cycle [17]. In fact, circadian misalignment leads to an increase in markers of insulin resistance and inflammation regardless of sleep loss [13]. The role of the clock in cellular metabolism is currently a subject of vast and ongoing research interest, including recent experimental ([17], [15]) and dynamical modeling ([18]) works alike. In this work, we will explore some ideas about clock connection with metabolism on Chapter 3.

As revealed by genome-wide studies, the majority of drug targets show circadian patterns of control [19]. Moreover, timed drug delivery, or chronotherapy, is an effective control of drug efficacy, that maximizes the desired drug effect while simultaneously minimizing undesired side-effects [19]. Chronotherapy is of importance in the delivery of a variety of treatments, including chemotherapy, though it is not clearly understood exactly what is behind increased efficiency of drugs at certain times. A better understanding of this phenomenon involves studying the circadian clock as well as its possible interactions with the cell cycle.

Concerning the relation between the mammalian circadian clock and cell cycle, rhythms of cell division are observed to be circadian in a variety of organisms [14], which led to an hypothesis of "gating" of the cell cycle by the clock mechanism [20]. This means that the clock mechanism would control the cell cycle so as to only allow mitosis to occur at certain time windows. Under the gating hypothesis the circadian clock would act as a fourth cell cycle checkpoint for the mitotic phase.

Furthermore, several molecular interactions revealing direct action of the clock on the cell cycle have been discovered. Firstly, the CLOCK:BMAL1 protein complex, essential for the circadian clock, induces expression of the *wee1* gene [21]. The kinase wee1 phosphorylates and inactivates the cdk1 and cdk2 kinases, thus inhibiting the essential cell cycle complex cyclin B-cdk1, or mitosis promoting factor (MPF). Secondly, the clock components REV-ERB-α/β and ROR-α/γ regulate the cell cycle inhibitor p21 [22]. Finally, there is also evidence for clock repression of c-Myc, a promoter of cell cycle progression by cyclin E induction [23], that is deregulated in mice deficient in the gene encoding for the core clock protein PER2 [24].

An example of a model of cell cycle gating by the clock is provided by Zámborszky et al.,

(2007), where critical size control of the mammalian cell cycle was found to be triggered by the clock [25]. By contrast, Gérard and Goldbeter, (2012), simulate entrainment of the cell cycle by the clock, while also suggesting a possible form of gating by the clock at the entry of G1 phase through a mechanism of oscillating growth factor [26].

Moreover, Nagoshi et al., (2004), have analyzed NIH3T3 mouse fibroblasts in real time and in individual cells and observed autonomous cellular clocks in these cells and that the cell cycle in a population of synchronized cells shows a trimodal frequency distribution of mitosis for specific circadian clock phases [27]. Up until now, the state of the art included clock control of the cell cycle, exclusively. A breakthrough was made by Feillet et al.,(2014), and Bieler et al., (2014), demonstrating phase-locking between clock and cell cycle with strong evidence for bi-directional coupling [1], [30]. In the same work, the trimodal peak distribution is also obtained for synchronized cells (similarly to Nagoshi et al., (2004) [27]).

1.3 Phase-locking of the Mammalian Circadian Clock and Cell Cycle

This Section describes the main results of Feillet et al., (2014), [1] that strongly motivate this dissertation.

The work of Feillet et al., (2014), changed the previous state of the art concerning the interconnection between the clock and cell cycle systems in that it showed substantial evidence for a control of the cell cycle on the clock [1]. This is evidenced by observing the periods of the clock and cell cycle systems in NHI3T3 mouse fibroblasts under different growth conditions. The authors are able to measure the phases of both cell cycle and clock in NHI3T3 mouse fibroblasts at each point in time, using two independent reporter systems: a single-live-cell imaging of a REV-ERBα::VENUS fusion protein, as a clock reporter, and two fluorescent cell cycle reporters, Cdt1 and Geminin, based on fluorescent ubiquitination of the cell cycle (FUCCI).

The cell cycle oscillator is known to be period-responsive to the concentration of growth factors in the medium – these are expressed as % of FBS (Fetal Bovine Serum) and comprised of a variety of nutrients and growth factors, such as insulin-like growth factor 1 (IGF-1), that stimulate the cell cycle in a variety of mammalian cells. The rate of cell division increases with FBS concentration.

Feillet et al., (2014), observe that increasing the concentration of growth factor in the medium results not only in the expected increased frequency of the cell cycle, but also in an equal trend of increase in clock frequency [1], such that the two oscillators always remain synchronized for a variety of values of % of FBS.

Furthermore, they verify that cell cycle division occurs at a specific clock phase for all cells. This means their observations are consistent with a model of oscillators that are phase-locked. Phase locking is characterized by convergence of the combined phase of oscillation $\phi(t) = (\phi_1(t), \phi_2(t))$ to a closed curve – an attractor. The phase-locking is distinct from the gating model, as phase-locked oscillators are synchronized through the entire cycle – knowing the phase of one oscillator determines the phase of the other, in ideal noise-free systems. By

contrast, in the gating hypothesis only the mitotic phase would have to align with specific clock phases.

Fig. 1.1 shows the 1:1 phase-locking results of Feillet et al., (2014), [1], for 10 % FBS and 15 % FBS. For cells grown in 10 % FBS the mean clock period is 21.9 ± 1.1 h and the mean cell-cycle period is 21.3 ± 1.3 h, while for cells grown in 15 % FBS the mean clock period is 19.4 ± 0.5 h and the mean cell-cycle period is 18.6 ± 0.6 h. Furthermore, the peak in REV-ERBα::VENUS expression is phase-locked with the mitotic phase: the mean delay of REV-ERBα::VENUS after mitosis is of 8,6 h for 10 % FBS and of 7,1 h for 15 % FBS (see also Traynard et al., (2016), [28]).

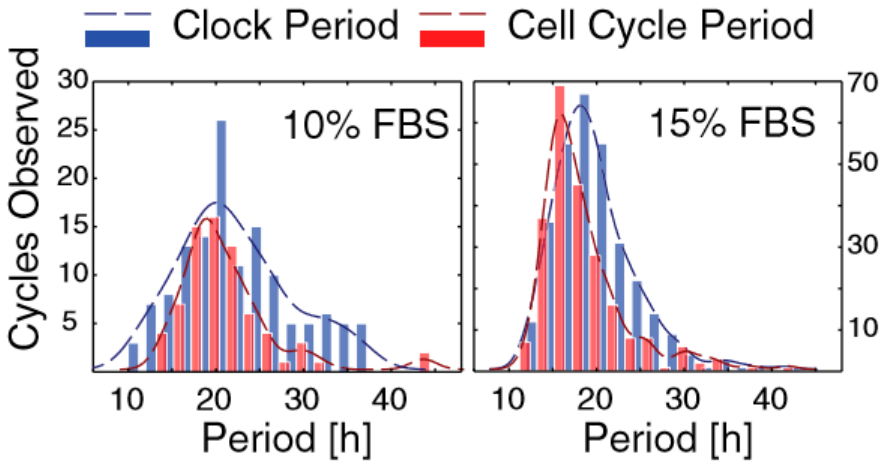

Figure 1.1: **Result from Feillet et al., (2014) for 1:1 clock/cell cycle phase-locking [1].** The increase in growth factor concentration in the culture medium of NHI3T3 mouse fibroblasts increases the frequency of the cell cycle, which results in an increase in clock frequency as well. The oscillators are in 1:1 phase-locking. For 10 % FBS mean clock period is 21.9 ± 1.1 h and mean cell-cycle period is 21.3 ± 1.3 h and REV-ERBα::VENUS peaks on average 8,6 h after mitosis. For 15 % FBS mean clock period is 19.4 ± 0.5 h and mean cell-cycle period is 18.6 ± 0.6 h and REV-ERBα::VENUS peaks on average 7,1 h after mitosis

Moreover Fig. 1.2 shows an histogram of cell density versus clock phase from Feillet et al., (2014), [1]. For 15 % FBS, increases in cell density, due to cellular division, occur at a preferential clock phase.

Furthermore, Feillet et al., (2014), observe synchronization of cells under the application a of Dexamethasone pulse (during 2 hours) in the medium [1]. Dexamethasone is a corticosteroid drug, known to synchronize clocks in populations of mammalian cells by inducing PER expression in all cells. Corticosteroids induce expression of circadian clock PER proteins via activation of transcriptional activator glucocorticoid receptor GR [29]. Feillet et al., (2014), verify that application of a Dexamethasone pulse results in different synchronization ratios depending on the concentration of growth factor [1].

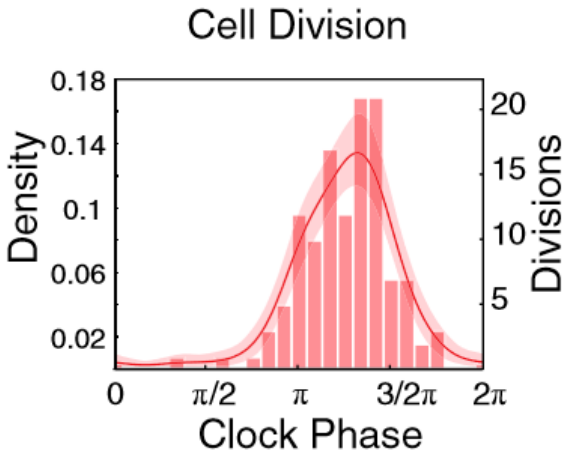

Figure 1.2: **A result from Feillet et al., (2014) for distribution of cell densities with clock phase [1].**
There is a preferencial clock phase for mitosis. For 15 % FBS the mean phase of division is 3.97 ± 0.14 radian.

For cells grown in 20% FBS, the population of cells segregates into two groups, one with cells and synchronizing in 1:1 phase-locking (just as without Dexamethasone application) and the other group of cells showing a slower clock than cell cycle. From several analysis of cells grown in 10% FBS and 20% FBS the period locked ratios are determined to be roughly 5:4 for 10% FBS and 3:2 for 20% FBS (second group); this is further predicted by mathematical modeling [1]. The synchronization dynamics of the second group for 20% FBS after Dexamethasone application is similar to that observed by Nagoshi et al., (2004), under a similar protocol [27].

Fig. 1.3 A) shows the clustering of cells in one simulation for 20% FBS after synchronization by a pulse of Dexamethasone. In this particular case the clock to cell cycle period ratios are 1,8 and 1,09. Fig. 1.3 B) shows the distribution of cell density with clock phase for the two groups of cells.

From these results as well as mathematical modeling, the authors conclude the existence of multiple attractors for clock and cell cycle phase-locked behavior [1], i.e. that the input of Dexamethasone may be shifting the oscillators from one limit-cycle to another.

While the three peak distribution of cell density on itself doesn't exclude the "gating" hypothesis, the observations of 1:1 period-lock are supportive of the phase-locked coupled oscillators hypothesis and suggests coupling from the cell cycle to the circadian clock in mammalian cells. Thus, there is likely bidirectional coupling between the oscillators. Our work aims at gaining insight on dynamical mechanisms that may be behind the observations of Feillet et al., (2014), [1] presented in this Section, in particular the different synchronization ratios, and explore uni- and bi- directional forms of coupling.

Furthermore, Bieler et al., (2014), have obtained similar results concerning the 1:1 phase-lock

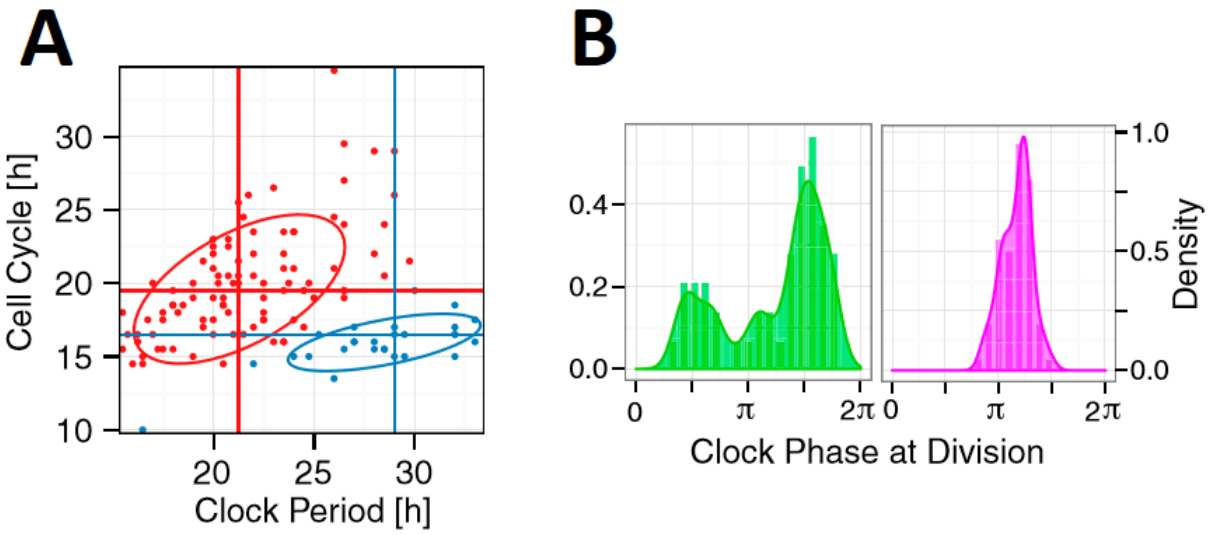

Figure 1.3: **Results from Feillet et al., (2014) for clustering of clock and cell cycle periods and distribution of cell densities with clock phase [1].**
A) Scatter plot showing segregation of two groups of cells in terms of their clock and cell cycle period ratios. In the blue cluster, the median clock period is 29 h ± 1,05 h and the median cell cycle period is 16,5 h ± 0,48 h; in the red cluster, the median clock period is 21,25 h ± 0,36 h and the median cell cycle period is 19,5 h ± 0,42 h. In this experiment the mean period ratios are 1,8 for the blue group and 1,09 for the red group. B) Distribution of cell densities with clock phase for the two cluster groups. On the left plot, the first group shows a three peak distribution, where the middle, left and right peaks correspond respectively to the first, second, and third divisions (hence the increase in cell density). On the right plot, the second group phase-locks in 1:1 ratio, similarly to the system without Dexamethasone (see Fig. 1.2).

of clock and cell cycle with the increase of growth factor [30], thus further corroborating this hypothesis. A recent study by Traynard et al., (2016) has presented model-based investigations of possible bidirectional mechanisms of clock and cell cycle coupling, that didn't result in recovering the rational period-lock ratios [28].

1.4 Models of the Mammalian Cell Cycle and Circadian Clock Oscillators

In this Section, we present a brief review of reference models for the cell cycle and the circadian cellular clock systems.

1.4.1 Cell Cycle Models

In 1991, Tyson first proposed a cell cycle modeling approach centered on MPF, the essential cell cycle component, by modeling the interactions of cdc2 (cdk1) with cyclin B and showed the existence of three modes of stability: a steady state with high MPF activity, a spontaneous

oscillator and an excitable switch [31]. Following this work, Novak and Tyson, (1993), were the first to select the regulatory loops between MPF and cdc25/wee1, as well as the negative feedback loop where MPF stimulates its own degradation by activation of the ubiquitination pathway, as essential mechanisms that in themselves form the central cell cycle network of eukaryotic cells [32]. This work resulted in a model for the cell cycle in Xenopus oocyte extracts.

A decade later, Pomerening et al., (2003), studied the negative feedback-loop between MPF and APC:cdc20, by developing a model that includes auto-regulatory positive loops [33]. This model generates relaxation oscillations. Furthermore, the authors verify experimentally that the activation response of cdc2 to non-degradable cyclin B is consistent with a bistable dynamical behavior [33]. Moreover, Qu et al., (2003), presented a generic mathematical model of the eukaryotic cell cycle that allows simulation of both the G1/S and G2/M transitions [34]. In this model, the cell cycle checkpoint is a Hopf bifurcation point. Later, Pomerening et al., (2005), highlighted the importance of positive feedback loops in maintaining sustained cell cycle oscillations and verified experimentally that the cdc2/APC system in Xenopus egg extracts behaves like a relaxation oscillator [35].

In more recent years, Gérard and Goldbeter, (2009), proposed a detailed, 39-variable model of the mammalian cell cycle, containing four cdk modules regulated by reversible phosphorylation, cdk inhibitors, and protein synthesis or degradation [36]. This model extensively describes the network of cyclin-dependent kinases and first includes the role of growth factors in inducing the system's transition from a quiescent state to an oscillatory cdk network. Later, the authors reduced this model ([36]) to a skeleton model of 5 variables (see Gérard and Goldbeter, (2011)), where the growth factor role in stability control is maintained and progression along the G1, S, G2 and M phase is still verified via sequential activation of the cyclin/cdk complexes [37]. Moreover, Gérard et al., (2012), extended this skeleton model via the incorporation of phosphorylation/dephosphorylation cdk regulation as well as the positive feedback loops between MPF and cdc25/wee1 and verified that these controls promote the occurrence of bistability and increase the amplitude of oscillations in the various cyclin/cdk complexes [38]. Furthermore, including these regulatory mechanisms improves robustness of the cdk oscillations with respect to molecular noise, as shown by stochastic modeling [38].

Finally, Gérard et al., (2015), built and analyzed a mathematical model of the molecular interactions controlling the G1/S and G2/M transitions in yeast cells with a minimal cdk network consisting of a single cyclin-cdk fusion protein [39].

1.4.2 Circadian Clock Models

The first circadian clock oscillatory model was proposed by Goodwin, (1975), and is based on a negative feedback loop between a protein and its own gene [40]. In later years, Leloup and Goldbeter, (2003), developed a detailed model of the mammalian circadian clock (of 16 to 19 variables) and observe sustained versus damped oscillations as well as entrainment of the system by light/dark cycles [41]. Furthermore, the authors verify a sensitivity of the oscillator's phase in relation to changes of parameters that potentially relates to syndromes of advanced or delayed

sleep phase observed in humans [41]. In the same year, Forger and Peskin, (2003), propose a different yet also detailed model of the mammalian circadian clock, using mass action kinetics, that is calibrated to data and accurately reproduces characteristics of oscillatory clock proteins and mRNAs, such as the shape and amplitude of oscillation and the phase of entrainment to the 24 h light/dark cycle [42].

Moreover, Leloup and Goldbeter, (2004), further extend studies on the Leloup and Goldbeter, (2003) [41], model and observe that the oscillatory behavior and period of the system are most sensitive to parameters involved in the synthesis or in the degradation of Bmal1 mRNA and BMAL1 protein, and that these regulatory mechanisms may be sufficient for generating sustained oscillations [43]. Furthermore, in the same study the authors verified that the phase of oscillations upon entrainment to the light/dark cycle strongly depends on the parameters that govern the level of CRY protein [43]. On the same year, Becker-Weimann et al., (2004), propose a model using a reduced number of species, that is able to reproduce the rescue of circadian oscillations in $Per^{2Brdm1}/Cry2^{-/-}$ double-mutant mice [44]. Differently, Mirsky et al., (2009), propose a model minimizing post-translation modified species that is evaluated against experimental knockout phenotypes in what concerns retention of rhythmicity and changes in expression levels of clock species [45].

Relógio et al., (2011), developed a circadian clock model based on data for the amplitude and phase of the core clock components that highlights the role of the ROR/BMAL1/REV-ERB loop as important to the circadian clock [46]. Moreover, Comet et al., (2012), identified mechanisms common to circadian clocks across species, using differential equations as well as discrete models [47]. The authors simplified as much as possible in order to obtain minimal networks of essential interactions and reduced the model of Leloup and Goldbeter, (2004) [43], to eight and four variables [47].

A different type of model is proposed by Korenčič et al., (2012), describing a six-variable gene regulatory network of the liver core clock, whose negative feedback includes time-delayed variables [48]. This model is able to reproduce time profiles, amplitudes and phases of clock genes and shows that intrinsic combinatorial gene regulation governs the liver circadian clock [48]. Moreover, Jolley et al., (2014), propose a simplified clock model that highlights the role of the clock controlled genomic binding region D-box and reproduces predictions on the dual regulation of *Cry1* by D-box and REV-ERBα/ROR [49].

Furthermore, a complete comparative review on these models is provided by Podkolodnaya et al., (2017) [50].

Finally, as mentioned in Section 1.2, mammalian clock models have been applied in studying connection with important cellular systems: the cell cycle (see Gérard and Goldbeter, (2012), [26], Zámborszky et al., (2007), [25], Bieler et al., (2014), [30] and Traynard et al., (2016), [28]) and metabolism (see Woller et al., (2016), [18]).

1.5 Principles, Methods and Goals

This work is the first part of the ICycle Project, [2], that seeks to uncover mechanisms behind the dynamics of the mammalian clock and cell cycle coupled systems and to build synthetic oscillators.

Because at the beginning of this thesis there is little knowledge of what mechanisms result in the dynamical clock/cell cycle synchronization ratios ([1]), it is crucial to first perform modeling work in order to verify their existence in reduced models and to establish principles for the design of synthetic oscillators. As it is not guaranteed that any two coupled models of mammalian cell cycle and circadian clock will phase-lock in rational ratios under the application of a specific input, especially one that accurately models the Dexamethasone effect, designing synthetic oscillators "in the dark", i.e. without first reproducing and studying these dynamics, offers less guarantees of recovering clock/cell cycle phase-locked dynamics in synthetic biology settings.

Thus, our work aims to reproduce the dynamical synchronization ratios, described on Section 1.3, observed by Feillet et al., (2014), [1], Bieler et al.,(2014), [30] and Nagoshi et al., (2004) [27]. Moreover, understanding the clock and cell cycle dynamical coupling and observation of synchronization dynamics are itself the main motivations and points of interest of this work. Furthermore, we seek to test protocols that may be of relevance for the real system, such as chronotherapies, and methods of oscillator period control and synchronization state control.

Fig. 1.4 shows a scheme of the philosophy behind the organization of the entire project ([2]) and the interplay between biology and methods of modeling and simulation. Starting from real systems, with a variety of complex interactions, our work aims for several steps of simplication: in the creation of average-sized models via selection of the main biological interactions, then dynamical reduction of these models in order to find the essential central mechanisms. From here we study the coupling between the two models. The insight gained on reduced models and their coupling can then be used in the design of synthetic oscillators.

We opted for designing new models, rather than using pre-existing models, such as those of Section 1.4. This is because, being part of a broader work, we sought a combination of characteristics for our models, that would simultaneously favor their use in synthetic oscillator design and coupling studies. For the design of synthetic oscillators we require a reduced number of variables and simultaneously to recover the essential mechanisms capable of generating oscillations. Moreover, we should be able to tune the period of the system and oscillations should be robust to variations in parameters. Furthermore, we seek to be able to relate our coupling results to the observations of Feillet et al., (2014), [1]. Therefore, modeling is conducted with the perspective of allowing the integration of Growth Factor and Dexamethasone, the control inputs in that experimental work, in subsequent coupling studies. The use of mechanistic rather than phenomenological terms is another property that helps relate our models both to the real system and to future synthetic circuits.

Thus, the basic principles of modeling used in this work are:

- Identification and choice of main mechanisms;

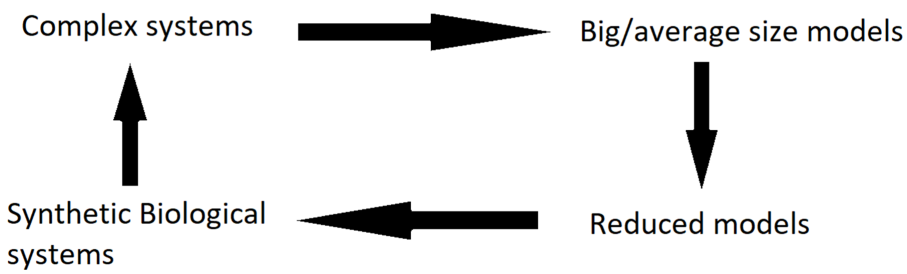

Figure 1.4: **General scheme of the philosophy behind this work.** Biological systems are on the left and mathematical models on the right. Our work performs the first two arrows: identifying main mechanisms to build intermediate average-sized models, and further pushing the simplicity to unveil skeleton reduced networks for both systems. We then use the reduced systems to study coupling and to discover the main points of interest for synthetic oscillator design.

- Reproducibility of oscillation and the essential properties of each oscillator;
- Tunable and robust oscillations;
- Reduced number of variables;
- Mechanistic rather phenomenological terms;
- Possibility of using the models to inform future design of synthetic oscillators;

To develop our models, we use differential ordinary equations (ODEs), with mechanistic terms, such as Michaelis-Menten and Hill functions, and terms derived by mass action kinetics. These are some of the classical tools used to model genetic and signaling networks (see de Jong, (2002), [51]). For dynamical model reduction we often use the quasi-steady-state approximation ([52], [53]) which is based on the comparison of the system's timescales. The "faster" variables can be obtained in terms of the "slower" variables, via an algebric equation. Moreover, we use the Matlab software for all simulation studies.

The main mathematical modeling and computational methods used in this thesis are:

- Ordinary Differential Equations using mass action kinetics, Michaelis-Menten and Hill functions;
- Calibration of models to data via numerical optimization methods;
- Analysis of numerical data – period computation based on a numerical implementation of the first return map [54];
- Model reduction using the quasi-steady-state approximation;

- Piecewise quadratic approximation of the reduced model to establish a parameter region for existence of oscillations;
- Matlab: ODE solvers and optimization tools based on non-linear cost minimization;

Thus, our work seeks to reproduce and study the synchronization state of the two oscillators, to investigate forms of coupling from the clock to the cell cycle as well as to propose mechanisms that may be relevant for the inverse, less studied, type of coupling, directed from the cell cycle to the clock. Uncovering these dynamics would also allow studying strategies of controlling the period of any or both of the two oscillators as well as the synchronization ratio between the two, which is a main motivation of this work. The relevance of period and synchronization control lies in the relation these two oscillators have with a variety of cellular states of health and disease, as was discussed on Section 1.2, namely cancer that is uncontrolled cell cycle.

Therefore, our main research goals are:

- ✓ To gain insight and increase the understanding of the mammalian cell cycle and clock oscillators via dynamical modeling analysis;
- ✓ To investigate several coupling mechanisms;
- ✓ To verify entrainment of one oscillator by the other, i.e. the 1:1 period-lock, in both directions of unidirectional coupling as well as in bidirectional coupling;
- ✓ To obtain clock to cell cycle rational synchronization ratios under application of Dex as a PER input, compatible with the experiments of Feillet et al., (2014), [1], Bieler et al., (2014) [30], and Nagoshi et al., (2004), [27];
- ✓ To observe the dynamical behavior of the coupled system and parametric control of synchronization ratios;
- ✓ To analyze strategies of period control of one oscillator on the other – in particular strategies to slow down the cell cycle;

By extension, some of the questions that we will keep in mind are: By which type of mechanisms may the cell cycle exert control on the clock? Is it possible to recover the synchronization ratios under the replication of experimental protocols *in silico*? If so, which parameters allow to control the synchronization state of the oscillators? Are there multiple attractors? Why is there a population of cells that synchronizes in a 3:2 period-lock ratio and another in a 1:1 ratio upon treatment with Dexamethasone? What if the clock is responding directly to Growth Factor? Is it possible to control the period of one oscillator by adding an input affecting the other?

1.6 Work Overview

Following the discussion and goals established in the previous Section, we develop non-linear dynamical models to study the mammalian clock and cell cycle systems.

As stated above, we aim for a reduced perspective that simultaneously focuses on the main goal of later using these models to study coupling mechanisms. We aim also to be able to relate our coupling results with the observations of Feillet et al., (2014), [1]. Thus, the cell cycle modeling work largely focuses on exploring an effect of growth factor (GF) control on the period and stability of the system and the clock model largely focus on a transcriptional-base, so as to take into account the action of Dexamethasone (Dex) in indirectly causing induction of the *Per* gene. Another point of clock modeling is the focus on obtaining an antiphasic oscillation of CLOCK:BMAL1 and PER:CRY, not only because these two main clock elements relate to opposite phases of the day/night cycle, a central influence on the evolution of clocks, but also because this property may be of relevance for Dexamethasone application, that exerts an asymmetric effect in promoting the repressor phase.

Thus, on Chapter 2 we identify the main dynamics underlying the mammalian cell cycle and start by creating an intermediate seven variable model based on post-translational modifications of MPF, and in its degradation by the APC:cdc20 complex [4]. This model gives rise to relaxation oscillations whose frequency increases with growth factor GF, a result in agreement with observations [1]. From here, dynamical reduction results in a two variable cell cycle model maintaining the essential properties of the initial model. We calibrate this reduced model against experimental data and perform sensitivity analysis. When given as the input of an open-loop configuration GF controls not only the period, but also the stability of the system.

The cell cycle model is then used, on Appendix B, to investigate coupling with a preliminary clock model based on the essential core clock transcriptional network, where all clock components oscillate in phase. The variation of the ratio of clock to cell cycle periods with GF resulted, for weak coupling, in the *devil's staircase* pattern ([55]), with the synchronization ratio being constant by intervals at integer values. However, the effect of Dex application is not recovered with this preliminary coupling. Nevertheless, the preliminary study of Appendix B allowed to formulate the hypothesis that in a more complete clock model, that recovers the appropriate phase differences between the core clock protein peaks, the experimentally observed effect of Dex application ([1]) could be reproduced.

From here, we moved on to build a transcription-based clock model presenting antiphasic oscillation of the CLOCK:BMAL1 and PER:CRY protein complexes as a key feature, on Chapter 3. Thus, the circadian clock modeling work, presented in Chapter 3, is an in-depth study where the relevance of the CLOCK:BMAL1/PER:CRY antiphasic oscillation is related to opposite phases of the fast/feeding, light/dark and rest/activity cycles. Uncovering the dynamical network behind this property is achieved by describing competition between activators and repressors of certain genomic regions called clock controlled elements (CCEs) and the rate of change of the core clock species as a combination of independent CCEs. The three modeled CCEs are E-box, R-box and D-box.

We also calibrate our clock model against experimental data and verify robustness of oscillation in relation to changes in parameters. The model reproduces the expected phase response curve to external pulses and the region of entrainment by an external oscillatory signal forms an Arnold Tongue pattern. We then applied our clock model in the simulation of the *tau* mutation

and in the simultaneous application of one signal representative of the light/dark cycle and another signal representing the fast/feeding cycle and observe the response in changes of duration of peak expression of the different core clock proteins. Moreover, we identify, by means of model reduction, the essential transcriptional core network that still guarantees the antiphasic BMAL1 and PER:CRY oscillation. The reduced clock model has four variables.

On Chapter 4 we study the coupling of our mammalian cell cycle and circadian clock reduced models. We address unidirectional cell cycle $\rightarrow$ clock coupling, unidirectional clock $\rightarrow$ cell cycle coupling, bidirectional coupling and unidirectional coupling with a GF-controlled clock. Unidirectional cell cycle $\rightarrow$ clock coupling is achieved by modeling MPF-controlled phosphorylation and subsequent degradation of REV-ERBα [56]. Unidirectional clock $\rightarrow$ cell cycle coupling, in turn, is performed by modeling CLOCK:BMAL1-induced expression of *wee1*, that leads to the repression of MPF activity [21]. Bidirectional coupling combines the two aforementioned mechanisms.

Furthermore, we model a direct effect of GF on the clock by means of chromatin remodeling near R-box ([102]), which is included in the model as GF repressing R-box. This is analyzed in conjunction with the previously studied unidirectional clock $\rightarrow$ cell cycle coupling via *wee1* induction.

We observe the *devil's staircase* pattern of synchronization state response in all forms of coupling except for the GF-controlled clock system. Moreover, we study the coupling dynamics under changes in control parameters and Dexamethasone application.

Final considerations and future work regarding synthetic oscillator design and further clock and cell cycle dynamical studies are presented on Chapter 5.

2

Modeling the Mammalian Cell Cycle

This Chapter presents the work done in the first part of this thesis in creating and exploring a dynamical model of the mammalian cell cycle, with a mechanistic, biologically meaningful, approach and reduced number of variables. Thus, this Chapter consists in the article "A comprehensive reduced model of the mammalian cell cycle" (Almeida et al. (2017)), published in the proceedings of the 20th IFAC World Congress [4].

Because this is a short technical paper, some explainations of specific methods of function approximation used in the article of Section 2.1 are provided on Section 2.2 of this Chapter. Following this Chapter, Appendix B shows the application of the model here developped in the coupling with a simple mammalian circadian clock model (developed in Appendix B), allowing to take a preliminary look into what type of information may be obtained from the unidirectional **cell cycle** $\rightarrow$ **clock** coupling between the two oscillators, which largely influenced the basis for the development of a better, more complete, clock model in Chapter 3.

As this work is included in a larger project of synthetic oscillators' design, the model developed in this Chapter seeks to minimize the number of variables, while simultaneously maintaining mathematical terms that allow for biological interpretation, such as Michaelis-Menten and Hill functions, as opposed to more phenomenological models. These characteristics allow to obtain a reduced final cell cycle scheme that can form a basis for the development of a synthetic biological oscillator (that is limited in the number of species it can contain, with 2 or 3 being ideal).

The cell cycle model built in this Chapter results in a relaxation oscillator, whose period control is made by an input of growth factors. A particularly important observation that is recovered by this model is the cell cycle period reponse to growth factor, whereby a small amount of growth factor is required for oscillation and the frequency of the cell cycle increases for increasing growth factor (both results in agreement with observations).

2.1 A comprehensive reduced model of the mammalian cell cycle

2.1.1 Abstract

The cellular division cycle is an essential process to ensure healthy tissue development and homeostasis which can, due to its periodicity, be interpreted as a biological oscillator. This work focuses on identifying the main dynamics underlying cell cycle rhythms in mammals and proposes a mathematical model to describe them. The model is based on post-translational modifications of cyclin B-cdk1, also called mitosis promoting factor (MPF), known to be the essential protein of the mammalian cell cycle, as well as in its degradation by the APC:cdc20 complex. The final result is a two variable reduced model of the mammalian cell cycle that is able to reproduce oscillatory behaviors and properties consistent with observations, namely the period being tunable by an external input of growth factor. We calibrate and validate this model and study its behavior in a simple open-loop control configuration, showing that it can exhibit bistability and oscillations. The model presents an advantage to work with due to its low variable and parameter size.

Keywords: cell cycle, biological oscillator, tunable period, open-loop control, bistability

2.1.2 Introduction

The cycle of life of eukaryotic cells is under tight control of a vast network of regulatory molecular processes in order to ensure cells grow, proliferate and die at proper rhythms and in a manner consistent with cell homeostasis. As such, the cell cycle is a key process involved in DNA synthesis and repair, cellular differentiation and programmed cell death, making it one of the most essential mechanisms to life. Uncontrolled cell proliferation on the other hand is characteristic of cancer, while insufficient cell proliferation may result in cell loss as seen in aging. Thus understanding and controlling the cell cycle is of the utmost importance in the treatment of cancer and other diseases.

The cell cycle occurs rhythmically resulting in a periodic oscillation of protein levels and activity, gene activation patterns and cellular morphology: it produces a biorhythm and can thus be interpreted as an oscillator. The cell cycle of several mammalian cells has a period of approximately 24 h and is coupled to the cellular circadian clock, another important biological oscillator, see [1] and [20]. Furthermore, the rate of division in a culture of mammalian cells varies accordingly with the amount of "growth factors", which are represented by a specific class of peptidic hormones added to the medium, allowing to tune the period of the oscillator.

Mathematical modeling has become particularly instrumental to study the cell cycle due to the increasingly known complexity of molecular controls involved in the process, see [57]. Models have become a powerful tool to study cell division systems, investigate the core mechanisms behind cell cycle rhythms and make predictions. [32], [36], [33] and [37] are successful examples of reference models for the mammalian cell cycle that vary in complexity and approach. The drawback of these models is their size which prevents analytical study of the parameter space in order to explore the various dynamical regimes.

With the goal of studying the main circuits underlying cell cycle rhythms and prove existence of oscillations and other properties we develop a reduced variable mechanistic model of ordinary differential equations (ODE) based on MPF (mitosis promoting factor, the cyclin B:cdk1 complex) which is the active component of the G2/M transition phase and is known to be necessary and sufficient to carry out the mitotic process (as seen in [6] and [32]).

The model here proposed includes phosphorylation and dephosphorylation steps carried out between MPF, wee1 and cdc25 ([7]), responsible for positive feedback-loops on MPF, as well as degradation of MPF by the APC:cdc20 complex ([8]) forming a negative feedback loop. While negative feedback loops are essential for oscillation, positive feedback-loops allow to tune the period of systems without compromising the amplitude of the signal, see [60]. The MPF/APC:cdc20 feedback loop has also been previously studied and modeled, see [39], [59].

Section 2.1.3 presents an intermediate-sized model, based on the reference mechanisms already described in [32] and [39]. This model is then reduced to a 2D model (section 2.1.4) containing all the mechanisms and is calibrated against cyclin B-cdk1 data [35] in order to obtain a physiological parameter set. Finally, in section 4 we present a numerical and analytical analysis of the parameter space, we observe that the 2D model captures well the period variation with growth factor and study a scenario of bifurcation between bistability and oscillations.

2.1.3 A 7D intermediate model

To obtain a low dimension model of the cell cycle, we first develop and then reduce an intermediate model.

First, the schematic of Fig. 2.1 summarizes some main processes responsible for MPF activation and inactivation. The inactive form of MPF has an extra phosphate group relative to the active one; cdc25 is a phosphatase responsible for removing this phosphate group leading to MPF activation, while wee1 is a kinase that phosphorylates MPF promoting its inactive form, [7]. Furthermore, MPF itself phosphorylates cdc25, activating it and forming a positive feedback-loop, and also phosphorylates wee1, inactivating it and forming a double-negative feedback loop, that acts as a positive loop.

Here, we consider that there is no production or destruction of cdc25 and wee1, meaning $[cdc25_{inactive}] = cdc25_{TOT} - [cdc25]$ and $[wee1_{inactive}] = wee1_{TOT} - [wee1]$, where $cdc25_{TOT}$ and $wee1_{TOT}$ are total amounts. Equations (2.1) to (2.4) model these processes.

The growth factor GF binds to receptors of the cellular membrane and initiates a signalling cascade that leads to the production of cyclin B, here represented by a synthesis term S_{GF} in equation (2.4) given by $S_{GF} = V_f \frac{GF^n}{GF^n + k_f^n}$. If GF is constant, so is S_{GF} and we assume that S_{GF} is a direct representation of the input.

$$\frac{d[cdc25]}{dt} = V_1 \frac{cdc25_{TOT} - [cdc25]}{cdc25_{TOT} - [cdc25] + k_1}[MPF] - V_2 \frac{[cdc25]}{[cdc25] + k_2} \tag{2.1}$$

$$\frac{d[wee1]}{dt} = V_3 \frac{wee1_{TOT} - [wee1]}{wee1_{TOT} - [wee1] + k_3} - V_4 \frac{[wee1]}{[wee1] + k_4}[MPF] \tag{2.2}$$

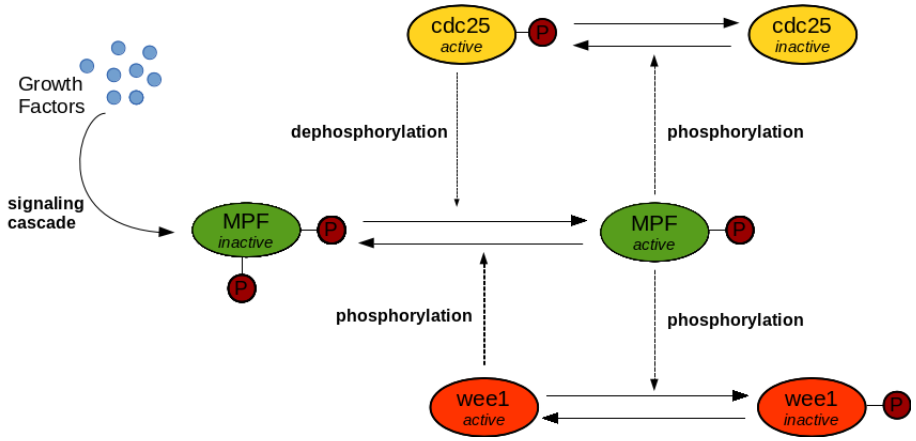

Figure 2.1: **Schematic representation of the positive feedback loop between MPF and cdc25 and of the double-negative feedback loop of MPF with wee1.**
MPF indirectly promotes its own activation by activating cdc25 and inactivating wee1: cdc25 promotes the active form of MPF while wee1 promotes its inactive form.

$$\begin{aligned}\frac{d[MPF]}{dt} =& V_5 \frac{[MPF_{inactive}]}{[MPF_{inactive}]+k_5}[cdc25] - V_6 \frac{[MPF]}{[MPF]+k_6}[wee1] \\ & - \gamma_1 [APC:cdc20][MPF]\end{aligned} \tag{2.3}$$

$$\begin{aligned}\frac{d[MPF_{inactive}]}{dt} =& S_{GF} - V5 \frac{[MPF_{inactive}]}{[MPF_{inactive}]+k_5}[cdc25] \\ & + V_6 \frac{[MPF]}{[MPF]+k_6}[wee1] \\ & - \gamma_2 [APC:cdc20][MPF_{inactive}]\end{aligned} \tag{2.4}$$

The second part of the model is represented in the scheme of Fig. 2.2 and describes the degradation of MPF by the complex APC:cdc20. These two components form a negative feedback-loop, with MPF phosphorylating the anaphase-promoting complex APC, leading it to a configuration that will dimerize with cdc20. The APC:cdc20 complex promotes the ubiquitination of MPF, targetting it for degradation. MPF has an opposite effect on cdc20 causing its inactivation and we include this step on the model as a first approach. The complex APC:cdc20 can dissociate into cdc20 and APC, see Fig. 2.2. Once more, we consider that there is no synthesis or degradation of cdc20 and APC, which allows us to write $[APC_{inactive}] = APC_{TOT} - [APC] - [APC : cdc20]$ and $[cdc20_{inactive}] = cdc20_{TOT} - [cdc20] - [APC : cdc20]$. Equations (2.5) to (2.7) model these steps.

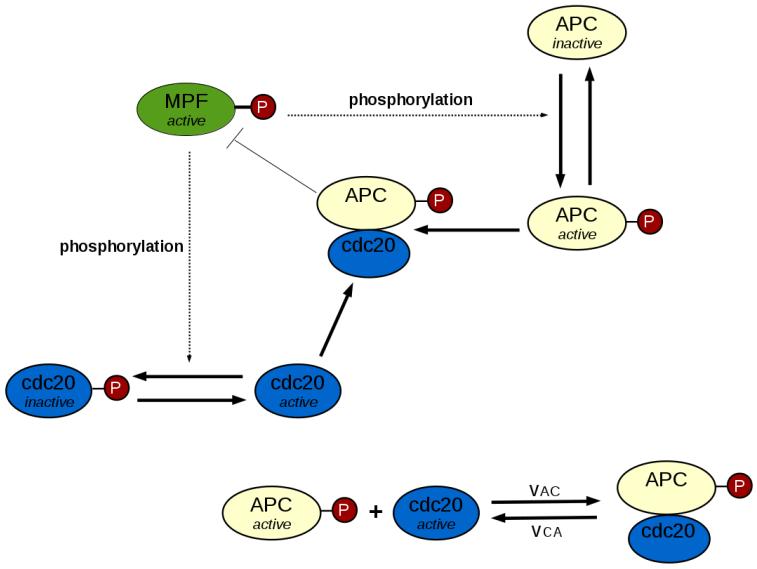

Figure 2.2: **Schematic representation of the negative feedback loop between MPF and the APC:cdc20 complex.**
MPF promotes the formation of APC:cdc20 by activating APC, while APC:cdc20 represses MPF by degradation. The APC:cdc20 complex can also dissociate.

$$\begin{aligned}\frac{d[APC]}{dt} =& V_7 \frac{APC_{TOT} - [APC] - [APC:cdc20]}{APC_{TOT} - [APC] - [APC:cdc20] + k_7}[MPF] \\ & - V_8 \frac{[APC]}{[APC] + k_8} - v_{AC}[APC][cdc20] + \\ & v_{CA}[APC:cdc20]\end{aligned} \tag{2.5}$$

$$\begin{aligned}\frac{d[cdc20]}{dt} =& V_9 \frac{cdc20_{TOT} - [cdc20] - [APC:cdc20]}{cdc20_{TOT} - [cdc20] - [APC:cdc20] + k_9} \\ & - V_{10} \frac{[cdc20]}{[cdc20] + k_{10}}[MPF] - v_{AC}[APC][cdc20] \\ & + v_{CA}[APC:cdc20]\end{aligned} \tag{2.6}$$

$$\frac{d[APC:cdc20]}{dt} = v_{AC}[APC][cdc20] - v_{CA}[APC:cdc20] \tag{2.7}$$

This model has an oscillatory behavior as shown in Fig. 2.3, for representative parameters. A calibration of the parameters is shown below for the reduced model. We also verify the tunability of the period with the input S_{GF}, for example for $S_{GF} = 0.24\ nmol.min^{-1}$, $T = 1942\ min$ and for $S_{GF} = 2.0\ nmol.min^{-1}$, $T = 1139\ min$. We verify that our total amounts of concentrations are close to those obtained by [35] and we chose the units of our preliminary parameters based

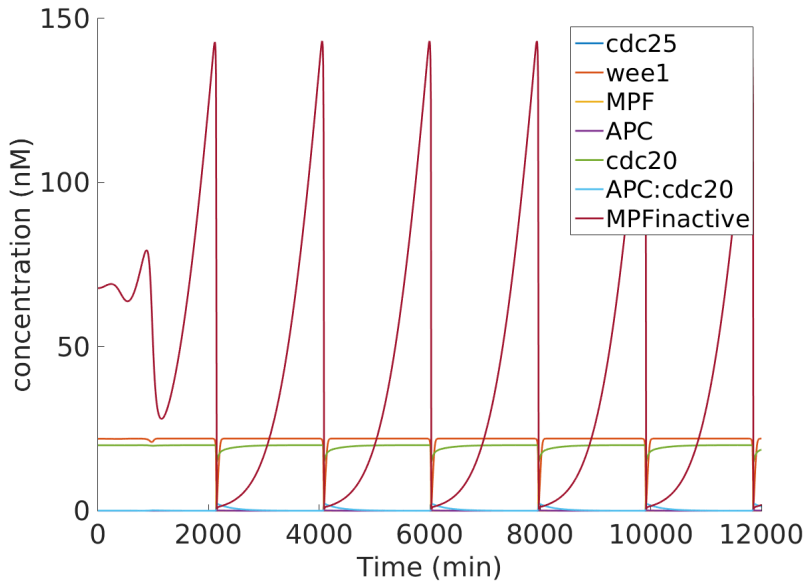

Figure 2.3: **Oscillations of the components of the cell cycle model.** Parameters: $wee1_{TOT} = 22.0$, $cdc25_{TOT} = 20.0$, $APC_{TOT} = 40.0$, $cdc20_{TOT} = 20.0$, $\gamma_1 = 3.0$, $\gamma 2 = 0.1$, $V_1 = 0.1$, $k_1 = 7.6$, $V_2 = 2.5$, $k_2 = 7.6$, $V_3 = 0.5$, $k_3 = 5.4$, $V_4 = 5.0$, $k_4 = 4.3$, $V_5 = 70.0$, $k_5 = 50.0$, $V_6 = 20.0$, $k_6 = 50.0$,$V_7 = 0.1$, $k_7 = 10.2$, $V_8 = 1.0$, $k_8 = 10.5$, $V_9 = 1.5$, $k_9 = 50.6$, $V_{10} = 0.5$, $k_{10} = 60.1$, $V_{AC} = 0.2$, $V_{CA} = 0.15$ and $S_{GF} = 0.24$. Units for V_1, V_4, V_5, V_6, V_7, V_{10} and V_{CA} are min^{-1} for V_2, V_3, V_8, V_9 and S_{GF} are $nM.min^{-1}$, for γ_1, γ_2 and V_{AC} are $min^{-1}.nM^{-1}$ and for all $k's$ are nM.

on that work. This model can be interpreted in relation to the cell cycle with the peaks of MPF corresponding to mitosis and the times when wee1 is high as the remaining phases of the cell-cycle preceeding mitosis.

2.1.4 Model Reduction and Calibration

The model has relaxation oscillations with certain variables varying through plateaus (see Fig. 2.3), thus in order to reduce it we start by setting cdc25 and wee1 at steady-state, i.e. $\frac{dx_i}{dt} = 0$ with x_i representing a generic variable. This results in:

$$MPF(cdc25) = \frac{V_2}{V_1}\frac{[cdc25]}{[cdc25]+k_2}\frac{cdc25_{TOT}-[cdc25]+k_1}{cdc25_{TOT}-[cdc25]} \tag{2.8}$$

and

$$MPF(wee1) = \frac{V_3}{V_4}\frac{wee1_{TOT}-[wee1]}{wee1_{TOT}-[wee1]+k_3}\frac{[wee1]+k_4}{[wee1]} \tag{2.9}$$

We want to replace the variables cdc25 and wee1 in equation (2.3) by a term dependent on MPF, thus we invert the functions given by equations (2.8) and (2.9) and verify that the inverse functions can be well approximated by Hill functions, as follows:

$$cdc25(MPF) = cdc25_{TOT}\frac{[MPF]^m}{[MPF]^m + k_m^m} \tag{2.10}$$

and

$$wee1(MPF) = wee1_{TOT}\frac{k_n^n}{[MPF]^n + k_n^n} \tag{2.11}$$

where the cdc25 equation (2.10) is that of an activator or promoter and wee1 equation (2.11) represents a repressor (further visualization of this method is given in Section 2.2).

Next, we observe that cdc20 isn't an essential variable for the oscillary behavior and we can make it constant.

Now focusing on the APC equation, we study the variations on parameters in equation (2.5). We verify that the parameter k_7 can be decreased to very low values without changing the output of the model: $k_7 \simeq 0$, implying that the first Michaelis-Menten term of equation (2.5) is saturated and can be approximated by a constant. Furthermore, we also verify that almost all the time $k_8 > [APC]$ and k_8 can be very large without dramatically affecting the system, which in its turn implies that the second Michaelis-Menten term of equation (2.5) can be approximated by a linear function. Thus,the equation for APC becomes:

$$\begin{aligned}\frac{d[APC]}{dt} =& V_7[MPF] - \frac{V_8}{k_8}[APC] - v_{AC}[APC][cdc20] \\ &+ v_{CA}[APC : cdc20]\end{aligned} \tag{2.12}$$

Now we put APC at steady-state to obtain:

$$[APC] = \frac{V_7[MPF] + v_{CA}[APC : cdc20]}{v_{AC} + \frac{V_8}{k_8}} \tag{2.13}$$

substituting in equation (2.7), leads to:

$$\frac{d[APC : cdc20]}{dt} = V_m[MPF] - V_k[APC : cdc20] \tag{2.14}$$

with parameters
$V_m = \frac{v_{AC}V_7}{v_{AC}+\frac{V_8}{k_8}}$ and $V_k = v_{CA}(1 - \frac{v_{AC}}{v_{AC}+\frac{V_8}{k_8}})$.

Lastly, we procceed to merge the two MPF equations (2.3 and 2.4). We look to remove the equation for $MPF_{inactive}$ as well as keeping Michaelis-Menten terms in the final equation to represent the phosphorylation and dephosphorylation of MPF, in coherence with the previous model. We verify that for non-negligible values of S_{GF} enough $MPF_{inactive}$ is created so that the production of MPF is never compromised. Thus, we consider an average maximum amount $\overline{MPF_{max}}$ from where we can define $MPF_{inactive} = \overline{MPF_{max}} - MPF$. The parameter $\overline{MPF_{max}}$ doesn't represent a total amount of MPF since there is also a production term S_{GF}. In section 4.2 we will include the effect of S_{GF} on the total amount of MPF.

In equation (2.15) we observe the simplified MPF reduced equation, which also contains the growth factor input:

$$\begin{aligned}\frac{d[MPF]}{dt} =& S_{GF} + V_c \frac{\overline{MPF_{max}} - [MPF]}{\overline{MPF_{max}} - [MPF] + k_c} \frac{[MPF]^m}{[MPF]^m + k_m^m} \\ & - V_w \frac{[MPF]}{[MPF] + k_w} \frac{k_n^n}{[MPF]^n + k_n^n} \\ & - \gamma_1 [APC : cdc20][MPF]\end{aligned} \tag{2.15}$$

The exponents m and n take the value of 2 and V_c and V_w represent $V_5 cdc25_{TOT}$ and $V_6 wee1_{TOT}$ respectively (see equations (2.3), (2.10) and (2.11)). The $APC : cdc20$ complex is as given by equation (2.14).

Our final model is thus given by equations (2.15) and (2.14). The numerical simulations give again rise to relaxation oscillations as observed in Fig. 2.4 (period 126.8 min), with the peaks of MPF indicating mitosis. Parameters are presented in Table 2.1 and were obtained through adjustment to data points by means of a computational optimization, see Fig. 2.4. Data points for calibration were collected from [35] that presents experimental results of normalized cyclin levels and cdc2 activity for the Xenopus egg.

Table 2.1: Calibrated parameters

p	Numerical Value
γ_1	0.016 min^{-1}
V_c	226 min^{-1}
k_c	130
V_w	748 min^{-1}
k_w	138
k_m	98.5
k_n	0.116
V_m	1.68×10^{-2} min^{-1}
V_k	1.07×10^{-2} min^{-1}
S_{GF}	5.69 min^{-1}
$\overline{MPF_{max}}$	284

It is clear that our model faithfully represents the dynamics of cyclin B, with a set of physiological parameters that leads to oscillatory behavior. The fact that the reduced model again produces relaxation oscillations for MPF as well as tuning of the period through GF (see section 3.12), allows us to consider that the essential mechanistic steps of our first model are conserved.

2.1.5 Mathematical Analysis

Next, we analyse how oscillations are originated by an unstable fixed-point inside a limited phase-plane region. The nullclines are shown in Fig. 2.6. As discussed before, $\overline{MPF_{max}}$ will be

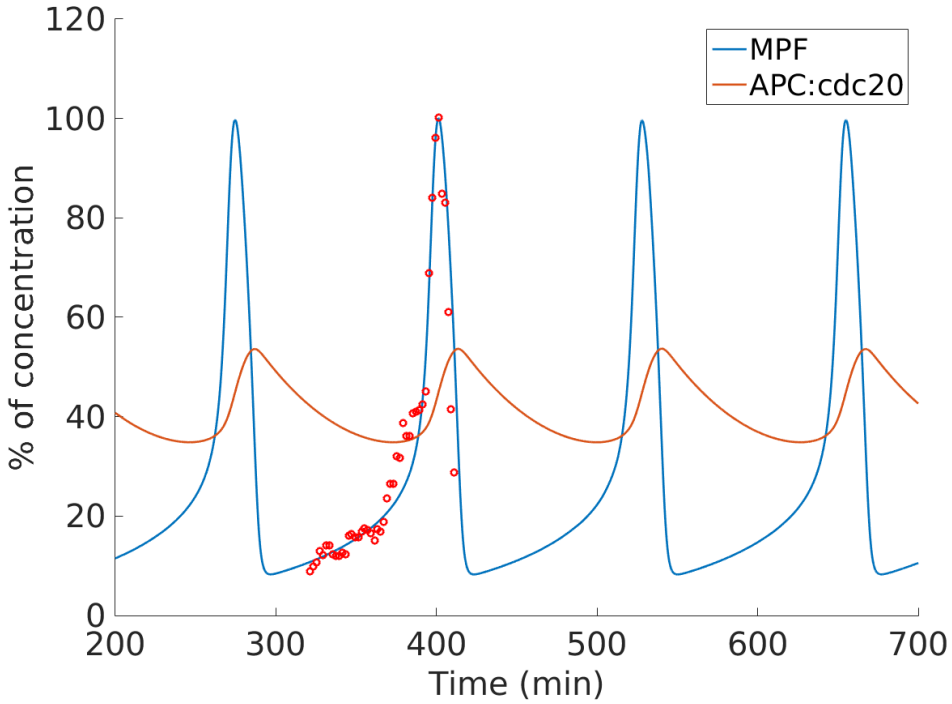

Figure 2.4: **Oscillations of MPF and APC:cdc20 over time.**
Adjustment of the 2D model to data points for the Xenopus egg normalized to 100, retrieved from [35]. Obtained parameters are presented in Table 2.1. The model results in relaxation oscillations with T = 126,8 min. The peaks of MPF indicate mitosis.

an approximate limit for the maximum value of MPF, which in its turn will limit the amount of APC:cdc20, thus forming a foward-invariant region for this system. Inside this region there is a unique fixed point, which is unstable when the two nullclines intersect in an interval where both are increasing. For this set of parameters, the nullclines intersect at $(23.03, 36.16)$ and this is an unstable fixed point. Under these conditions, applying the Poincaré-Bendixson Theorem to this 2D system proves the existence of a periodic orbit.

The rate of production of the APC:cdc20 complex by MPF (V_m) and the natural degradation of APC:cdc20 (V_k) control the slope of the APC:cdc20 nullcline. For the parameters of Table 2.1 the nullclines intersect near the beginning of the oscillatory region (Fig. 2.6), however the calibration with data for the Xenopus egg gives us mostly the order of magnitude for the parameters of a mammalian cell, thus we can change slightly the value of V_k in order to have a broader study of the parameters in the oscillatory region in Fig. 2.5. From observation of Fig. 2.5 we can conclude that V_m, V_k and k_m are the parameters that produce greater changes in period and that overall the system is robust in relation to parameters' changes.

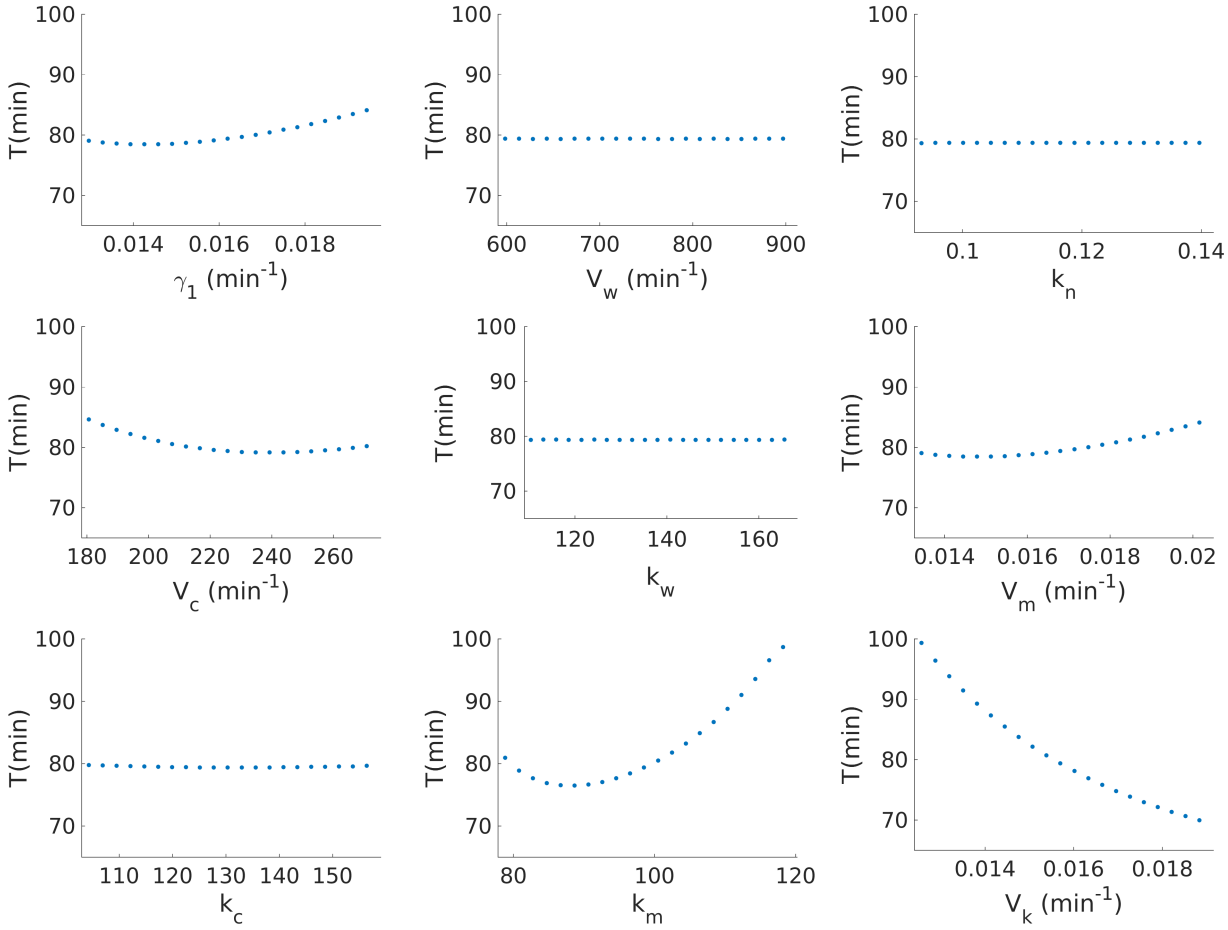

Figure 2.5: **Sensitivity analysis of the model.**
Parameters are varied 20 % around a value in the middle of the oscillation region - (Table 2.1, with $V_k = 0.0157\ min^{-1}$).

Parameters Analytical Characterization

In order to obtain broader limits for the parameters than those that numerical simulations allow and to better understand how each term of the model equations affects the dynamics we analyse possible relations between parameters that can guarantee existence of oscillation.

From the observed dynamics of our oscillations (Fig. 2.6), we require the MPF nullcline to be increasing when it intersects with the APC:cdc20 nullcline in order to obtain an unstable fixed-point. Thus, we consider now the MPF nullcline as $g_1(x)$ and the APC:cdc20 nullcline as $g_2(x)$, represented in equations (2.16) and (2.17), with $\overline{MPF_{max}}$ now called X_M for simplicity:

$$\begin{aligned} g_1(x) = & \frac{S_{GF}}{\gamma_1 x} + \frac{V_c}{\gamma_1 x}\frac{X_M - x}{X_M - x + k_c}\frac{x^2}{x^2 + k_m^2} \\ & - \frac{V_w}{\gamma_1 x}\frac{x}{x + k_w}\frac{k_n^2}{x^2 + k_n^2} \end{aligned} \tag{2.16}$$

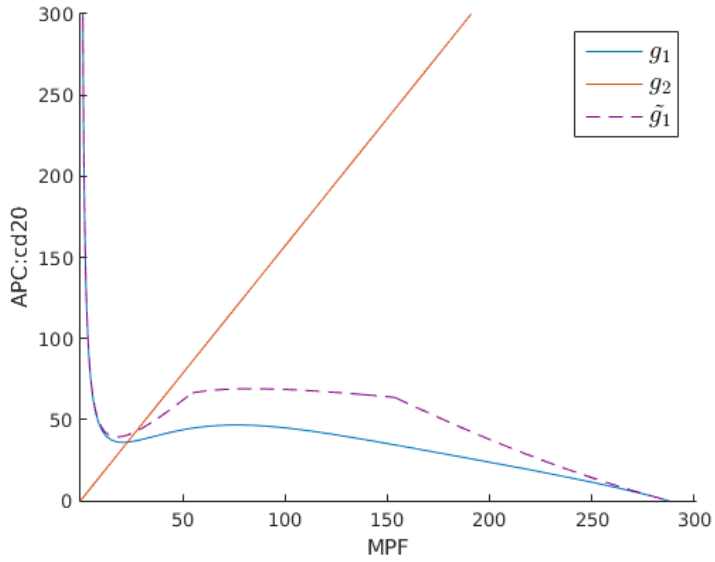

Figure 2.6: **Nullclines and piece-wise quadratic approximation.**
Blue curve (g_1): MPF nullcline, red curve (g_2): APC:cdc20 nullcline (parameters given in Table 2.1), dashed purple curve ($\tilde{g}_1$): piecewise quadratic approximation of the MPF nullcline.

$$g_2(x) = \frac{Vm}{Vk}x \tag{2.17}$$

and determine the local minimum and maximum points x_1 and x_2 that will delimit the region of increasing g_1. The intersection point of g_1 and g_2 must satisfy $\frac{g_1(x_2)}{x_2} < \frac{V_m}{V_k} < \frac{g_1(x_1)}{x_1}$ (see equation 2.17) in order for the nullclines to intersect in the growing region of g_1. For the set of calibrated parameters (Table 2.1) we determine x_1 and x_2 numerically and verify $0.61 < \frac{V_m}{V_k} < 1.73$.

We now proceed to approximate the terms of $g_1(x)$ by piecewise quadratic functions (a more complete explanation of this process is given in Section 2.2). For example, considering $h_1(x)$ as the activator Hill function in equation (2.16) we design an approximation given by:

$$h_1(x) = \frac{x^2}{x^2 + k_m^2} \approx \begin{cases} \alpha x^2 & \text{if } x < x_a \\ -a(x - X_M)^2 + h_1(X_M) & \text{if } x_a \leq x < X_M \end{cases}$$

We choose $\alpha = 8 \times 10^{-7} k_m$ in order to define a quadratic function that approximates well the first region of h_1, $x_a = \sqrt{\frac{1-\alpha k m^2}{\alpha}}$ is the point where the function intersects h_1. The second equation defines an inverted parabola whose maximum is set at X_M, with a defined as $a = \frac{h_1(X_M)+\alpha k m^2 - 1}{(x_a - X_M)^2} > 0$ in order to have continuity at x_a.

The space is split into five intervals: $0 < x < \sqrt{2}k_n$, $\sqrt{2}k_n < x < x_a$, $x_a < x < k_w$, $k_w < x < X_M - k_c$ and $X_M - k_c < x < X_M$ that define the limits of the piecewise quadratic approximation $\tilde{g}_1$ (shown in Fig. 2.6).

Intervals 2 and 3 contain the region where the function increases (Fig. 2.6), at these intervals $\tilde{g}_1$ is defined as:

$$\tilde{g}_1^2(x) = \frac{S_{GF}}{\gamma_1 x} + \frac{V_c \alpha x}{\gamma_1} \tag{2.18}$$

$$\tilde{g}_1^3(x) = \frac{1}{\gamma_1 x}[S_{GF} + V_c(-a(x - X_M)^2 + h_1(X_M))] \tag{2.19}$$

The derivative of $\tilde{g}_1^2(x)$ has a zero at $\tilde{x}_1 = \sqrt{\frac{S_{GF}}{\alpha V_c}}$ that marks the begining of the increasing region, the derivative of $\tilde{g}_1^3(x)$ as a zero at $\tilde{x}_2 = \sqrt{\frac{V_c(aX_M^2 - h_1(X_M)) - S_{GF}}{aV_c}}$ that limits the upper bound of the interval. Thus, in a broad manner we may conclude that the parameters need to satisfy $\tilde{x}_1 < \tilde{x}_2$, or:

$$S_{GF} < V_c \frac{\alpha(aX_M^2 - h_1(X_M))}{a + \alpha} \tag{2.20}$$

which we can interpret as giving the maximum value of the growth-factor dependent synthesis term S_{GF} in relation to V_c that guarantees oscillations. S_{GF} and V_c together account for the total production of MPF in the model, with V_c being the maximum value of the positive Michaelis-Mentem term (representing formation of MPF from $MPF_{inactive}$) in equation (2.15), this allows us to conclude that the limit of growth factor above which oscillations stop is dependent on the rate of MPF phosphorylation by cdc25. Using the parameters presented in Table 2.1 and the mentioned value of α we obtain $S_{GF} < 21.6$ and verify the condition (2.20).

The piecewise quadratic approximation shows that an interval where $g_1([MPF])$ increases appears due to a dominance of the Hill term coming from the cdc25 positive loop, $V_c \frac{MPF^2}{MPF^2 + k_m^2}$. It furthermore captures the properties needed to generate sustained oscillations, yielding relations between the parameters that allow to characterize the oscillatory behavior.

Open-loop Control and Bistability

In Fig. 2.7 we can see that the model reproduces the trend of period tunable with a Growth Factor input, where an adjustment is made between our output and experimental data from Table 2.2. The experimental data points come mostly from [1], with the exception of the 5% FBS (fetal bovine serum) value, that is an additional measurement done under the exact same experimental conditions (unperturbed NIH 3T3 mouse fibroblasts). We do a scaling in our model such as $t \to \beta t$, which leads to $S_{GF} \to \frac{S_{GF}}{\beta}$, with $\beta = 0.1$.

Lastly, seeking to improve the approximation made in section 3 as: $MPF_{inactive} = \overline{MPF_{max}} - MPF$, we study the case in which $\overline{MPF_{max}}$ also depends on the input: $\overline{MPF_{max}} = \overline{MPF_{max}} + \beta S_{GF}$ in equation (2.15). This recovers a property of our 7D model in which S_{GF} will have an effect in the amount of $MPF_{inactive}$ available to generate MPF.

An interesting result is that for certain values of $\overline{MPF_{max}}$, the model switches from the oscillatory regime to a bistable regime as the input S_{GF} increases. Fig. 2.8 presents the MPF steady states for different values of S_{GF}, with $\overline{MPF_{max}} = 150$ and $\beta = 20$. We can observe,

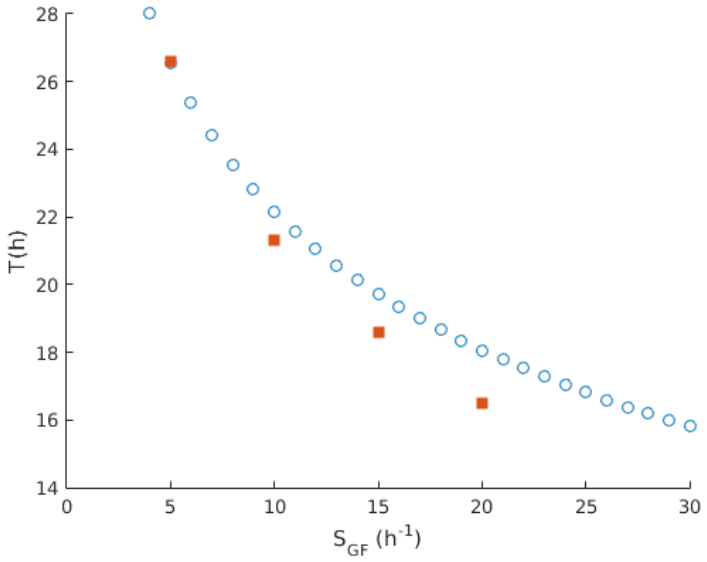

Figure 2.7: **Period tunable with the input S_{GF}: open-loop control.** We do a scaling correspondance of our numerical simulations (blue circles) with data from Table 2.2 (red squares).

Table 2.2: Experimental data for the period tunable with GF ([1])

$\%FBS$	$T(h)$
5	26.6
10	21.3
15	18.6
20	16.5

with increasing S_{GF}, the passage from a monostable regime to bistability, to again monostability, then entering the oscillation region with one unstable fixed point and finally monostability again. The entrance in the oscillatory region is marked by a Hopf bifurcation.

The input parameter S_{GF} controls the change between dynamic regimes and we can delimit the oscillatory regime for 3.3 $min^{-1} < S_{GF} < 17.7\ min^{-1}$.

From a biological point of view this raises the question of whether cells grown with low growth factor and unable to divide would present bistability. Bistability in the activation of cdc2 has been observed by [33] on a modified system.

Additionally, Fig. A.1 shows an extended analysis of Fig. 2.8 complemented with the envelope of oscillations and Fig. A.2 shows the intersection of nullclines for several values of S_{GF} (these Figures are not part of the original paper).

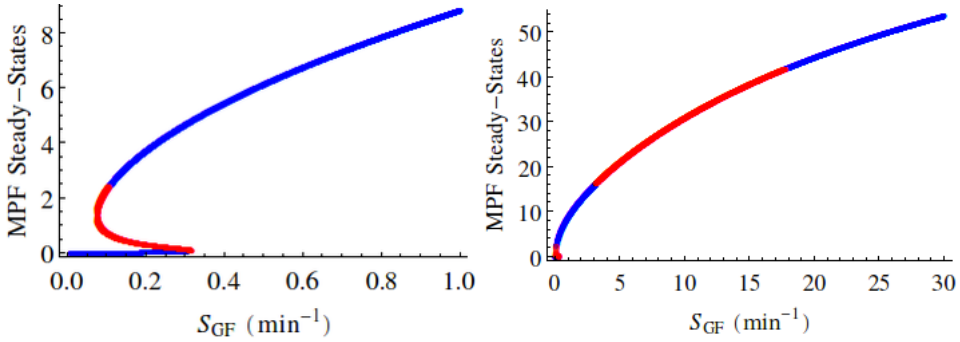

Figure 2.8: **MPF steady-states as a function of the parameter S_{GF}.** Left side of image shows a zoom for S_{GF} between 0 and 1. Stable steady states are represented in blue and unstable steady-states in red. A Hopf bifurcation marks the entrance in the oscillatory region.

2.1.6 Conclusion

A two variable cell cycle model based on the negative feedback loop between MPF and the APC:cdc20 complex and on a positive feedback loop of MPF was calibrated from experimental data for cyclin B from one study ([35]) and was able to reproduce experimental data from another study ([1]) for the tunability of the period with the growth factor input.

The growth factor input controls the output of the system determining switching behavior between bistability, monostability and oscillations. The cell cycle is understood in terms of relations between parameters representing the G2 phase, with the activity of cdc25 being dominant over the other components, producing the biorhythm.

2.1.7 Aknowledgments

The authors are part of the Labex SIGNALIFE Network for Innovation on signal Transduction Pathways in Life Sciences (Grant ANR-11-LABX-0028-01), ANRHyClock project (ANR-14-CE09-0011) and iCycle project (ANR-16-CE33-0016-01).

2.2 Function Approximation in Cell Cycle Modeling

In this Section we provide complementary explanations and visualizations on methods of function approximation used in the previous Section.

2.2.1 Graphical Function Approximation

In Section 2.1.4 quasi-steady-state approximation of $\frac{d[cdc25]}{dt}$ and $\frac{d[wee1]}{dt}$ led to the substitution of cdc25 and wee1 by functions (2.10) and (2.11). In this case function approximation is graphical. Figs. 2.9 and 2.10 respectively show the plot of MPF(cdc25) and MPF(wee1) along with the

inverse plot for the same functions, allowing to see that both can be well approximated by Hill functions.

The true inverse functions of Eqs. 2.8 and 2.9 contain terms such as square roots that are less biologically meaningful than Hill functions. For simplicity and readability of the reduced model, we approximate the true inverse functions by straightforward Hill functions representing one activator and one repressor for cdc25 and wee1 respectively. These accurately represent the role of these two cell cycle components.

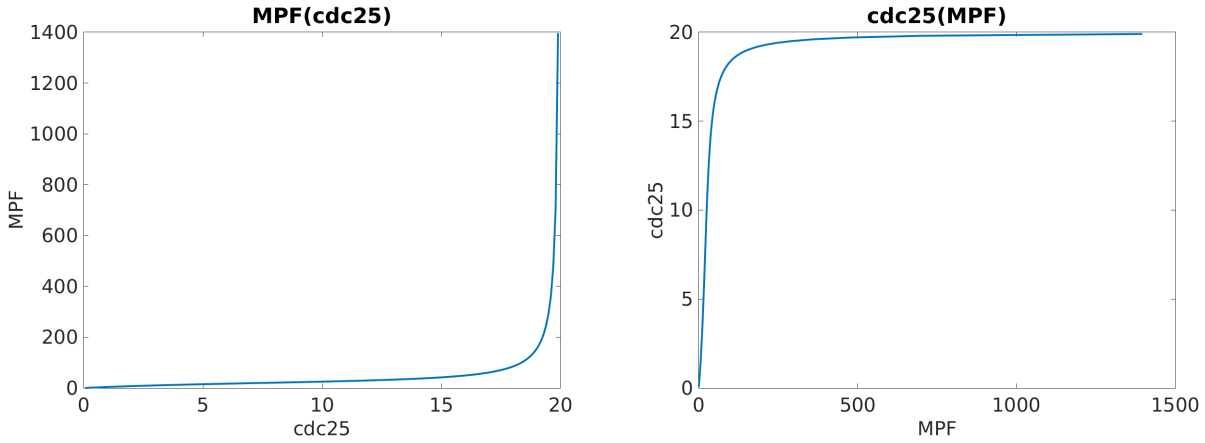

Figure 2.9: **Quasi-Steady-State Approximation of cdc25.**
On the left: MPF as function of cdc25 as given by 2.8. On the right: the inverse plot of MPF(cdc25) allows to visualize that cdc25(MPF) can be well approximated by an activator Hill function of the type $V_m \frac{x^m}{x^m+k_m^m}$ (Eq. 2.10).

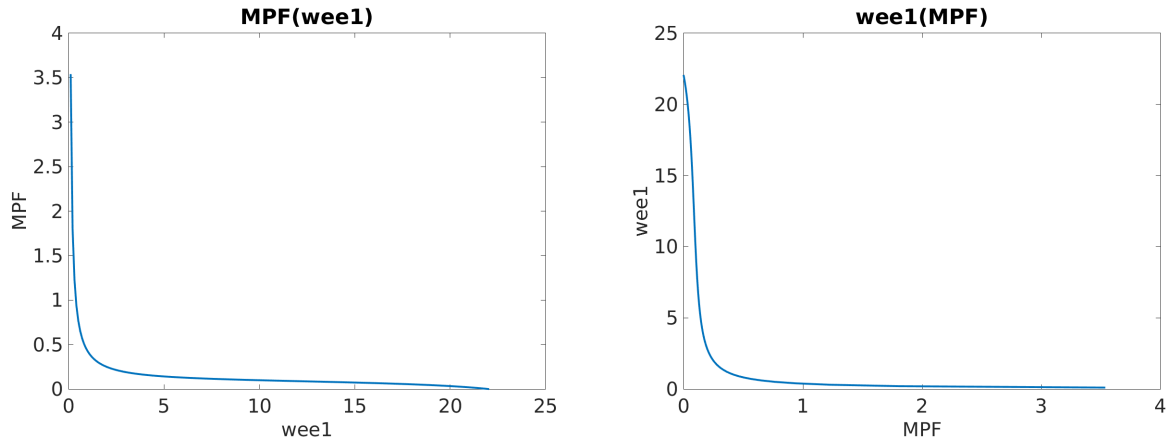

Figure 2.10: **Quasi-Steady-State Approximation of wee1.**
On the left: MPF as function of wee1 as given by 2.9. On the right: the inverse plot of MPF(wee1) allows to visualize that wee1(MPF) can be well approximated by a repressor Hill function of the type $V_n \frac{k_n^n}{x^n+k_n^n}$ (Eq. 2.11).

2.2.2 Piecewise Quadratic Approximation

In Section 2.1.5 approximation of the MPF nullcline g_1 by a piecewise quadratic function allowed to establish a relation between the parameters representing MPF production, either by synthesis (S_{GF}) or by activation via the cdc25 mechanism (V_c). This method consisted in approximating each Michaelis-Mentem or Hill term of g_1.

Recall g_1:

$$g_1(x) = \frac{S_{GF}}{\gamma_1 x} + \frac{V_c}{\gamma_1 x}\frac{X_M - x}{X_M - x + k_c}\frac{x^2}{x^2 + k_m^2} - \frac{V_w}{\gamma_1 x}\frac{x}{x + k_w}\frac{k_n^2}{x^2 + k_n^2} \tag{2.16}$$

Thus, we begin by approximating the Hill terms.

The repressor term representing wee1 action on MPF, given by $h_2(x) = \frac{k_n^2}{x^2+k_n^2}$, is decreasing and tends to zero as $x \to \infty$, thus after a certain value k_s we approximate h_2 by zero. To devise the function for $x < k_s$ we found the quadratic approximation to fit better than the linear. We design a funcion of the type $q(x) = -ax^2 + bx + c$ so as to have $q(0) = 0$, $q'(0) = 0$ and $q(k_n) = \frac{1}{2}$, just as h_2. Thus the approximation becomes:

$$h_2(x) = \frac{k_n^2}{x^2 + k_n^2} \approx \begin{cases} -\frac{1}{2k_n^2}x^2 + 1 & \text{if } x < \sqrt{2}k_n \\ 0 & \text{if } x \geq \sqrt{2}k_n \end{cases} \tag{2.21}$$

And we set $k_s = \sqrt{2}k_n$ so as to have continuity between the two steps of the function.

The activator term representing cdc25 action on MPF and given by $h_1(x) = \frac{x^2}{x^2+k_m^2}$ is increasing and tends to 1 when $x \to \infty$. In this case approximating by two quadratic functions yielded better results in terms making our approximation $\tilde{g_1}$ closer to g_1. The approximation was shown in Section 2.1.5 and is given by:

$$h_1(x) = \frac{x^2}{x^2 + k_m^2} \approx \begin{cases} \alpha x^2 & \text{if } x < x_a \\ -a(x - X_M)^2 + h_1(X_M) & \text{if } x_a \leq x < X_M \end{cases} \tag{2.22}$$

Fig. 2.11 shows h_1 as well as the two approximate parabolas, the inverted parabola has its maximum at $h_1(X_M)$.

We now approximate the Michaelis-Menten functions by linear terms.

The term $h_3(x) = \frac{x}{x+k_w}$ represents MPF inactivation via phosphorylation and is multiplied by the wee1 term h_2. As h_3 is increasing and tends to 1 as $x \to \infty$, for $x > k_s$ we define h_3 as 1, while for $x < k_s$ we take the linear approximation of the Michaelis-Menten function near the origin $\frac{x}{k_w}$ and set $k_s = k_w$ so as to have continuity of h_3:

$$h_3(x) = \frac{x}{x + k_w} \approx \begin{cases} \frac{x}{k_w} & \text{if } x < k_w \\ 1 & \text{if } x \geq k_w \end{cases} \tag{2.23}$$

Similarly, the term $h_4(x) = \frac{X_M - x}{X_M - x + k_c}$, representing activation of MPF from an available constant amount X_M is decreasing and flat at the origin. Thus we approximate it by 1 for $x < k_s$ and take the linear approximation of h_4 for $x > k_s$. In this case $k_s = X_M - k_c$ and the approximation becomes:

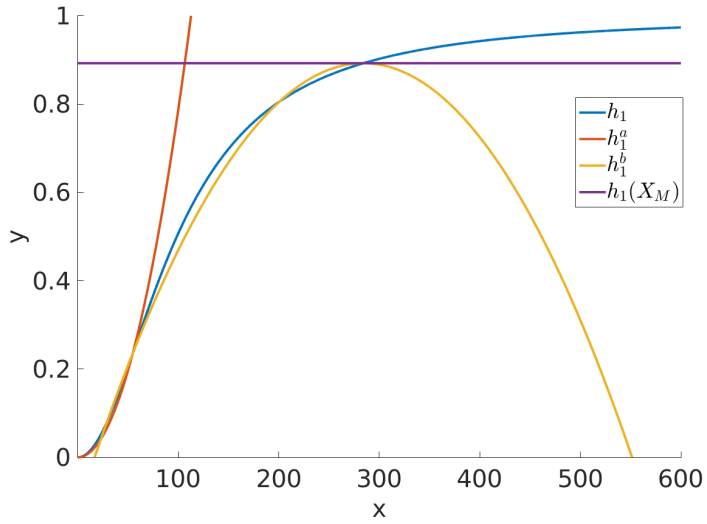

Figure 2.11: **Activator Hill term of g_1.**
Plot of h_1 as well as the parabolas of Equation 2.22 and the line $y = h1(X_M)$. X_M is the upper limit of x. In this case $k_s = x_a$ is the point where the two parabolas intersect.

$$h_4(x) = \frac{X_M - x}{X_M - x + k_c} \approx \begin{cases} \frac{X_M - x}{k_c} x & \text{if } x < X_M - k_c \\ 1 & \text{if } X_M - k_c \leq x \leq X_M \end{cases} \tag{2.24}$$

Finally we order the five intervals obtained above, defining the points where the quadratic approximation $\tilde{g}_1$ changes: $0 < x < \sqrt{2}k_n$, $\sqrt{2}k_n < x < x_a$, $x_a < x < k_w$, $k_w < x < X_M - k_c$ and $X_M - k_c < x < X_M$.

And we define $\tilde{g}_1$ for each interval:

$0 < x < \sqrt{2}k_n$:

$$\tilde{g}_1^1(x) = \frac{1}{\gamma_1 x}[S_{GF} + V_c \alpha x^2 - V_w \frac{x}{k_w}(1 - \frac{1}{2}\frac{x^2}{k_n^2})] \tag{2.25}$$

$\sqrt{2}k_n \leq x < x_a$:

$$\tilde{g}_1^2(x) = \frac{1}{\gamma_1 x}[S_{GF} + V_c \alpha x^2] \tag{2.18}$$

$x_a \leq x < k_w$:

$$\tilde{g}_1^3(x) = \frac{1}{\gamma_1 x}[S_{GF} + V_c(-a(x - X_M)^2 + h_1(X_M))] \tag{2.19}$$

$k_w \leq x < X_M - k_c$:

$$\tilde{g}_1^4(x) = \frac{1}{\gamma_1 x}[S_{GF} + V_c(-a(x - X_M)^2 + h_1(X_M))] \tag{2.26}$$

and $X_M - k_c \leq x \leq X_M$:

$$\tilde{g}_1^5(x) = \frac{1}{\gamma_1 x}[S_{GF} + V_c(-a(x - X_M)^2 + h_1(X_M))\frac{X_M - x}{k_c}] \tag{2.27}$$

The plot of this approximation is shown in Fig. 2.6 together with g_1 and g_2.

3

Modeling the Mammalian Circadian Clock

This Chapter is written in the form of an article, with the provisory title: "Timing of circadian clock regulatory inputs controls duration of activating and repressing phases in a transcriptional D-box-based model". In this article a transcription-based mammalian cellular clock model is built, analyzed and reduced to a reasonable number of variables. Moreover, some applications of this model are explored, namely the response to timed signaling inputs, allowing for an increased understanding of how the circadian clock may control metabolic health and disease.

The mammalian circadian clock system presents a characteristic orderly expression of its core proteins, where the phase-opposition between CLOCK:BMAL1 and PER:CRY, relating to opposite states of the day/night cycle, is a key feature. Following the discussion of Appendix B, we intend to study the implications of the essential circadian topology leading to an antiphasic oscillation between CLOCK:BMAL1 and PER/PER:CRY in relation to the period-lock dynamical behavior of the coupled clock/cell cycle system (this will be done on Chapter 4). Because pre-existing circadian clock models tend to have a large number of variables and/or account for a lot of post-translation protein modifications, we are not using already existing clock models, but rather rely on the most recent experimental data to construct a more comprehensive model with the desired properties. As such, the work here developed focus in obtaining this property as a result of our model and also as a part of the essential oscillatory network. This is verified when upon dynamical model reduction the BMAL1 and PER:CRY variables remain a part of the circadian skeleton network. Their antiphasic oscillatory behavior is also maintained after model reduction, making it a "built-in " feature of our model, which after reduction has a small number of variables (four).

The circadian clock being a mechanism of physiological adaption to daily external changes consists in a system that coordinates the modulation of gene expression by certain external and internal inputs, such as light and hormones. In this Chapter, we relate the different clock phases with different metabolic states and use this to make inferences of the interconnection between clock and metabolism, without including metabolic modeling directly. This is done, among other methods, by analyzing the clock response to inputs that relate to the day/night and fast/feeding cycles and observing the differences in clock dynamics when these two signals are given in proper phase alignment versus in phase misalignment.

3.1 Timing of circadian clock regulatory inputs controls duration of activating and repressing phases in a transcriptional D-box-based model

Abstract

The molecular oscillator of the mammalian circadian clock consists of a dynamical network of genes and proteins, largely uncovered by experimental studies and dynamical modeling, whose regulation occurs essentially at the transcription level with some degree of post-transcriptional/post-translational regulation. From a dynamical point of view, the mechanisms leading to an oscillatory solution following an orderly peak protein expression pattern and a clear day/night phase distinction remain unclear. Our goal is to identify the essential interactions needed to generate phase opposition between the activating CLOCK:BMAL1 and the repressing PER:CRY complexes and to better distinguish two main clock molecular phases relating to rest/activity and fast/feeding cycles. To do this, we develop a transcriptional-based model centered on linear combinations of clock controlled elements (CCEs): E-box, R-box and D-box, where each CCE is modeled as an effector of activators and repressors. After calibration with single-cell data, the model is analyzed and used to explore entrainment and period tuning via interplay with metabolism as well as asymmetric changes in the duration of the different clock phases in the *tau* mutation. Furthermore, when exposing the clock mechanism to two regulatory inputs, one relating to the fast/feeding cycle and the other to the light-dependent SCN synchronization signaling, the phase difference between these two signals impacts on the relative duration of the different molecular clock phases. Simulated circadian misalignment, known to correlate with insulin resistance, leads to decreased duration of BMAL1 and CRY1 peak expression, thus supporting their role in promoting insulin sensitivity. The circadian clock mechanism controls the relative duration of activating and repressing molecular clock states in response to hormonal signaling inputs. Finally, dynamical reduction of the model allows us to conclude that D-box plays an essential role in guaranteeing oscillations with CLOCK:BMAL1 and PER:CRY in anti-phase.

Author summary

In this work we investigate whether rhythmicity and phase differences between the main mammalian clock proteins can be recovered by a transcription-based model that minimizes post-translational effects. We show that a model centered on the CCEs E-box, R-box and D-box recovers the desired properties. This model is calibrated against experimental data and validated through properties such as robustness to changes of parameters and ability of entrainment by an external signal. To allow for period tuning, we develop a non-linear closed-loop control function representative of CLOCK:BMAL1 chromatin remodeling via PGC1-α. Through quasi-steady-state reduction, we conclude that D-box is an essential topological element for antiphasic oscillation between BMAL1 and PER:CRY, indicating a possibly important role for PAR transcription factors in the core clock. Furthermore, we simulate the *tau* mutation and verify that a decrease in the period of the system leads to a proportional decrease in the duration of the

molecular night only. Following this, we explore interactions between clock and metabolism by observing the clock response to the alignment state between fast/feeding and light/dark cycles and propose that a decrease in the duration of BMAL1 peak expression may explain why circadian misalignment is correlated with insulin resistance.

3.1.1 Introduction

In the vast majority of organisms the circadian clock is a fundamental, highly conserved, mechanism that governs daily behavior and cell physiology providing adaptation to external changes. In mammals, coordination between cycles of rest/activity and fast/feeding with the external light/dark cycle is ensured by a complex and hierarchical timing system: in brief, a hypothalamic central clock receives light inputs and in turn coordinates clocks in peripheral organs, tissues and cells along the 24 h cycle via internal signaling. Importantly, both central and peripheral clocks share the same molecular makeup.

Experimental studies and mathematical models have uncovered a dynamical network of clock components. The core clock mechanism consists of the CLOCK:BMAL1 protein complex that promotes transcription of the *Per* and *Cry* mRNA. The PER:CRY protein complex subsequently formed in the cytoplasm then translocates into the nucleus where it both blocks CLOCK:BMAL1 transcriptional activity and displaces the CLOCK:BMAL1 heterodimer from its cognate promoters [65]. Another negative feedback loop between CLOCK:BMAL1 and REV-ERBα is also a part of the core clock mechanism mechanism [10] [46]. In spite of the phase differences between core clock mRNAs and core clock proteins not being exactly the same, specific peak order between the core clock components, such as BMAL1, REV-ERBα, PER and CRY occurs already at the mRNA level [61].

Endogenous circadian clocks coordinate gene activation patterns and protein concentrations that oscillate in individual cells with a 24 hour period, such that different times of day are characterized by different cellular protein profiles. Of particular importance is the antiphasic relation between BMAL1 and PER:CRY that strongly correlates with the day/night separation. We note that the terminology "phase" is formally used as to denote the angle of rotation of the oscillator relative to a reference value. However, by abuse of language, throughout this article we sometimes use "phase" in a more general sense, to designate a given stage of the molecular circadian oscillation, as for instance to refer to an activating phase (when BMAL1 is up and PER:CRY is down) or to a repressing phase (with BMAL1 down and PER:CRY up).

A combination of experimental and computational approaches has helped increase knowledge on the circadian clock. Goodwin proposed in 1975 a model based on a simple negative feedback loop between a protein and its own gene, [40]. Such a feedback loop was indeed uncovered, first in *Drosophila* (Zehring et al. (1984) [62]) and later in other organisms (Bell-Pedersen et al. (2005) [63]). Since then a number of dynamic modeling studies have furthered the discussion on the mammalian cellular clock (see Podkolodnaya et al., (2017), for a comparative review [50]). Examples of these models are Leloup and Goldbeter (2003), [41], Forger and Peskin (2003), [42], Relógio et. al (2011), [46], and Yan et al. (2014), [64], that present varying ways

of studying the system, from the use of high number of variables/parameters to the addition of explicit time delays. Differently, Mirsky et al. (2009), propose a model that purposely minimizes post-translation modified species [45] and Becker-Weimann et al. (2004) focus on clock modeling using a reduced number of species [44]. In this work, we attempt to simultaneously minimize the number of variables and restrict posttranslational modifications to the PER/CRY mediated transrepression in order to investigate whether major mammalian clock properties such as oscillation, orderly peak protein expression and clear day/night phase distinction can be recovered by a transcription-based model that includes the majority of the core clock components and uses simple equation modeling terms. Applications of clock models are useful for studying the interconnection between the mammalian clock and other essential cellular processes, such as the cell cycle (Gérard and Goldbeter (2012), [26], Zámborszky et al. (2007) [25], Feillet et al. (2015) [20], Bieler et al. (2014) [30]) and metabolism (Woller et al. (2016) [18], Woller and Gonze (2018) [100]).

While post-transcriptional mechanisms, including RNA-based mechanisms, are essential for the proper functioning of the clock, this doesn't mean these mechanisms are dynamically significant for oscillation or for the correct order of protein peak expression and their contribution may be mainly to create specific delays that in a modeling perspective can be achieved by adjusting parameters on the essential dynamical interactions. In fact, transcription/translation feedback loops are usually shorter than circadian periods and delays such as that of PER degradation or that of PER nuclear entry via phosphorylation are known to contribute to the 24h circadian period [12]. Furthermore, post-translational mechanisms may be a way to rapidly incorporate a variety of signals and may even consist on the majority of circadian regulation interactions; notwithstanding the integration of all these signals seems to occur at the gene transcription level and uncovering a transcriptional network that reproduces the main mammalian clock properties can provide insight on the system.

The process of designing the model in order to describe an experimentally-supported transcriptional network, with a minimal yet plausible number of elements, led us to approach the problem by focusing on the clock controlled elements (CCEs): E-box, D-box and R-box. Some previous models have also represented the effect of CCEs on the clock: Korencic et al., (2012), focus exclusively on regulation between CCEs modulation factors, proposing independent competition between CCEs modeled by a multiplicative relation [48], and Jolley et al., (2014), highlight the role of D-box in a model that reproduces expected timing of CRY1 peak expression via linear combined action of D-box and R-box [49]. In our model we consider independent multiplicative competition between the terms of the majority of pairs of activator/repressor of each CCE, but additive relations between the contributions of each CCE to gene promoters, as has been observed for the activation of the *mPer1* promoter [67]; basing our choice of CCEs on the work of Ueda et al., (2005), [69], D-box is included in the equations for REV-ERBα and PER rates of change – a topology that is later found to be essential. Fig. B.2 shows a scheme of the molecular mechanisms and interactions included in our model.

Our model reproduces the expected peak order expression of the core clock proteins: BMAL1, then PER, then CRY1 [61], and the expected antiphasic relation between BMAL1 and PER:CRY

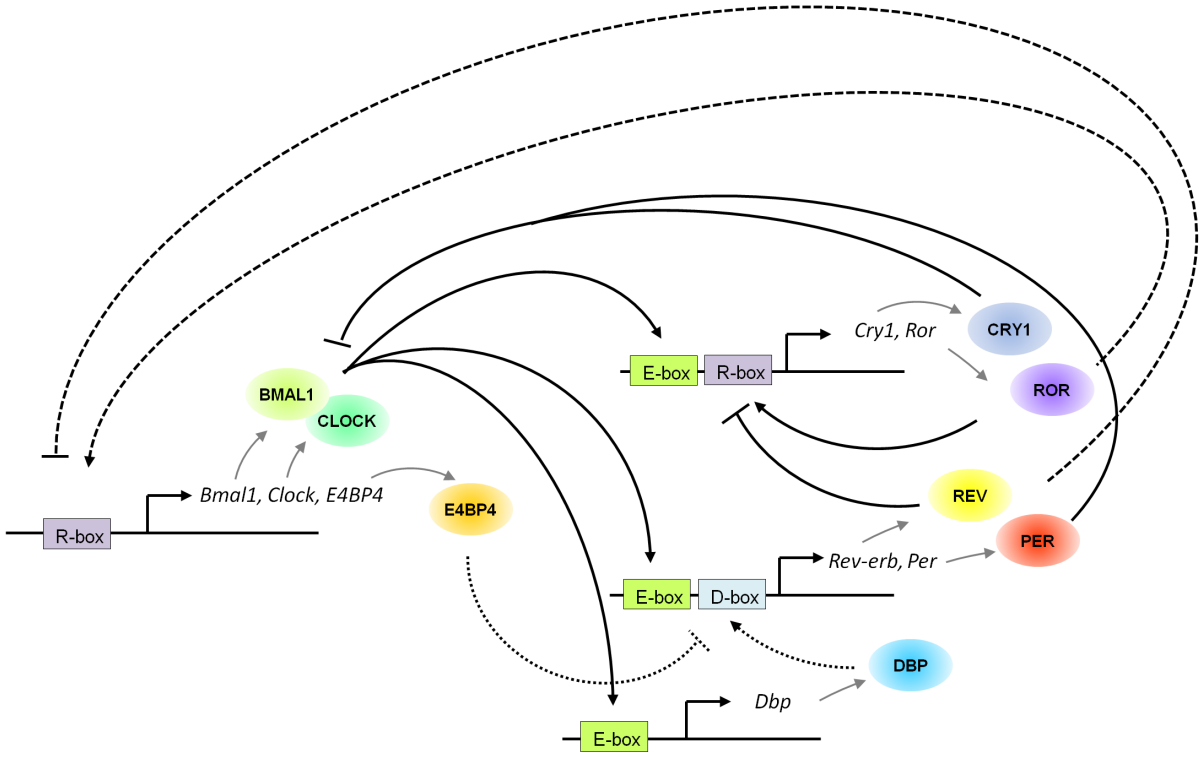

Figure 3.1: **Simplified molecular mechanisms of the mammalian circadian clock.** The CLOCK:BMAL1 protein complex promotes transcription of *Per*, *Cry*, *Ror*, *Rev-erb* and *Dbp* via E-boxes. CRY1 and PER:CRY block CLOCK:BMAL1 transcriptional activity, forming the main transcription-translation feedback loop. RORs (activators) and REV-ERBs (repressors) compete for R-box binding, coordinating expression of *Clock*, *Bmal1*, *E4BP4*, *Ror* and *Cry1*. Finally, D-box, activated by DBP and repressed by E4BP4, also contributes for expression of *Rev-erb* and *Per*.

is obtained. Aside from protein degradation/sequestration and formation/dissociation of the PER:CRY complex no other post-translational protein effects such as multiple phosphorylation states or shuttling between nucleus and cytoplasm are included in this model. Overall the model presents an essential skeleton for the mechanisms driving the mammalian circadian rhythm, consisting of eight molecular species described by a system of ordinary differential equations. The CCE modeling terms are based mostly on Michaelis-Menten and one low exponent Hill function (n=2), making it in agreement with experimentation, where cooperative binding of clock proteins to target genes hasn't been observed [66]. Parameters are obtained by fitting to high temporal resolution REV-ERBα expression data from single cells, from Feillet et al. (2014) [1], and oscillatory behavior is robust to parameter variations.

We improve on this model by adding an extra loop representative of the impact of the CLOCK:BMAL1 controlled transcriptional coactivator PGC1-α on ROR activity This function allows to control the period of the oscillator. Furthermore, we assess entrainment to external

stimulus, typical of circadian clocks, and verify that the region of model entrainment forms an Arnold tongue on the period and amplitude of the external signal, with sinusoidal waves allowing for a larger entrainment region than rectangular waves.

As an application, the model is then used to simulate the *tau* mutation [80]. This is achieved by increasing the PER degradation rate which leads to period diminution and variations in the full width at half maximum (FWHM) of clock protein expression. FWHM decreases linearly with the circadian period in the majority of clock proteins, with exception of CRY1 and BMAL1, where FWHM almost doesn't change, which recovers the experimental result of the asymmetric shortening of the molecular night on the *tau* mutation [81][82]. We conclude that the dynamic clock mechanism behind two distinct circadian phases (activating and repressing) is able to protect the duration of one of these main phases from alterations that occur at the other.

Furthermore, we analyse what happens to the duration of clock protein expression in a situation of circadian misalignment, by simultaneously applying two oscillatory input signals mimicking the effect of regulatory events. The first signal acts on PER and represents glucocorticoid signaling activity, indirectly correlating with the day/night cycle (see discussion below). The second signal acts on BMAL1 and represents insulin signaling, correlating with the feeding/fast cycle. One of the outcomes of our analysis is that the integration of the roles of feeding-related and light-related signals affects the percentage of circadian period that is spent at each of the two main molecular clock phases (BMAL1 and PER:CRY). This in turn may directly or indirectly affect the duration of insulin sensitivity/resistance states and may be taken into consideration in the study of altered metabolic physiology (further discussed below). We hypothesize that the time spent at each circadian molecular phase may be related to states of metabolic health or disease. Our proposal thus differs from the currently accepted view that considers the cause of metabolic diseases in circadian misalignment to be the internal circadian desynchrony of tissues and systems. Moreover, the here proposed clock control of molecular phase duration can potentially be linked to a variety of cyclic cellular processes, such as metabolism or DNA repair, explaining metabolic homeostasis. The circadian clock is thus interpreted as a mechanism that reads hormonal signaling inputs and outputs time spent at different molecular and cellular states.

A deeper analysis of our mathematical system includes model reduction to identify the minimal set of components and interactions that are crucial for generating the antiphasic oscillatory response. From here, we conclude D-box plays an essential role.

3.1.2 Model Design, Calibration and Robustness

To construct a concise yet biologically meaningful mathematical model, we use ODEs and favor mass action kinetics terms as well as Michaelis-Menten and low exponent Hill function terms that reasonably describe complex formation.

We restrict post-translational effects to protein natural degradation, formation/dissociation of the PER:CRY complex and nuclear export of the CLOCK:BMAL1:PER:CRY complex. Focusing on transcriptional details, we center the model on the competition of pairs of tran-

scription factors in binding to certain specific regions of genome: the clock controlled elements (CCEs), summarized on Table B.7. These CCEs are the E-box (enhancer box) activated by CLOCK:BMAL1 whose promoter activity can be blocked by CRY binding, the R-box (REV-ERBα/ROR response element) activated by ROR and repressed by REV-ERBα and the D-box activated by DBP, HLF and TEF and repressed by E4BP4.

Repressors	Activators	Targets	Response element (box)	Mechanism
REV-ERBα, REV-ERBβ	RORα, RORβ, RORγ	*Bmal1, Clock, Cry1, RORc, E4BP4*	R-box	Competition on DNA
PER1, PER2, PER2, CRY1, CRY2	CLOCK, BMAL1	*Per1, Per2, Per3, Cry1, Rev-erba Rev-erbβ, RORc, Dbp*	E-box	Protein-protein interaction
E4BP4	DBP, HLF, TEF	*Per1, Per2, Per3, Rev-erba Rev-erbβ, RORa, RORb,*	D-box	Competition on DNA

Figure 3.2: **Regulatory mechanisms of the three major CCEs.**
RORs and REVs compete for R-box binding. CLOCK:BMAL1 acts as an E-box activator and CRYs or PER:CRYs can bind to a previously bound CLOCK:BMAL1 repressing its E-box promoter activity. D-box can be activated by DBP, HLF and TEF and repressed by E4BP4.

The transcriptional interactions used in this work (Fig. B.2) are based on the work of Ueda et al., (2005), [69], that report the CCEs sufficient to guarantee clock rhythmicity in phase with PER2 and antiphase with BMAL1. Several other experimental results point to more extensive clock networks. For instance, Yang et al., (2013), found three functional E-boxes at the REV-ERB promoter [70], Yamamoto et al., (2004), show the presence of R-box elements in DBP and REV-ERB promoters as well as a higher number of CCEs in general [71] and Ukai-Tadenuma et al., (2011), present substantial evidence for a D-box in combination with R-box at the CRY1 promoter [72]. Here, we focus on understanding the mininimal mechanisms for orderly clock protein expression, in particularly anti-phase between CLOCK:BMAL1 and PER2/PER:CRY.

We start by deriving appropriate equations to describe the effect of each CCE (E-box, D-box and R-box), which include an activator with a positive effect and a repressor with a negative effect, that compete for binding, shown in Eqs 3.1, 3.2 and 3.3:

$$E_{box} = V_E \frac{[BMAL1]}{[BMAL1] + k_E + k_{Er}[BMAL1][CRY]} \tag{3.1}$$

$$R_{box} = V_R\left(\frac{[ROR]}{[ROR] + k_R}\right)\left(\frac{k_{Rr}^2}{k_{Rr}^2 + [REV]^2}\right) \tag{3.2}$$

$$D_{box} = V_D\left(\frac{[DBP]}{[DBP] + k_D}\right)\left(\frac{k_{Dr}}{k_{Dr} + [E4BP4]}\right) \tag{3.3}$$

Independent competition as in the R-box and D-box cases (Fig. B.7) is well described by multiplying the terms of activation and repression. As for the E-box, CRY binds to a previously bound BMAL1 on the target gene, blocking its promoter activity rather than directly blocking the gene itself, and the competition is not independent

The model is shown in Eqs. (3.4) to (3.11): the eight variables are the 3 pairs of activators/repressors mentioned above (Equations (3.1) to (3.3)) as well as PER and the PER:CRY complex. BMAL1 promoter activity is assumed to represent the CLOCK:BMAL1 complex, as their transcriptional regulation is similarly achieved by 1 R-box and BMAL1 is rate-limiting in the formation of CLOCK:BMAL1 [68]. All variables directly represent the rate of change of protein concentrations. Each CCE contributes additively to protein production, which is in agreement with observations of the activation of the *mPer1* promoter by DBP and CLOCK:BMAL1 [67]. As such, the model is given by Equations (3.4) to (3.11):

$$\frac{d[BMAL1]}{dt} = R_{box} - \gamma_{bp}[BMAL1][PER:CRY] \tag{3.4}$$

$$\frac{d[ROR]}{dt} = E_{box} + R_{box} - \gamma_{ror}[ROR] \tag{3.5}$$

$$\frac{d[REV]}{dt} = 2E_{box} + D_{box} - \gamma_{rev}[REV] \tag{3.6}$$

$$\frac{d[DBP]}{dt} = E_{box} - \gamma_{db}[DBP] \tag{3.7}$$

$$\frac{d[E4BP4]}{dt} = 2R_{box} - \gamma_{E4}[E4BP4] \tag{3.8}$$

$$\frac{d[CRY]}{dt} = E_{box} + 2R_{box} - \gamma_{pc}[PER][CRY] + \gamma_{cp}[PER:CRY] - \gamma_{c}[CRY] \tag{3.9}$$

$$\frac{d[PER]}{dt} = E_{box} + D_{box} - \gamma_{pc}[PER][CRY] + \gamma_{cp}[PER:CRY] - \gamma_{p}[PER] \tag{3.10}$$

$$\frac{d[PER:CRY]}{dt} = \gamma_{pc}[PER][CRY] - \gamma_{cp}[PER:CRY] - \gamma_{bp}[BMAL1][PER:CRY] \tag{3.11}$$

where the negative term $-\gamma_{bp}[BMAL1][PER:CRY]$ represents the nuclear export of CLOCK:BMAL1 via complex formation with PER:CRY and the terms $\gamma_{pc}[PER][CRY]$ and $\gamma_{cp}[PER:CRY]$ represent formation and dissociation of the PER:CRY complex respectively. The model includes the two step mechanism of the repression of CLOCK:BMAL1 by PER:CRY [65], with CRY also being a repressor of BMAL1 activity on E-box (Equation 3.1). The variables

CRY and ROR directly model CRY1 and RORc, via the appropriate combination of CCEs (see Ueda et al. (2005) [69]) (though we take them as representative of all CRYs and RORs).

Fig. 3.3 shows a solution of the model for the calibrated parameters (see Table D.1). The model fits well to the high temporal resolution experimental data for relative fluorescence intensities of VENUS-tagged REV-ERBα protein obtained from Feillet et al., (2014), [1] (Fig. 3.3 B). These data are here filtered and repeated three times and normalized as percentage of the REV-ERBα mean value ($\%\ of \overline{REV}$). The period of the system converged to the period of the data (20,1 h). We can observe an appropriate separation and correct order between peaks of protein expression of BMAL1, PER and CRY1 as well as total phase opposition between BMAL1 and PER:CRY, the property of interest (Fig. 3.3 A). The phase relation between CLOCK:BMAL1 and REV-ERBα (Fig. 3.3 B) of 7,1 h is also in agreement with experimental observation [77].

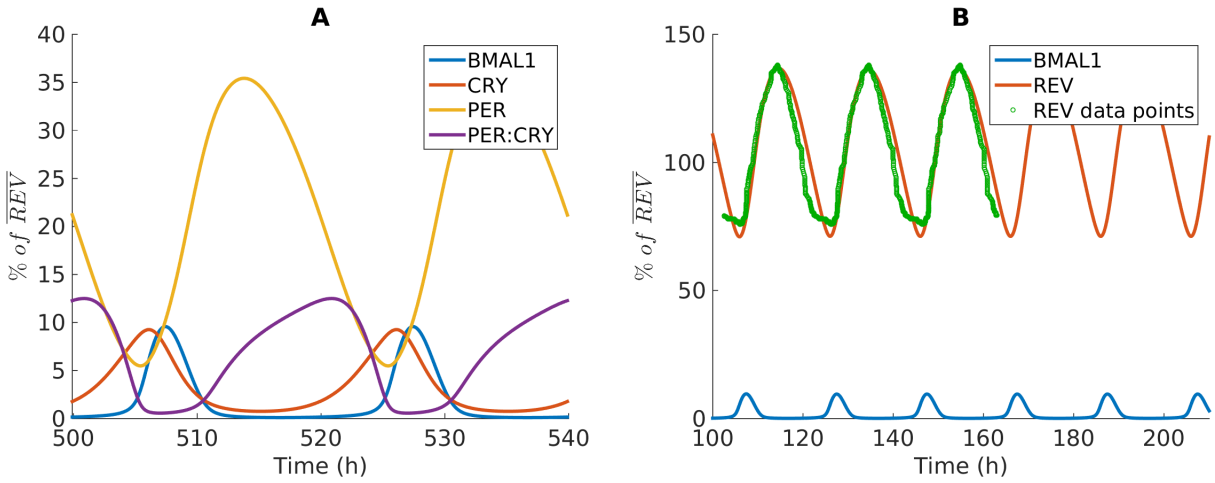

Figure 3.3: **The mammalian circadian clock can be described by a model focused on transcriptional regulation.**
Output of the mammalian circadian clock model for parameters of Table D.1. A) The expression of clock proteins follows an order in accordance with experimental observation: BMAL1, then PER, then CRY1. BMAL1 and PER:CRY have an antiphasic relation. B) Calibration of the model using data from Feillet, (2014), [1] for a peak of REV-ERBα in mouse fibroblast cells (NIH-3T3) repeated three times; a filter was applied to smooth the data. Oscillation occurs with a 20,1 h period.

We note that all modeling terms have low Hill coefficient n, with the majority being Michaelis-Menten terms, except the repression achieved by REV-ERBα. In the case of REV-ERBα, active repression occurs via recruitment of co-repressor to genes, which requires two REV-ERBα molecules; monomer REV-ERBα binding is not sufficient for active gene repression acting exclusively as an inhibitor of ROR binding [76] [75]. REV-ERBα monomer repression may indeed be what happens at gene promoters where R-boxes are not in close proximity at the genome [74], however, here we assume REV-ERBα active repression and study the model with n = 2, respecting the stoichiometry of co-repressor activation. Nevertheless, simulations for n = 1 yield very similar results to simulations with n = 2, as seen in supplementary Fig. D.1. We consider

low value Hill coefficients to be desirable in circadian models, because cooperative binding of clock proteins to their target genes hasn't been experimentally demonstrated.

The model is robust to perturbations in its parameters as shown by the sensitivity analysis in Fig. 3.4. Each parameter is varied by 20% around the calibrated point and oscillations are never lost although the period may change, which suggests period tuning is possible within a range of 18 - 23 h approximately. We can observe that parameters such as V_R and γ_{db} impact the period most, while variations on, for instance, k_{Er} and γ_{bp} have little impact. We may conclude that in general R-box promotes longer periods, as parameters that lead to an increase in R-box value, V_R and k_{Rr}, have a positive effect on the period, similarly D-box promotes shorter periods and E-box has a very mild effect on the period (with V_E and k_{Er} having opposite effects). Additionally, the increase in the rate of complex formation γ_{pc} leads to an increase in the clock period and unsurprisingly the rate of complex dissociation γ_{cp} has an opposite effect, meaning that favoring the repressor PER:CRY favors longer periods – as such the rate of formation of the BMAL1:PER:CRY complex γ_{bp} that favors the removal of both the repressor PER:CRY and the activator BMAL1 has almost no effect on clock period. The increase in PER degradation rate γ_p leads to shorter periods, while decreasing it lengthens the period, which is in accordance with observations on both the *tau* mutation phenotype and the knockout of the ($CK1\epsilon$) enzyme [79] [81].

3.1.3 Results and Discussion

Chromatin remodeling by CLOCK:BMAL1 as an internal mechanism of period control

Recently, more relevance has been attributed to the role of CLOCK:BMAL1 in promoting a transcriptionally permissive chromatin state for other transcription factors, allowing to integrate sensors of cellular energy status and nutrient availability with the molecular clock [85].

From a modeling point of view, this means that CLOCK:BMAL1 may be rhythmically altering specific model parameters that reflect chromatin states, thus acting as a closed-loop control function that modulates one or more specific parameters.

The circadian clock oscillates with a period close to 24 hours, but is observed to vary in a larger range, from 18 to 26 hours approximately (see Saini et al. (2012) [86] and Feillet et al. (2014) [1]) and as indicated by our sensitivity analysis. Hence, we explore ways to control and tune the period of the system. A straightforward approach is to change the value of a specific parameter or sets of parameters, but a more challenging and insightful approach is to verify if a biologically derived function representative of the oscillatory chromatin permissiveness state could be used to tune a parameter thus validating our modeling architecture while complementing the model.

Biologically, PGC1-α appears as an important transcription coactivator that facilitates ROR connection to the genome at the R-box binding site. CLOCK:BMAL1 can possibly promote PGC1-α in more than one way, particularly by promoting expression of the NAMPT enzyme [87] and the sirtuin SIRT1 [97] via E-boxes: NAMPT is rate-limiting in the biosynthesis of

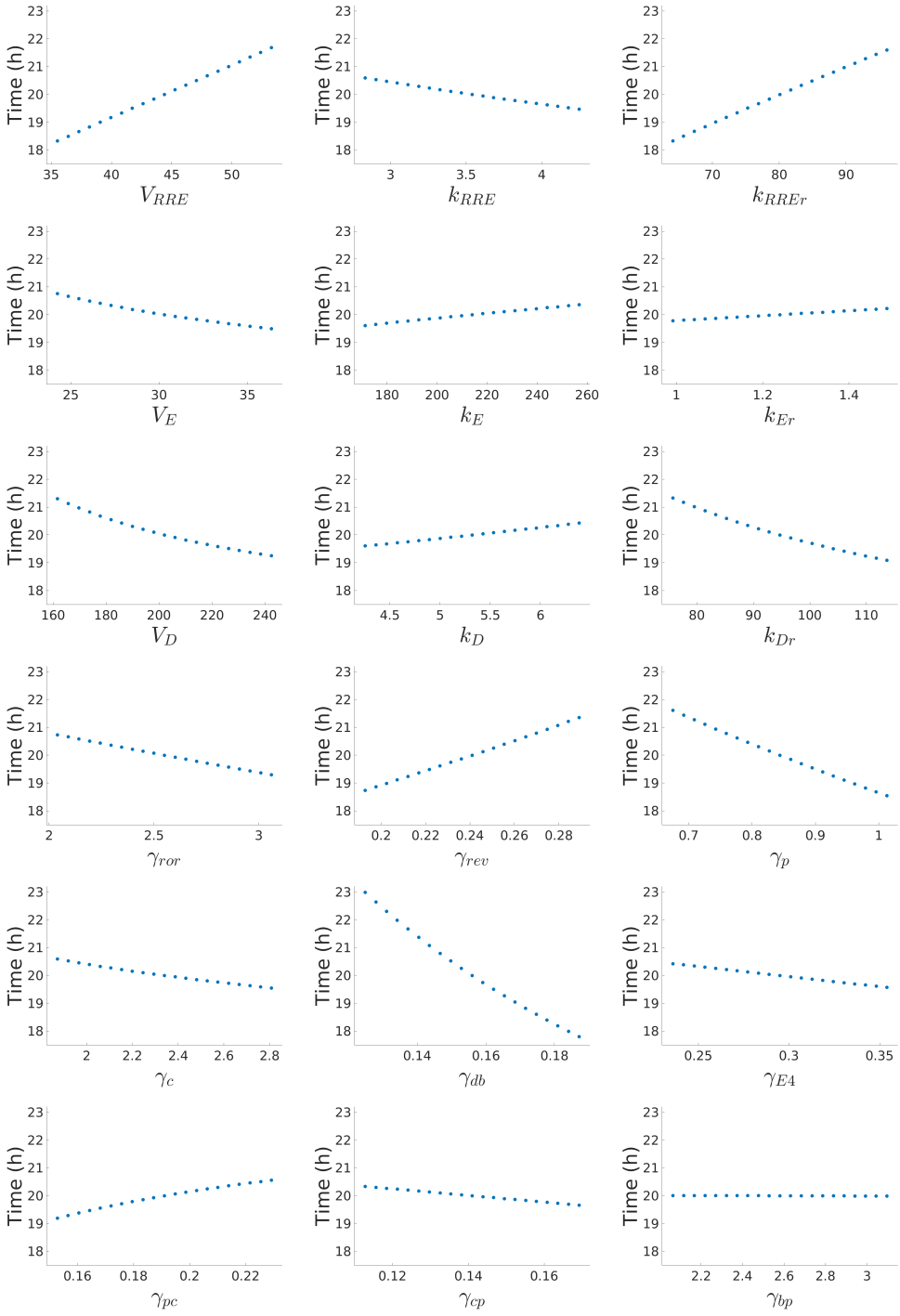

Figure 3.4: **Sensitivity analysis: the model is robust to the variation of parameters.** Each parameter is varied 20% around the calibrated point (Table D.1) and oscillations are always present. Variations in the value of V_R, k_{Rr}, γ_{rev}, γ_{db} and γ_p significantly alter the period of the system, while varying k_E, k_{Er}, γ_{bp}, γ_{E4} and k_D has little impact on the oscillatory period.

NAD+ that acts as a cofactor of SIRT1 which deacetylate and activate PGC1-α [88]. This control loop is shown in Fig. 3.5.

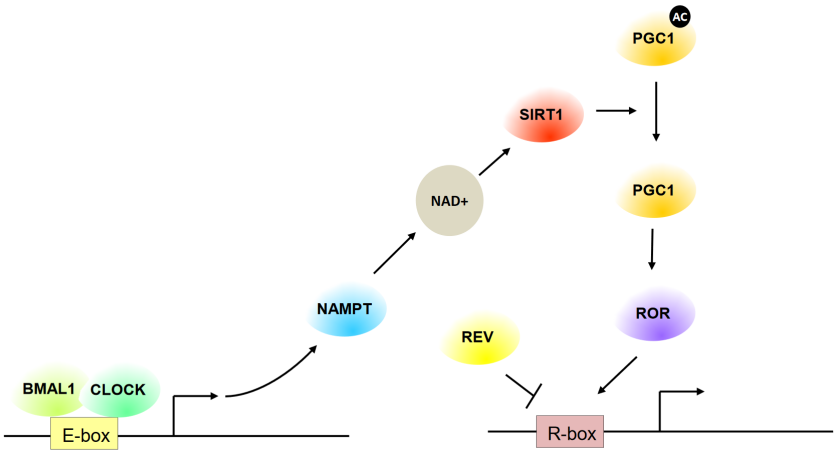

Figure 3.5: **PGC1-α integrates cellular metabolism and the mammalian circadian clock.**
CLOCK:BMAL1 promotes PGC1-α indirectly by promoting expression of NAMPT, rate-limiting in NAD+, and SIRT1 via E-boxes; the NAD+ dependent SIRT1 deacetylates and activates PGC1-α. PGC1-α in turn binds to ROR facilitating its activation of R-box.

Thus, PGC1-α activity on R-box is a good candidate to represent the oscillatory chromatin status. As such, we design a non-linear function μ that allows to control the period: consider PGC1-α to be given by an E-box (PGC1-α = E-box) and its activity as a facilitator of the binding of ROR to R-box can be expressed as causing a decrease in the parameter k_R of R-box, by making $k_R \rightarrow \mu\ k_R$ in Equation 3.2, where μ is given by:

$$\mu = V_1 \frac{k_1}{k_1 + Ebox} \tag{3.12}$$

and setting $V_R = 50$ (and keeping the rest of parameters as shown in D.1) allows to obtain period control, without altering any other feature of the behavior of the system, see Fig. 3.6.

Part of the interest of this analysis is that period control via a closed loop function is not always possible, for example applying this control function in other terms results in complex behavior. The fact that a biologically-derived closed-loop function allows period control and doesn't interfere with the qualitative dynamical behavior of the system illustrates one of the many ways in which the circadian clock is able to tune and integrate signals via internal loops in order to optimize circadian output, i.e. the system has the ability to regulate itself via this function. The period-control response to the internal closed-loop function, highlights the ability of our model to correctly include chromatin remodeling terms. Incorporation of this term increases the ability of entrainment to an external signal, to be discussed bellow.

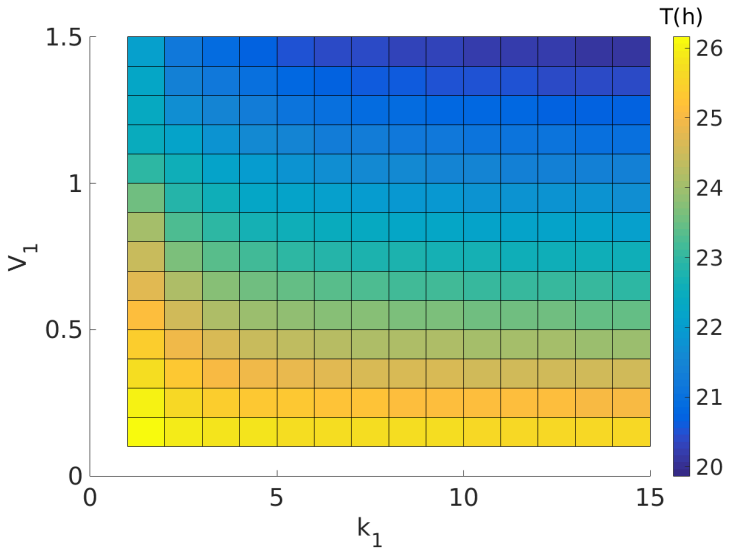

Figure 3.6: **Tuning of the period by the function μ.**
Variations in the period of the system with the parameters V_1 and k_1 of μ (Eq. 3.12). In this region the system behaves with the exact same features of Fig. 3.3.

We use values of $V_1 = 0.41$ and $k_1 = 10$ to take the period of the oscillator to 24 h and we will now work with this tuned system and explore its response to external signals.

Phase Response Curves and Entrainment

A particularly important characteristic of the circadian clock is its ability to synchronize to external signals, as well as the phase response induced by an external input pulse. In order to explore these properties, an input I_{pulse} is added in the equation of the PER protein, such as $\frac{d[PER]}{dt} = I_{pulse} + E_{box} + D_{box} - \gamma_{pc}[PER][CRY] + \gamma_{cp}[PER:CRY] - \gamma_p[PER]$. The idea is to mimic the PER promoter's response in transducing a variety of external signals such as stress hormones [29] [89] [90].

Fig. 3.7 shows the phase-response curve (PRC) of the system when we make a temporary perturbation on PER: the transient phase-shift is measured when the phase of the perturbation is varied over the course of one circadian cycle. For this, we consider the first BMAL1 peak that occurs after the perturbation and compute the difference between the time at which this peak occurs in the perturbed and non-perturbed cases. Data from Pendergast et al., (2010), from photic entrainment in wild type mice, are shown for comparison [91]. Our simulation shows a type I PRC, for two pulse intensities I_{pulse}, with shape similar to those of wild type mice, with the delay zone being larger than the advance zone. The majority of organisms typically have PRCs of this type, illustrating an ability to synchronize to external signals. Observe that phase shifts are more pronounced for higher intensity pulses.

We next analyse the entrainment of our model to a sinusoidal and to a rectangular wave, for different periods and amplitudes. In Fig. 3.8 we observe that, for both the sinusoidal (Fig.

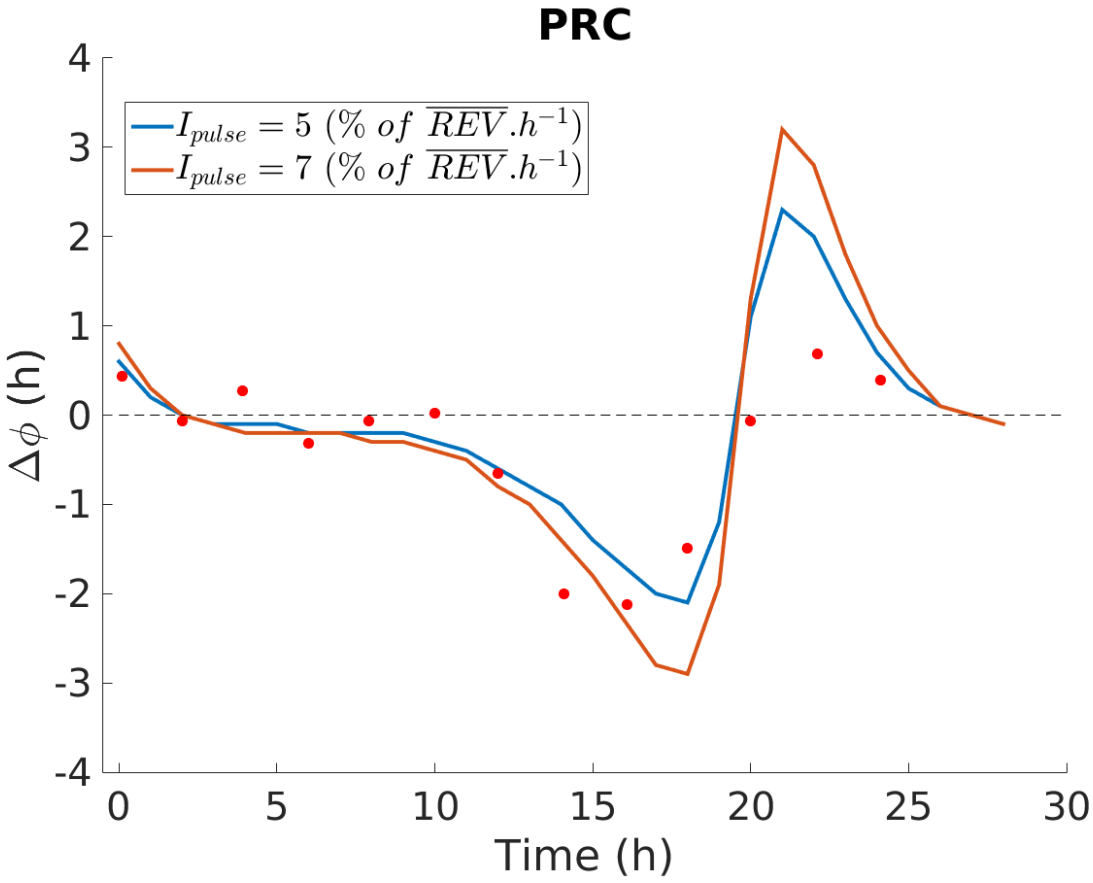

Figure 3.7: **Phase response curves.**
Phase response curves of the system (measured as the phase shift in BMAL1) to two external pulses of different intensities, acting via stimulation of PER expression. Data points from Pendergast et al., (2010), of photic entrainment in wild-type mice are shown for comparison [91].

3.8 A) and the rectangular (Fig. 3.8 B) waves, the region of entrainment forms a characteristic shape known as the Arnold tongue with entrainment becoming possible for larger period ranges with increasing amplitude. Entrainment with a sinusoid in general allows for larger regions of entrainment than with a square wave, a result that is obtained experimentally in observations of photic entrainment in hamsters [94], as well as in numerical simulations of temperature entrainment in circadian clocks [92] and of stochastic population-level entrainment of cellular oscillators [93]. Entrainment via a sinusoidal wave leads to some points of period doubling, where the ratio between the period of the clock and that of the entraining signal is 2:1, as well as one point where the ratio between periods becomes 3:1. Rectangular waves also allow for a couple of points where the period of the clock becomes three times the period of the entraining wave.

Furthermore, Fig. D.2 shows the same simulation for the model without the closed loop control function (Equation 3.12) introduced above. The closed-loop control increases the region

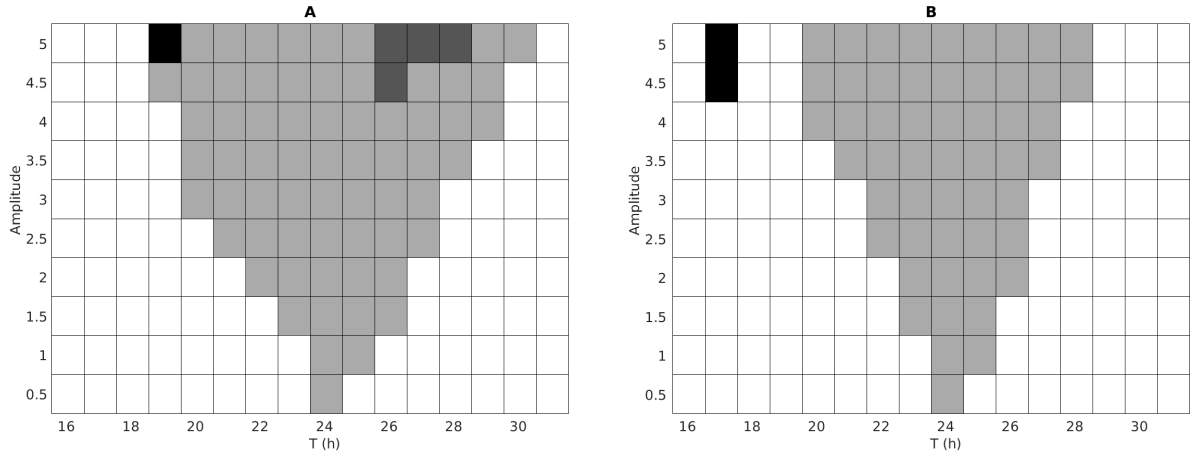

Figure 3.8: **Entrainment of the clock to an external oscillatory input.** The amplitude and the period of an entraining wave are varied and the resulting regions of entrainment form Arnold tongues. A) The entraining wave is a sinusoid. B) Entrainment is done with a rectangular wave. A black/white gradient represents the ratio between the clock period and the period of the entraining wave: white - no entrainment, grey - 1:1 entrainment, dark grey - 2:1 entrainment and black - 3:1 entrainment.

of entrainment of the system by an external oscillatory input, thus revealing a possible role of chromatin remodeling in improving the ability of clock entrainment to signals.

Asymmetric variations in the duration of molecular clock phases on the *tau* mutation.

We now apply our calibrated and validated model to assess changes in the duration of the different clock phases. An important experimental example of asymmetric changes in the duration of molecular clock phases is observed in animal models of the *tau* mutation, that have shorter circadian periods. This mutation of the enzyme casein kinase 1ϵ ($CK1\epsilon$) is thought to result in a gain of function on certain PER residues leading to its accelerated degradation, which is at the basis of the reduced period [79] [81].

In this model increased PER phosphorylation is achieved by increasing the parameter γ_p, which as seen in Fig. 3.4 leads to a shortening of the circadian period. The same effect is observed in the controlled model, oscillating at 24 h (see Fig. D.3). Though animals affected by the *tau* mutation have a shorter behavioral day, the underlying mechanism is a shortening of the molecular night, caused by accelerated degradation of PER after its peak expression [81]. However, it remains unclear whether ($CK1\epsilon$) acts at a specific time phase or if a generalized increase in the phosphorylation of PER could lead to asymmetric changes in the duration of the core clock proteins. Here, we investigate if the model is able to reproduce the asymmetric changes in the duration of clock phases when a decrease in period is caused by increasing γ_p.

As a measure of the average duration of peak expression, we compute the full width at half maximum (FWHM) as the length between the two instances at which the solution crosses half

peak height: $FWHM = t_{up} - t_{down}$, where $x(t_{up}) = x(t_{down}) = \frac{1}{2}\, x(t_{peak})$, $t_{up} < t_{peak} < t_{down}$ and t_{peak} is the instant at which the solution $x(t)$ is at its maximum. Fig. 3.9 shows the ratio of FWHM to circadian period of all clock proteins, plotted against γ_p. Values of γ_p between 0.8 and 1.2 yield periods in the range from 24 h to 20 h, most relevant for comparison with experimentations (see Fig. D.3).

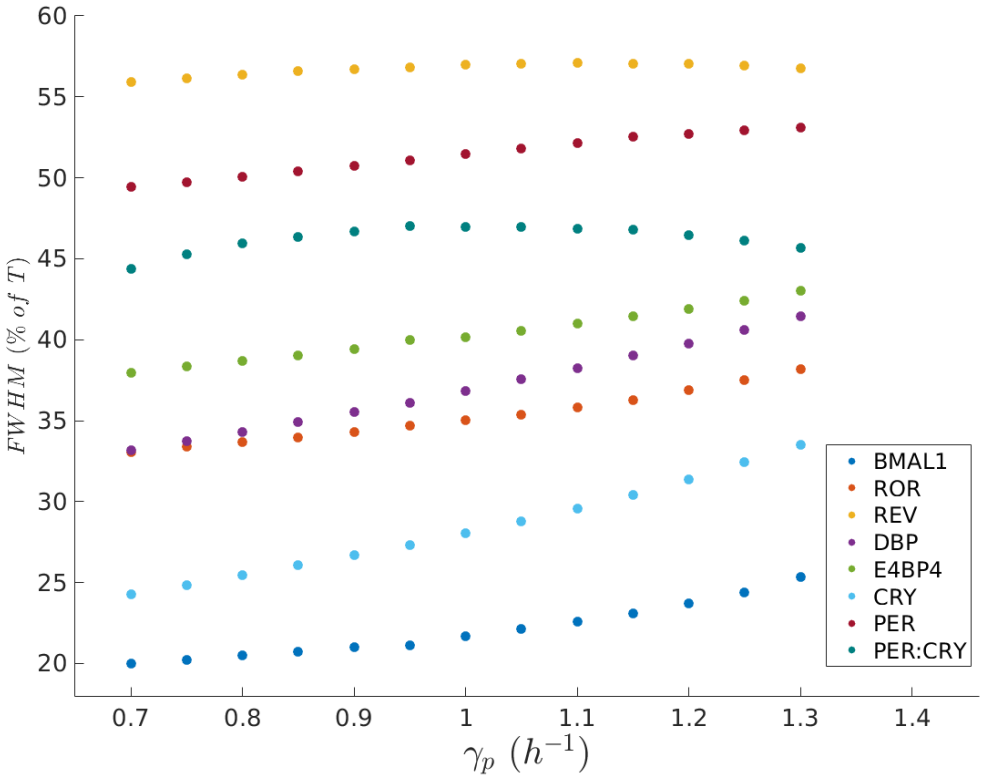

Figure 3.9: **Ratio of FWHM to circadian period T of several clock proteins is unchanged as γ_p increases.**
When the period of the system is varied in a manner consistent with the *tau* mutation the majority of clock proteins, except for CRY1 and BMAL1, maintain an approximately constant relation between its FWHM and the period of oscillations, i.e. the duration of protein expression increases linearly with the circadian period (decrease of γ_p), with effects more pronounced in REV.

We observe in Fig. 3.9 that the ratio of FWHM to circadian period T of a large group of proteins remains constant, more pronouncedly in REV, but also seen in PER, ROR, DBP and E4BP4, meaning that as the period decreases, the duration of expression these proteins also decreases in a linear manner. The exceptions are BMAL1 and CRY1, whose duration doesn't decrease linearly with the period, with FWHM of CRY1 keeping approximately constant as the period decreases in the *tau* mutation (see Fig. D.4 for a different representation of the same results). This is consistent with observations on the asymmetric shortening of the molecular night observed in animal models of the *tau* mutation and suggests an ability of the clock circuit

to protect the duration of one of its molecular phases (BMAL1, CRY1) against changes that affect the other (PER), see Fig. 3.3. Moreover, the fact that this phenotype can be reproduced by a general increase in the PER degradation rate indicates that the dynamic clock mechanism behind two distinct circadian phases is at the basis of this phenomenon.

The existence of two markedly distinct phases may be implicated in metabolic processes and states, such as insulin sensitivity/resistance, that oscillate with the states of sleep and alertness: a state of feeding/alertness tends to be also of increased insulin sensitivity so as to allow cells to uptake glucose, in particular at the beginning of the activity phase [83]. The *tau* phenotype is characterized by a cluster of altered features that includes altered rates of growth and reproduction, body size and lifespan. Furthermore, metabolic rate relative to body mass is observed to increase proportionally to the increase in circadian frequency [84]. Whether these phenomena are caused by pleiotropic effects of $CK1\epsilon$ kinase or by the altered ciradian rhythm is still a matter of discussion. In fact, mammalian clock proteins not only control the formation of rate-limiting enzymes of several metabolic processes, but are also themselves directly involved in metabolism [97] [99]. Furthermore, we observed that amplitudes and mean values of all clock proteins decrease proportionally to the period variation (see Fig. D.5 and Fig. D.6), which could also contribute to altered metabolic features. However, while amplitudes and mean values vary similarly for all clock proteins, the FWHM is clearly different between the two main clock phases, suggesting there may be a role of the circadian clock in optimizing the time spent in each molecular phase. Hence, the relative duration of different clock phases may be a factor to take into consideration when investigating metabolic diseases.

Clock integration of hormonal signaling and circadian alignment

To expand and deepen the relationship between the duration of the different circadian phases and metabolism, we investigate the role of the mammalian clock mechanism in integrating hormonal signaling.

A subject of interest is the response of the system to aligned and misaligned states between suprachiasmatic nucleus (SCN)-driven circadian light sensing and food/activity-related signaling. Circadian misalignment between the sleep/feeding schedule of individuals and the external light environment (occurrent, for instance, in shift-workers) is known to increase the risk of several metabolic diseases such as diabetes, obesity, displidemia, and insulin resistance which are all manisfestations of the metabolic syndrome [16] [13].

Peripheral clocks are incapable of directly sensing light inputs. Nevertheless, light-induced SCN-driven hormonal signaling is likely to be relevant for metabolic homeostasis in the entire organism, as phase misalignment between the internal clock and the external light environment decreases metabolic efficiency [17]. Ishida et al. demonstrate that the SCN of mice gates external light signals inducing phase-dependent corticosterone release by the adrenal gland via the sympathetic nervous system [95]. Furthermore, this effect is proportional to the light intensity and indicates that external environmental light signals instantly provoke blood glucocorticoid signals [95].

Thus, adrenal production of glucocorticoids (GCs) is coordinated by the central nervous system and can be either humoral, via activation of the hypothalamic pituitary adrenal (HPA) axis as provoked by stress and fasting, or nervous via activation of the SCN-sympathetic nervous system by light [95]. GCs in turn act on peripheral cells via activation of the glucocorticoid receptor GR and are known to regulate the circadian clock and to cause an increase in PER expression. In general, a high GC state also correlates with the fasting state, but unlike insulin or glucagon that are exclusively dependent on nutrient status, GC plasma levels in mice can be induced by light, making it the hormonal signal of choice to represent indirect sensing of the light/dark cycle in peripheral molecular clocks. In fact, in aligned nocturnal animals, the fasting phase corresponds to the light part of the daily circadian cycle.

As such, to represent the light-dependent GR cycle we add an input in the equation of PER, Eq. (3.10), as done above for the entrainment study, which is a sinusoidal wave with a 24 h period (the same as the intrinsic period of the system), as *Per* genes have been shown to be the ultimate transcriptional targets of gluccorticoid signaling [29]. On the other hand, the hormonal signal that better represents a feeding cycle is insulin. Insulin is known to trigger BMAL1 exclusion from the nucleus, suppressing its promoter activity [96]. Thus, we introduce the degradation term: $-insulin(t)\ [BMAL1]$ in Eq. (3.4), where $insulin(t)$ is also sinusoidal wave with period $T = 24\ h$, meaning that a gradual change occurs between a feeding (activity) and a fasting (rest) phase (of 12 hours each). We keep the two signals with the same amplitude $A = 1$ and period $T = 24\ h$ and vary only the phase $\Delta\phi$ between them, as in $GR(t) = A\ cos(\frac{2\pi}{24}t)$ and $insulin(t) = A\ cos(\frac{2\pi}{24}t + \Delta\phi)$. As our model was built on and calibrated to data of nocturnal animals (mice and rats) [1] [69], we consider the aligned state to be represented by $\Delta\phi \approx 12$ and compute the FWHM of all clock proteins in response to the phase difference between these signals.

In Fig. 3.10 we observe how the FWHM of each clock protein changes as the phase difference $\Delta\phi$ between the two signals varies from 0 to 24 hours. Strikingly, duration of BMAL1 and PER:CRY peak expression has opposite trends in change, meaning that $\Delta\phi$ affects the time spent at each main circadian clock phase. This can possibly result in different time spent at different metabolic states or processes, as well as in alteration of the quantities of metabolic enzymes for which clock proteins are rate-limiting. Duration of BMAL1 peak expression has a maximum when the signals are in phase opposition (circadian alignment) and a minimum when the signals are in phase (circadian misalignment), with FWHM of CRY1, ROR and E4BP4 also increasing when signals move out of phase. On the other hand, REV and PER:CRY seem to have a maximum for signals in phase. Curiously, average duration of PER peak expression seems to be constant. In a general manner, amplitudes and mean values are higher for smaller $\Delta\phi$ for all clock proteins (Fig. D.7 and Fig. D.8). In all simulations the order of peak expression of clock proteins was unaltered, and the same as in Fig. 3.3.

These simulations show dynamic variations in the core clock components due to changes in regulatory inputs. An interpretation of these results can be provided in the light of the wide involvement of the circadian clock in metabolism and noticing that circadian misalignment has been shown to promote insulin resistance independently of sleep loss [13]. Considering the role

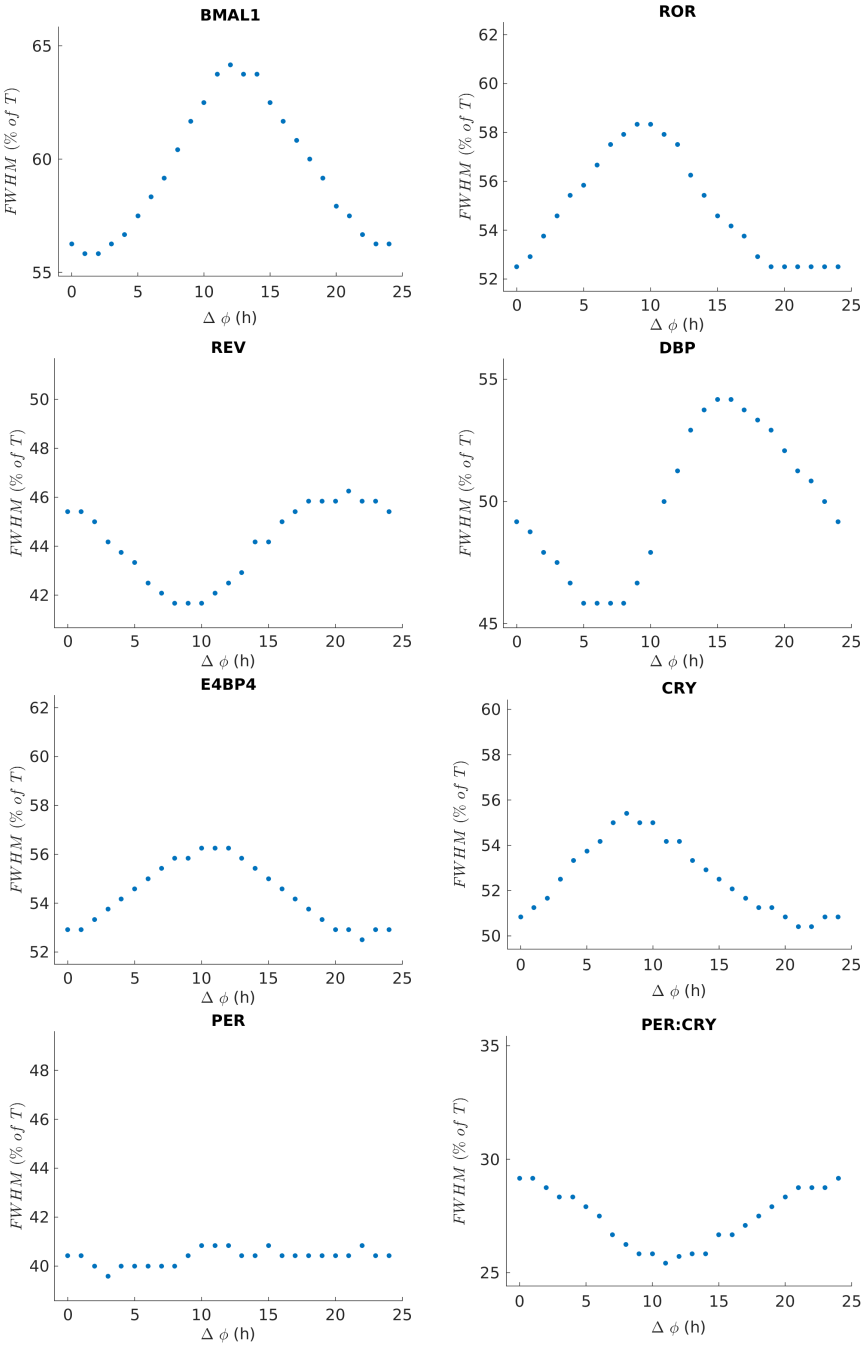

Figure 3.10: **Variations of FWHM with the phase difference between two external hormonal signals.**
The ratio of FWHM to the 24 h period is measured, as the phase difference between two crossed regulatory inputs changes. We can observe that duration of BMAL1, ROR, CRY1 and E4BP4 expression increases when the signals move out of phase, while duration of REV and PER:CRY decreases. FWHM of PER seems to be constant with $\Delta\phi$.

of BMAL1 in promoting insulin sensitivity in mouse liver and muscle [97] [98], as well as the fact that CRY1, here presenting a similar trend as BMAL1, also plays a role in improving hepatic insulin sensitivity [99], these results may help to explain the higher incidence of insulin resistance in indiviuals subjected to circadian misalignment: as duration of circadian phases varies and the percentage of circadian period with higher BMAL1 and CRY decreases so does the time spent in (directly or indirectly) promoting processes of insulin sensitivity.

We note that light is a known stressor in mice, that are prey animals, and its role in provoking GC adrenal release can't for the moment be extrapolated for diurnal or predator animals. However, not only a similar type of signaling is conceivable in other organisms, but also the impact of misalignment in generating changes in the duration of the different clock phases as seen in Fig. 3.10 may be relevant in all systems. Overall, Fig. 3.10 (as well as Fig. D.7 and Fig. D.8) give predictions of the response of the system to the phase relation between any two input signals (one acting via promoting PER and other via BMAL1 removal from target promoters) and show that different states of circadian alignment/misalignment result in different percentage of time spent at different clock phases and processes.

The analysis presented in this Section pieces together information on the mammalian clock, namely that misalignment with the light evironment is observed to decrease metabolic efficiency [17] and that light activates adrenal release of GCs [95]. Furthermore, a feeding-dependent 24 h insulin cycle is here proposed to be a decisive factor in determining the aligned/misaligned state. This allowed to construct an idea of what type of signals could be acting on peripheral clocks and how. Consequently, the obtained results in response to one food-related signal and one SCN-dependent signal are here interpreted as a possible way by which the 24 h insulin sensitivity cycle can be affected by peripheral clocks. This idea thus suggests a mechanism for how the control of the 24 h glucose tolerance rhythm may be done by the SCN [83].

Furthermore, Woller and Gonze, (2018), have also investigated this subject by means of a mathematical model for the clock-dependent pancreatic regulation of glucose homeostasis in rodents and found that the conflict between light/dark and fast/feeding cycles creates a differential phase shift in the expression of core clock genes and induces misalignment between clock-controlled exocytosis and glucose cues on insulin secretion [100].

The currently accepted view of how circadian misalignment causes metabolic disease states that circadian misalignment causes metabolic disease by desynchronizing the clocks of different internal organs and systems. Our hypothesis aims to provide a new insight whereby circadian misalignment can change the relative duration of activating and repressing clock phases and consequently promote a higher percentage of time spent in processes that favor insulin sensitivity/resistance, thus leading to altered metabolic markers. A similar reasoning could be made for other cyclic processes that may have a circadian control. For example, the time spent at a specific stage of the DNA repair/damage cycle could be related with observations of altered lifespan as is the case of *tau* mutation animals and in several studies of altered feeding. The circadian clock is here seen as a system that receives hormonal signaling inputs and outputs time spent at different cellular processes.

Oscillation of ROR, E4BP4 and CRY1 is not required for oscillations: PER is rate-limiting in the formation of the PER:CRY complex

This Section focuses on identifying the minimal network that still guarantees antiphasic oscillation for the clock system in Equations (3.4) to (3.11).

We observe that rhythmicity of ROR, E4BP4 and CRY is not required in order for the system to oscillate. Oscillation of CRYs has in fact been shown not to be necessary for clock oscillation in mouse fibroblasts by Fan et al., (2007), who were able to recover circadian oscillation in $CRY1^{-/-}CRY2^{-/-}$ mouse fibroblasts by means of introduction of a cell permeable CRY protein of constant concentrations [101]. Furthermore, considering that PER:CRY is one of the main repressors of the circadian clock, the maintenance of clock oscillation when CRY is arrhythmic can only be possible if PER is rate-limiting in the formation of the PER:CRY complex, which is verified experimentally [102].

Fig 3.11 shows the variation in the period when the formation of each of the three proteins is put at an equilibrium ($\frac{d[CRY]}{dt} = 0$, $\frac{d[ROR]}{dt} = 0$ and $\frac{d[E4BP4]}{dt} = 0$) and their constant concentration (given as an initial condition) is varied. In general, we verify that greater protein concentrations lead to greater periods, with a saturation being observed in the case of ROR.

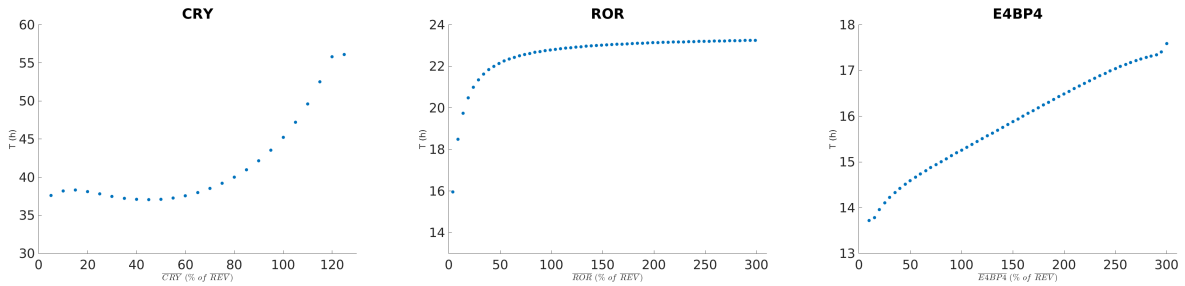

Figure 3.11: **Oscillation of CRY, ROR and E4BP4 is not required for oscillation of the system.**
The system yields oscillations when the variables CRY, ROR and E4BP4 are individually put at an equilibrium. Variation in circadian clock period with the variation of total protein concentration is shown for the three cases.

To better understand the fundamental variables and interactions of our system, while focusing on maintaining oscillations with phase opposition between BMAL1 and PER:CRY, a dynamical reduction is the next step in the analysis of our model.

3.1.4 Model Reduction

In order to obtain the core structural dynamical network of our system, we perform a sequence of quasi-steady-state approximations and other simplifications, verifying at each step both the existence of a periodic solution and antiphase between PER:CRY and BMAL1. The goal is to reduce the number of variables and possibly simplify equation terms in order to obtain a skeleton

model with dynamical properties similar to those of the system of equations (3.1 –3.11).

The fist step is to set E4BP4 at quasi-steady-state:

$$\frac{d[E4BP4]}{dt} = 0 \tag{3.13}$$

leading to a system without loss of oscillations and allowing to approximate the Michaelis-Menten term with a negative effect on D-box($\frac{k_{Dr}}{k_{Dr}+[E4BP4]}$) (see Eq. 3.3) by a constant $\frac{1}{2}$. Furthermore, as $k_D \gg [DBP]$, the Michaelis-Menten term with a positive effect on D-box ($V_D \frac{[DBP]}{[DBP]+k_D}$) can be approximated by a linear function, which leads to the equation of D-box being well approximated by:

$$D_{box} = \frac{1}{2}\frac{V_D}{k_D}[DBP] \tag{3.14}$$

Secondly, setting the equation for the formation of ROR at the quasi-steady-state:

$$\frac{d[ROR]}{dt} = 0 \tag{3.15}$$

also maintains the desired oscillatory properties and eliminates one more variable. REV, however, can't be removed, and as such R-box can now be simplified as:

$$R_{box} = V_R \frac{k_{Rr}^2}{k_{Rr}^2 + [REV]^2} \tag{3.16}$$

As a third step, the system doesn't require oscillation of CRY (Fig. 3.11) and we also verify the dependence of E-box on CRY can be set to zero ($k_{Er}[BMAL1][CRY] = 0$ in equation 3.1). Furthermore, $k_E \gg [BMAL1]$ allows the following approximation for E-box:

$$E_{box} = \frac{V_E}{k_E}[BMAL1] \tag{3.17}$$

Finally, consider the quasi-steady-state approximation of the Equation 3.10:

$$\frac{d[PER]}{dt} = 0 \tag{3.18}$$

that leads to:

$$PER = \frac{E_{box} + D_{box} + \gamma_{cp}[PER:CRY]}{\gamma_{pc}[CRY] + \gamma_p} \tag{3.19}$$

furthermore is also possible to take:

$$\gamma_p = 0 \tag{3.20}$$

which impacts the period of the system, but not the existence of oscillations. From (3.19) and (3.20), replacing PER in the PER:CRY equation (3.11) leads to cancelling out the term $\gamma_{pc}[CRY]$ and dependence on CRY is automatically eliminated.

The reduced model has now four variables: BMAL1, DBP, REV and PER:CRY. We further observe that, contra-intuitively, the E-boxes in the equations of REV and of PER:CRY can be removed, while preserving oscillation and antiphasic relation between BMAL1 and PER:CRY, but the D-boxes can't. Finally, the skeleton reduced model is given by:

$$\frac{d[BMAL1]}{dt} = V_R \frac{k_{Rr}^2}{k_{Rr}^2 + [REV]^2} - \gamma_{bp}[BMAL1][PER:CRY] \tag{3.21}$$

$$\frac{d[DBP]}{dt} = V_B[BMAL1] - \gamma_{db}[DBP] \tag{3.22}$$

$$\frac{d[REV]}{dt} = V_{D2}[DBP] - \gamma_{rev}[REV] \tag{3.23}$$

$$\frac{d[PER:CRY]}{dt} = V_{D2}[DBP] - \gamma_{bp}[BMAL1][PER:CRY] \tag{3.24}$$

where $V_B = \frac{V_E}{k_E}$ and $V_{D2} = \frac{1}{2}\frac{V_D}{k_D}$ and all parameters (now shown in Table D.2) come directly from the previous ones (Table D.1). The boxes here have become $R_{box} = V_R \frac{k_{Rr}^2}{k_{Rr}^2+[REV]^2}$, $E_{box} = V_B[BMAL1]$ and $D_{box} = V_{D2}[DBP]$. Fig. 3.12 A) and Fig. 3.12 B) show a simulation of the reduced model, with BMAL1 and PER:CRY maintaining an antiphasic relation; the solution has an oscillatory period of 18,6 h. Fig. 3.12 C) shows a scheme of the reduced model, the dashed red line represents the E-boxes at PER and REV promoter that can be removed as in Eqs. (3.23) and (3.24); the direct double negative loop between BMAL1 and PER:CRY is due to their mutual removal from the nucleus as the BMAL1:PER:CRY complex.

Fig. 3.12 A) shows that DBP varies slowly, but with very small amplitude. To better understand the role of DBP dynamics, the reduced model of Eqs. (3.21) to (3.24) is explored as a Boolean model, which provides an overall qualitative view of the dynamics. The corresponding Boolean equations are given in Appendix E. Fig. 3.12 D) shows the asymptotic behavior of the Boolean model, where several possible cycles are observed: when DBP (third variable) is removed the dynamics converge to the cycle on the right side of the image where PER:CRY (fourth variable) is always 1 and doesn't oscillate (see Appendix E). In the minimal network (Eqs. (3.21) to (3.24)) BMAL1 is therefore acting on PER:CRY on two different time-scales: fast in its direct degradation and slow via DBP (here representing a generic D-box activator). The dynamical condition for oscillation with BMAL1/PER:CRY in antiphase is that we need to have D-box as an intermediate step, a topology that provides an element of delay.

Generally, D-box has been considered of lesser importance for the core clock mechanism and its presence in the dynamic network is thought to affect mostly clock robustness than clock period or the existence of oscillations. Our findings point to the necessity of a network topology that includes two alternative pathways for the action of BMAL1 on the PER:CRY complex, allowing for the possibility of delay effects and distinct time-scales phenomena. In our model this role is achieved by D-box.

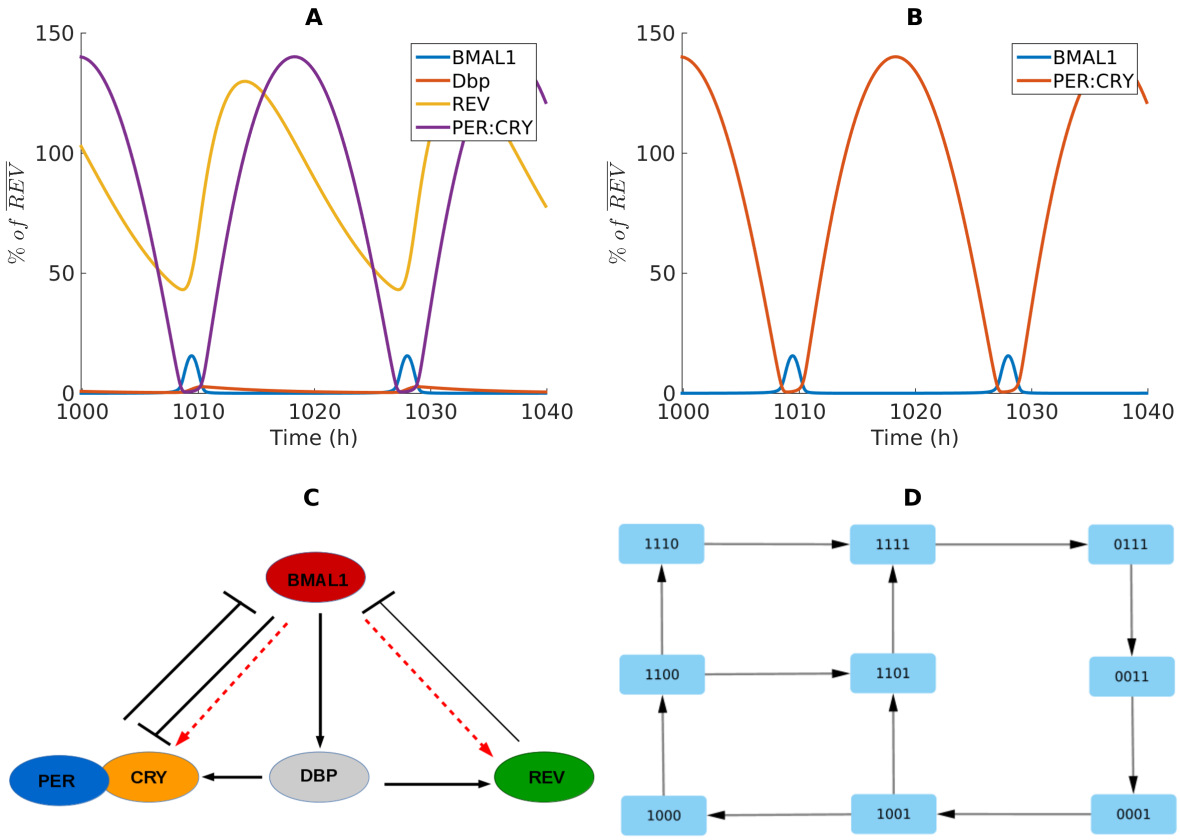

Figure 3.12: **The reduced model can recover the main properties of the circadian clock**
A) Output of the reduced model, oscillations have a period of 18,6 h. B) BMAL1 and PER:CRY maintain an antiphasic oscillation. C) A scheme of the reduced model. Red dashed arrows show the effect of E-boxes on REV and PER:CRY and can be removed. D) The asymptotic behavior of the Boolean model showing the possible limit-cycles. A Boolean model without the third variable (DBP) converges to the cycle $1111 \rightarrow 0111 \rightarrow 0011 \rightarrow 0001 \rightarrow 1001 \rightarrow 1101$ where the fourth variable (PER:CRY) is always 1 and doesn't oscillate.

The known activators of D-box are the PAR transcription factors that aren't thought of as part of the molecular core clock. In fact, the triple knockout mouse ($Dbp^{-/-}/Hlf^{-/-}/Tef^{-/-}$) is rhythmic [103] [104] (though showing a clear change in their activity pattern). As such, molecules other than DBP/HLF/TEF and E4BP4 could possibly also affect D-box, as for example proteins of the C/EBP family (CCAAT/enhancer-binding protein), known basic leucine zipper (bZip) transcription factors that recognize similar, though less specific, amino-acid sequences to the PAR proteins [105] [106]. More importantly, we note that rhythmicity in the triple knockout mouse model doesn't prove non-essentiality of D-box in peripheral clocks, as locomotor activity and central clock controlled behavior may be influenced by a number of factors and external inputs and we hypothesize that D-box may play a more important role in the cell-autonomous

mammalian clock than what is generally accepted.

Ukai-Tadenuma et al. (2008), first propose that various combinations of transcription factors with CCEs might, via the transcriptional cascade, generate all possible circadian phases [107]. In this work, linear combinations of CCEs at gene promoters were useful for circadian clock modeling and while we started the modeling process by favoring mechanisms that underly the circadian BMAL1/PER:CRY phase relation, we nevertheless end up obtaining results that point for a topological role of significance of D-box on the circadian clock, via PER and REV-ERBα, essential for oscillation and timely protein expression, a similar conclusion to that presented by Ukai-Tadenuma et al., (2001), for the role of D-box via CRY1 [72].

Conclusion

Our analysis tends to illustrate that the circadian clock mechanism is well described by a network of regulations occurring mostly at the transcription level. This is due to the ability of circadian genes to transduce a variety of signals, as well as to the whole architecture of the system that is able to sense and integrate external and internal inputs, with likely implications in a variety of cellular processes, including metabolic processes. In this perspective, we developed a transcription-based dynamic model, with standard mathematical formalism and a reduced number of equations and parameters, that is indeed capable of reproducing the relative order of expression of the main clock proteins, with special emphasis on the antiphasic relation between BMAL1 and PER:CRY that relate to opposite phases of the fast/feeding, rest/activity cycles. The modeling framework here developed is a tool that can be used for dynamic modeling of genetic networks of this type, and consists generally in describing protein rates of change as a combination of independent responses to certain regions of the genome, that in this case are the CCEs: E-box, R-box and D-box. Change at these regions of the genome in turn is modeled by the competition between activators and repressors.

Simulation of the *tau* mutation has shown that the peak duration of protein expression adjusts linearly to the period for the majority of clock proteins with the exception of BMAL1 and CRY1. Moreover, when one signal representative of the light/dark cycle and another signal representing the fast/feeding cycle are simultaneously applied, the peak duration of BMAL1 is maximal when the feeding behavior occurs at a correct time (in mice) and minimal when the feeding behavior occurs the most out of its expected phase (an opposite effect is observed for PER:CRY). As we may directly connect BMAL1 with increased insulin sensitivity, these observations help to connect the state of insulin resistance with altered time pattern of feeding behavior that is observed for shift-workers and in people affected by metabolic syndrome [16], leading us to propose that in the same way we may talk of two opposite phases of feeding behavior, activity or light, we may talk of two main metabolic phases related to insulin sensitivity/resistance. Overall these results point to the relevance of the absolute and relative duration of each core clock protein expression/activity in experimental observations of healthy and altered circadian systems.

Finally, we identify the essential transcriptional core network that still guarantees the an-

tiphasic clock property. The topology of this network includes D-box, where its activator acts as an intermediate step between BMAL1 and PER/REV and is essential for oscillatory clock transcriptional dynamics, with antiphase of BMAL1 and PER:CRY. This observation leads us to propose that D-box plays an important role in establishing the correct phase delays in the transcriptional clock network.

Acknowledgments

The authors are part of the Labex SIGNALIFE Network for Innovation on signal Transduction Pathways in Life Sciences (Grant ANR-11-LABX-0028-01) and ICycle project (ANR-16-CE33-0016-01).

4

Coupling the Mammalian Cell Cycle and Circadian Clock Oscillators

In this Chapter we study the coupling of the mammalian cell cycle model developed in Chapter 2 with the mammalian circadian clock model developed in Chapter 3 and investigate several possibilities for the coupling mechanism. We use the reduced versions of both models: the two variable model of the cell cycle given by Eqs. 2.15 and 2.14 and the four variable circadian clock model given by Eqs. 3.21 to 3.24. The cell cycle model produces relaxation oscillations whose period is controlled by the growth factor input GF; the clock model is based on transcriptional regulation and is able to recover the antiphasic relation in the oscillation of the CLOCK:BMAL1 and PER:CRY proteins. Dynamical oscillations of these models were shown in Figs. 2.4 and 3.12 (A and B), respectively. Additionally, sensitivity analysis of the reduced clock model is shown in Fig. D.9 for parameters of Table D.2, allowing to understand how the period of the system varies with changes in parameters.

A repetition of the model equations is here shown again as a summary:

$$\frac{d[BMAL1]}{dt} = R_{box} - \gamma_{bp}[BMAL1][PER:CRY] \tag{4.1}$$

$$\frac{d[DBP]}{dt} = V_B[BMAL1] - \gamma_{db}[DBP] \tag{4.2}$$

$$\frac{d[REV]}{dt} = V_{D2}[DBP] - \gamma_{rev}[REV] \tag{4.3}$$

$$\frac{d[PER:CRY]}{dt} = V_{D2}[DBP] - \gamma_{bp}[BMAL1][PER:CRY] \tag{4.4}$$

$$\begin{aligned}\frac{d[MPF]}{dt} =& GF + V_c\frac{\overline{MPF_{max}} - [MPF]}{\overline{MPF_{max}} - [MPF] + k_c}\frac{[MPF]^2}{[MPF]^2 + k_m^2} \\ & - V_w\frac{[MPF]}{[MPF] + k_w}\frac{k_n^2}{[MPF]^n + k_n^2} \\ & - \gamma_1[APC:cdc20][MPF]\end{aligned} \tag{4.5}$$

$$\frac{d[APC:cdc20]}{dt} = V_m[MPF] - V_k[APC:cdc20] \tag{4.6}$$

where

$$R_{box} = V_R \frac{k_{Rr}^2}{k_{Rr}^2 + [REV]^2} \tag{4.7}$$

and the previously named parameter S_{GF}, representing an MPF synthesis term due to the presence of GF, is here renamed GF for simplicity.

In order to have oscillation of both systems with periods of the same order of magnitude and consistent with values of experimental observations we scale parameters of both models, by multiplying those referring to rates of change by a constant. This type of scaling changes only the oscillatory frequency without interfering with the dynamical behavior of the system. Thus, for the cell cycle model a time scaling $t \to \beta t$, with $\beta = 10$, is performed on parameters of Table 2.1, making the dynamics 10 times faster (as was previously done in Section 3.12). For the clock model, the scalling $t \to \mu t$, with $\mu = 0.775$ is performed on parameters of Table D.2, normalizing the period to 24 h, the typical circadian clock period (see Section F.1 of appendix F for a brief description). As both systems were previously normalized to a certain concentration value, the solution of the coupled system (referring to concentration) is now unitless. Table F.1 shows the final parameter values (except the parameter GF that will be varied during this Chapter). Additionally, for all simulations we use the initial condition: BMAL = 1,2; DBP = 1,6; REV= 1,5; PER:CRY = 1,2; MPF = 2,0; APC:cdc20 = 1,0.

Moreover, the main topics explored in this Chapter are:

- possible ways of coupling the clock and cell cycle systems;
- joint dynamics of the oscillators in response to different forms of coupling;
- period response of the coupled system under single-parameter changes and/or external inputs;

We will focus specifically on states of synchronization of the two oscillators with respect to their period, or period-lock (PL), for the various types of coupling mechanisms. Phase-locking (that implies period-locking) is also obtained (shown in some figures with oscillatory solutions), but the analysis will largely focus on the evolution of the ratio of clock to cell cycle period r_T under different forms of coupling mechanisms, added inputs and parameter changes. In particular, strategies for period control of one oscillator through the dynamics of the other are investigated. The effects of Dexamethasone (Dex) are also recovered by using the new clock model, in contrast to the preliminary model of appendix B.

As we intend to relate our work with experimental observations of the ratios of period locking observed in mammalian cells ([1]), we want to develop an algorithm to compute these numerical ratios in a systematic manner. We opted by computing the period of oscillations by counting the number of relevant peaks in the numerical solutions, during a sufficiently long time

interval. We consider that the relevant peaks of a protein are those above a certain threshold concentration, and assume this is given by the mean protein concentration in that interval. In our algorithm, the period is then the average of the differences between the times of relevant peak occurrence. Therefore, in certain cases, this period will not correspond to the mathematical period T of the solution, $x(t) = x(t+T)$, but will nevertheless provide a more realistic estimate of the period-lock ratios. In fact, in many cases, small amplitude peaks can be observed in the numerical solutions, which would not be distinguishable in experimental results, motivating our introduction of the relevant peaks above a certain threshold. For example, two peaks of MPF with different amplitudes but above mean MPF concentration both represent a mitotic event.

As discussed in Chapter 1, not much precise knowledge is available on how the cell cycle may influence the clock. Following the breakthrough made by Feillet et al., (2014), and Bieler et al., (2014), we know that in NIH3T3 cells the oscillators show 1:1 phase-lock and the influence of the cell cycle on the clock seems to be as relevant as the reverse [1] [30]. A general idea explored in this Chapter is that MPF (cyclin B-cdk1) likely phosphorylates an essential clock component. Specifically, MPF-mediated REV-ERBα phosphorylation and subsequent degradation is an experimental observation [56]. Notably, this is supported by the observation that cells arrested in G2 upon treatment with nocodazole show a significant decrease in REV-ERBα abundance. On the other hand, mechanisms denoting a clock influence on the cell cycle are a consensual observation. Of these, CLOCK:BMAL1 promoting the MPF repressor *wee1* [21] is a mechanism that involves the essential cell cycle and clock complexes (MPF and CLOCK:BMAL1) as well as the *wee1* interaction included in our model via an MPF negative regulatory term.

Thus, we begin, in Section 4.1, by analyzing the coupling mechanism in which the cell cycle influences the clock, which is the MPF-induced degradation of REV-ERBα [56] previously analyzed in appendix B for the preliminary clock model. We are able to recover not only the 1:1 and the 3:2 period-lock ratios, but also the experimentally observed effect of a Dex input, unlike with the model of appendix B. Furthermore, the application of a PER/PER:CRY input such as Dex and the application of an hypothetical BMAL1 input I_B have opposite effects in the control of synchronization states: Dex drives the system from a 1:1 to a 3:2 period-lock state and I_B drives the system from 3:2 to 1:1 period-lock. In Section 4.2 we study the unidirectional entrainment of the cell cycle by the clock via the known molecular interaction whereby CLOCK:BMAL1 indirectly represses MPF. This repression occurs via CLOCK:BMAL1-controlled activation of the *wee1* gene [21]. Strategies for controlling the cell cycle period by tuning the clock period and controlling the coupled state of the system are also explored in this Section, by tuning the parameters k_{Rr}, γ_{rev} and γ_{db}. Following this, we study, in Section 4.3, the bidirectional coupled system combining the two aforementioned interactions and find that certain combinations of growth factor (GF) and the coupling parameters (c_m and c_b) result in a very slow mitotic rate. Moreover, we analyze the effect of a Dex pulse (instead of a constant Dex input) and find the time of pulse application T_{pulse} to be a control parameter for the synchronization state response of the system: there is a responsive and a non-responsive region of the oscillators phase. Besides this, the system's period-lock response to a Dex pulse is transient, with the system returning to its initial synchronization state some time after the application of the pulse. Finally, because

unidirectional coupling can be sufficient for 1:1 PL and observations show the increase of both clock and cell cycle frequencies with growth factor (GF), we also propose a different hypothesis in Section 4.4 in which GF is not only a cell cycle input but also acts on the circadian clock system, making it a common input for both systems. This mechanism is explored in conjunction with the clock entrainment of the cell cycle via *wee1* induction and results in a different dynamical evolution of r_T with GF, that nevertheless provides an alternative explanation to experimental phase-lock observations [1]. For all coupling mechanisms, growth factor GF and the coupling parameters (c_m and c_b) provide a way of controlling the oscillators' synchronization state.

A summary of the coupling interactions and control parameters analyzed in this Chapter is shown in Table 4.1.

Table 4.1: Coupling mechanisms and control parameters studied in this Chapter.

Coupling mechanisms	Unidirectional cell cycle → clock	Unidirectional clock → cell cycle	Bidirectional cell cycle ⇄ clock
MPF —|REV (Section 4.1)	Control Parameters: ✓ GF, c_m; ✓ Dex, I_B;	-	-
BMAL1 —|MPF, (Section 4.2)	-	Control Parameters: ✓ GF, c_b; ✓ k_{Rr}, γ_{rev}, γ_{db};	-
MPF —|REV, BMAL1 —|MPF (Section 4.3)	-	-	Control Parameters: ✓ GF, c_m, c_b; ✓ Dex, T_{pulse};
BMAL1 —|MPF GF —|BMAL1 (Section 4.4)	-	Control Parameters: ✓ GF, c_b, k_s; ✓ Dex;	-

4.1 Coupling via MPF-induced phosphorylation of REV-ERBα

We begin by studying the unidirectional cell cycle to clock coupling, whereby MPF phosphorylates REV leading to its subsequent degradation, [56], and compare results with those of the simplistic clock model of appendix B. A scheme of the coupled system is shown in Fig. 4.1.

As such, we multiply the degradation term of REV by $c_m[MPF]$, where c_m is a constant, representing the coupling strength between oscillators. The equation for the REV rate of change

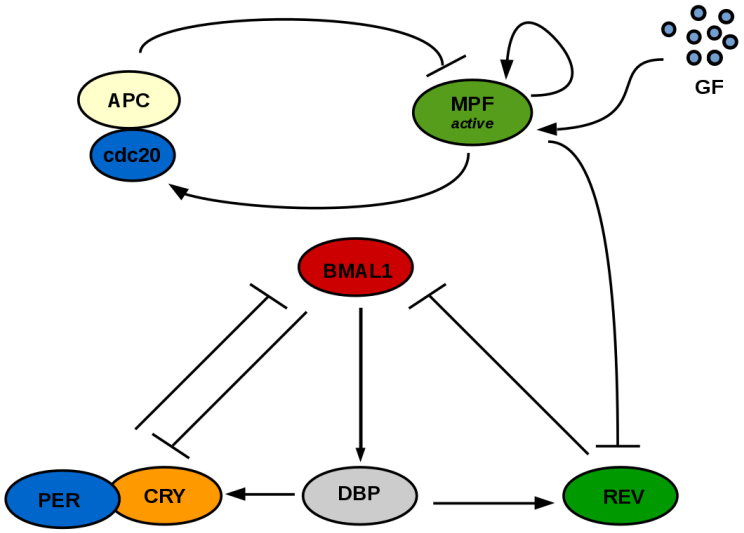

Figure 4.1: **Schematic of the first coupling mechanism**
MPF in its active form represses REV via its phosphorylation and subsequent degradation: this is a unidirectional form of coupling, with exclusive action of the cell cycle on the clock.

becomes:

$$\frac{d[REV]}{dt} = V_{D2}[DBP] - c_m[MPF]\gamma_{rev}[REV] \tag{4.8}$$

As MPF has an enzymatic activity, catalyzing the reaction without being consumed in it, we consider its rate of change to be unaffected by this interaction.

We start by verifying that entrainment of the clock by the cell cycle is possible for $c_m = 0.2$, see Fig. 4.2 (the variation of the cell cycle period with GF is also observed in this Figure).

Fig. 4.3 shows an example of an oscillatory solution for $c_m = 0.2$ and GF $= 40$, where the 1:1 synchronization state can be seen along with phase portraits. Here, REV peaks 7,2 h after MPF, which is in agreement with observations of REV-ERB peaking approximately 7 h after mitosis [1].

Conversely, for weak/moderate coupling we verify different values for the period-lock ratio $r_T = \frac{T_{clock}}{T_{cellcycle}}$, where the *devil's staircase*-like pattern ([55]) is again observed with GF as a control parameter. Fig. 4.4 shows results for $c_m = 0.04$ (left) and $c_m = 0.08$ (right). We verify that different c_m values induce different r_T values and that non-integer rational ratios are now present, including the experimentally observed 3:2 period-lock in both cases, a ratio inferred from experimental analysis [1]. Increasing GF increases r_T, while increasing c_m has the opposite effect and shifts the point where the system "jumps" from 3:2 to 2:1 period-locking for a higher value of GF. From this analysis, it follows that GF and c_m are control parameters for the oscillators' synchronization state.

Non-integer values of r_T, such as 1,5, are now being recovered with the new clock model (Eqs. (3.21) - (3.24)) for a large range of GF (see Fig. 4.4). In contrast, the preliminary model

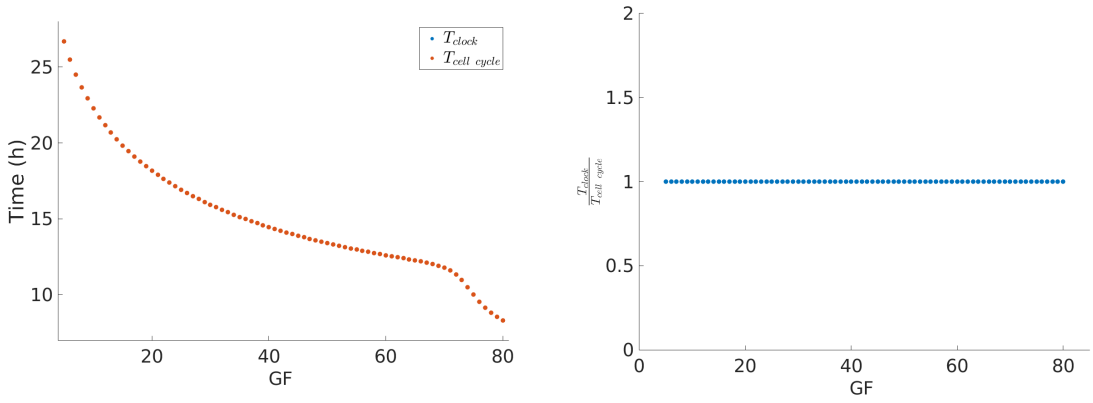

Figure 4.2: **Strong coupling of the circadian clock and cell cycle models by MPF-induced degradation of REV.**
For $c_m = 0.2$ the system is strongly coupled with 1:1 period-lock. The period of the clock follows that of the cell cycle that decreases with GF. Cell cycle oscillations occur for $4 \leq \text{GF} \leq 80$.

of appendix B could only obtain integer values of r_T for very specific values of GF (see Fig.B.6). These numerical results illustrate the more realistic and adaptable properties of the clock model developed in Chapter 3.

A similar observation holds for c_m as seen in Fig. 4.5, which shows the system's period-lock response to variation of this control parameter for fixed GF.

Additionally, supporting Figs. F.1 and F.2 show oscillatory solutions of $c_m = 0.08$ and $c_m = 0.04$ respectively. These are done for fixed GF = 40 and result in 3:2 and 2:1 period-locked oscillations (compare to Fig. 4.3 where GF = 40, $c_m = 0.2$ results in 1:1 period-lock). See that in Figs. 4.4 and 4.5 there are some points that fall outside the *devil's staircase* pattern. This sometimes constitutes a numerical error that occurs due to a difficulty of our algorithm in computing the period, however often the system has a complex behavior. An example is shown in Fig. F.3 for the point of $c_m = 0.1$, GF = 40 that, as shown in Fig. 4.5, falls outside the pattern.

The next important step is to test the ability of the model in simulating the effect of Dexamethasone on the system, namely on the ratios of period-locking. To do so, the constant term Dex is added to the equation of $\frac{d[PER:CRY]}{dt}$ that in the reduced system encompasses the transcriptional terms of PER activation (see Section 3.1.4). The equation now becomes:

$$\frac{d[PER:CRY]}{dt} = Dex + V_{D2}[DBP] - \gamma_{bp}[BMAL1][PER:CRY] \tag{4.9}$$

With $c_m = 0.1$ the system couples in a 1:1 ratio for $4 \leq GF \leq 24$ and we verify that introducing Dex = 10 drives the system from the 1:1 to the 3:2 PL ratio, as shown in Fig. 4.6, confirming the ability of the model of reproducing the PL response to Dexamethasone. This

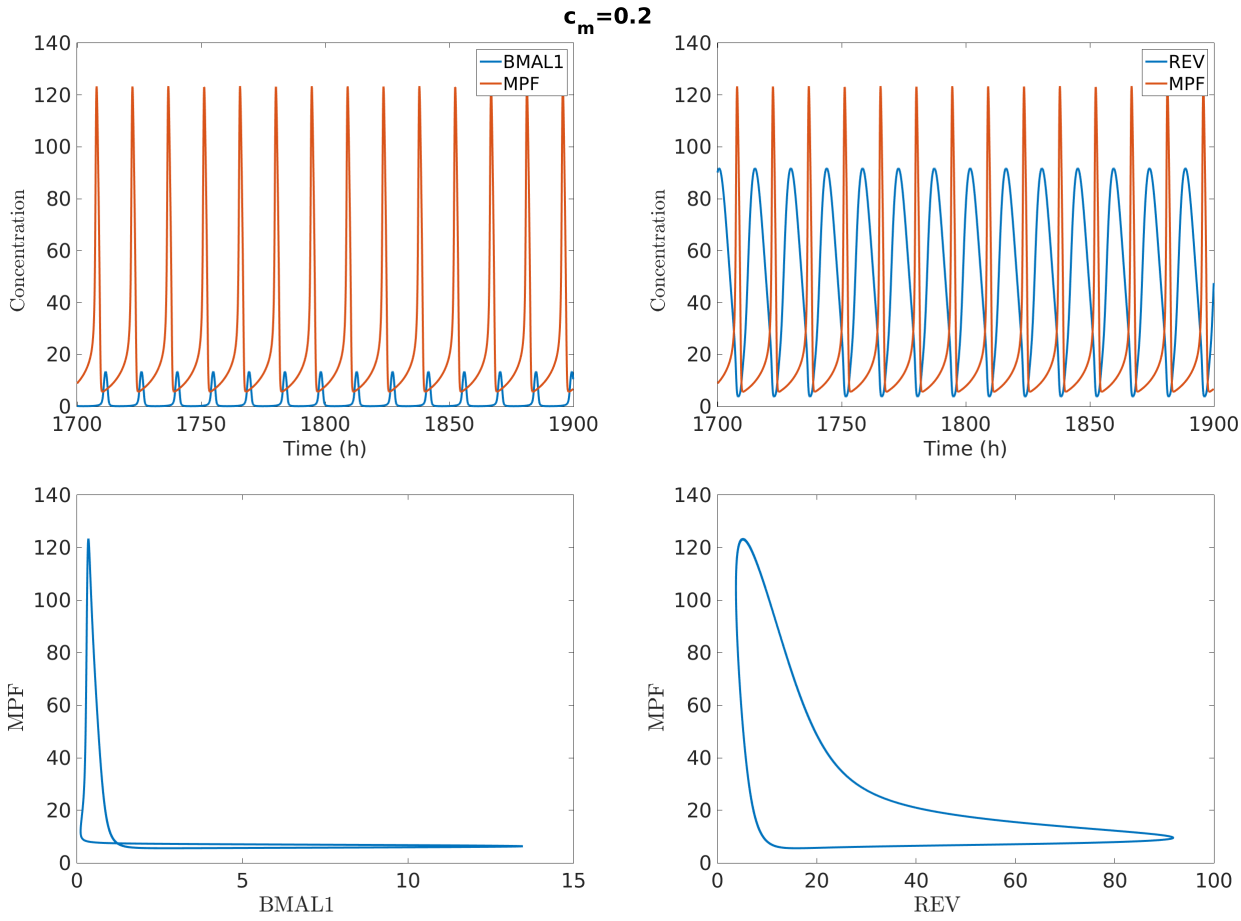

Figure 4.3: **Oscillations and phase portraits of BMAL1, REV and MPF in a 1:1 period-lock.**
With GF=40, the coupling strength $c_m = 0.2$ results in a solution with a 1:1 period-lock, where $T_{clock} = T_{cell\ cycle} = 14{,}5$ h. The system is synchronized and phase-locked.

differs from coupling with our preliminary clock model (appendix B), where the application of Dex didn't recover the 3:2 period-lock from experimental observations [1].

These results mean that introducing an input on PER/PER:CRY has a similar effect to decreasing the coupling strength parameter c_m, in terms of driving the system from 1:1 PL to a higher PL ratio. Furthermore, the fact that more of the clock/cell cycle experimental period-lock observations are now being accurately reproduced by our mammalian clock model further helps to validate it and highlights the importance of the circadian transcriptional topology.

Finally, note that the circadian clock dual state property (CLOCK:BMAL1 and PER:CRY in phase opposition, as seen in Figs. 3.3 and 3.12) is important to generate the wide range of period-lock ratios, confirming our hypothesis (developed in appendix B). For model 4.9, interference with one of the phases of the clock, say by promoting the state of high PER:CRY/low BMAL1 (as is the case of Dex application) is in a way equivalent to decreasing the coupling strength c_m. These numerical experiments show that there is more than one way to drive the system between

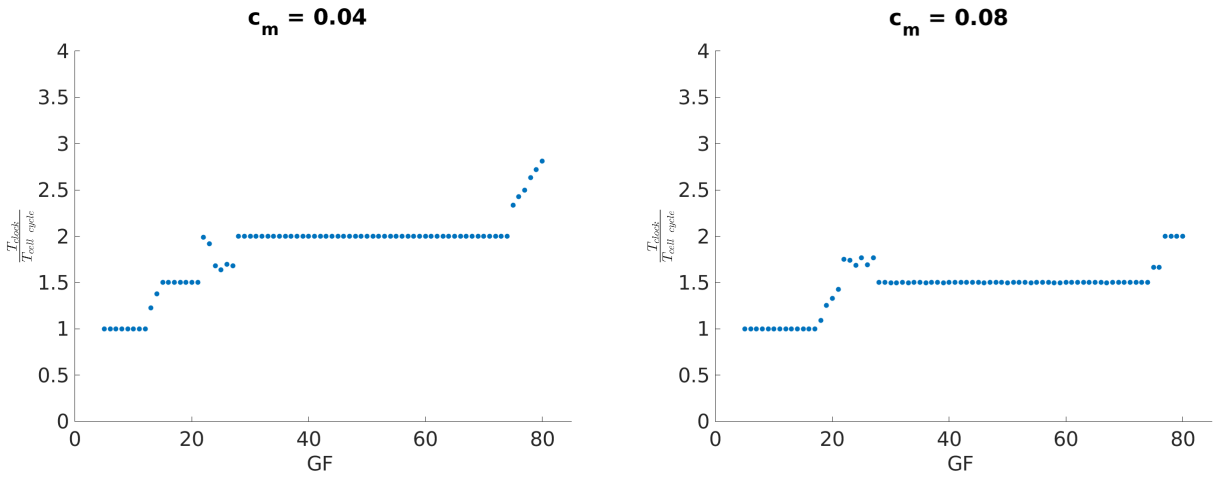

Figure 4.4: **Weak coupling of the circadian clock and cell cycle models by MPF-induced degradation of REV.**
For $c_m = 0.04$ (left) and $c_m = 0.08$ (right) the system is in weak/moderate coupling and distinct period-lock ratios are obtained depending on GF, forming a pattern similar to that of the *devil's staircase*, where the period-lock ratio is increasing but remains constant by intervals of GF. GF and c_m are control parameters for the PL ratios. The 3:2 experimentally observed period-lock state is obtained.

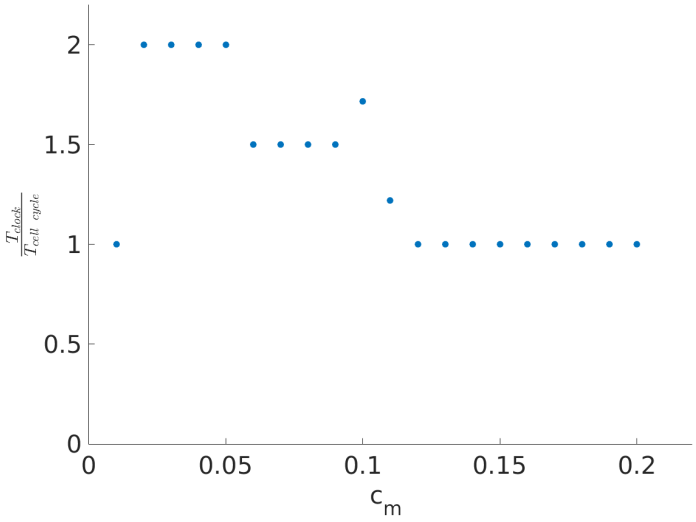

Figure 4.5: **c_m is a control parameter for the period-lock dynamics of the coupled system.**
Varying c_m with fixed GF = 40 causes the ratio of clock to cell cycle period to vary in steps, where the 2:1, 3:2 and 1:1 period-lock ratios are obtained.

different PL states, suggesting that in wild type cells the cell cycle may play an important role in regulating the clock period, as recently proposed by Feillet et al., (2014), [1]. To further explore

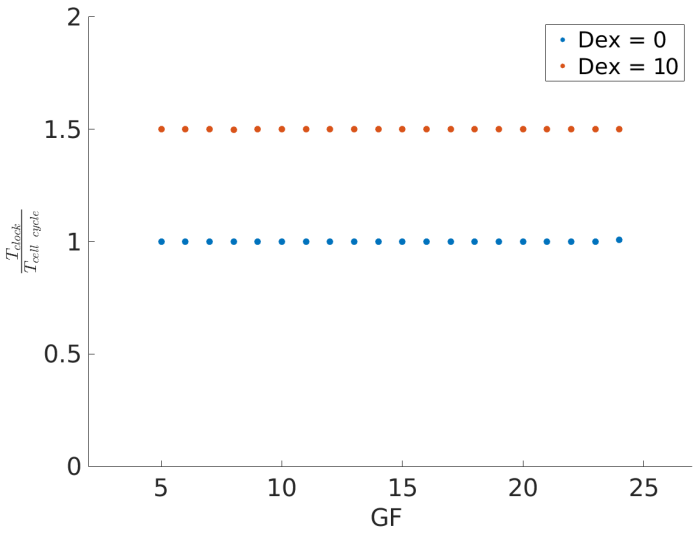

Figure 4.6: **An input of Dexamethasone drives the system from 1:1 to 3:2 period-lock.** With $c_m = 0.1$ and Dex $= 0$ the system is in strong coupling and in 1:1 PL for $4 \leq GF \leq 24$. With $c_m = 0.1$ and Dex $= 10$ the 3:2 PL ratio is obtained.

our phase opposition hypothesis we devise a symmetric study where the system is in 2:1 PL and an input I_B is applied to induce a high BMAL1 state. In contrast to the Dex input, we now anticipate the system will evolve to a state of 1:1 PL. The equation for $\frac{d[BMAL1]}{dt}$ now becomes:

$$\frac{d[BMAL1]}{dt} = I_B + V_R \frac{k_{Rr}^2}{k_{Rr}^2 + [REV]^2} - \gamma_{bp}[BMAL1][PER:CRY] \tag{4.10}$$

In Fig. 4.7 we verify that our hypothesis is correct as the I_B input drives the system from $r_T > 1$ to $r_T = 1$.

Promoting 1:1 PL either by increasing Dex (thus PER:CRY) or by decreasing c_m (thus increasing REV), can lead to similar effects in BMAL1 as both PER:CRY and REV repress BMAL1. However, coupling via BMAL1 is not being modeled yet, which means changes applied on the clock system impact the dynamics of the coupled system because they affect the clock period. Fig. F.4 shows that Dex increases the clock period, while I_B decreases it. As the cell cycle has a shorter period than the clock for GF $>$ 7,5 the I_B input is promoting closer clock/cell cycle periods, whilst Dex has an opposite effect. Thus, unsurprisingly, the relative periods of the oscillators are a preponderant factor for the control of synchronization states: the closer the intrinsic periods of the oscillators are the more the 1:1 period-lock is favored.

Furthermore, in this Section we have observed that for low GF values the oscillators tend to couple in a 1:1 fashion: this could be because for low GF the clock and cell cycle intrinsic periods are closer, as the GF value for which the cell cycle and the clock have the same intrinsic period (24 h) is 7,5 (Fig. 4.2 (left) shows how the cell cycle period varies with GF). Accordingly, PL states with $r_T > 1$ that occur for higher GF values always represent a slower clock. Thus, the idea of the intrinsic period of the oscillators being determinant of the coupling state is

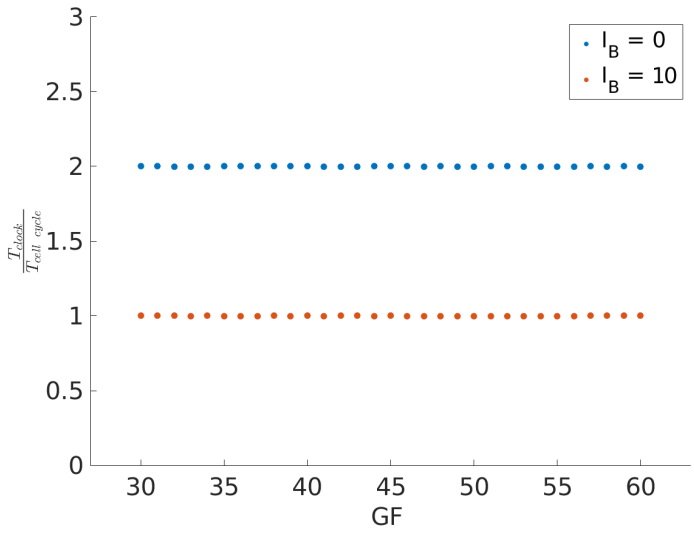

Figure 4.7: **The input I_B drives the system from 2:1 to 1:1 period-lock.** With $c_m = 0.04$ and $I_B = 0$ the system period-locks in 2:1 for $30 \leq GF \leq 60$ (see also Fig. 4.4). With $c_m = 0.04$ and $I_B = 10$ the 1:1 period-lock is obtained.

highlighted. Though a slower clock is in agreement with the experimental observations of Feillet et al. [1], the possibility of using the PL state dynamics to slow down the cell cycle is of interest and will be explored in following Sections.

Moreover, the application of Dex is able to induce the system from the 1:1 to the 3:2 PL ratio as in experimental observations by Feillet et al., (2014), [1], which doesn't occur for a clock model without the characteristic CLOCK:BMAL1/PER:CRY antiphasic relation (see appendix B). The circadian clock topology recovering CLOCK:BMAL1/PER:CRY antiphase is in turn essential for reproduction of period-lock state changes induced by Dex application or by the application of inputs that asymmetrically promote one of the two main clock phases. Specifically, promoting the high PER phase of the circadian clock favors $r_T > 1$, similarly to weak coupling, while promoting the high CLOCK:BMAL1 phase favors $r_T = 1$, similarly to strong coupling, in the system of unidirectional coupling where the cell cycle entrains the clock via MPF-induced degradation of REV.

Finally, we remark that a large part of experimental observations can be reproduced with this unidirectional **cell cycle** $\rightarrow$ **clock** coupling, which is in itself a relevant result and helps to validate not only the mechanism of MPF-controlled REV degradation in particular, but also the cell cycle-mediated clock control in general.

4.2 Coupling via BMAL1-mediated *wee1* activation (indirect repression of MPF)

We now study the reverse unidirectional coupling where the clock entrains the cell cycle (the coupling mechanism studied in Section 4.1 is removed). As discussed before, unlike coupling via the cell cycle, coupling via the clock has been known and documented for a long time. One notable mechanism and the one we will focus on here is the induction of the *wee1* gene by CLOCK:BMAL1 [21], as it involves the variable BMAL1 present in our clock model as well as the *wee1* interaction with MPF that is included in our cell cycle model. Fig. 4.8 shows a scheme of the coupled system to be analyzed in this Section.

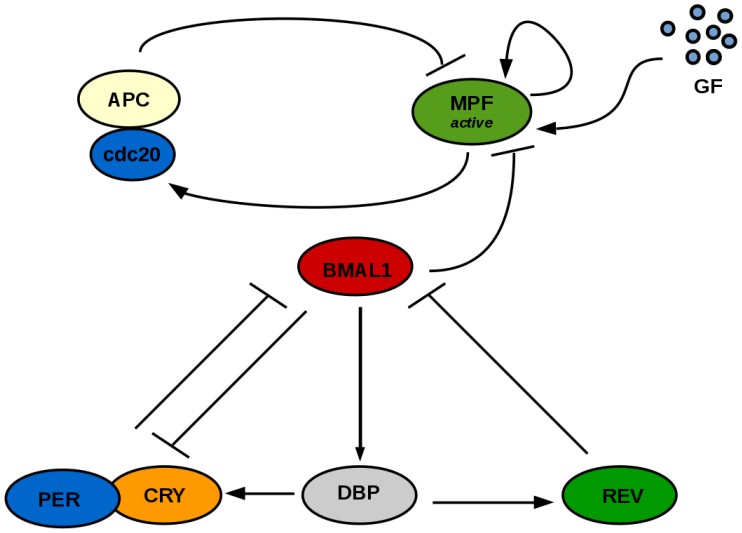

Figure 4.8: **Schematic of the second coupling mechanism**
The CLOCK:BMAL1 protein complex (here the variable BMAL1) represses MPF_{active} due to its action in promoting *wee1* gene expression. This is a form of unidirectional coupling, with exclusive action of the clock on the cell cycle.

The action of wee1 on MPF is included in the self-regulatory loop where MPF represses the negative loop representative of its inactivation by wee1 (see Section 2.1). Thus, the effect of CLOCK:BMAL1 in promoting wee1 is represented by promoting the wee1 term (and thus repression of MPF), for which the equation for $\frac{d[MPF]}{dt}$ now becomes:

$$\begin{aligned}\frac{d[MPF]}{dt} =& GF + V_c \frac{\overline{MPF_{max}} - [MPF]}{\overline{MPF_{max}} - [MPF] + k_c} \frac{[MPF]^2}{[MPF]^2 + k_m^2} \\ & - c_b[BMAL1]V_w \frac{[MPF]}{[MPF] + k_w} \frac{k_n^2}{[MPF]^n + k_n^2} \\ & - \gamma_1[APC : cdc20][MPF]\end{aligned} \tag{4.11}$$

where c_b is the coupling parameter indicative of the coupling strength.

In Fig. 4.9 we observe the effect of GF and the coupling parameter c_b on the ratios of period locking. For higher GF the ratio of clock to cell cycle period tends to increase; for higher c_b the GF parametric region for which the 1:1 period-lock occurs is wider, with $r_T > 1$ beginning at higher values of GF.

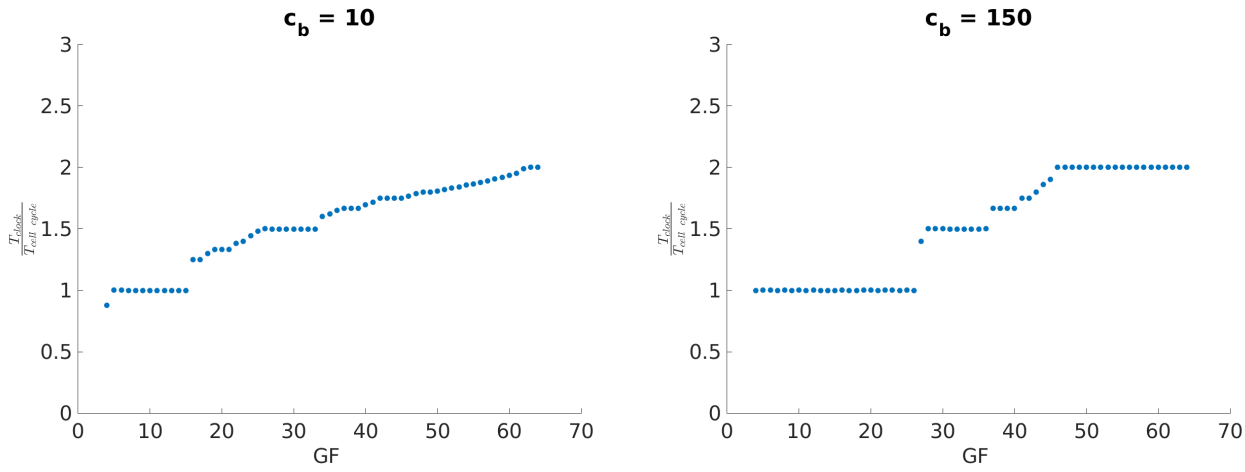

Figure 4.9: **Coupling of the circadian clock and cell cycle models by BMAL1 repression of MPF via *wee1* induction.**
Coupling strength c_b and growth factor GF control the period-lock ratio. Increasing c_b increases the GF region of 1:1 period-lock.

Furthermore, Fig. 4.10 shows the system's period-lock response to variation of the control parameter c_b for fixed GF, which predicts the appearance of 4:3 and 5:3 synchronization states.

With the **clock** $\rightarrow$ **cell cycle** coupling, the effect of a Dexamethasone input in changing the system's PL dynamics is not as marked as with **cell cycle** $\rightarrow$ **clock** of the previous Section. However, it may still be observed for a small GF interval near the point of period-lock state change, as shown in Fig. F.5.

Fig. 4.9 shows that once again the periods couple in a 1:1 manner for low values of GF and that when other period-lock ratios appear the clock is always slower than the cell cycle. This points to the importance of the intrinsic oscillatory period, as argued above, since the natural frequency of the uncoupled cell cycle increases with GF (see Figs. 2.7 and 4.2 (left)). In Fig. 4.11 the periods of both oscillators are shown for the same simulation as Fig. 4.9 (right), with $c_b = 150$. Observe that as expected for the **clock** $\rightarrow$ **cell cycle** unidirectional coupling, the period of the clock is kept at 24 h, while the period of the cell cycle changes: in the region of $r_T > 1$, the period of the cell cycle adapts in such a way that it changes by steps with GF, showing period ratios between 1 and 2.

As the intrinsic period of the cell cycle is lower than that of the clock for GF > 7,5, for the majority of the GF region, a higher value of GF represents a sped up cell cycle. A question of interest is the possibility of tuning the period of each oscillator, by using the knowledge gained on the coupled system. In particular, the ability of slowing down the cell cycle would be relevant for cancer treatment. From Fig. 4.11 this would roughly mean either promoting a slower clock

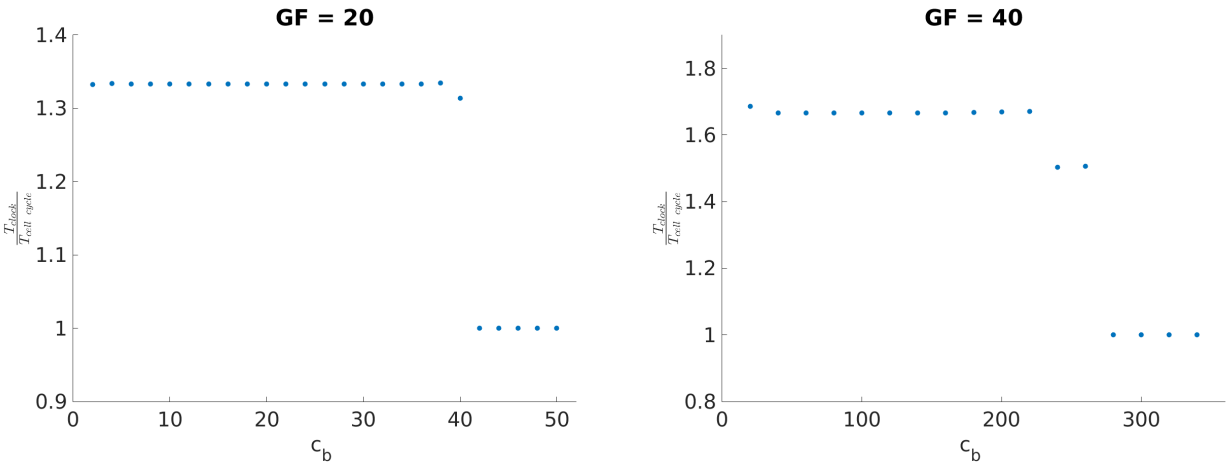

Figure 4.10: **c_b is a control parameter for the period-lock dynamics of the coupled system.**
Varying c_b with fixed GF causes the ratio of clock to cell cycle period to vary in steps. For GF = 20, the 4:3 and 1:1 period-lock ratios are obtained, while GF = 40 results in 5:3, 3:2 and 1:1 period-lock ratios. GF = 40 requires a much higher value of c_b for 1:1 period-lock than GF =20.

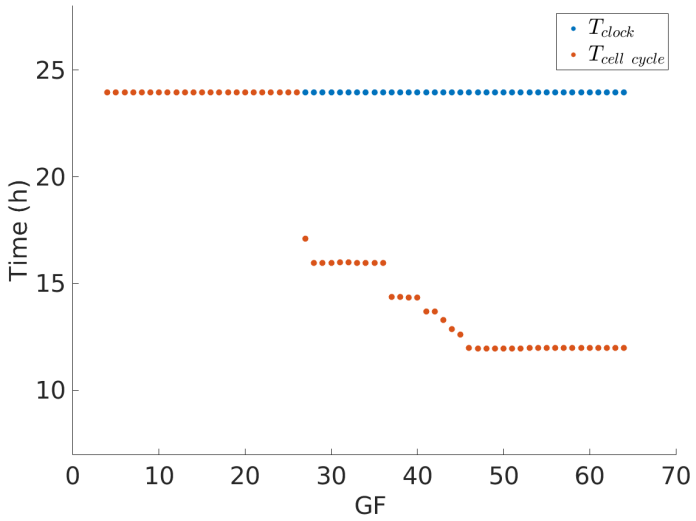

Figure 4.11: **Circadian clock and cell cycle periods in the coupling via BMAL1 induction of *wee1*.**
The period of the clock doesn't change with GF in the unidirectional coupling, while the period of the cell cycle adapts in a stepwise manner ($c_b = 150$).

together with coincidental period ratios ($r_T = 1$) or a faster clock with $r_T > 1$ in order to cause the step-wise adaptation of the cell cycle, increasing its period relative to that of the coupled system.

4.2.1 Cell Cycle Period Control via the Clock

We will focus on procedures that are experimentally feasible, such as the addition of specific inputs and single parameter changes. Available inputs include GF and Dex. Other inputs are hypothetical so far, as is the case of the input I_B in $\frac{dBMAL1]}{dt}$ (Equation 4.10); single parameter changes in its turn have the potential to be reproduced in experimental settings contingent upon the discovery of target molecular compounds that specifically affect them (some examples will be discussed below).

From observation of Fig. D.9 we conclude that parameters that affect R-box (V_R and k_{Rr}) as well as the degradation rates of REV and DBP (γ_{rev} and γ_{db}) affect clock period the most and are thus the best candidates for period-lock state control analysis.

We start by introducing the parameter α_1 in the R-box equation as: $R_{box} = V_R \frac{k_{Rr}^2}{k_{Rr}^2+(\alpha_1[REV])^2}$, which generally acts as a R-box antagonist or REV potentiator. Here, $\alpha_1 = 1$ represents the original system oscillating with the intrinsic period, while the parameter α_1 can either represent an R-box agonist (REV antagonist) for $\alpha_1 < 1$ or an R-box antagonist (REV agonist) for $\alpha_1 > 1$ by comparison with the control state. Note that this application is identical to rescalling the parameter $k_{Rr} \rightarrow \frac{k_{Rr}}{\alpha_1}$. The way this change relates to existing clock chemical modulators is not obvious. On one hand agonists and antagonists of REV have been developed and are well studied, on the other hand REV ligand agonists affect mostly the amplitude of the clock with little impact on the period [109]. However, these drugs affect different tissues differently, causing alterations of circadian gene expression that are distinct in the hypothalamus and in the liver [109], for which we can't conclude whether or not their action occurs specifically by changing REV modulation of R-box. In our model, parameters of R-box strongly affect the period and oscillation of the system, which is compatible with observations since our variable REV represents all REV-ERBs. Therefore, the parameter α_1 appears to be a good candidate for period control of the coupled oscillators.

Fig. F.6 shows the variation of the clock period with α_1, where we can observe that clock period increases with α_1, up to a saturation value. Fig. 4.12 shows how α_1 affects the period of both oscillators and the ratio of clock to cell cycle period: for $c_b = 10$ and GF = 7 the system is naturally in a state of strong coupling when $\alpha_1 = 1$, with a 1:1 period-lock (see Fig. 4.9); when $\alpha_1 < 1$ higher values of R-box expression and shorter clock period are obtained resulting in a substantially increase in cell cycle period.

We now move on to explore variations of REV and DBP rates of natural degradation, γ_{rev} and γ_{db} respectively. Some available compounds are known to interfere with γ_{rev} that could thus be used for tuning this parameter. These drugs act mostly via inhibition of GSk3β, known to increase phosphorylation of REV-ERB, and can lead either to a decreased or increased clock period [110] depending on the GSK-inhibitor used [111] [112]. Concerning γ_{db}, we have found no readily available compounds that specifically target this parameter yet. Nevertheless, we will investigate how changes in both γ_{rev} and γ_{db} interfere with the oscillators' period. We thus introduce α and β as modulators of these parameters as: $\gamma_{rev} \rightarrow \alpha\gamma_{rev}$ and $\gamma_{db} \rightarrow \beta\gamma_{db}$ and observe the change in period and the synchronization state of the system when individually

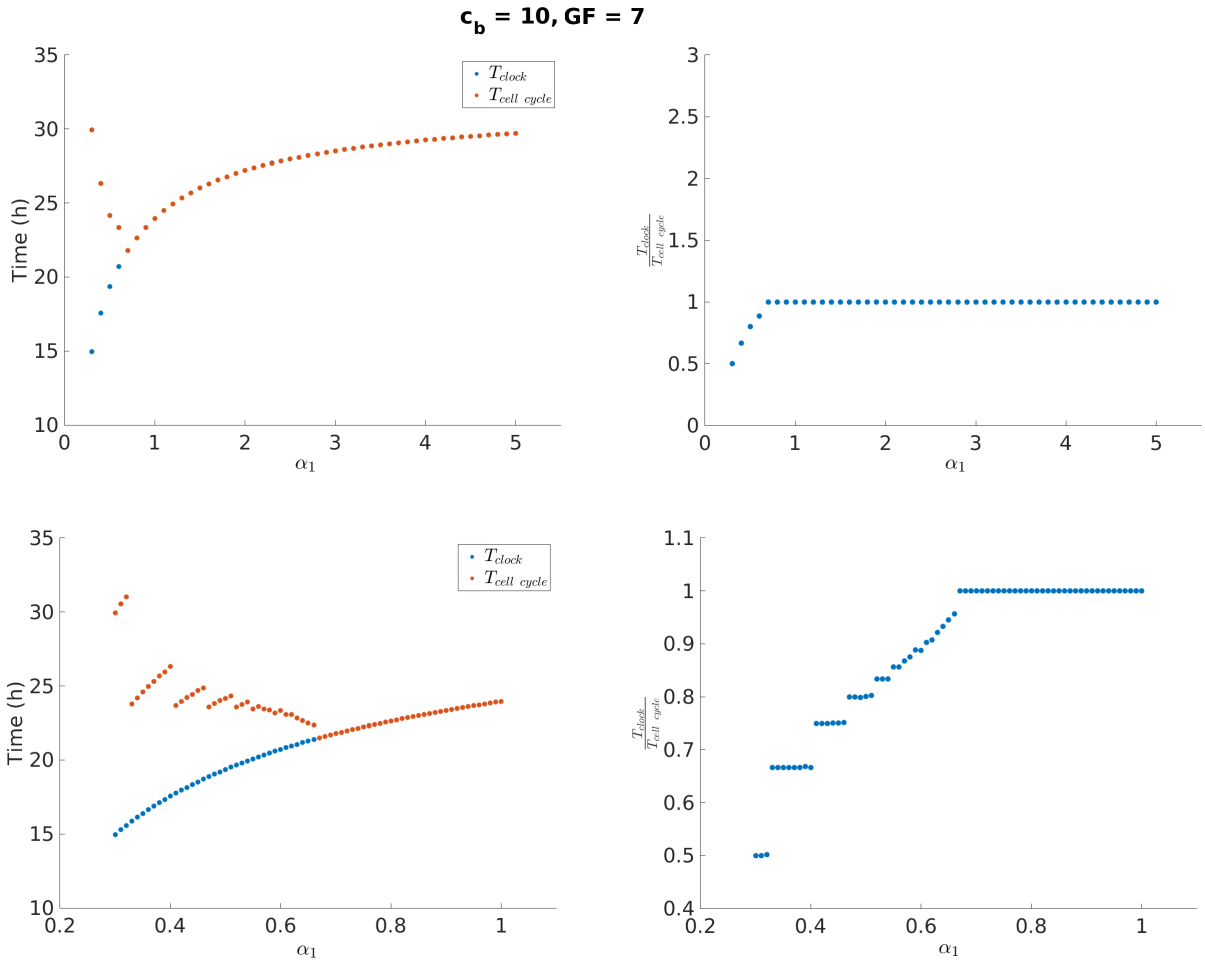

Figure 4.12: **Evolution of the oscillators period with α_1 in the unidirectional coupling via clock wee1 activation.**
For $c_b = 10$ and GF $= 7$ the system is in a 1:1 synchronization state when $\alpha_1 = 1$. On top: values of $\alpha_1 < 1$ accelerate the clock and the cell cycle "adapts" by slowing down (left), which makes the ratio between the two periods smaller than 1 (right); for $\alpha_1 > 1$ the system synchronizes in a 1:1 manner. On bottom: the same as on top but for $0 < \alpha_1 < 1$, to allow a more detailed visualization. Ratios such as 1:2, 2:3, 3:4 and 4:5 are obtained.

varying each of these modulators.

Fig. 4.13 shows that tuning γ_{rev} by varying α leads to variations of the oscillators synchronization state. For $\alpha < 1$ the period of the clock slows down which effectively slows down the cell cycle. For $\alpha > 1$ the clock frequency increases resulting in a cell cycle oscillator that is slower than the clock. This implies that regulating the parameter γ_{rev} is a successful strategy for clock/cell cycle period control.

Fig. F.7 shows the periods and the ratio between periods of both oscillators, when $\alpha = 2$, while varying GF. We observe a region where the cell cycle is much slower than the clock, for low values of GF: the 1:2 and the 3:4 synchronization states are present. More importantly, α

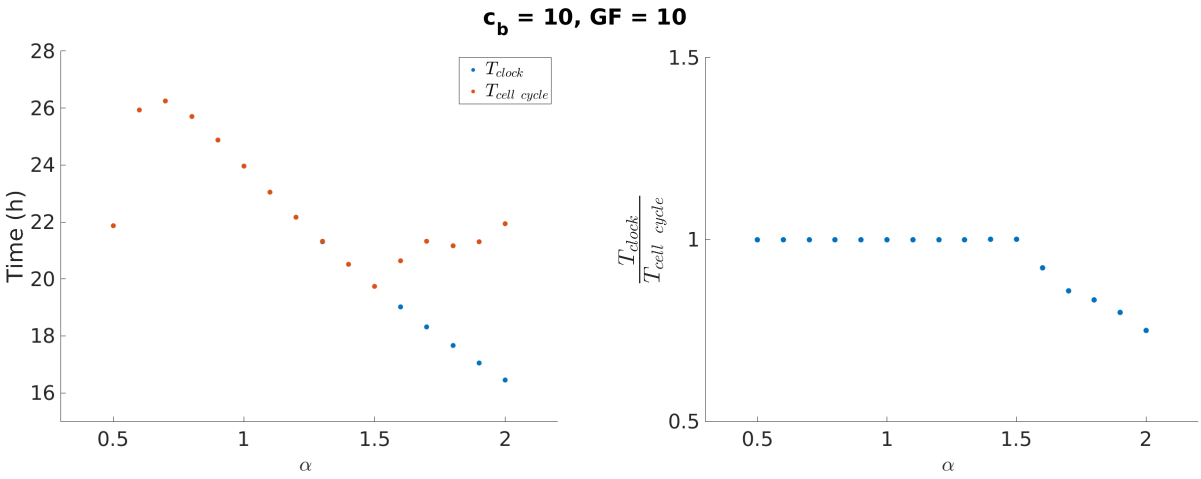

Figure 4.13: **Evolution of the oscillators period and synchronization state with α in the unidirectional coupling via clock-controlled wee1 activation.**
Tunning the parameter γ_{rev} is effective for period control: slowing down the clock period for $\alpha < 1$ effectively slows down the cell cycle, while speeding up the clock for $\alpha > 1$ results in a region ($\alpha > 1,5$) with a slower cell cycle than clock, thus representing two opposite forms of slowing down the cell cycle.

= 2 induces higher cell cycle periods than that of the original locking ($T_{cellcycle}$ = 33 h, for GF $\leq$ 5, whereas $T_{cellcycle}$ = 24 h with α = 1). As GF increases and the cell cycle speeds up the system enters a region of 1:1 period entrainment, followed by a region of $r_T > 1$. Though this strategy is successful in slowing down the cell cycle by inducing $r_T < 1$, the cell cycle is slower than the clock in only a narrow GF interval.

In contrast, Fig. 4.14 shows that tuning γ_{db} by changing β is less effective in changing the cell cycle period comparatively to the clock period, for a fixed value of GF. On the other hand, as variations in γ_{db} cause more dramatic changes in clock period, control of the cell cycle period to higher values than that of the coupled system (24 h) or that of the intrinsic cell cycle period (22 h, for GF = 10) may still be possible via this parameter.

To further analyze the effect of an increased DBP degradation rate γ_{db}, we vary GF in the region of oscillation for $\beta = 1,5$. Fig. F.8 shows that increasing γ_{db} leads to a wider GF region where the cell cycle is slower than the clock (compare to Fig. F.7). However, the region where the cell cycle is slower than 24 h ($\beta = 1$) is still small.

The combination of the two upgraded degradation rates is shown in Fig. 4.15. In this case, $\alpha = 2$ and $\beta = 1,5$ leads to a much slower cell cycle overall (T= 31,5 h) and a 1:3 period entrainment, while keeping GF =10.

In this Section, we have focused on controlling the cell cycle, because of its relation to cancerous cell's division rate, but it is important to note that healthy cells are likely to have same period clock and cell cycle internal oscillators and the state of $r_T \neq 1$ may be an indicator or precursor of cellular disease [116]. In this case, it would be helpful to explore forms of tuning

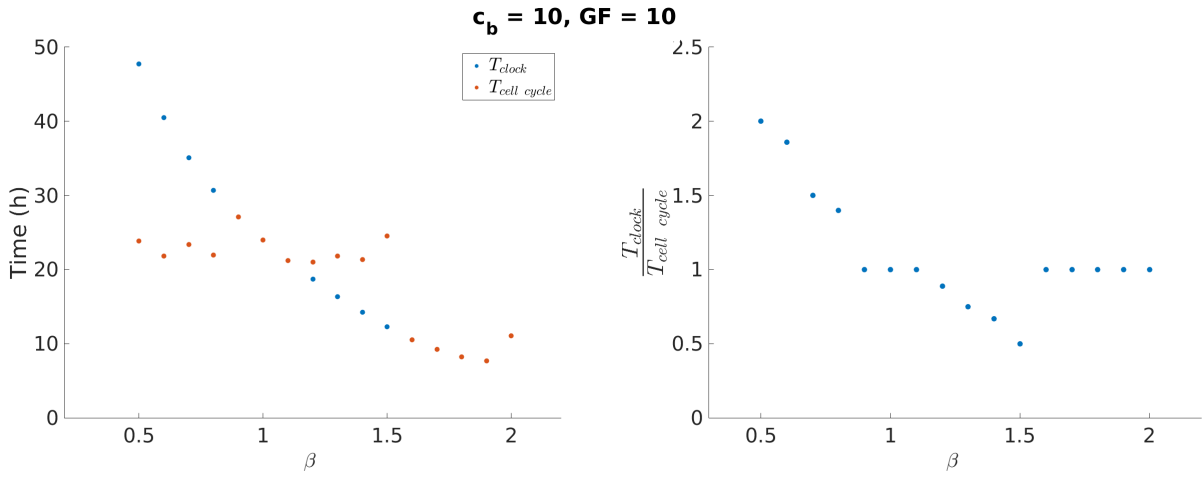

Figure 4.14: **Evolution of the oscillators period and synchronization state with β in the unidirectional coupling via clock-controlled wee1 activation.**
When tuning the parameter γ_{db} the period of the cell cycle changes less than that of the clock, breaking the 1:1 period-lock. Because the period of the clock varies greatly with γ_{db}, the cell cycle can only entrain to values close to its intrinsic period (of 22 h), oscillating around this value.

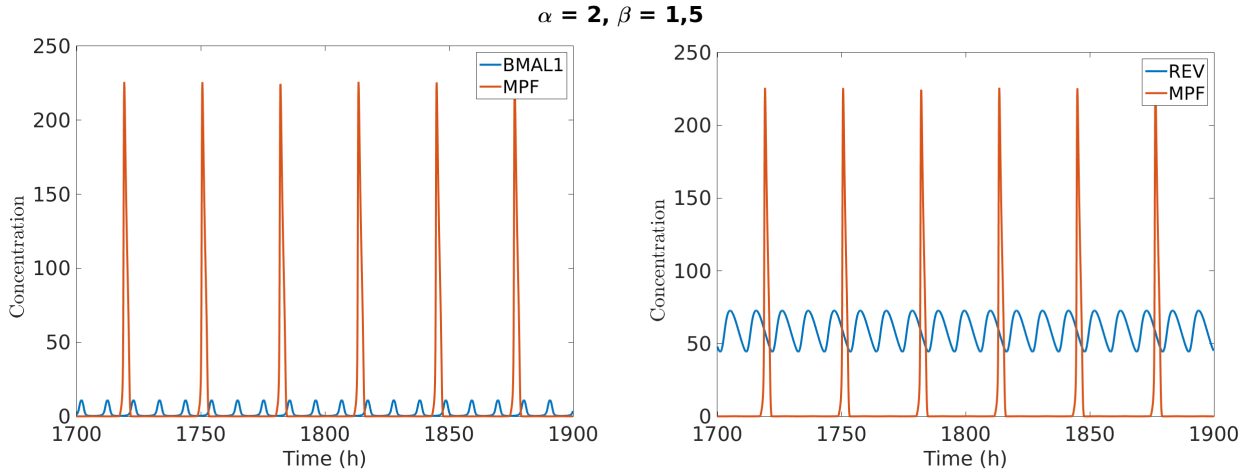

Figure 4.15: **Oscillation of clock and cell cycle variables for $\alpha = 2$ and $\beta = 1,5$ in the unidirectional coupling via clock-induced wee1 activation.**
Oscillations of MPF and the clock variables BMAL1 and REV with GF =10, $\alpha = 2$ and $\beta = 1,5$: the system locks in a 1:3 fashion: $T_{clock} = 10{,}5$ h and $T_{cell\ cycle} = 31{,}5$ h. The cell cycle is three times slower than the clock and overall slower than the intrinsic coupled oscillators' period (for $\alpha = 1$ and $\beta = 1$) of 24 h.

the coupling strength parameters in order to promote clock and cell cycle synchronization.

The intrinsic periods of the oscillators are the determinant factor for the system's period-lock state and promoting either the 1:1 synchronization state or other period entrainment ratios

is a consequence of tuning the periods of the two oscillators by changes in parameters or the introduction of inputs. In the next Section, we study the dynamical behavior of the bidirectional coupled system that puts together the two unidirectional forms of coupling here studied.

4.3 Bidirectional coupling

In this Section we investigate the oscillators' behavior under the simultaneous application of the two coupling mechanisms studied above (given by Equations 4.8 and 4.11). Fig. 4.16 shows a scheme of the system with bidirectional coupling.

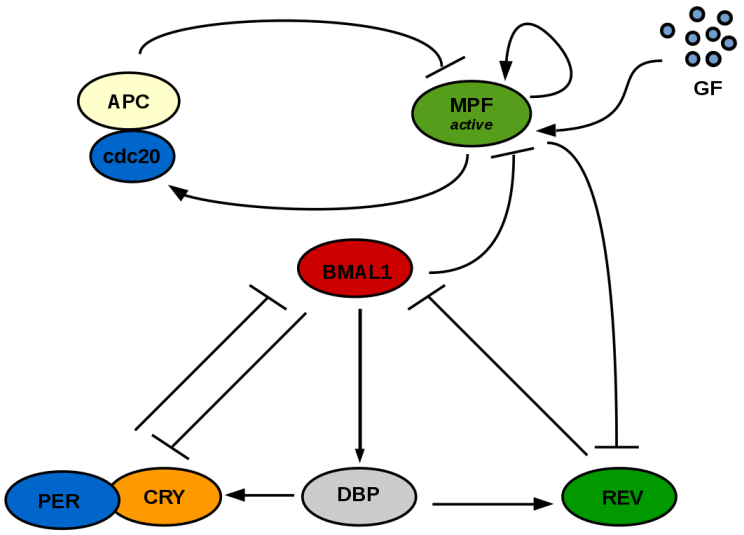

Figure 4.16: **Schematic of the bidirectional coupling mechanism.** Bidirectional coupling between the cell cycle and clock oscillators that includes the two previously studied forms of coupling: MPF phosphorylates REV inducing its degradation and BMAL1 represses MPF by promoting its repressor wee1.

First, we start by verifying the system's period response to variations of growth factor to be compatible with observations. Fig. 4.17 shows that entrainment occurs for values of the coupling strength parameters $c_m = 0.2$ and $c_b = 30$ and the trend of period decrease with GF fits well the four data points of Table 2.2 ([1], [4]) when making a correspondence between our parameter GF and % FBS in the real system (similarly to what was done in Fig. 2.7). In this case a 1 to 1 correspondence works well, i.e. $GF = \%FBS$. Furthermore, the phase difference between the peak of REV and the peak of MPF $\Delta\phi_{[REV,MPF]}$ is also shown in Fig. 4.17. Observe that $\Delta\phi_{[REV,MPF]}$ follows a very similar trend of the oscillators' period ($T_{oscillators}$). From [1] we know that REV-ERBα is phase-locked with the mitotic phase and $\Delta\phi_{[REV,MPF]}$ is 8,6 h for 20 h $\leq T_{oscillators} \leq$ 23 h and 7,1 h for 18 h $\leq T_{oscillators} \leq$ 20 h (see also[28]), i.e. $\Delta\phi_{[REV,MPF]}$ falls between 35 % and 45 % of the period. However, $\Delta\phi_{[REV,MPF]}$ of our experiments has higher values for 18 h $\leq T_{oscillators} \leq$ 23 h than experimental observations, falling somewhere between

50 and 60 % of the period. This may be due to our clock model being too simplistic, but perhaps more interestingly this observation raises the question of testing further coupling mechanisms to attempt to fit not just the systems' period response but also $\Delta\phi_{[REV,MPF]}$. In particular other coupling mechanisms that, similar to the mechanism of **cell cycle→ clock** coupling here proposed, involve MPF-controlled phosphorylation of an essential clock component are a subject of future work. Phase control in itself has not been a subject of focus in this work and is also a topic for further research. Nevertheless phase results of Fig. 4.17 give a broader view and prediction of the trend of $\Delta\phi_{[REV,MPF]}$ with the period of the system.

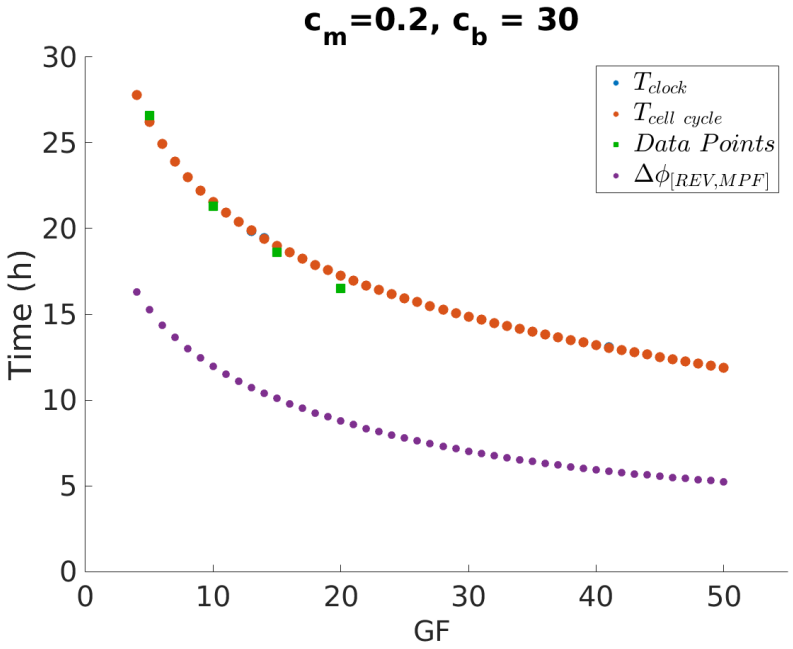

Figure 4.17: **Period response of the bidirectional coupled system.**
Our bidirectional coupling mechanisms are able to reproduce the overall observed oscillators' period response of acceleration with GF and result in a good fit to experimental data ([1], [4]) when making GF = % FBS, with $c_m = 0.2$ and $c_b = 30$. Phase difference between the peak of REV expression and MPF, $\Delta\phi_{[REV,MPF]}$, follows the same trend as the period of the system.

An oscillatory solution of a 1:1 synchronization state is shown Fig. 4.18 along with phase-portraits.

Furthermore, we extend the simulation of Fig. 4.17 so as to include the entire GF region of oscillation. Thus, Fig. F.9 shows that similarly to the two unidirectional coupling cases observed above GF is a control parameter for the oscillators' synchronization state that is constant by intervals. In this case, for $c_m = 0.2$ and $c_b = 30$, the system couples in 1:1 synchronization for the majority of GF values, while for high GF values ratios such as 4:3, 2:1 and even 2:3 appear. Given that in Fig. 4.17 we observed that a 1 to 1 correspondence between GF and % FBS accurately allows to reproduce the system's period response, the values of GF that in Fig. F.9 lead to $r_T \neq 1$ are outside of experimental feasible values of % FBS, which could mean that in

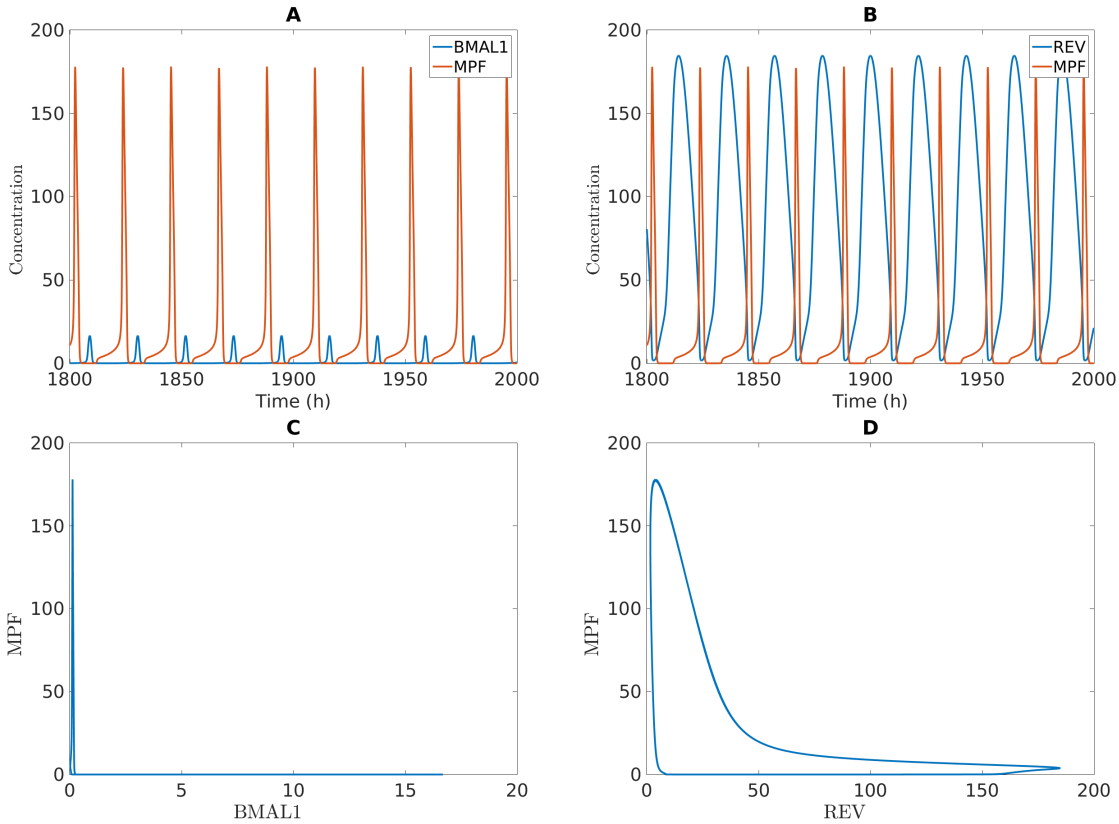

Figure 4.18: **An oscillatory solution with 1:1 period-lock in bidirectional coupling via MPF-conrolled REV degradation and BMAL1-induced wee1 expression.**
The solution for $c_m = 0.2$, $c_b = 40$ and GF=10 shows a 1:1 period-lock, with $T_{cell\ cycle} = T_{clock} =$ 21,5 h. Moreover, the system is phase-locked, with REV peaking 11,8 h after MPF.

the real system we would reach the saturation of GF increase before arriving at period-lock ratios differing from 1:1. On the other hand, because the period response doesn't depend exclusively on GF, but also on the coupling parameters c_b and c_m, the control of period-lock ratios in the real system by GF might still be possible for other combinations of c_b/c_m.

Following this discussion, Fig. 4.19 shows the system's synchronization state for varying c_m and c_b with fixed GF = 20. Patterns of entrainment include the Arnold Tongue for the 3:2 ratio. Because GF = 20 causes a faster cell cycle than clock, synchronization states aside from the 1:1 represent a slower clock than cell cycle. Additionally, the same study is shown for GF = 5, GF = 10, GF = 30 and GF = 40 in Figs. Fig. F.10, Fig. F.11, F.12 and F.13, respectively. For GF = 5 (Fig. F.10) the intrinsic cell cycle period is higher than the clock, which for certain combinations of c_m and c_b results in $r_T < 1$.

Furthermore, Fig. 4.20 shows the periods of clock and cell cycle for GF = 20 (same simulation as Fig. 4.19). Extremely long periods are present for certain regions of entrainment. One example from Fig. 4.20 is given in Fig. F.14, of a solution with a 1:1 synchronization and with $T_{clock} = T_{cellcycle} = 956$ h – the intervals without mitosis correspond to elevated REV expression.

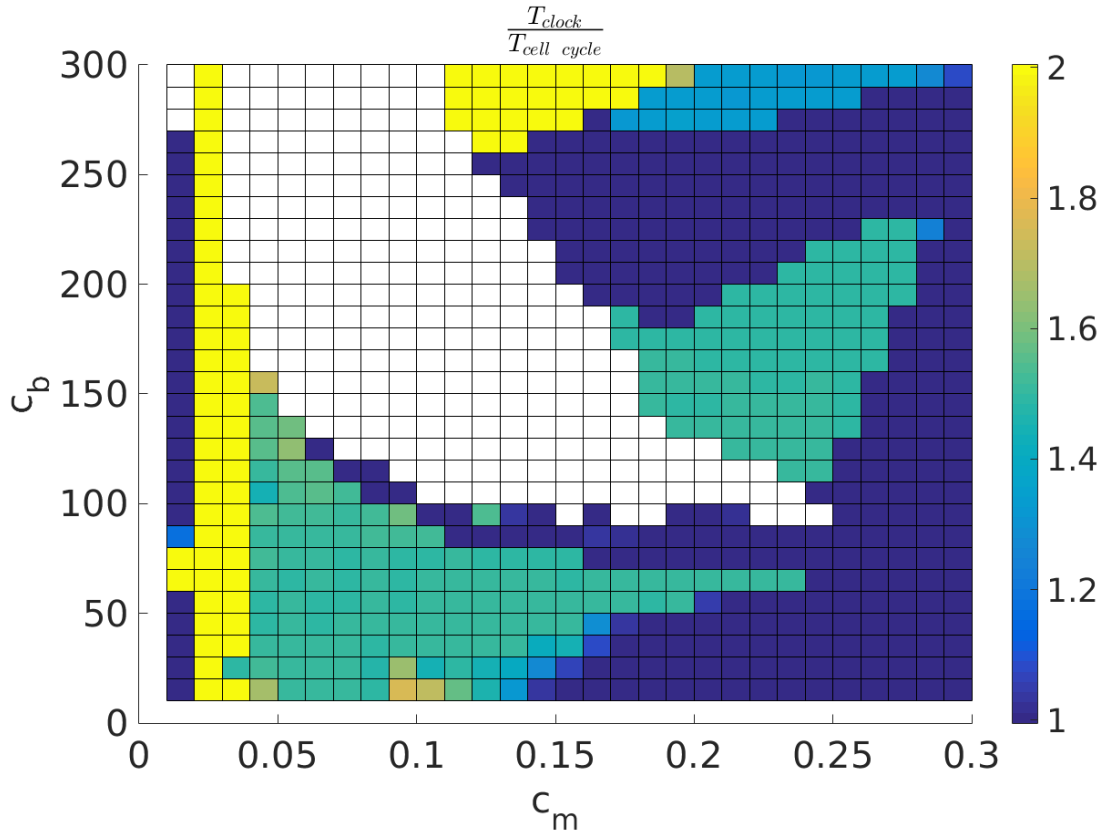

Figure 4.19: **Period-lock for different values of c_b and c_m with GF = 20.** Varying c_b and c_m for fixed GF = 20 results in different period-lock ratios. In the white region there is no oscillation. The 1:1, 3:2, 2:1 and 4:3 ratios are the most prevalent.

Moreover, in certain parametric regions the system has a complex behavior where long periods without mitosis occur – these also correspond to periods of high REV – followed by periods where some peaks of MPF and BMAL1 occur typically with $r_T \neq 1$. Fig. 4.21 shows one solution of this region, where $T_{clock} = T_{cellcycle} = 531$ h. Another example is given in Fig. F.15. Although these periods are not currently biologically viable, they are interesting as a model indicator: this model predicts that particular combinations of c_b, c_m and GF are an effective srategy for clock and cell cycle period control, capable of inducing a very slow mitotic rate. These coupling combinations represent simultaneous weak degradation of REV and strong/moderate repression of MPF (low c_m and high/medium c_b).

Next, we perform the Dex experiment, similarly to what was done above (Equation 4.9), by inputting a constant amount of Dex in the system with 1:1 synchronization and observing its period-lock response. Fig. 4.22 shows that the bidirectional coupling allows to recover the experimentally observed effect of Dex ([1]) in shifting the system from 1:1 to 3:2 period-lock.

Moreover, Fig. 4.23 shows the oscillators' period-lock response to different values of Dex for fixed GF = 10. Dex is a control parameter for the oscillators' synchronization state that is once again constant by intervals. Additionally, Fig. F.16 shows the evolution of the clock

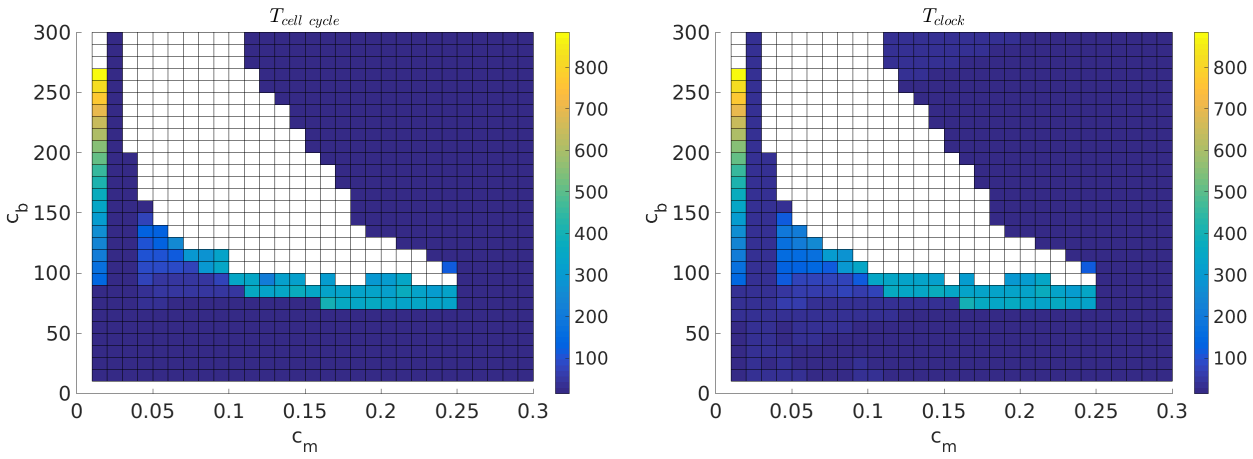

Figure 4.20: **Oscillators' period for different values of c_b and c_m with GF = 20.** Periods of clock and cell cycle for the same simulation as Fig. 4.19, when varying c_b and c_m for fixed GF = 20. In the white region there is no oscillation. Some small regions with very long periods appear.

and cell cycle periods for the same simulation as Fig. 4.23: Dex can either decrease or increase the period of both clock and cell cycle oscillators in the system with bidirectional coupling, in contrast to its effect in increasing the clock period when applied exclusively on the clock (Fig. F.4).

So far Dex has been introduced in the system as a constant input and the period-lock of the two different systems (with and without Dex) compared. To better reproduce experimental settings, where Dex is applied for some time and then removed, we will apply a Dex pulse and observe the transient period-lock change. Fig. 4.24 shows the period-lock response to a pulse of Dex applied over the course of two periods. Parameters of the system are the same as in Fig. 4.22 ($c_m = 0.2$ and $c_b = 40$, with fixed GF = 15), which result in a $T_{clock} = T_{cellcycle} =$ 18,9 h without Dex. A pulse of Dex = 40 is apllied during 1 hour and the period-lock response measured on the second and third cycles following the application of the pulse. As shown in Fig. 4.24, the system's synchronization response is dependent on the time of pulse application T_{pulse}, i.e. the system responds by shifting away from the 1:1 period-lock only when the pulse is applied at particular clock/cell cycle phases. More specifically, we have verified that the Dex response peak occurs when BMAL1 is up.

This could mean that cells would only be able to respond to a Dex pulse when at specific phases of these cycles. Conversely, as a population of cells contains cells that are asynchronous among themselves in their clock and cell cycle oscillations, this result provides insight on the observed existence of two groups of cells after Dex application mentioned in Section 1.3. Namely, that the existence of two period-lock groups of cells observed by Feillet et. al, (2014), [1] – one with cells locking in a 1:1 manner and the other with cells locking in a 3:2 manner – may be due to the clock or cell cycle phase cells are in at the moment of Dex application. To further explore this hypothesis, for instance by extending modeling to populations of cells, is a topic for future

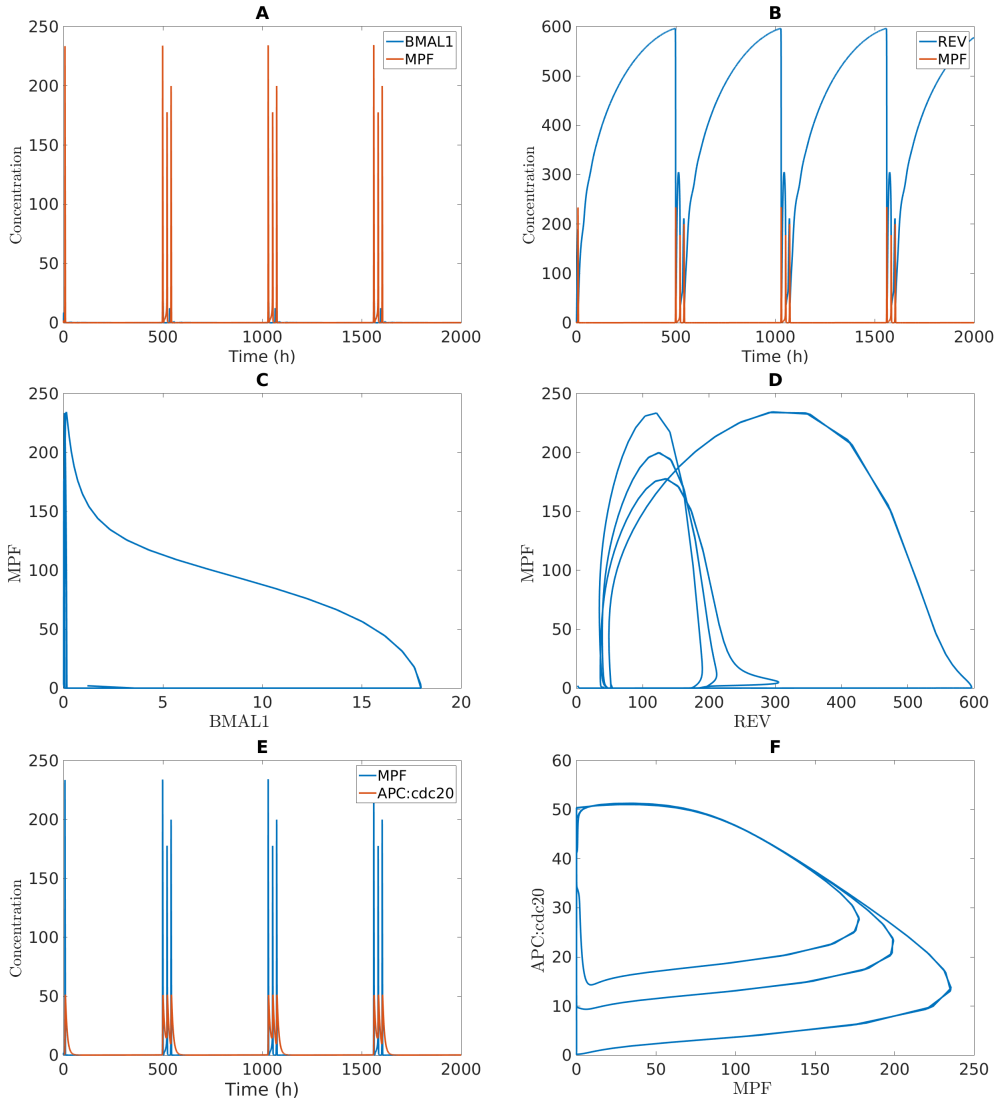

Figure 4.21: **An oscillatory solution with complex behavior and a very long period in bidirectional coupling.**
The solution for $c_m = 0.04$, $c_b = 70$ and GF=10 results in a very long period with a complex behavior, where three peaks of MPF occur every 531 h, interleaved by a long time interval where REV is up; $T_{clock} = T_{cellcycle} = 531$ h and in the region of MPF/BMAL1 peaks the two oscillators lock in 3:2 synchronization.

research. Furthermore, a small region of period-lock with $r_T < 1$ occurs in Fig. 4.24, which gives a prediction that for a small phase interval a Dex application could result in a slower cell cycle than clock, thus providing yet another strategy of cell cycle period control.

It is not clear, in theory, whether the clock or the cell cycle would be the preponderant oscillator in determining the synchronization state response. On one hand cells in the G0 phase of the cell cycle are known to be unresponsive to a variety of inputs and cells in M phase don't respond to Dex-treatment [114]. On the other hand, a recent crosstalk between REV-ERBα and

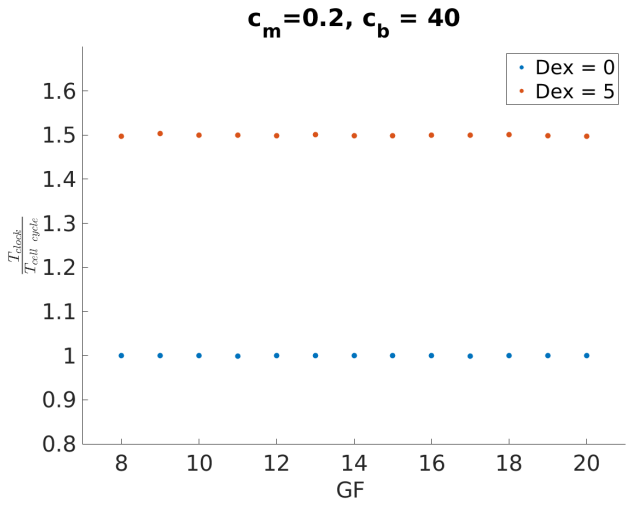

Figure 4.22: **A Dex input induces the system from a 1:1 to a 3:2 period-lock in bidirectional coupling.**
With $c_m = 0.2$ and $c_b = 40$ the system locks in 1:1 synchronization for $8 \leq \text{GF} \leq 20$. Inputting Dex $= 5$ shifts the system to a 3:2 period-lock ratio for the same values of GF.

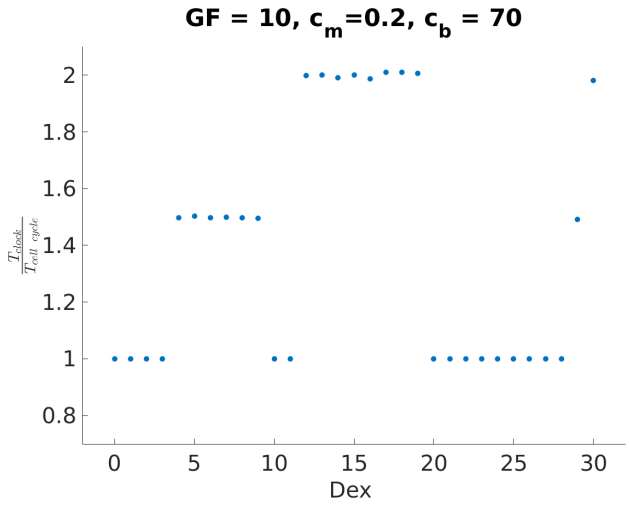

Figure 4.23: **Period-lock response to different values of Dex**
Different values of the input Dex result in different period-lock ratios. For $c_m = 0.2$, $c_b = 70$ and GF =10 synchronization states are constant by intervals and the 1:1, 3:2 and 2:1 period-lock ratios appear.

glucocorticoid receptor signaling has been uncovered [115]. Therefore, both systems could play a role in the resulting synchronization state of a cell under the application of Dex or other inputs. In our work, we found that the system is Dex-responsive at the molecular phase where BMAL1 is up and PER:CRY is down. This makes sense intuitively, as is when PER:CRY is down that an additive input in its expression would result in bigger changes, whereas when PER:CRY is

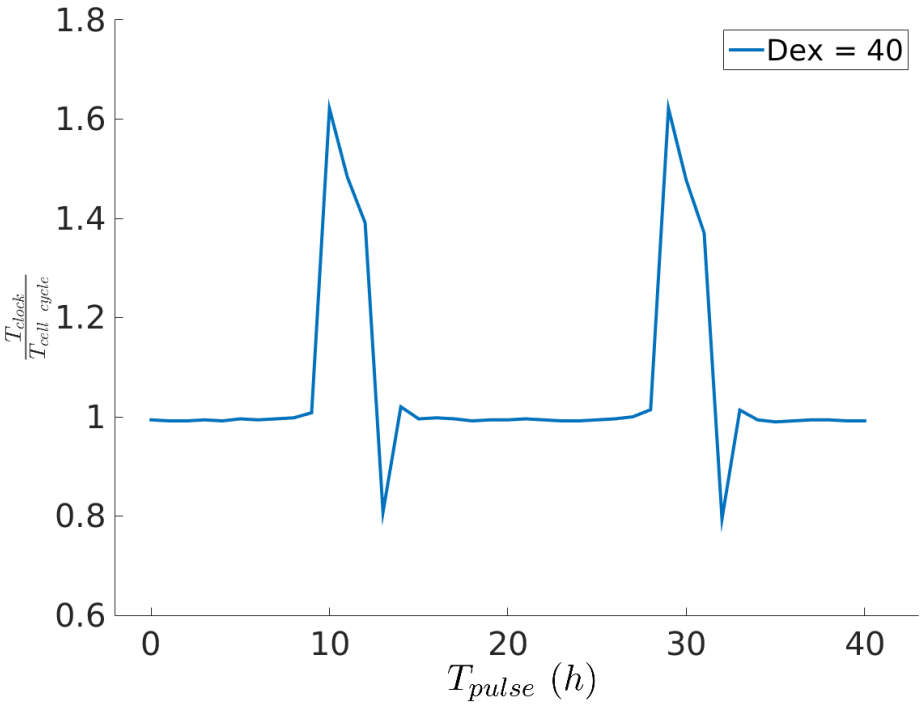

Figure 4.24: **Period-lock phase response of the bidirectional coupled system.** An 1 hour Dex pulse is applied over the course of two periods (i.e. during 38 h). Parameters are $c_m = 0.2$ and $c_b = 40$ and GF =15. The system's synchronization state changes only for certain times of pulse application T_{pulse}. The responsive phase corresponds to increasing BMAL1.

already up adding more won't affect the system as much, specially because in this model mean values of PER:CRY are much higher than mean values of BMAL1. An experimental test that would help to further increase the understanding of this topic would be to observe whether or not Dex-induced synchronization of cellular clocks in a population is indeed occurring in cells of the 1:1 period-lock group, as synchronization points to a Dex-responsive clock, which would in this case highlight the role of the cell cycle phase in the period-lock response. From this analysis, the time of pulse application T_{pulse} is a new control parameter for the synchronization state.

Furthermore, this insight may be relevant for a variety of chemical therapies, including apoptosis-inducing chemotherapies that are usually efficient for only a part of the cell population, with a percentage of cells remaining resistant. In particular, a group of apoptosis-resistant cells is observed *in vitro* after repeated exposure to death-inducing ligands: each re-exposure of the surviving group of cells results always in fractional killing [113]. This is thought to be due to cell-to-cell variations of protein levels, though the mechanisms behind the fractional death response remain unclear [113]. In this regard, our results uncover a possible role of the clock and cell cycle systems in controlling the response of cells to inputs, whether this response is a change in period or another physiological response, such as apoptosis. Moreover, this idea relates the increased efficiency demonstrated by chronotherapies *in vivo* over normal therapies to clock/cell

cycle time-dependent responses.

Finally, Fig. 4.25 shows the same simulation of Fig. 4.24 at a later point in time (1000 h after the pulse), showing that after a transient shift in synchronization state, the system returns to the 1:1 period-lock. As mentioned in Section 1.3, the different period-lock ratios observed by Feillet et al., (2014), were considered to be caused by the existence of multiple attractors [1], i.e. that the change caused by Dex occurs because the system shifts to a different limit-cycle, with each ratio of period-lock corresponding to a different attractor. In this regard our results contradict this hypothesis, pointing instead to the Dex-induced period-lock change being transient. Experimental observation of cells after the application of the Dex pulse was done over the course of three days [1], which can easily fall within the transient period. For this reason, a longer observational time would help to clarify the existence (or non-existence) of attractors. Additionally, Fig. F.17 shows two time series for different values of T_{pulse} and Fig. F.18 shows a longer time series with the return to 1:1 synchronization.

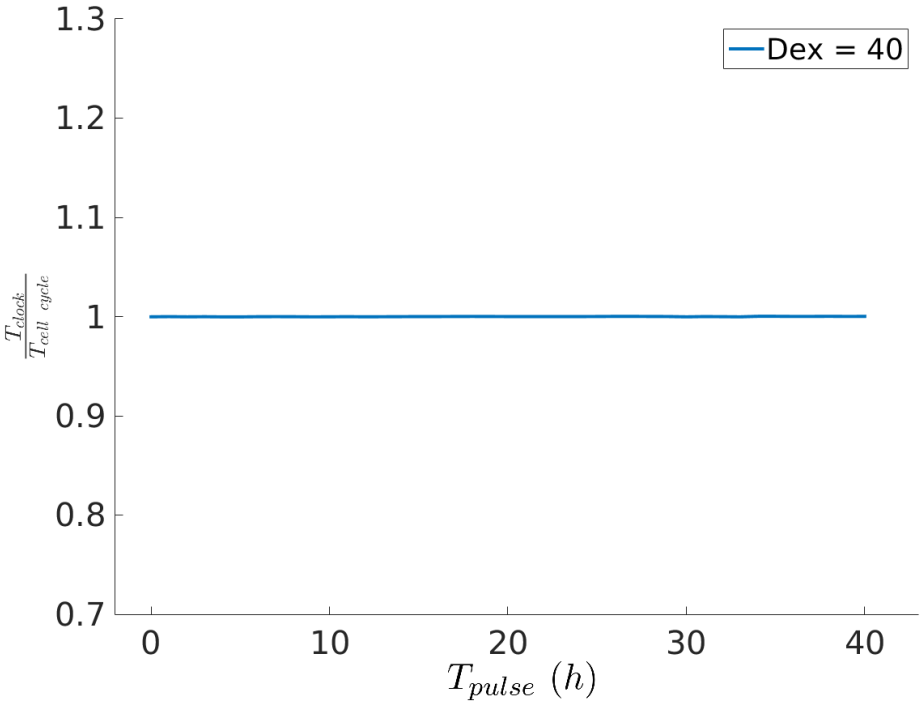

Figure 4.25: **Convergence to the 1:1 period-lock state after the application of a Dex-pulse at different circadian phases over the course of two periods.**
1000 hours after the shift caused by the Dex pulse (observed in Fig. 4.24) the system has returned to 1:1 synchronization: changes in period-lock caused by Dex input are transient.

A similar conclusion to ours is given in the work of Traynard et al., (2016), albeit in the context of non-recovery of experimental period-lock ratios [28]. By contrast, here we consider the occurrence of rational synchronization ratios and the existence of multiple attractors as two separate and different questions. Thus, in this work, we verify the occurrence of specific

experimental synchronization ratios in agreement with the work of Feillet et al.. (2014), while at the same time demonstrating a transient nature of these ratios when occuring in response to a pulse, which is in disagreement with the hypothesis of that same work [1]. Following this reasoning, we further searched for multiple attractors in our system by changing the initial conditions under the same parameters as the simulations of Figs. 4.24 and 4.25, without Dex, and didn't find multiple attractors, though numerical analysis can't be conclusive to prove their non-existence, due to the impossibility of exploring the entire phase space.

Finally, our observations also indicate that a lasting effect of altered synchronization state can be achieved by means of a constant Dex input (of a smaller value than that given in a pulse).

4.4 Coupling via GF-induced inhibition of R-box

In this Section we propose a different mechanism for the coupling of cell cycle and clock. One of our goals is to reproduce and understand the dynamical interactions behind the phase-lock experimental observations of Feillet et al., (2014), described in Section 1.3, where observations show increasing amounts of GF speed up both the cell cycle and the clock in a 1:1 period-lock state [1]. Thus, here we study GF as a common input to both oscillators. So far we have assumed a coupling hypothesis where GF acts on the cell cycle that in turn acts on the clock. Here, we take a look at a pathway connecting GF with the clock, such that GF is included in the model as a direct clock input.

Growth factors promote cyclin D, a non-essential cell cycle cyclin that is active when in a complex with either cdk4 or cdk6, via β-catenin mediated pathways [117]. Despite cyclin D being approximately constant during the cell cycle, it is a precursor for the activation of the subsequent cyclins. However, because cyclin D is non-essential (its deletion mutants still have a functioning cell cycle) and considering cells can't divide without GF, there must be other ways for GF to affect the essential cell cycle elements, namely the cyclin B-cdk4 complex (MPF). In our cell cycle model MPF responds directly to GF – an approximation that allows focusing on this exclusively essential cell cycle species.

The cyclin D-cdk4 complex is known to negatively regulate PGC1-α, by promoting its repressor GCN5 [102]. PGC1-α is an important clock component, whose role in promoting binding of ROR to R-box has been shortly discussed in the previous Chapter. As such, the pathway GF $\rightarrow$ cyclinD-cdk4 $\rightarrow$ GCN5 —|PGC1-α is of interest in the study of GF as a direct input to the clock. The model term of R-box dependency on ROR has been simplified to a constant in the previous Chapter (see Section 3.1.4). Nevertheless, the effect of GF as a repressor of R-box via the cyclin D/PGC1-α pathway can be introduced by making the change $V_R \rightarrow V_R \frac{k_s}{k_s+GF}$. R-box now becomes:

$$R_{box} = V_R(\frac{k_s}{k_s + GF})\frac{k_{Rr}^2}{k_{Rr}^2 + [REV]^2} \tag{4.12}$$

The hypothesis introduced in Equation 4.12 raises the question of whether or not a certain amount of GF is needed for clock oscillation, as cells in experimental settings usually require

some growth factor (often in the form of % of FBS) to be alive and functional. Because we built and calibrated our model based on the established assumption of a cell autonomous clock, the removal of GF (from Equation 4.12) doesn't affect clock oscillations. Observations clearly show a dependency of both cell cycle and clock periods on GF [1], whilst not being clear whether or not the influence of GF on the clock involves essential components of the cell cycle, such as MPF. These observations provide some basis to consider the hypothesis of clock oscillation being dependent on the presence of GF, which is largely in disagreement with the long held assumption of circadian clock oscillatory autonomy. Nevertheless, if that were to be the case, in our model this could be achieved by adjusting the parameter V_R to a higher value, incompatible with oscillations at GF =0, and then modulate V_R by the presence of GF (see Equation 4.12). However, for simplicity, we will assume GF as a clock input that can control its period but it's still not required for oscillation. This modeling implies that GF = 0 yields the 24 h intrinsic clock oscillation that has been the basis of our clock studies so far.

For $k_s = 100$, Fig. F.19 shows the evolution of the clock period with GF when introducing the GF repressing effect (Equation 4.12): the clock period decreasing for increasing GF, which is in agreement with observations [1]. Clock oscillations are maintained in the entire GF region of cell cycle oscillation ($4 \leq \text{GF} \leq 80$).

Next, we study the coupled system that includes the established interaction of BMAL1 repression of MPF via wee1, studied above. A schematic of the coupled system is shown in Fig. 4.26. Coupling is in this case unidirectional from the clock to the cell cycle achieved by introducing the term $-c_b[BMAL1]$ that multiplies the term denoting the wee1-mediated inactivation of MPF (Equation 4.11) and GF is a common input.

We start by analyzing the effect of the coupling strength parameter c_b on the oscillators' synchronization state. Fig. 4.27 shows a wide region of 1:1 period-lock for $c_b = 50$ differing from the dynamics with $c_b = 10$ that by contrast yield a narrow region of 1:1 period-lock ($6 \leq \text{GF} \leq 21$) followed by a region where the ratio of clock to cell cycle period increases to values close to 1, or a state of "quasi-entrainment", approaching the 1,25 period ratio. This behavior differs from that of the other forms of coupling previously explored in the sense that, in this case the *devil's staircase* pattern is not visible (r_T is not constant by intervals), but rather the transition between period ratios is smoother, while simultaneously maintaining a certain stability around the 5:4 synchronization state. Interestingly, this dynamical behavior though quite different from that of the previous coupling mechanisms still reproduces desired properties, such as a slower clock than cell cycle and the stabilizing near a 5:4 period-lock that adequately compares to the experimental observations of Feillet et al. (2014) [1].

A more complete view of the dynamical behavior of this system is shown for $c_b = 10$ for the entire GF region of cell cycle oscillation in Fig. 4.28 (left), where the absence of period-lock "jumps" is more visible. More importantly, a Dex input alters slightly the system's behavior, in particular shifting the changes of period-lock dynamics to lower values of GF (Fig. 4.28 (right)), namely the presence of Dex narrows the 1:1 synchronization region of GF response. This "shift to the left" effect is similar to that observed for Dex application in the coupling mechanisms studied above and provides an explanation for the experimental observations of

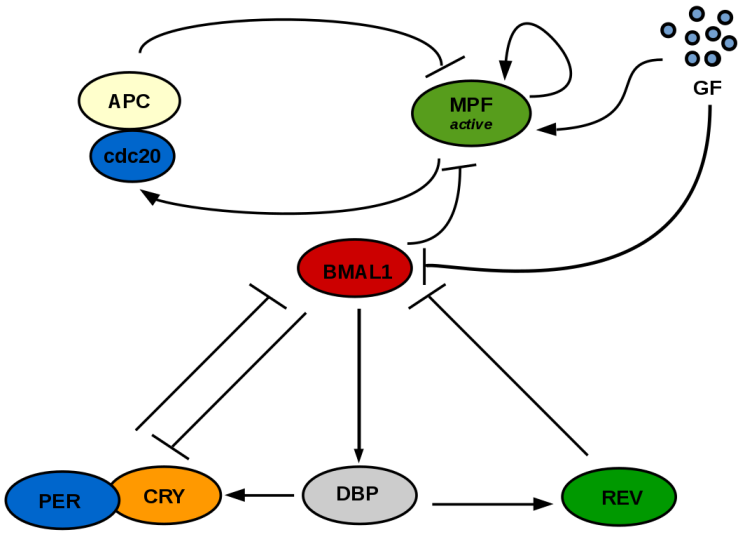

Figure 4.26: **Schematic of the GF-responsive clock system coupled via BMAL1 repression of MPF.**
GF controls both the cell cycle and the clock: GF represses R-box (at the BMAL1 promoter) via the cyclin D-cdk4/$PGC1_\alpha$ pathway. Coupling from the clock to the cell cycle is made via BMAL1 repression of active MPF (via the wee1 pathway).

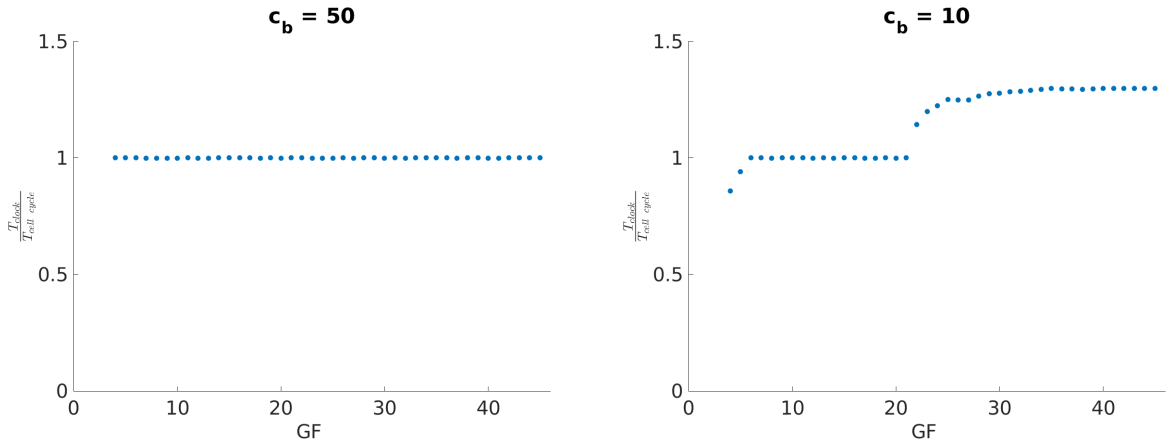

Figure 4.27: **Variation of period-lock with GF for two values of c_b.**
With $4 \leq GF \leq 40$, for a fixed value of $c_b = 50$ the system shows 1:1 period lock, while for $c_b = 10$ a region of 1:1 period-lock is followed by a region where clock to cell cycle period ratios are above but near 1 ("quasi-entrainment") stabilizing around the 5:4 synchronization state.

Feillet et al. (2014), where introducing Dex leads to period-lock period ratios differing from 1 [1]. Thus, assuming GF as a clock input in conjunction with the unidirectional clock-to-cell cycle coupling is also successful in reproducing experimental observations and may provide an alternative or complementary explanation for the oscillators' behavior to that of cell cycle-mediated phosphorylation of some clock element, as studied above for the MPF phosphorylation

of REV.

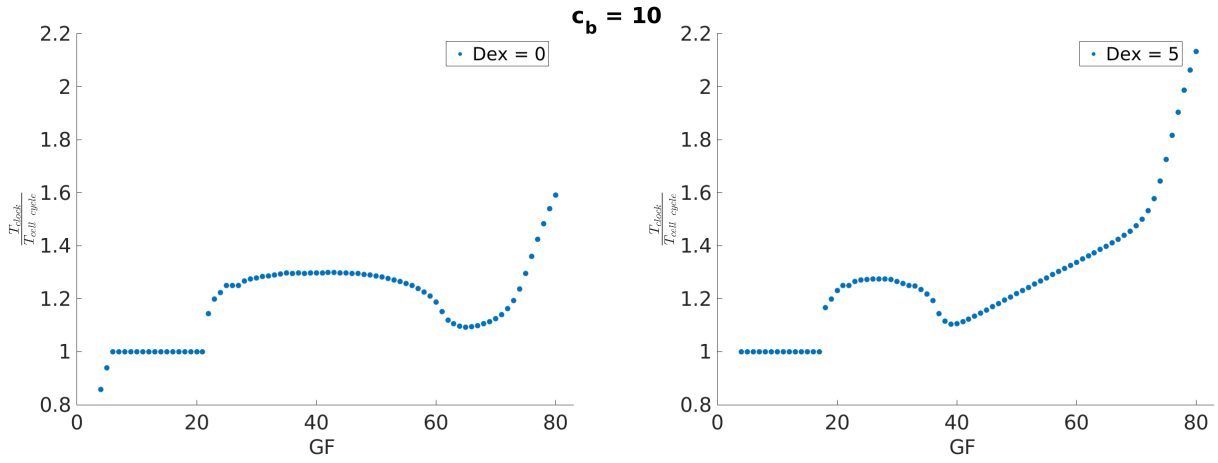

Figure 4.28: **Dex input reduces the required GF value for changing the period-lock state.**
For $c_b = 10$ the ratio of clock to cell cycle period is observed with and without Dex as GF varies between 4 and 80: the presence of Dex causes dynamical changes in the system's synchronization state. In particular, inputting Dex ends the 1:1 period-lock state for a smaller value of GF (without Dex the change in dynamics occurs at GF > 20 and with Dex at GF < 20).

Additionally, Fig. 4.29 shows the period of the system as GF varies, for $c_b = 10$ with no Dex, where as expected for the unidirectional coupling we observe the cell cycle adapting its period to that of the clock. This is a situation with similarities to that of the unidirectional clock to cell cycle coupling (see Section 4.2) and raises the question of the possibility of cell cycle period control via tuning of the clock period. Thus, we test this possibility by making $\gamma_{rev} \to \alpha\gamma_{rev}$ as above and varying α for values around 1, see Fig. 4.30 . In this case, we can vary $0.6 \leq \alpha \leq 2{,}5$ and observe that slowing down the clock by decreasing α effectively slows down the cell cycle while maintaining 1:1 synchronization. For $1 < \alpha < 1,4$ we observe that speeding up the clock results in a sped up cell cycle in 1:1 period-locking and for $\alpha \geq 1,4$ the system breaks out of the 1:1 synchronization state and states of $r_T < 1$ appear again in a step-like form, where the cell cycle is slower than the clock. Thus, tuning the parameter γ_{rev} is also successful in cell cycle period control and in the synchronization of the coupled oscillators in the unidirectional clock to cell cycle coupling with a GF-responsive circadian clock.

Simulations have shown very different dynamic behavior between this form of direct GF influence on the clock and the other where GF acts on the clock via MPF. A step-like response with intervals of constant period ratio was present only in the coupling via MPF, while a continuous period ratio response was obtained, in the coupling with GF as a common input. However, both simulations yield period-lock ratios that are compatible with experiments (3:2 and 5:4 respectively) and reproduce the impact of Dex as a promoter of $T_{clock} > T_{cellcycle}$ (period-lock ratios higher than 1). Because living cells have a large amount of interactions and pathways (including redundant pathways and species) it is not clear which of these two experimentally established interactions is preponderant and whether this is influenced by the cellular (and extracellular)

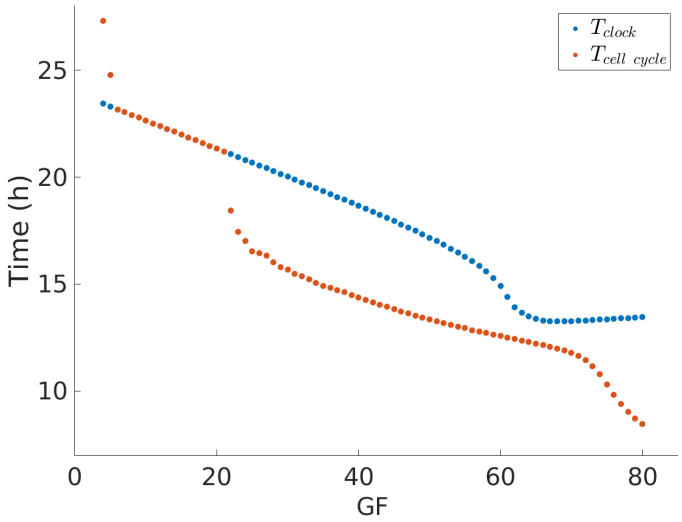

Figure 4.29: **Periods of clock and cell cycle oscillators as GF varies in the GF-responsive clock system coupled via BMAL1 repression of MPF.**
For $c_b = 10$ and Dex $= 0$ the periods of the clock and cell cycle oscillators are shown in the GF region of cell cycle oscillation ($4 \leq$ GF ≤ 80). As the coupling is done from the clock to the cell cycle, it is the cell cycle that may adapt its period to that of the clock; both systems respond to GF, but an approximately constant relation between them ($r_T = 1,25$) is observed for the middle region of GF.

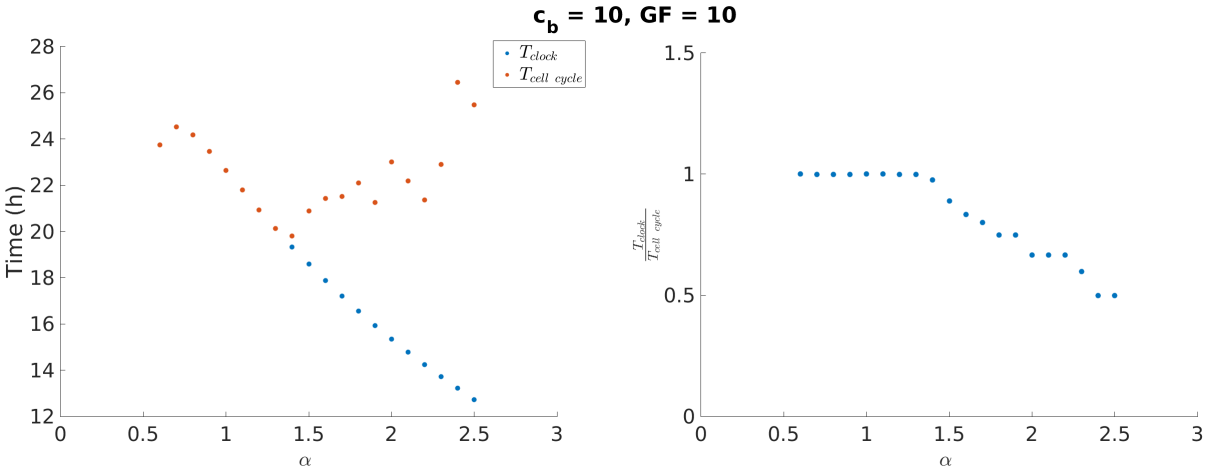

Figure 4.30: **Variation of clock and cell cycle periods and period-lock ratio with the parameter α in the system coupled via BMAL1 repression of MPF with a GF-responsive clock.**
Slowing down the cell cycle is possible either by slowing down the clock (that maintains the 1:1 synchronization) or by speeding up the clock and inducing the breaking of the 1:1 synchronization.

context (metabolism, signaling). Thus, experimental observations where GF is varied in a larger

interval with and without Dex (or other period tuning inputs) would allow comparison with our simulations for both cases and to understand which one of these interactions more accurately reproduces the behavior of the system and is thus more relevant.

4.5 Final Discussion

In this Chapter we have observed the dynamics of our models of the mammalian cell cycle and cellular clock under different forms of unidirectional/bidirectional coupling. Our work recovers the emergence of rational period-lock ratios in unidirectional and bidirectional coupling. Differing approaches have been taken in other studies. We next discuss two main articles.

Gérard and Goldbeter, (2012), [26], for instance, have analyzed three different coupling mechanisms of unidirectional **clock** $\rightarrow$ **cell cycle** coupling: CLOCK:BMAL1-mediated wee1 activation, CLOCK:BMAL1-mediated c-Myc repression and REV-ERBα-mediated repression of the cdk inhibitor p21. They have verified the size of the period entrainment region under these three different forms of unidirectional coupling and that combining multiple forms of coupling doesn't necessarily increase this region. Furthermore, for entrainment via CLOCK:BMAL1-induced wee1 expression they found a parametric region with a complex MPF dynamics that is similar to what we found in Section 4.3 for the bidirectional coupling (where the wee1 interaction is also incorporated), albeit in our case BMAL1 followed a similar cycle as MPF and this dynamics was associated with a very slow mitotic rate, while in the work of Gérard and Goldbeter, BMAL1 was expressed in the period of low MPF and this complex dynamical behavior was associated with a faster mitotic rate [26]. More importantly, their approach differed from ours in that they opted for detailed models incorporating more molecular interactions, while we favored reduced models that allow to understand which cellular mechanisms are essential.

Unidirectional **cell cycle** $\rightarrow$ **clock** coupling, in its turn, has been studied by Traynard et al., (2016), via the incorporation of transcription regulation of clock genes during the mitosis stage [28]. Their approach is fairly different from ours in that they focus on transcription regulation, while we focus on MPF phosphorylation activity. Their model is centered on the observed transcription activation of clock genes at the mitosis stage and proposes a role of MPF in this regulation, using a periodic coupling parameter, while our model is based on the established kinase activity of MPF in a particular experimentally verified interaction of REV-ERBα phosphorylation. Another difference is that all of our coupling mechanisms are achieved by constant multiplicative terms and, in our study, it is the natural periodicity of variables that represents the different molecular phases (ex: MPF up represents the mitotic phase, etc.) [28]. Furthermore, our **cell cycle** $\rightarrow$ **clock** coupling mechanism represents a degradation of REV-ERBα by the MPF, while one of their coupling mechanisms represents REV-ERBα gene activation during mitosis. Even though these are opposed forms of regulation, simultaneous co-existence of both mechanisms isn't, in our opinion, contradictory, as often such complex levels of regulation exist in mammalian cells. In fact, not yet identified factors may tune the balance between these two opposite regulations. In addition the mechanism proposed by Traynard relates to gene (or protein) synthesis, whereas we considered a posttranslational regulation

(ubiquitination and degradation of the REV-ERBα protein). Therefore, both mechanisms may well represent fine tuning of REV-ERBα expression/activity regulation at the G2/M transition. Furthermore, as discussed in Section 4.3 the conclusions of Traynard et al., (2016), about the Dex period-lock response being transient are similar to ours [28]. However, in their work the rational period-lock ratios were not obtained, which was interpreted as demonstrating non-existence of multiple attractors. In our work, the appearance of period-lock ratios is understood as a separate issue from the existence of multiple attractors. Moreover, in their work simultaneous fitting of period and phase response is possible and achieved by adjusting the coupling parameters, while in our work coupling parameters affect only the synchronization state (and thus the period) of the oscillators.

A main result of our work is that there is more than one way of controlling the synchronization state of the oscillators. Specifically, a 1:1 period-lock can be obtained when the intrinsic periods between the oscillators are close to each other or when the coupling strength is high. Conversely, period-lock ratios that differ from 1 ($r_T \neq 1$) can be obtained when the periods of the oscillators are further apart or when the coupling is weak. In particular, inputs such as GF, Dex or single-parameter changes induced changes in synchronization state by changing the proximity between the periods of the oscillators. This in turn can be used to control the period of one oscillator by applying modifications to the other oscillator.

A common observation to all of our results, in the various types of coupling studied in this Chapter, is that GF is a control parameter to the synchronized state of the oscillators. This in theory predicts that synchronization states differing from 1:1, such as the experimental results described in Section 1.3, could be reproduced by further increasing GF. However, this verification is contingent upon the GF region of $r_T \neq 1$ falling within the physiological limit of GF increase in cells, which we can't yet predict, because this depends on the real period response of the oscillators to GF. Nevertheless, it would be interesting to analyze period-locking (and phase-locking) in cells grown in high GF (% FBS > 15) and with no Dex, as for example the 20 % FBS culture was tested only in the presence of Dex (see Section 1.3). On the other hand, if the natural coupling between the oscillators is strong enough the oscillators will remain in 1:1 period-lock even for increasing GF.

The hypothesis we made in the discussion of Appendix B of the importance of the dual state clock property in modeling clock response to Dex was validated in this Chapter. In particular, observations of a Dex pulse on the bidirectional coupled system reveal a sensitivity of the CLOCK:BMAL1 molecular phase, where there is no PER:CRY, in period-lock response, while when PER:CRY is up the system's period-lock doesn't change. In contrast, because the 3:2 period-lock occurs when Dex is introduced in the unidirectional **cell cycle** $\rightarrow$ **clock** coupling, the idea that Dex introduction would be a form of indirect action on the coupling mechanism is not verified, but rather Dex acts on the synchronization state of the oscillators by changing the clock period (when given as a constant input). The period-lock state is dependent on the relation between the intrinsic periods of the two oscillators, as well as on the strength of coupling.

In this Chapter, we investigated plausible molecular mechanisms for the coupling between the cell cycle and the circadian clock. A general idea explored in the unidirectional **cell cycle**

→ **clock** coupling is that MPF phosphorylates an essential clock component. This is compatible with observations on NIH3T3 cells denoting a preponderant action of the cell cycle on the clock [1] [30]. The particular mechanism modeled here was that of MPF-induced REV degradation (observed experimentally). This resulted in entrainment and allowed to recover the effect of Dex application. More than the validation of this particular coupling mechanism, these results reinforce the validity of a broader class of coupling mechanisms involving the phosphorylation of a core clock component by the essential cell cycle machinery.

Furthermore, Dex application as a PER/PER:CRY input recovered the experimentally observed change in synchronization state ($\{r_T = 1\} \rightarrow \{r_T > 1\}$) more faithfully in the **cell cycle** → **clock** coupling than in the **clock** → **cell cycle**, which again points to the increased relevance of the first coupling mechanism for the observations in Dex-treated cells. And an input I_B applied on BMAL1 had the opposite effect of Dex: $\{r_T > 1\} \rightarrow \{r_T = 1\}$, because inputs at the two main clock phases induce opposite effects on clock period. Unidirectional **clock** → **cell cycle** coupling in turn centered on the observed BMAL1-induced wee1 activation, which was modeled as an MPF repression. This allowed entrainment and period control of the cell cycle by means of single-parameter changes in the clock system.

In the bidirectional coupling combining MPF-mediated REV degradation and BMAL1-mediated MPF repression via wee1 activation we found a particular parametric region where both clock and cell cycle showed an oscillatory regime of very long periods. In this region, the dynamics exhibited a time interval of oscillation interleaved with a time interval without oscillation, providing a promising strategy for period control. Moreover, GF-period control fits well to data points and the effect of the Dex input in shifting the system from 1:1 to 3:2 synchronization is also recovered in the bicoupled system. Additionally, we found the system's response to a Dex pulse to be transient, which contradicts the multiple attractor hypothesis established by Feillet et al., (2014), [1]. Period-lock response to a Dex pulse applied at different times revealed the existence of a responsive and a non-responsive phase regions, which we relate to the existence of two populations of cells observed by Feillet et al., (2014), [1]. Thus, not only the amount of Dex and the duration of the pulse are control parameters for the system's dynamical response, but also the time of pulse application as it relates to the the clock/cell cycle oscillators' phase a at the time of Dex application. This in a broader sense may be extrapolated to any input/output cellular response, with possible implications for the improvement of chronotherapies.

Furthermore, we have modeled two very different forms of GF influence on the clock: one via the cell cycle, where MPF phosphorylates and induces degradation of the essential clock element REV and the other where GF acts on the clock via a pathway involving the non-essential cell cycle complex cyclin D/cdk4, both experimentally established interactions. Both models result in different dynamical behavior that nevertheless allows to reproduce experimental results whereby Dex induces period-lock states of $r_T > 1$. Dex application in the unidirectional **clock** → **cell cycle** with a clock that responds directly to GF also results in inducing $r_T > 1$, which is compatible with experimental observations. Moreover, cell cycle period control was also verified by inducing single-parameter changes in the GF-responsive clock.

Finally, for all coupling mechanisms we have observed that control parameters allow to shift

the system between different synchronization states. In general Dex induces a change similar to that of GF, because these two inputs both separate the period of the oscillators: GF by accelerating the cell cycle and Dex by slowing down the clock, leading to a $r_T > 1$ state. Diminishing the coupling strength in a situation where the clock is slower than the cell cycle has a similar effect. Thus, the GF point of synchronization state change depends on the strength of the coupling between the oscillators as well as on the proximity of the periods of the oscillators. Inputs such as Dex have the effect of decreasing the GF value required for period-lock dynamical change. This provides an explanation to the experimental observations of Feillet et al., (2014), (described in Section 1.3) that have influenced this thesis [1].

5

Conclusions and Perspectives

This dissertation aimed to expand the understanding of the coupled cell cycle and mammalian circadian clock oscillators. As exposed on Chapter 1, the observations of Feillet et al., (2014), establish evidence for a cell cycle control on the clock [1]. With the aim of reproducing some of these observations as well as of understanding which characteristics of the mammalian cell cycle and circadian cell clock oscillators are relevant for synchronization state determination we used ODEs to build non-linear dynamical models of the two oscillators, on Chapters 2 and 3, and applied our models to the study and exploration of coupling mechanisms and interconnection between the oscillators, on Chapter 4.

5.1 Conclusions

On Chapter 2 we identified and modeled the main dynamical processes of the mammalian cell cycle. Our model is based on post-translational modifications of the mitosis promoting factor (MPF) and on its degradation by the APC:cdc20 complex ([4]). This model was calibrated from data points and results in relaxation oscillations whose frequency increases with GF, a particular important result that is in agreement with observations ([1]), and was reduced to a two variable model with the same properties. Overall, our cell cycle model minimizes the number of variables while simultaneously maintaining mathematical terms that allow for biological interpretation.

On Chapter 3 we modeled the mammalian cellular clock and uncovered a dynamical network that generates antiphasic oscillation of the CLOCK:BMAL1 and PER:CRY protein complexes. This model is transcription-based and describes competition of activators and repressors at the clock controlled elements (CCEs) genomic regions: E-box, R-box and D-box. Furthermore, we calibrated our model against experimental data and observed the region of entrainment by an external signal as well as its phase response curve. We used this model to study the interplay between the clock system and metabolism and uncovered a circadian clock role as a controller for the duration of different molecular clock phases in response to the *tau* mutation and to the phase difference between signals pertaining to the fast/feeding and the light/dark cycles. These results allowed to formulate a mechanism explaining how metabolic states of health and disease,

such as insulin sensitivity and insulin resistance, can be related with normal or altered time patterns of feeding behavior (in mice and humans) by means of the internal circadian cell clock.

On Chapter 4 we investigated the coupling of our mammalian cell cycle and circadian clock models in unidirectional and bidirectional configurations. These were: the MPF-controlled phosphorylation and subsequent degradation of REV, the CLOCK:BMAL1-induced expression of *wee1* leading to the repression of MPF activity, the bidirectional application of the two aforementioned mechanisms, and a different mechanism whereby GF action on the clock occurs directly instead of by means of the cell cycle (in this case the clock entrains the cell cycle via *wee1* induction). We have observed that in all coupling cases GF itself is a control parameter for the oscillators' synchronization state, with higher GF driving the system from $r_T = \frac{T_{clock}}{T_{cell\ cycle}} = 1$ synchronization to $r_T > 1$. Dex application, in turn, reduced the minimal GF value for which this transition occurs and its effect in driving the system from the 1:1 to the 3:2 synchronization state is reproduced. A *devil's staircase* pattern of synchronization state response, where synchronization ratios are constant by intervals, is obtained in all forms of coupling, except in the GF-controlled clock system. These coupling forms resulted in different rational synchronization ratios such as 1:1, 2:1, 3:2, 4:3, 2:3 and 1:2.

Furthermore, we establish that inputs, such as GF and Dex, cause the intrinsic periods of the two oscillators to either be closer together or further apart, which in unidirectional coupling has a similar effect in synchronization state alteration as respectively increasing or decreasing the coupling strength parameter. In bidirectional coupling the combination of the two coupling parameters with GF determines the ratio of period-locking.

In the system under bidirectional coupling analysis of the oscillators' period-lock response to a Dex pulse revealed that only when the application of the pulse occurs at a certain clock/cell cycle phase region does the system respond by shifting from $r_T = 1$ to $r_T > 1$, while when at another phase region the system doesn't respond and is kept in 1:1 synchronization. Furthermore, our results predict that a third and smaller phase region of pulse application results in a slower cell cycle than clock ($r_T < 1$). Synchronization state response to the Dex pulse is transient in our system, which contradicts the multiple attractor hypothesis established by Feillet et al., (2014), [1]. We relate the existence of a responsive and a non-responsive region to the two populations of cells observed by Feillet et al., (2014), [1]. Therefore, the time of an input pulse application is highlighted as a control parameter for the input/output response of a cell, which is an idea relevant not just for synchronization state control but also for a variety of drug treatments, including chemotherapy.

Synchronization state response in unidirectional coupling with a GF-responsive clock contrasted with the other forms of coupling in that it didn't result in the *devil's staircase* pattern for changes in control parameters. Nevertheless $r_T > 1$ is observed for certain parametric conditions as well as in the response to a Dex input, that similarly to what was observed in other forms of coupling decreases the minimum GF value required to induce breaking of the 1:1 period-lock. Thus, this mechanism also provides a viable dynamical explanation for the results of Feillet et al., (2014), [1].

Overall, in all forms of coupling we have observed the system's response to different changes

in parameters and inputs and that there is more than one way of controlling the synchronization ratio. In a broader sense, our coupling results provide visualization and understanding of dynamical behaviors compatible with the experimental observations of Feillet et al., (2014), [1].

Moreover, this work is part of a larger project of designing and constructing synthetic biological oscillators representing the cell cycle and clock systems. These synthetic constructs will allow further investigation of some of the dynamics observed both in experimental settings of the real system ([1]) and *in silico* on Chapter 4 of this thesis.

5.2 Perspectives and Future Work

5.2.1 Design of Synthetic Oscillators

The results of this thesis directly influence the design of synthetic oscillators and experiments to be performed with them, as now we know which parameters would be more beneficial to control externally and how different controls may affect the resultant synchronization state. Furthermore, the period-control analysis performed on Chapter 4 offers an idea of the type of experimental protocols to be developed.

Firstly, possible methods of synthetic oscillator design are provided by Purcell et al., (2010), [3]. Simple configurations centering a main negative feedback loop between an Activator and a Repressor in conjunction with the possible inclusion of either positive or negative self-regulatory feedback loops, similar to our reduced cell cycle model (see Fig. B.1), are good starting points for the design of both oscillators. The clock model should be appropriately represented by a transcription-based circuit, while the cell cycle by a post-translational regulatory system.

Moreover, each synthetic circuit should have between two or three variables. Because we discovered during the course of this work that the effect of Dex application in period-lock control is due to its effect on the clock period, there won't be necessary to match the number of variables of our clock model (four) in a synthetic representation of the clock system. Instead the focus should be on increasing period range as well as on methods of tuning parameters of period control via external inputs. An example is provided by Kainrath et al., (2017), that makes use of cobalamin binding domains of bacterial CarH transcription factors to allow the breaking of protein complexes with an external green-light, thus creating an important tool to control the rate of protein release via an external input [119]. Another technique that allows tuning parameters is the use of drug-responsive gene promoters, whereby the control of gene expression rates can be made via an additive input [120]. A particular interesting development that improves control of the response of synthetic biological constructs is provided by Milias-Argeitis et al., (2011), where external *in silico* feedback is computed by taking real-time cellular measurements in order determine at each step the amount of an external light input to be applied on the synthetic system [121].

Concerning cell cycle representation, a possible regulatory mechanism to assist the design of a post-translational regulated oscillator is the toolbox proposed by Fernandez-Rodriguez and Voigt, (2016), that is based on proteases of *Potyvirus* and their cleavage sites [122]. This

toolbox allows external control of protein release and degradation by fusing the protein with an inactivating peptide or a degron. Protease controlled cleavage acts by removing the inactivating peptide, in the first case, thus activating the protein, or by exposing the degron, in the second case, thus targeting the protein for degradation.

Furthermore, another system that may be useful to assist the design of our circuits is the first ever implemented synthetic genetic oscillator, the repressilator, that has recently been simplified by Potvin-Trottier et al., (2016), [123]. The authors found that the removal of some of the initial circuit interactions allows for more regular oscillations and synchronization of populations of cells without any coupling between them.

Finally, chinese hamster ovary (CHO) cells and the human embryonic kidney (HEK293) are examples of mammalian cell lineages used in synthetic biology ([120]), that are good candidates for our work as well. This project may involve the use of the latest developed lab techniques and protocols of the field of synthetic biology engineering in eukaryots, such as Golden Gate shuffling [124] and the hierarchical modular cloning system [125], that are based on type II restriction enzymes and their ability for sequential assembly of multiple DNA streams.

5.2.2 Clock and Cell Cycle Modeling

In general, the modeling work presented on this thesis has expanded the state of the art concerning the dynamics of the coupled clock and cell cycle systems by addressing the goals established on Section 1.5, while at the same time opening topics of future research.

An immediate subject of future research is the use of our models in the investigation of the dynamics of other forms of coupling. In particular, the idea proposed in this thesis of phosphorylation of an essential clock component by MPF could be extended besides REV-ERB – in this case BMAL1, PER and CRY are good candidates due to their fundamental role in the clock system. Furthermore, clock regulation of the cell cycle can also be investigated via PER or BMAL1 controlled regulation of c-Myc, a repressor of the G1/S transition, which in our model can be represented by decreasing the effect of GF. Because we established the fundamental role of GF in synchronization state control, this coupling mechanism has a high potential of being relevant for the real system. Furthermore, as in this work we have focused on studying period-lock and period control, the study of phase-lock control remains open. In this sense, observing how differing types of coupling affect phase-locking is also a topic of interest; simultaneous period-lock and phase-lock fitting to data points can be a method of validating a particular coupling hypothesis over another, that hasn't been explored by us here.

Moreover, as the results of Chapter 4 on the response of the bidirectional coupled system to a Dex pulse suggest an explanation for the existence of the two period-locked populations of cells observed by Feillet et al., (2014), [1], follow up modeling work on cell populations is a subject of interest. In this regard, some questions that can be addressed under population modeling are: are all techniques of period control used in this work also effective when expanding to cell populations? Is it possible to make the non-responsive population responsive? Is it possible to control the number of cell populations that occur or the number of cells in each population?

Furthermore, the analysis and characterization of our reduced clock model could be expanded. This could include the investigation of its FWHM response and/or the possibility to simulate temperature compensation.

Concerning the expansion of the cell cycle model, earlier cell cycle stages and cyclins could be included in order to investigate the mechanistic interplay between cyclins: though it is well established that cell cycle cyclins precede each other, the entirety of the mechanism that leads GF to induce expression of cyclin B is not simple, as binding of other cyclins to the cyclin B promoter has not been identified. Instead the cyclin B promoter responds to a variety of molecular compounds that have a role in sensing cellular health and whether DNA replication during S phase has occurred correctly. It would be interesting to investigate how such a mechanism can be incorporated as well as how to connect MPF synthesis rate with, for instance, a previous cyclin stimulated by GF.

5.2.3 Experimental Studies

An important follow up to our clock modeling work would be the experimental exploration in mammalian cells of our observations on the role of the clock mechanism in controlling the duration of different molecular phases in response to input signals. Relatedly, another idea is to investigate whether this finding can be extrapolated to other clock systems, which could be done not only via modeling of other organisms, but also in experimental settings.

Moreover, an idea here proposed that could be experimentally explored is that of a GF-responsive clock. In particular, the pathway proposed by us on Chapter 4 could be tested via knock-out experiments of the intermediary components cyclin D/cdk4 and GCN5. Current available observations relating to the issue of a GF versus a cell cycle-responsive clock are those of confluent cells, that aren't physically allowed to grow or divide [1]. On one hand, confluent cells (with an arrested cell cycle) show a 24 h clock period regardless of the GF value, which supports the idea of the cell cycle mediating any effect GF might exert on the clock. On the other hand, only a very small percentage of cells (5 to 10 %) kept in confluency conditions exhibit a circadian rhythm at all, thus making these observations insufficient to exclude the hypothesis of GF directly affecting the clock of free dividing cells, in particular because we don't know how confluency affects GF-transducing pathways. Nevertheless, both the case where cell cycle arrest results in a 24 h clock and the case where cell cycle arrest results in a loss of circadian rhythmicity are consistent with a **cell cycle** $\rightarrow$ **clock** coupling effect, for which this is, in our opinion, the strongest hypothesis. In general, the hypothesis of a GF-responsive clock, formulated in this work, adds another layer of complexity to the coupling problem, as there isn't yet a way of knowing how relevant to circadian rhythms the effect of GF-transducing pathways is versus the effect of the cell cycle. Thus, further experimental study is needed on particular pathways establishing a direct connection between GF and the clock, such as the one proposed in this thesis.

A final idea of future experimental work is to test on mammalian cells some of the experiments and protocols proposed by us, so as to revisit and expand the work of Feillet et al., (2014),

[1], now with the broader view acquired by our work. The methods developed in our work may also be adapted into protocols testing the synchronization dynamics of synthetic biology oscillators.

In summary, the observations of synchronization state control via inputs and single parameter changes provided by this thesis form a basis for a design of synthetic oscillators consistent with the future goal of using these circuits to observe a variety of clock/cell cycle synchronization ratios and period control methods. This can be achieved by focusing on external tuning of parameters via the use of drug-responsive promoters of gene transcription as well as toolboxes that allow the external control of protein release and degradation, such as light-sensitive transcription factors. Finally, the work presented on this thesis has expanded the state of the art concerning the dynamics of the coupled clock and cell cycle system by revealing different ways of controlling the synchronization state of these oscillators as well as their dynamical behavior under different coupling methods and controls.

A

Supporting Information for the Cell Cycle Model

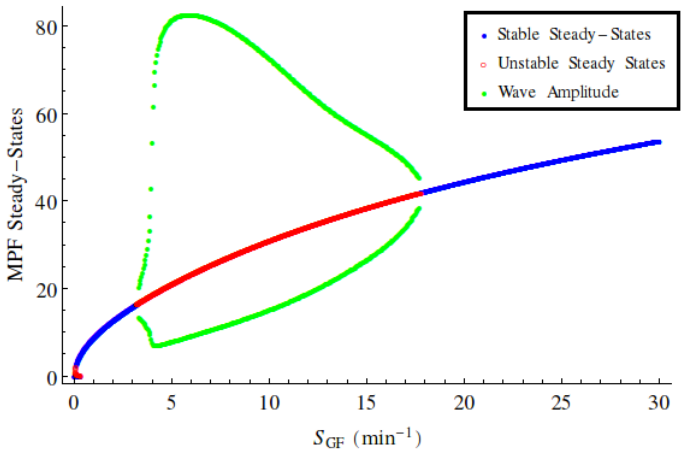

Figure A.1: **Bifurcation analysis of the cell cycle model with S_{GF}.** Stable steady states are represented in blue and unstable steady-states in red. A Hopf bifurcation marks the entrance in the oscillatory region. The wave envelope is shown in green.

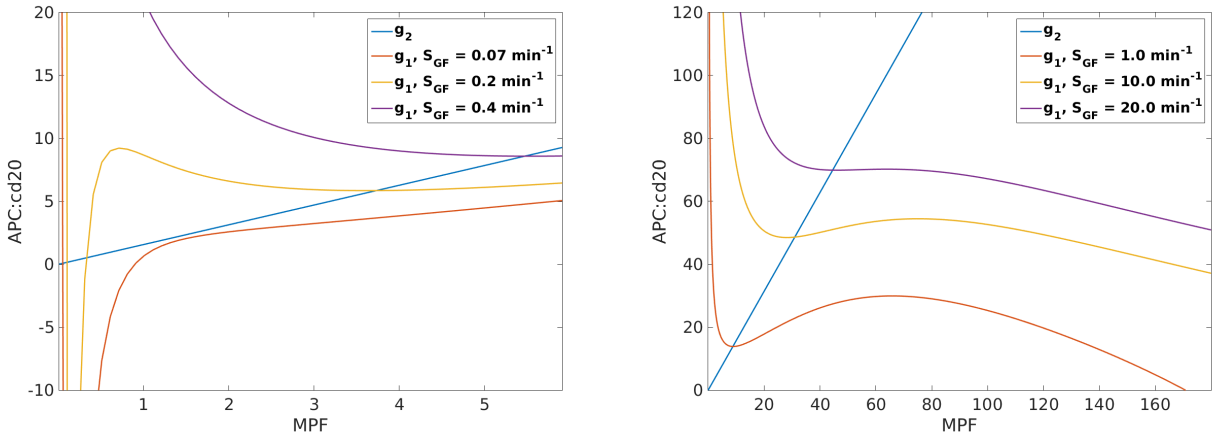

Figure A.2: **Nullclines for several values of S_{GF}.**
Varying S_{GF} varies the shape of g_1 and changes the number of fixed points. On the left, the region of low S_{GF}: two monostable regimes (red and purple), where intersection of g_1 and g_2 occurs only once, and a bistable regime (yellow), where the nullclines intersect three times – one unstable fixed point is in the middle of two stable fixed points and the system converges to one of the two stable points depending on the initial condition. On the right, higher values of S_{GF}: growth factor controls passage from monostability (red) to instability giving rise to oscillation (yellow) and again to monostability (purple).

B

Preliminary Coupling Studies

We now apply the 2 variables skeleton cell cycle model developed in Chapter 2, shown schematically in Fig. B.1, to perform a preliminary assessment of the coupling with a basic clock model developed in this Section, in order to investigate possible mechanisms behind different synchronization states.

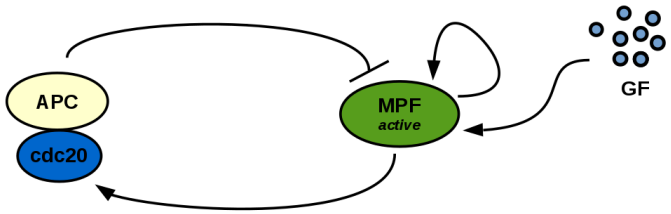

Figure B.1: **Schematic of the reduced cell cycle model.**
The reduced model consists of a central negative feedback-loop between the active form of MPF (activator) and the APC:cdc20 complex (repressor). An auto-regulatory positive feedback-loop of MPF represents the positive regulation of MPF on itself via inhibition of wee1 and activation of cdc25 and the effect of growth factor GF on the cell cycle is included via MPF synthesis.

This preliminary study seeks to investigate a known cell cycle/clock interaction of MPF-controlled REV-ERBα phosphorylation ([56]), namely to assess its ability in reproducing entrainment for various GF values as well as how the periods of the system relate to each other under this coupling mechanism and in the presence of a Dexamethasone input. The results presented in this Section allow for a better understanding of the flow of the coursework between the Chapters of this thesis, in specific because the questions raised by this preliminary study largely influence subsequent work.

First, we analyze the fundamental molecular clock network and develop a simple model to describe it. Fig. B.2 shows a scheme of the core molecular mammalian clock network, described in Section 1.1.

Based on these main features of the mammalian circadian cell clock, we develop a prelimi-

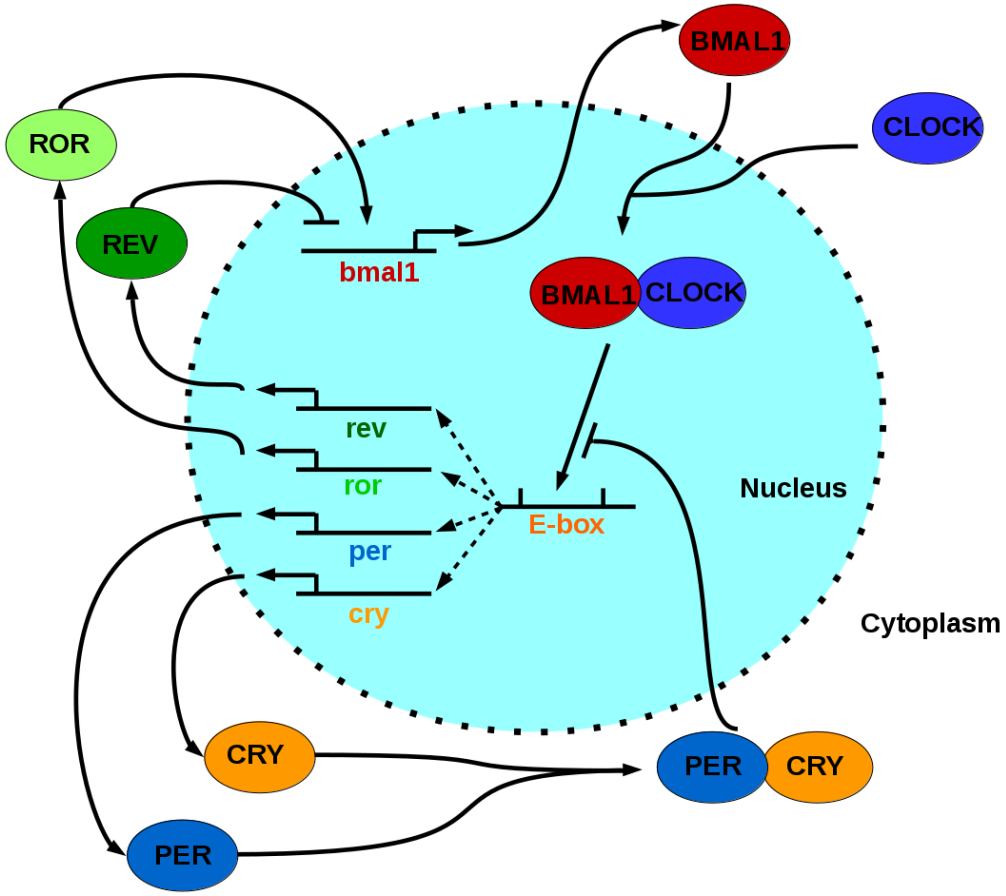

Figure B.2: **Main molecular mechanisms of the mammalian circadian clock.** The nuclear CLOCK:BMAL1 protein complex promotes transcription of *Per*, *Cry*, *Ror* and *Rev*. ROR and REV are transcription factors with an antithetical effect on BMAL1 transcription: ROR activates the BMAL1 promoter and REV represses it. The PER and CRY proteins form the PER:CRY complex that upon re-entrance in the nucleus will bind to CLOCK:BMAL1 repressing its promoter activity.

nary model to describe it, in Equations (B.1) to (B.5). In this model BMAL1 is representative of the CLOCK:BMAL1 complex and acts in promoting, REV, PER and CRY via Hill function terms, the positive loop between ROR and BMAL1 is modeled directly by BMAL1 self-activation, including competing REV-ERB inhibition, and there is formation and dissociation of the PER:CRY complex.

$$\frac{d[BMAL1]}{dt} = V_B \frac{V_{rb}\frac{k_{rb}^2}{k_{rb}^2+[REV]^2}[BMAL1]^2}{V_{rb}\frac{k_{rb}^2}{k_{rb}^2+[REV]^2}[BMAL1]^2 + k_b^2} - \gamma_{bp}[BMAL1][PER:CRY] \tag{B.1}$$

$$\frac{d[REV]}{dt} = V_{br}\frac{[BMAL1]^2}{[BMAL1]^2 + k_{br}^2} - \gamma_{rev}[REV] \tag{B.2}$$

$$\frac{d[CRY]}{dt} = V_C\frac{[BMAL1]^2}{[BMAL1]^2 + k_C^2} - \gamma_{pc}[PER][CRY] + \gamma_{cp}PER:CRY - \gamma_c[CRY] \tag{B.3}$$

$$\frac{d[PER]}{dt} = V_P\frac{[BMAL1]^2}{[BMAL1]^2 + k_P^2} - \gamma_{pc}[PER][CRY] + \gamma_{cp}PER:CRY - \gamma_p[PER] \tag{B.4}$$

$$\frac{d[PER:CRY]}{dt} = \gamma_{pc}[PER][CRY] - \gamma_{cp}[PER:CRY] - \gamma_f[PER:CRY] \tag{B.5}$$

This model yields oscillations, shown in Fig. B.3, with parameters of Table B.1. However, all variables oscillate in phase for a wide range of parameter sets, whereas experimental observations show a specific order of the core clock proteins peak expression, namely BMAL1 then REV-ERBα, then PER followed by CRY1. As such, we consider this approximate clock model insufficient for accurate description of the mammalian clock system. In Chapter 3, we develop a different transcription-based model, providing a deeper understanding of the system.

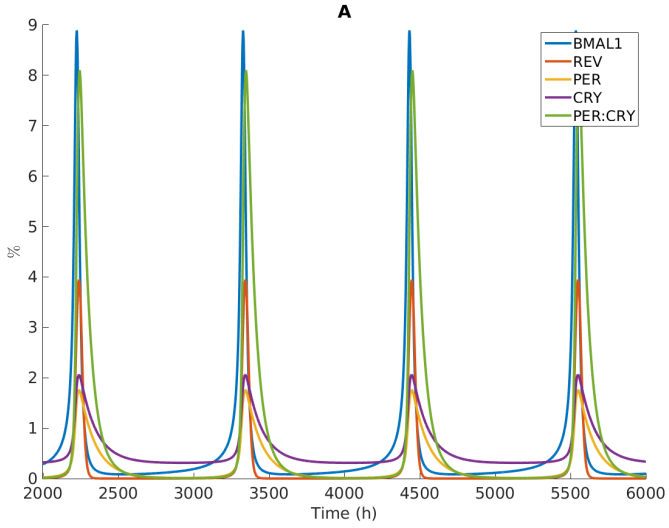

Figure B.3: **Oscillations of the simplified mammalian clock model.** The model of the core mammalian clock network yields oscillations (Equations (B.1) - (B.5)), for parameters of Table B.1. All variables oscillate in phase.

As preliminary work for the construction of a new, more realistic, clock model we will reduce this clock model and explore the coupling between it and our reduced cell cycle model. First,

we reduce the clock model (Equations B.1 to B.5) by approximating CRY and PER at quasi-steady-state and considering that $\gamma_p[PER]$ can be neglected without loss of oscillation. We now get the new $\frac{d[PER:CRY]}{dt}$ Equation:

$$\frac{d[PER:CRY]}{dt} = V_{PC}\frac{[BMAL1]^2}{[BMAL1]^2 + k_{PC}^2} - \gamma_f[PER:CRY] \tag{B.6}$$

whilst the equations for BMAL1 and REV remain unchanged. We aim to keep these three variables, because BMAL1 and PER:CRY form the essential circadian clock main feedback loop and REV-ERB is at the basis of the second, also essential, clock feedback loop. Furthermore, REV-ERB is the usual reporter in the experimental study that demonstrates coupling from the cell cycle to the circadian clock [1], whose results in part motivate this thesis.

We assess the unidirectional coupling, from the cell cycle to the clock system, one of the least explored interactions, whose possible mechanisms we intend to investigate in this work. Thus, we begin by observing the coupled systems via the MPF phosphorylation of REV-ERBα that leads to its degradation [56].

Firstly, in the reduced clock model, the degradation term of REV now becomes $-\gamma_{rev}\frac{[REV]}{[REV]+k_{rev}}$, instead of the previous $\gamma_{rev}[REV]$ in order to obtain a better mathematical description of the phosphorylation mechanism. A simulation of this model is shown in Fig. B.4 (with parameters in Table B.2) (the new parameters now take the values $V_{PC} = 0.6$, $k_{pc} = 15.0$, $\gamma_{rev} = 0.4$ and $k_{rev} = 4.0$, with all remaining parameters the same as in Table B.1). These parametric readjustments do not affect the global dynamics of the system.

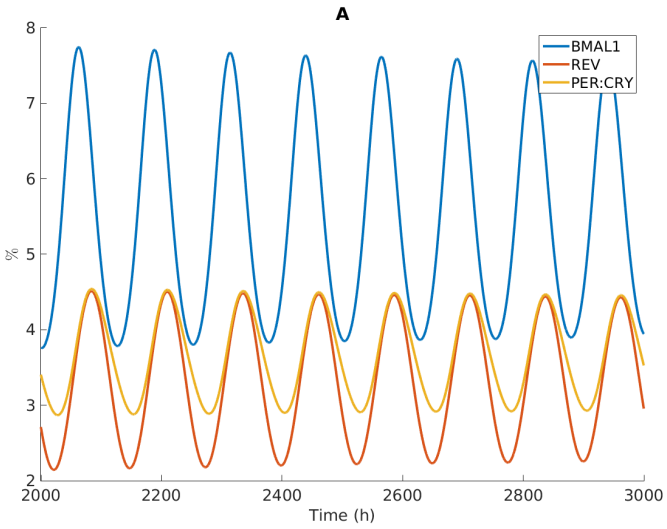

Figure B.4: **Reduced clock model.**
Oscillations of BMAL1, REV and PER:CRY in the reduced model for parameters of Table B.2.

We now use this model to make a tentative coupling with the cell cycle model developed in Chapter 2. The effect of MPF on REV natural degradation is modeled by a multiplicative term $c_m[MPF]$, where the constant c_m represents the coupling strength, for which the equation of REV becomes:

$$\frac{d[REV]}{dt} = V_{br}\frac{[BMAL1]^2}{[BMAL1]^2 + k_{br}^2} - c_m[MPF]\gamma_{rev}\frac{[REV]}{[REV] + k_{rev}} \tag{B.7}$$

For $c_m = 2$, we observe that the cell cycle entrains the circadian clock to its period, see Fig. B.5.

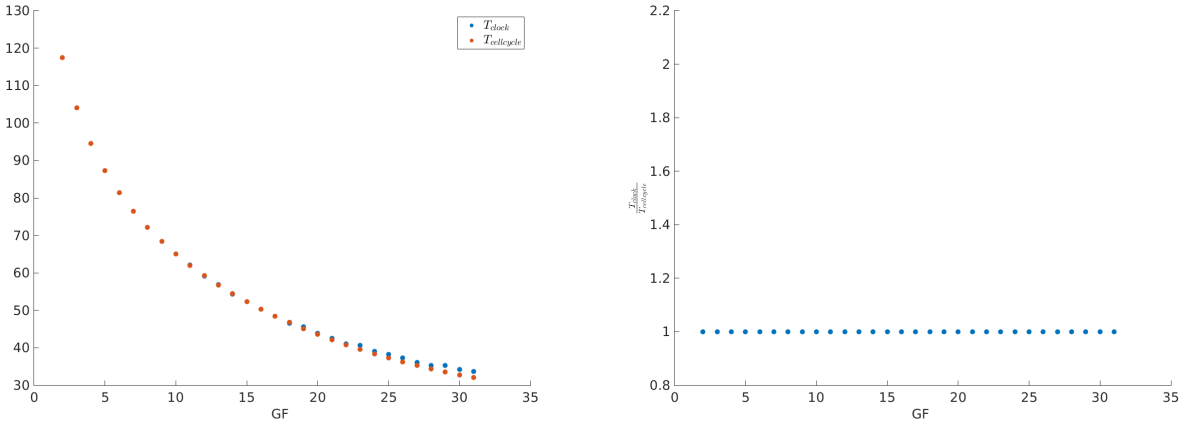

Figure B.5: **Strong coupling between the cell cycle and the circadian clock systems by MPF-mediated degradation of REV.**
For $c_m = 2$ the system is strongly coupled in a a 1:1 clock to cell cycle period ratio: the period of the clock follows that of the cell cycle, both decreasing with GF (left panel); the ratio between the periods is always close to 1 (right panel).

On the other hand, for a weak/moderate coupling we observe different period-lock relations. Fig. B.6 (left) shows results for a lower value of c_m ($c_m = 0.05$) where ratios between the two periods follow a specific pattern with increasing GF. Period-lock ratios remain constant at integer values for some GF intervals. This pattern has visual similarity to that of the *devil's staircase* fractal curve [55]. In Fig. B.6 (right) we observe how the ratio changes with variations of c_m for a fixed value of GF. The resulting variety of period-lock ratios obtained in these simulations includes rational ratios differing from 1:1, which resembles results in Dex-treated cells ([1]), though here period-lock regions often occur at integer values. These results hint at a possible phenomenon of weak coupling from the cell cycle to the clock to explain the observed period-lock phenomena in Dex-treated cells and support the coupling mechanism here proposed (MPF promoting REV degradation). It is also interesting to investigate whether non-integer period-lock ratios, such as 3:2 or 5:4, can also be obtained in a more comprehensive circadian clock model.

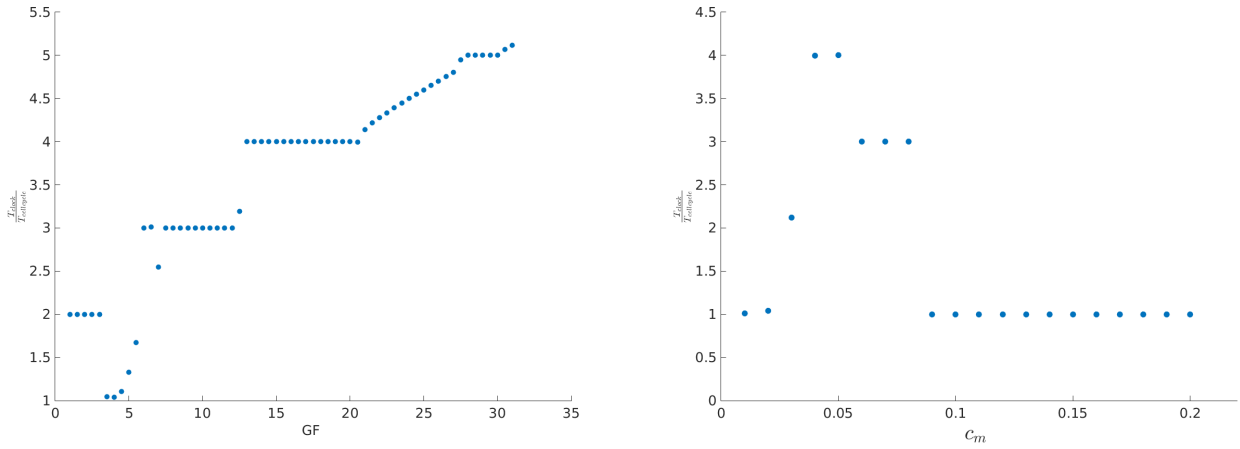

Figure B.6: **Weak coupling of the circadian clock and cell cycle models by MPF-mediated degradation of REV.**
On the left: for $c_m = 0.05$ the system is in weak/moderate coupling and several period-lock ratios are obtained. The ratio of clock to cell cycle period increases with increasing GF but is constant by intervals at integer values, forming a type of *devil's staircase*-like pattern. On the right: for a fixed value of growth factor, $GF = 15$, varying the coupling strength also leads to different period ratios.

These results allow to extrapolate some ideas for the variety of experimentally observed period-lock ratios between the cell cycle/circadian clock system, more specifically for the period ratios observed in cells synchronized by Dexamethasone [1]. In particular, the introduction of a Dexamethasone pulse may cause a perturbation in the system altering the GF-response of the ratio between the periods of the two oscillators, as occurs in Fig. B.6 (left). Starting from this point, a first idea would be that Dexamethasone could directly be affecting the coupling strength parameter, which in this case means acting on the term $c_m[MPF]\gamma_{rev}\frac{[REV]}{[REV]+k_{rev}}$. Though this hypothesis is not impossible, it consists in a high degree of extrapolation. A less speculative perspective arising from these observations is that the clock/cell cycle system behaves in such a way that the Dexamethasone perturbation affects the coupling between the systems, without necessarily exerting direct action on coupling terms.

Dexamethasone, used commonly as a clock synchronizer in populations of cells is known to induce a peak of PER expression. This phase-shifts the clocks of individual cells, synchronizing the population for a certain amount of time. The mechanism by which Dexamethasone mediates PER expression is likely to be the activation of the PER promoter by the glucocorticoid receptor GR, which is activated by Dexamethasone (and other corticoids).

Thus, following this discussion, specific synchronization ratios, as observed experimentally ([1]) or as obtained in Fig. B.6 (left), should appear when modeling the known effect of Dexamethasone on the clock system, i.e. by adding an input Dex on the equation of $\frac{d[PER{:}CRY]}{dt}$, representative of the Dexamethasone-driven activation of the PER promoter. The new model would have a constant input of Dexamethasone, allowing to study the new limit-cycle under

such conditions; alternatively, a pulse of Dex could be introduced to study the system's transient response to the perturbation. However, adding Dex to Eq. B.6 results in loss of oscillation.

From this, we conclude that a better understanding of the clock system dynamics is required via further modeling work. As the simplistic model here presented is a rough approximation of the mammalian clock and results in simultaneous BMAL1, REV and PER:CRY oscillation, which does not reflect reality, we move towards the construction of a more suitable model, that better reproduces circadian clock dynamics. We aim to keep emphasis on a transcriptional-based approach, as this is the basis of both the core clock circuitry (see Fig. B.3) and the known mechanistic effect of Dexamethasone on the clock, via GR-mediated PER activation, as discussed in this Section.

The most important mammalian clock negative feedback loop consists of CLOCK:BMAL1 and PER:CRY (Fig. B.2) and these two proteins tend to oscillate in phase-opposition, relating to opposite phases of the day/night cycle. The known interaction of Dexamethasone with the clock is via induction of PER expression, which favors one of these two main clock states (PER:CRY up and CLOCK:BMAL1 down). We recall that CLOCK:BMAL1 is a known clock/cell cycle coupling agent, via action in activating expression of the *wee1* gene. The numerical experiments of this Section show that weak coupling reproduces period-lock proportions differing from 1:1, similar to experimental observations, which raises the question the role of Dex in the dynamical behavior of the coupled system. Considering that PER:CRY represses CLOCK:BMAL1 activity, an activator of PER, such as Dex, could then lead to increased repression of CLOCK:BMAL1 and consequently affect the coupling state of the oscillator (in a **clock** $\rightarrow$ **cell cycle** type of coupling). Thus, the hypothesis here formed is that the mechanistic network behind the circadian clock two-state dynamics (where either CLOCK:BMAL1 or PER:CRY is high) may thus be a preponderant factor for the observed period-lock phenomena in cells treated with Dexamethasone. Furthermore, introducing a Dex input may lead to a similar period-lock outcome as changing the coupling strength.

In Chapter 4, this hypothesis will be verified with the new model (developed in Chapter 3), where the introduction of a Dex input drives the cell cycle/clock system from a 1:1 synchrony state to different rational period-lock ratios.

In summary, the experimentally observed period-lock phenomena in Dex-treated cells can't be reproduced using the model developed in this Section, raising the question of whether or not this problem would be solved by using a model capable of reproducing the appropriate order of protein expression. Understanding the topology that is behind the circadian clock CLOCK:BMAL1 and PER/PER:CRY phase opposition is in itself a subject of interest and the focus of Chapter 3. Nevertheless, the analysis of this Section helped to understand that period-lock proportions differing from 1:1 can be otained with a **cell cycle** $\rightarrow$ **clock** unidirectional coupling.

Finally, the main difference between the model of this Section, based on the scheme of Fig. B.2, and that of Chapter 3 lies on the clock controlled elements (CCEs): E-box, R-box and D-box, with the model variables now being the pairs of activators and repressors that act on these CCEs (see Fig. B.7). This leads to a more extensive model, which incorporates experimental

details, variables and interactions, while maintaining a core transcriptional basis.

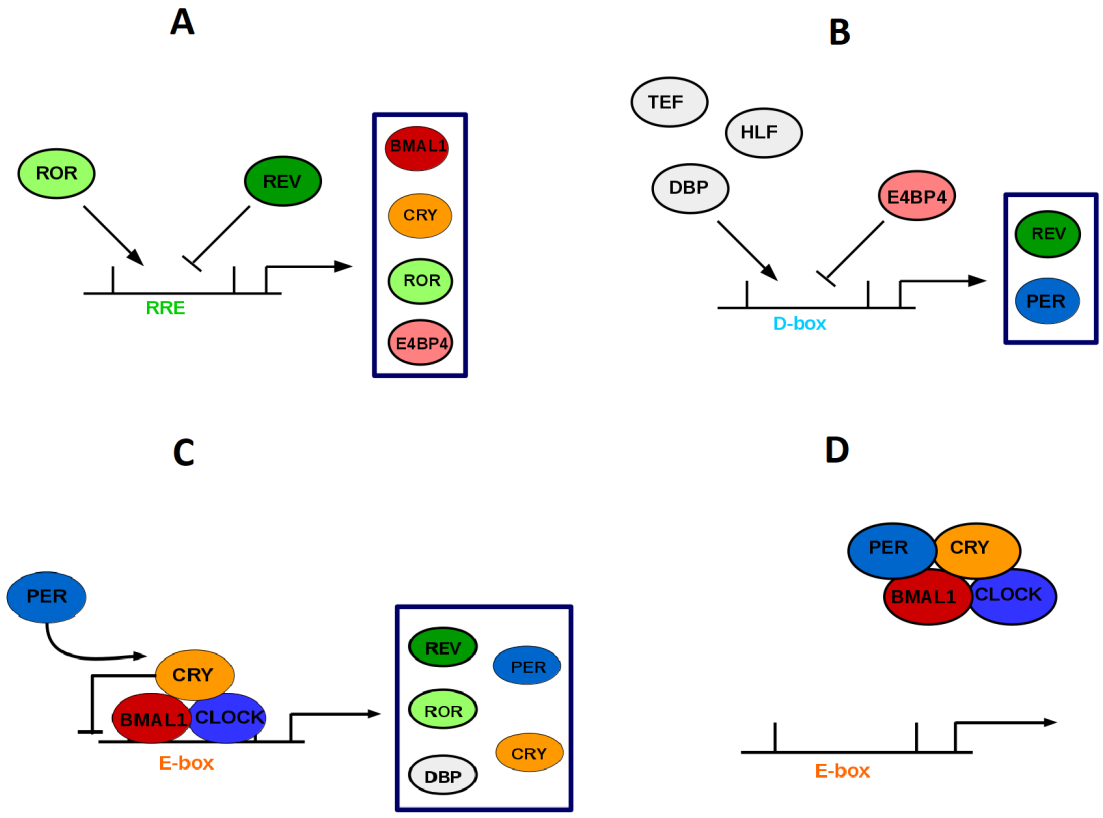

Figure B.7: **A scheme of the regulatory mechanisms of the three major CCEs.** A deeper look into the clock mechanism, by comparison with Fig. B.2. A) Competition between ROR (activator) and REV (repressor) in RRE (R-box) binding. B) D-box may be activated by DBP, HLF and TEF and repressed by E4BP4. C) CLOCK:BMAL1 acts as an E-box activator and CRY can bind to a previously bound CLOCK:BMAL1 repressing its E-box promoter activity. D) PER:CRY bound to CLOCK:BMAL1 removes it from target genes.

Supporting Tables

Table B.1: Parameters for the preliminary clock model

p	Numerical Value
V_B	1.4
k_b	4.0
k_{br}	6.0
V_{br}	0.4
k_P	15.0
k_C	15.0
V_P	1.6
V_C	1.6
V_{rb}	0.2
k_{rb}	3.0
γ_{rev}	0.4
γ_{pc}	0.5
γ_{cp}	0.2
γ_p	0.1
γ_c	0.1
γ_f	0.02
γ_{bp}	0.02

Table B.2: Parameters for the reduced preliminary clock model

p	Numerical Value
V_B	1.4
V_{br}	0.4
V_{rb}	0.2
V_{PC}	0.6
k_b	4.0
k_{br}	6.0
k_{rb}	3.0
k_{pc}	15.0
k_{rv}	4.0
γ_{rev}	0.4
γ_f	0.02
γ_{bp}	0.02

C

Modeling E-box Dynamics

In this Section we use mass action kinetics to derive a model term for the E-box activation dynamics. E-box is activated by [CLOCK]:[BMAL1], whose promoter activity is blocked by subsequent CRY binding. PER then binds to CRY and the [CLOCK]:[BMAL1]:[PER:CRY] complex exits target genes, freeing up E-box.

In more general terms an activator A binds to a promoter P, forming an activator complex C_a. Afterwards, the repressor R binds to C_a at the promoter site. A scheme of this process is shown on Fig. C.1.

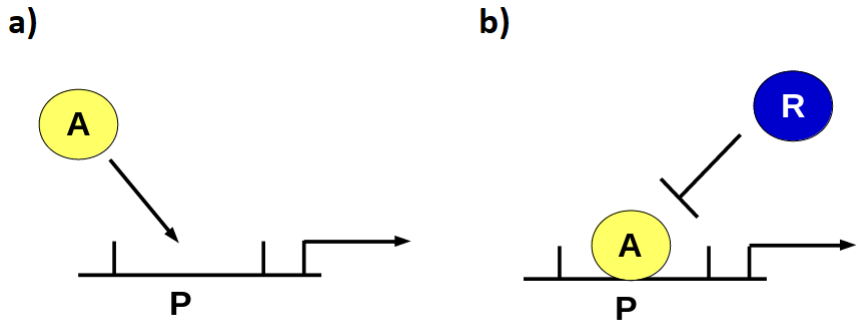

Figure C.1: **A scheme for a regulatory E_{box}-type mechanism.**
a) The activator A binds to the promoter site P initiating gene transcription. b) The repressor R binds to previously bound A blocking gene transcription.

Competition between activator and repressor is not independent as the complex $C_r = [C_a : R]$, is not formed by direct binding of R to P, but rather by the binding of R to the previously formed activator complex C_a.

These processes are given by the following kinetic reactions:

$$\begin{aligned} A + P &\underset{k_2}{\overset{k_1}{\rightleftarrows}} C_a \\ C_a + R &\underset{k_4}{\overset{k_3}{\rightleftarrows}} C_r \end{aligned} \tag{C.1}$$

which by the law of mass action result in the following system of equations:

$$\begin{aligned} \dot{C_a} &= k_1[A][P] - k_2[C_a] - k_3[C_a][R] + k_4[C_r] \\ \dot{C_r} &= k_3[C_a][R] - k_4[C_r] \\ \dot{P} &= -k_1[A][P] + k_2[C_a] \end{aligned} \tag{C.2}$$

And, from [73], the rate of gene transcription is given by:

$$\dot{G} = \alpha[C_a] \tag{C.3}$$

Observe that from (C.2) we have:

$$\begin{aligned} & \dot{P} + \dot{C_a} + \dot{C_r} = 0 \\ \Leftrightarrow\ & [P] + [C_a] + [C_r] = P_{TOT},\ P_{TOT} > 0 \\ \Leftrightarrow\ & [P] = P_{TOT} - [C_a] - [C_r] \end{aligned} \tag{C.4}$$

meaning the total amount of promoter sites P – free and occupied in the complexes C_a and C_r – is always a constant P_{TOT}.

Two further simplifications arise by taking the quasi-steady-state approximations:

$$\dot{C_a} \approx 0 \tag{C.5}$$

and

$$\dot{C_r} \approx 0 \tag{C.6}$$

which assumes the changes in the concentration of the intermediate complexes C_a and C_r are fast in relation to the rate of formation of the product G.

Thus, from (C.6) we have:

$$C_r = \frac{k_3}{k_4}[C_a][R] \tag{C.7}$$

and from Equations (C.4), (C.5) and (C.7):

$$
\begin{aligned}
& k_1[A][P] - k_2[C_a] - k_3[C_a][R] + k_4[C_r] = 0 \\
\Leftrightarrow\ & k_1[A](P_{TOT} - [C_a] - [C_r]) - k_2[C_a] - k_3[C_a][R] + k_4\frac{k_3}{k_4}[C_a][R] = 0 \\
\Leftrightarrow\ & k_1[A]P_{TOT} - k_1[A][C_a] - k_1[A]\frac{k_3}{k_4}[C_a][R] - k_2[C_a] - k_3[C_a][R] + k_3[C_a][R] = 0 \\
\Leftrightarrow\ & [C_a](k_1[A] + k_1\frac{k_3}{k_4}[A][R] + k_2) = k_1[A]P_{TOT} \\
\Leftrightarrow\ & [C_a] = \frac{k_1[A][P_{TOT}]}{k_1[A] + k_1\frac{k_3}{k_4}[A][R] + k_2} \\
\Leftrightarrow\ & [C_a] = P_{TOT}\frac{[A]}{[A] + \frac{k_3}{k_4}[A][R] + \frac{k_2}{k_1}}
\end{aligned}
\tag{C.8}
$$

From Equation C.3 the gene transcriptional rate is directly proportional to $[C_a]$, now becoming:

$$
\dot{G} = V_G\frac{[A]}{[A] + k_{GR}[A][R] + k_G} \tag{C.9}
$$

And replacing A and R by BMAL1 and CRY respectively, we arrive at our equation for E_{box} transcriptional activity:

$$
E_{box} = V_E\frac{[BMAL1]}{[BMAL1] + k_E + k_{Er}[BMAL1][CRY]} \tag{3.1}
$$

D

Supporting Information for the Circadian Clock Model

Table D.1: Calibrated parameters from REV-ERBα data from Feillet, (2014), [1], (as shown in Fig.3.3), for the circadian clock model.

p	Numerical Value
V_R	44.4 %.h^{-1}
k_R	3.54 %
k_{Rr}	80.1 %
V_E	30.3 %.h^{-1}
k_E	214 %
k_{Er}	1.24 %
V_D	202 %.h^{-1}
k_D	5.32 %
k_{Dr}	94.7 %
γ_{ror}	2.55 h^{-1}
γ_{rev}	0.241 h^{-1}
γ_p	0.844 h^{-1}
γ_c	2.34 h^{-1}
γ_{db}	0.156 h^{-1}
γ_{E4}	0.295 h^{-1}
γ_{pc}	0.191 $\%^{-1}.h$
γ_{cp}	0.141 h^{-1}
γ_{bp}	2.58 $\%^{-1}.h$

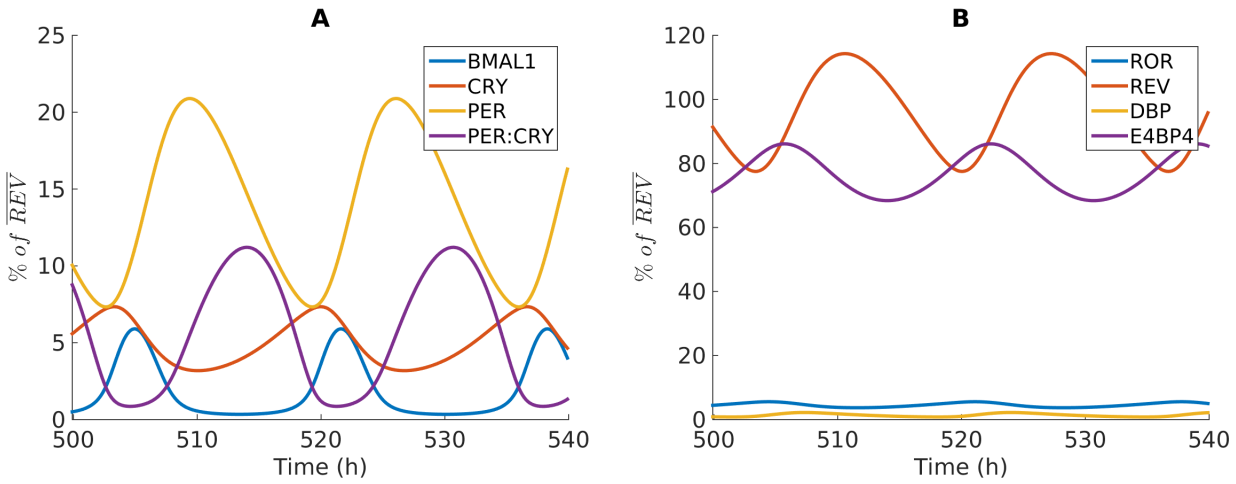

Figure D.1: **Output of the model with Hill exponent n=1.**
The model yields similar results with n=1 and n=2 and the peak expression of BMAL1, PER, CRY and PER:CRY appear in the same order. Parameters of simulation are those of Table D.1.

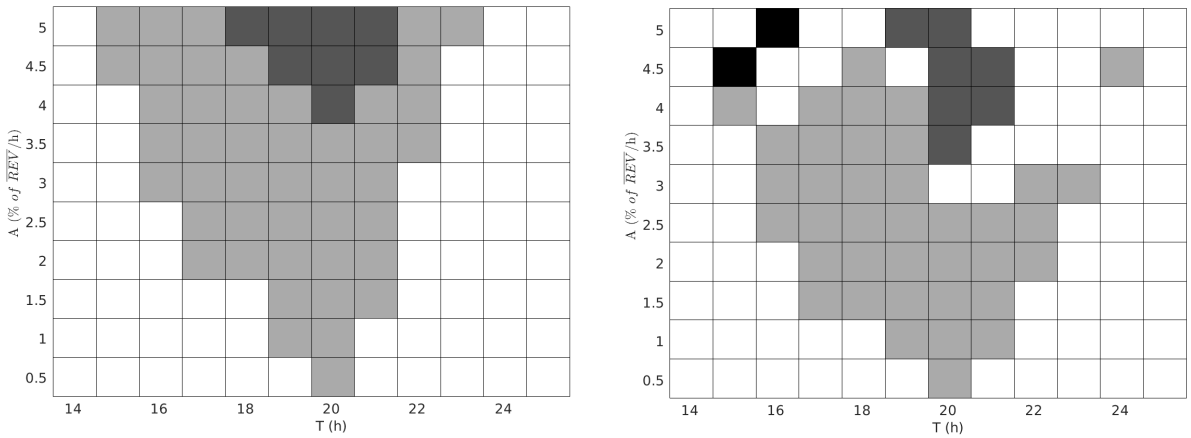

Figure D.2: **Entrainment of the clock model without chromatin remodeling to an external oscillatory input.**
The amplitude and the period of an entraining wave are varied and the resulting regions of entrainment form Arnold tongues. A) The entraining wave is a sinusoid. B) Entrainment is done with a rectangular wave. A black/white gradient represents the ratio between the clock period and the period of the entraining wave: white - no entrainment, grey - 1:1 entrainment, dark grey - 2:1 entrainment and black - 3:1 entrainment. By comparison with Fig. 3.8 incorporation of the chromatin remodeling function results in a larger region of entrainment for sinusoidal waves and an improved entrainment overall for square waves.

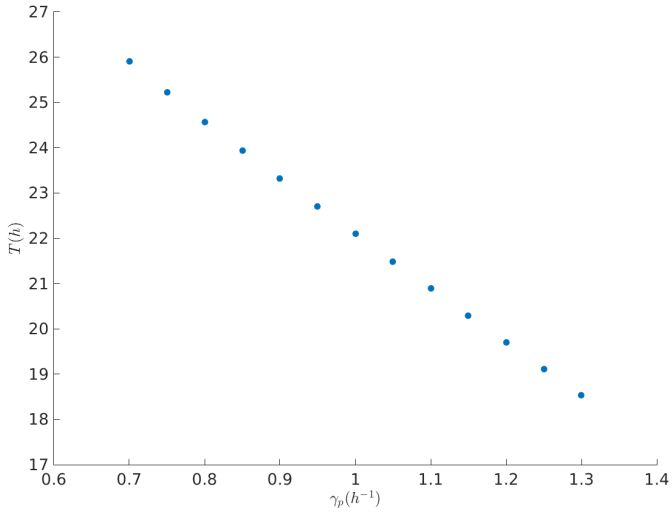

Figure D.3: **Period change with the parameter γ_p for the system with the closed-loop control.**
Period decreases as γ_p increases, similarly to what may be observed in Fig. 3.4.

Table D.2: Parameters of the reduced clock model.

p	Numerical Value
V_R	44.4 $\%.h^{-1}$
k_{Rr}	80.1 %
V_B	0.142 $\%.h^{-1}$
V_{D2}	19.0 $\%.h^{-1}$
γ_{rev}	0.241 h^{-1}
γ_{db}	0.156 h^{-1}
γ_{bp}	2.58 $\%^{-1}.h$

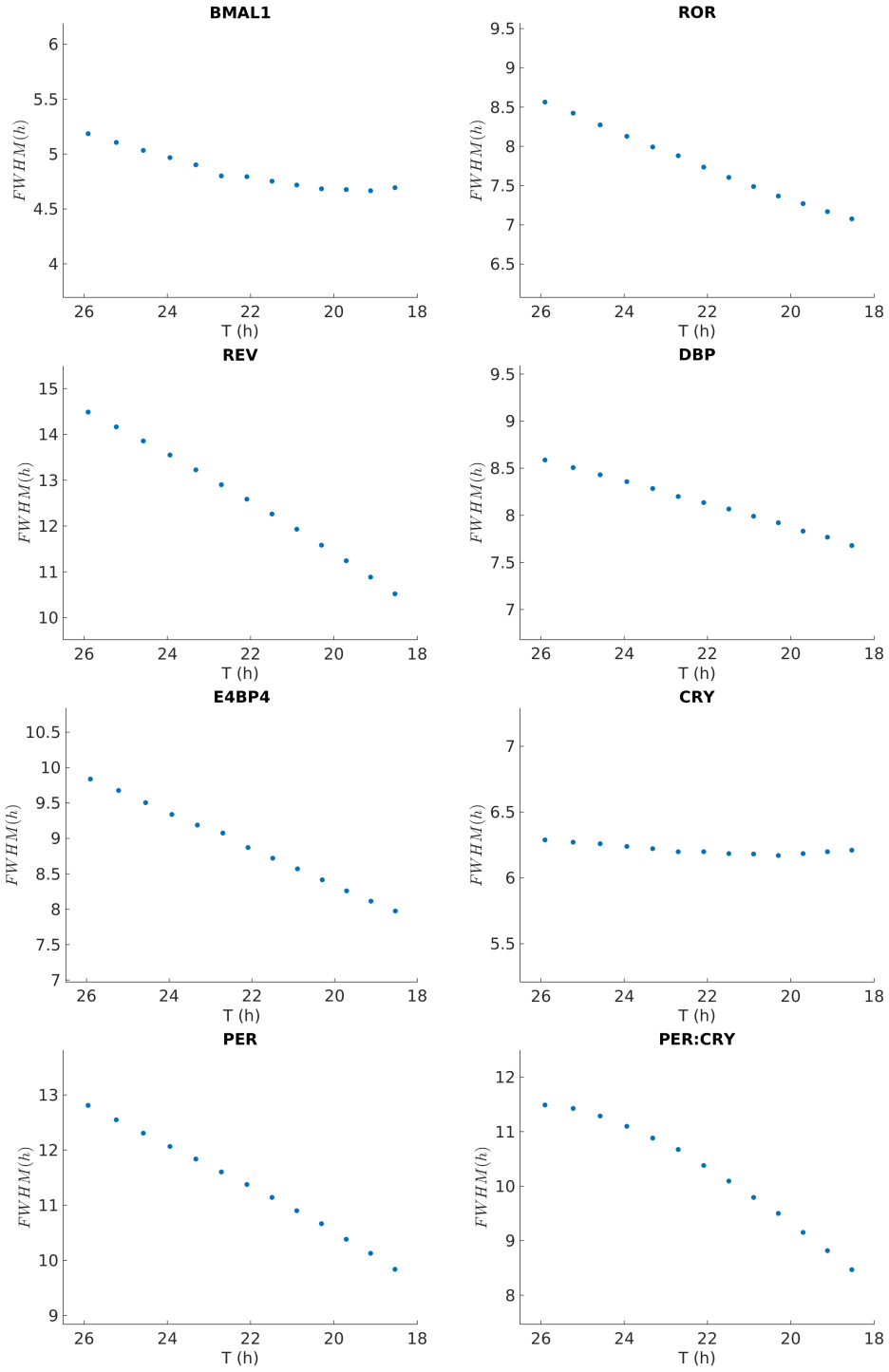

Figure D.4: **Changes of FWHM of the clock proteins as the period changes via increased PER phosphorylation.**
As the period decreases in a manner consistent with the *tau* mutation the FWHM of several clock proteins, such as REV and PER decrease in linearly with the period, while the FWHM of BMAL1 varies less and the FWHM of CRY1 is approximately constant. Here the results are the same of Fig. 3.9, but shown differently.

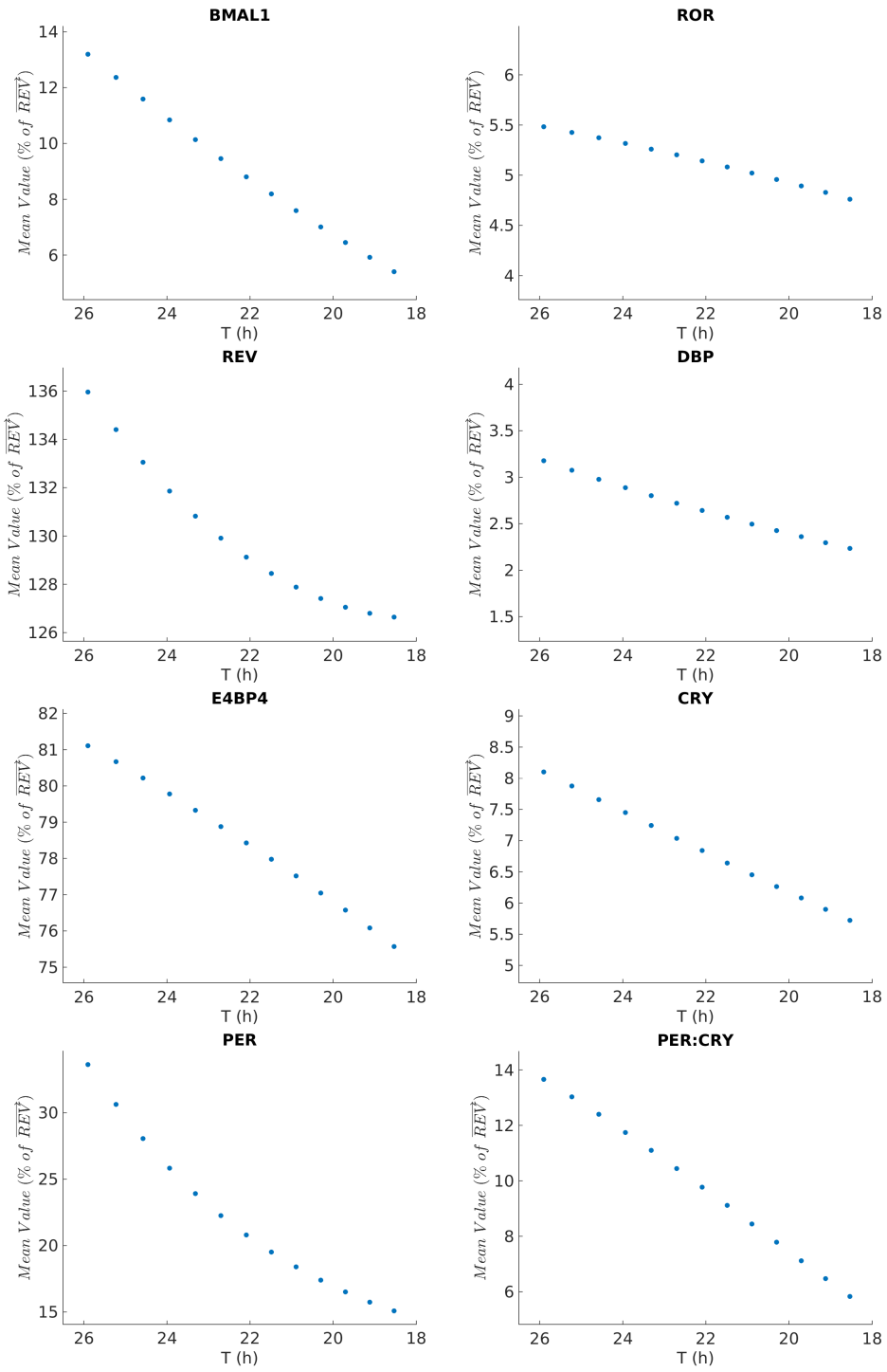

Figure D.5: **Changes of the mean value of the clock proteins as the period changes via increased PER phosphorylation.**
As the period decreases in a manner consistent with the *tau* mutation the mean value of expression of all clock proteins decreases.

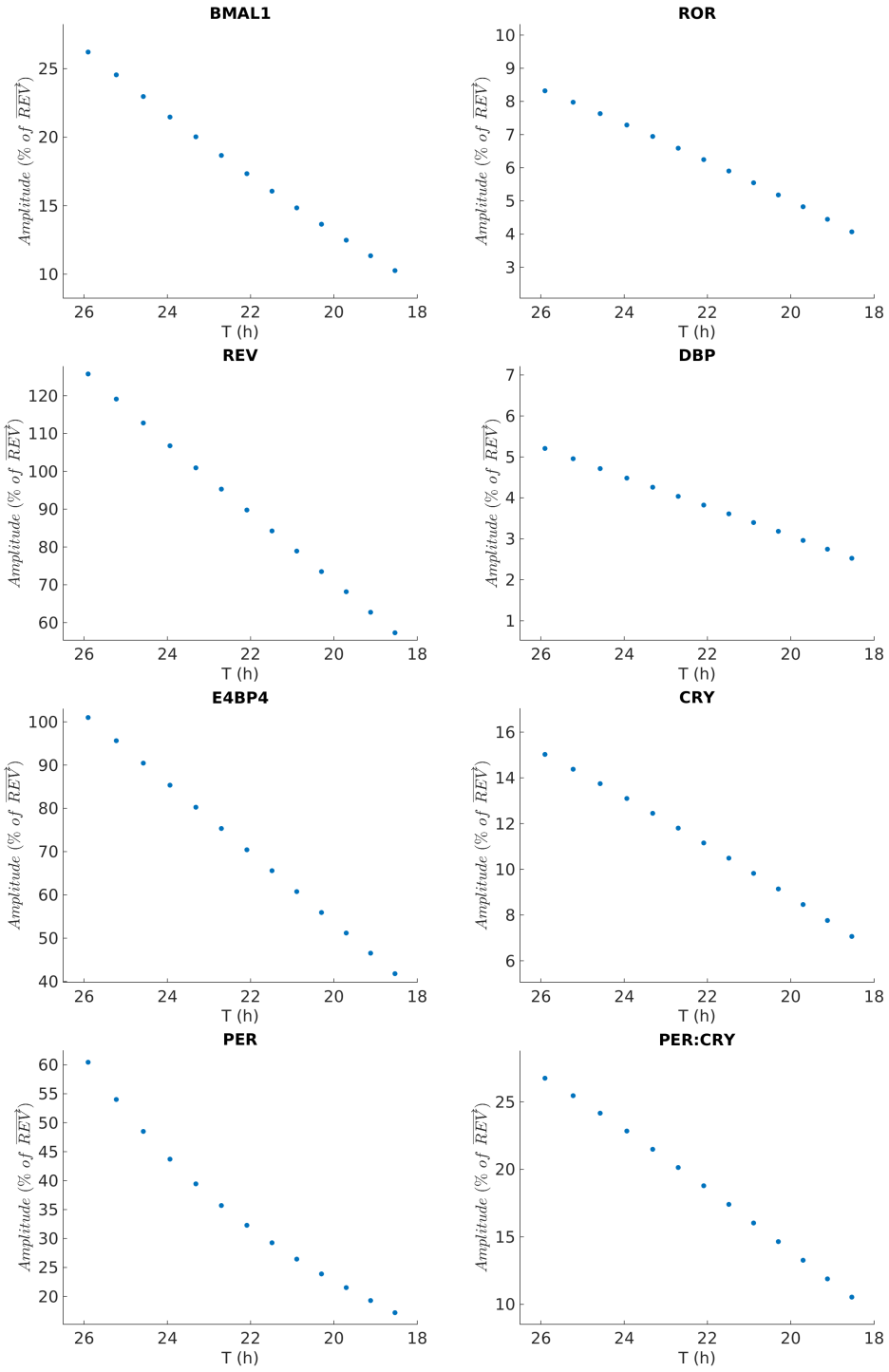

Figure D.6: **Changes of the amplitude of the clock proteins as the period changes via increased PER phosphorylation.**
As the period decreases in a manner consistent with the *tau* mutation the amplitude of all clock proteins decreases.

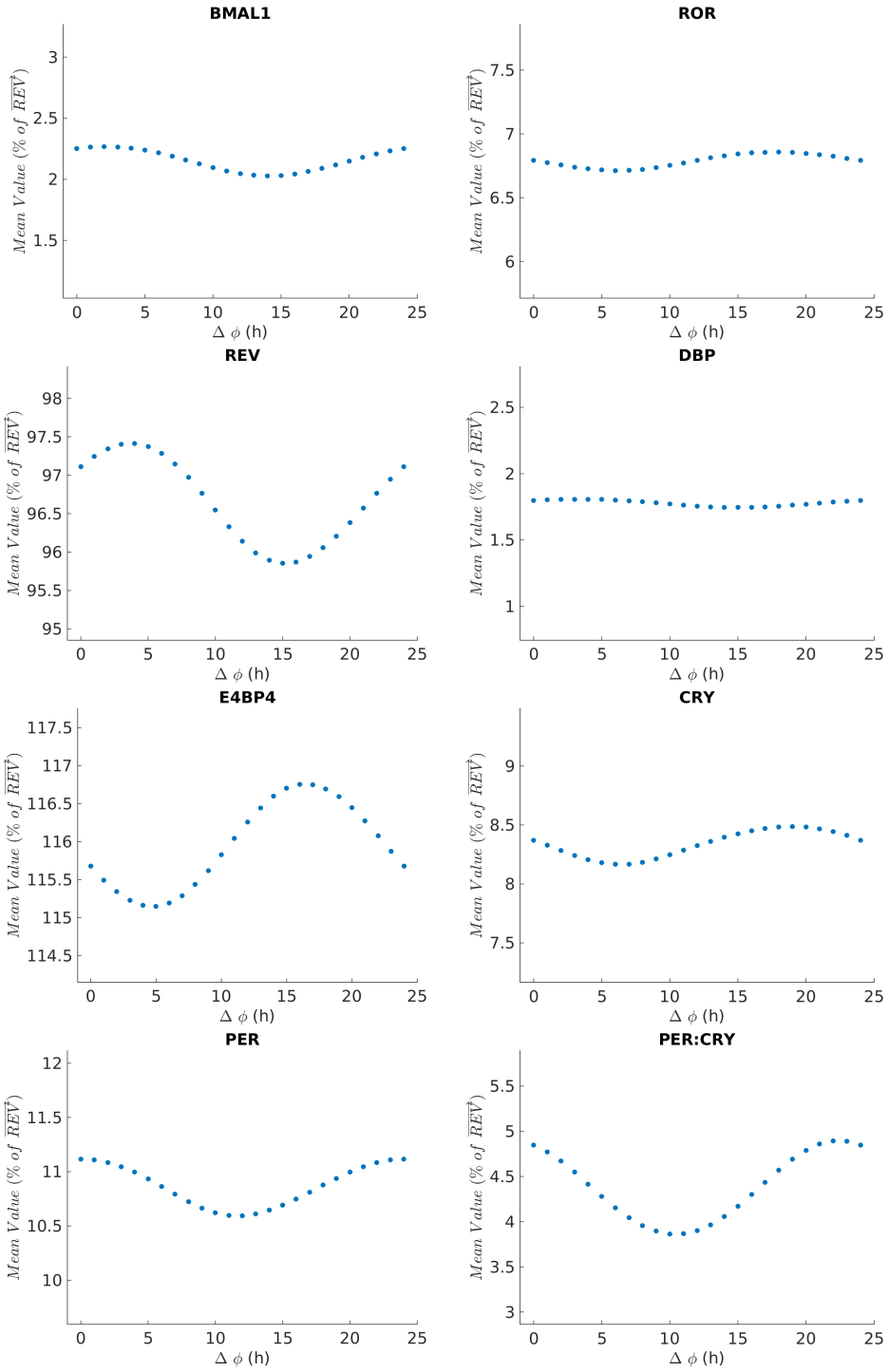

Figure D.7: **Variation in the mean values of clock core proteins with the phase difference between two external hormonal signals $\Delta\phi$.**
We observe that in general the mean value of most clock proteins is higher when the signals are more in phase.

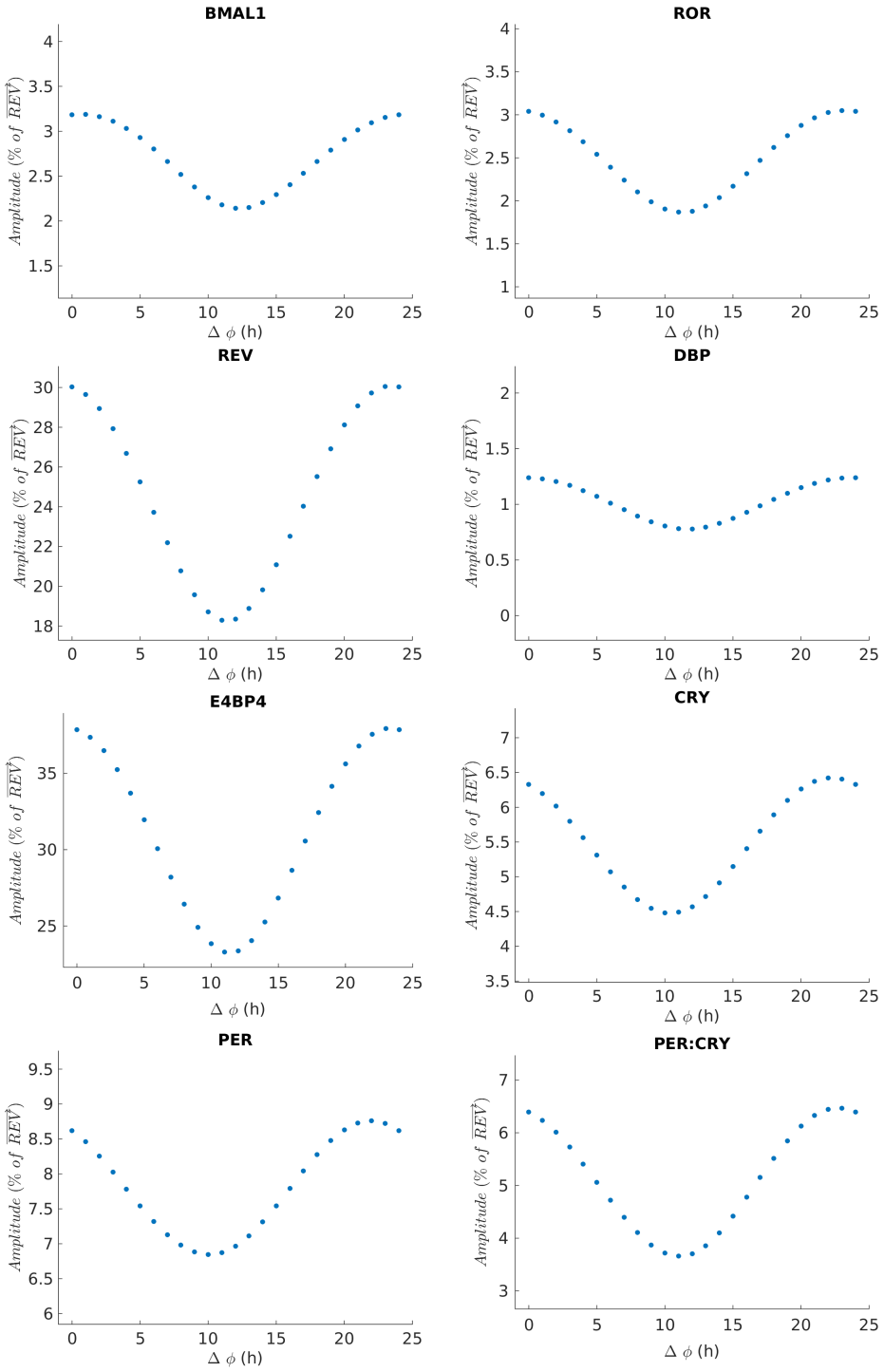

Figure D.8: **Variation in the amplitude of clock core proteins with the phase difference between two external hormonal signals $\Delta\phi$.**
We observe that in general the amplitude of most clock proteins is higher when the signals are more in phase.

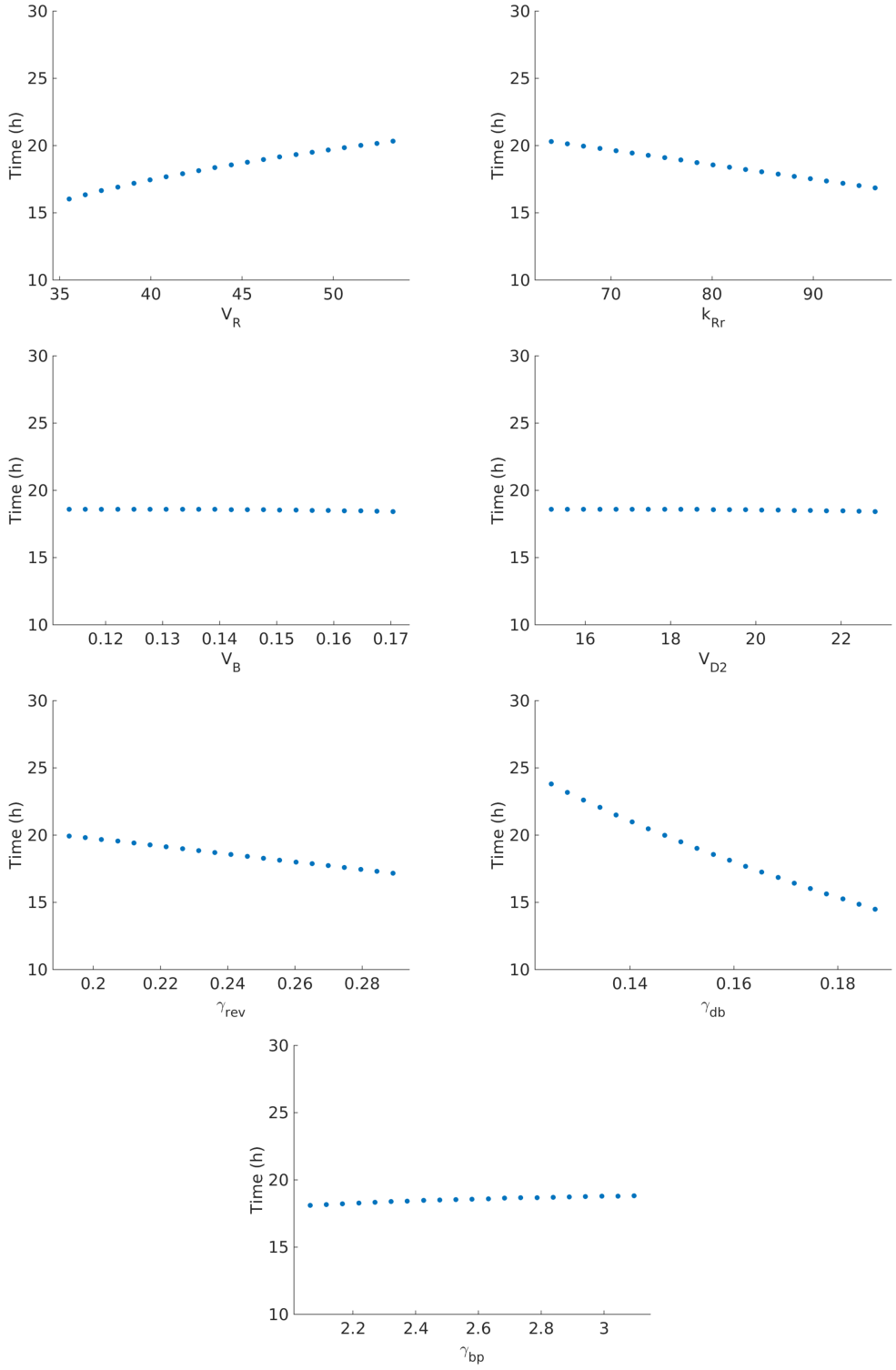

Figure D.9: **Sensitivity analysis and robustness of the reduced clock model (parameters of Table D.2).**
Each parameter is varied 20% around its central point and oscillations are maintained. Increasing the value of V_R increases the period of the system while increasing k_{Rr}, γ_{rev} and γ_{db} decreases the period.

E

Boolean Model of the Circadian Clock

Boolean Model Equations:

$$\frac{d[BMAL1]}{dt} = \overline{REV} \vee \overline{PER:CRY} \tag{E.1}$$

$$\frac{d[DBP]}{dt} = BMAL1 \tag{E.2}$$

$$\frac{d[REV]}{dt} = DBP \tag{E.3}$$

$$\frac{d[PER:CRY]}{dt} = DBP \vee \overline{BMAL1} \tag{E.4}$$

In order to reduce the model we consider the effect of BMAL1 via DBP directly acting on REV and PER:CRY.

Reduced Boolean Model Equations:

$$\frac{d[BMAL1]}{dt} = \overline{REV} \vee \overline{PER:CRY} \tag{E.5}$$

$$\frac{d[REV]}{dt} = BMAL1 \tag{E.6}$$

$$\frac{d[PER:CRY]}{dt} = BMAL1 \vee \overline{BMAL1} \tag{E.7}$$

Fig. E.1 shows a scheme of the reduced discrete model, the solution has collapsed into one of the sub-cycles of the bigger model (see main article). PER:CRY is always up (see equation E.7). This allows to understand why oscillation is not possible in the continuous model reduced model without DBP.

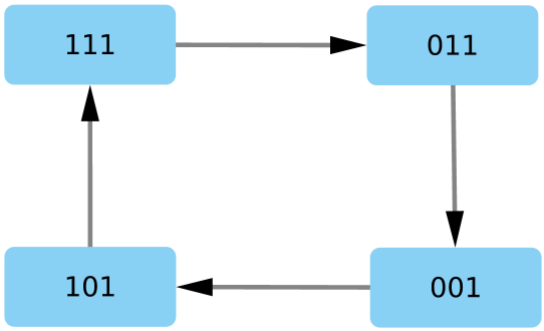

Figure E.1: **Reduced boolean model output.**
The solution of the reduced boolean model is a sub-cycle of the solution of the complete boolean model. Here PER:CRY doesn't oscillate.

F

Supporting Information of Chapter 4

F.1 Scaling of parameters for the coupled clock/cell cycle systems

Changes the time scale of the systems dynamics consists in multiplying by constants the subsets of calibrated parameters that represent rates of change (p_x and p_y for the cell cycle and clock respectively). Thus, for the cell cycle we make $p_x \rightarrow \beta\ p_x$ on parameters of Table 2.1, where:

$$p_x = \begin{bmatrix} \gamma_1 \\ V_c \\ V_w \\ V_m \\ V_k \\ GF \end{bmatrix} \tag{F.1}$$

and $\beta = 10$. Note that GF is varied through the majority of coupling studies. For the circadian clock we make $p_y \rightarrow \mu\ p_y$ on parameters of Table D.2, where

$$p_y = \begin{bmatrix} V_R \\ V_B \\ V_{D2} \\ \gamma_{rev} \\ \gamma_{db} \\ \gamma_{bp} \end{bmatrix} \tag{F.2}$$

and $\mu = \frac{18.6}{24} = 0.775$, thus changing the period from 18,6 h to 24 h. As both systems were previously normalized to a certain concentration value, the solution of the coupled system is unitless.

Table F.1: Parameters of the models for the two oscillators after scaling.

p	Numerical Value
V_R	34.4 h^{-1}
k_{Rr}	80.1
V_B	0.11 h^{-1}
V_{D2}	14.7 h^{-1}
γ_{rev}	0.187 h^{-1}
γ_{db}	0.121 h^{-1}
γ_{bp}	2.0 h
γ_1	0.162 h^{-1}
V_c	2260 h^{-1}
k_c	130
V_w	7480 h^{-1}
k_w	138
k_m	99
k_n	0.116
V_m	1.68 h^{-1}
V_k	1.07 h^{-1}
MPF_{max}	284

F.2 Supplementary Figures of Coupled Oscillators Analysis

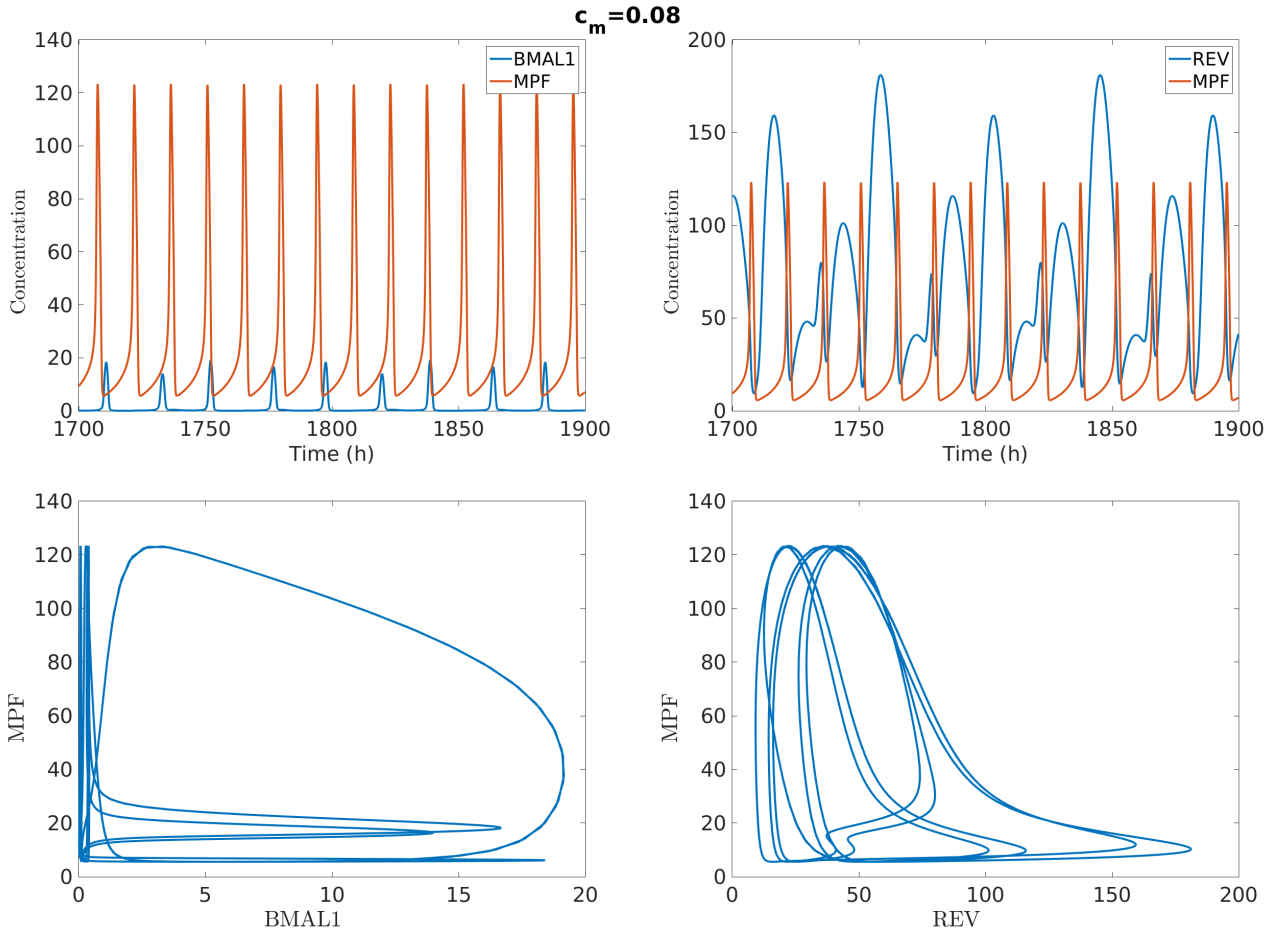

Figure F.1: **Oscillations and phase portraits of BMAL1 and MPF in a 3:2 period-lock.** With GF = 40 and coupling strength $c_m = 0.08$ the solution shows a 3:2 period-lock, where during each time interval where a periodic repetition of four peaks of BMAL1 occurs, there are six peaks of MPF. There are also two relevant peaks of REV (above mean REV value) for each three relevant peaks of MPF (above mean MPF value). The cell cycle period is kept constant at 14,5 h in the unidirectional coupling, the clock period (computed as the average of the time difference between peaks of BMAL1) is 21,7 h.

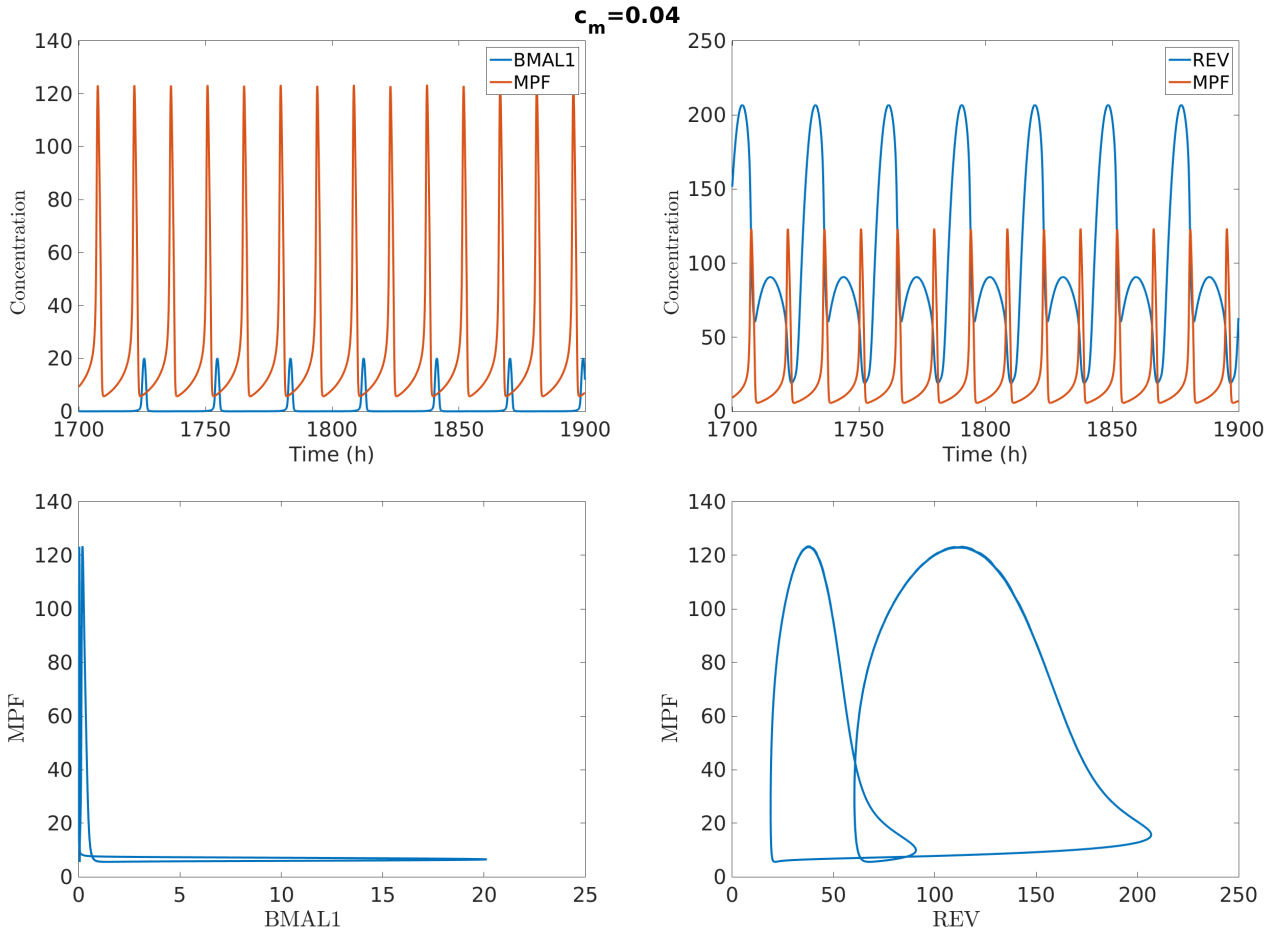

Figure F.2: **Oscillations and phase portraits of BMAL1, REV and MPF in a 2:1 period-lock.**
While keeping GF = 40, the cell cycle period is kept constant at 14,5 h in the unidirectional coupling. The coupling strength $c_m = 0.04$ results in a solution with a 2:1 period-lock, where the clock period is 28,9 h.

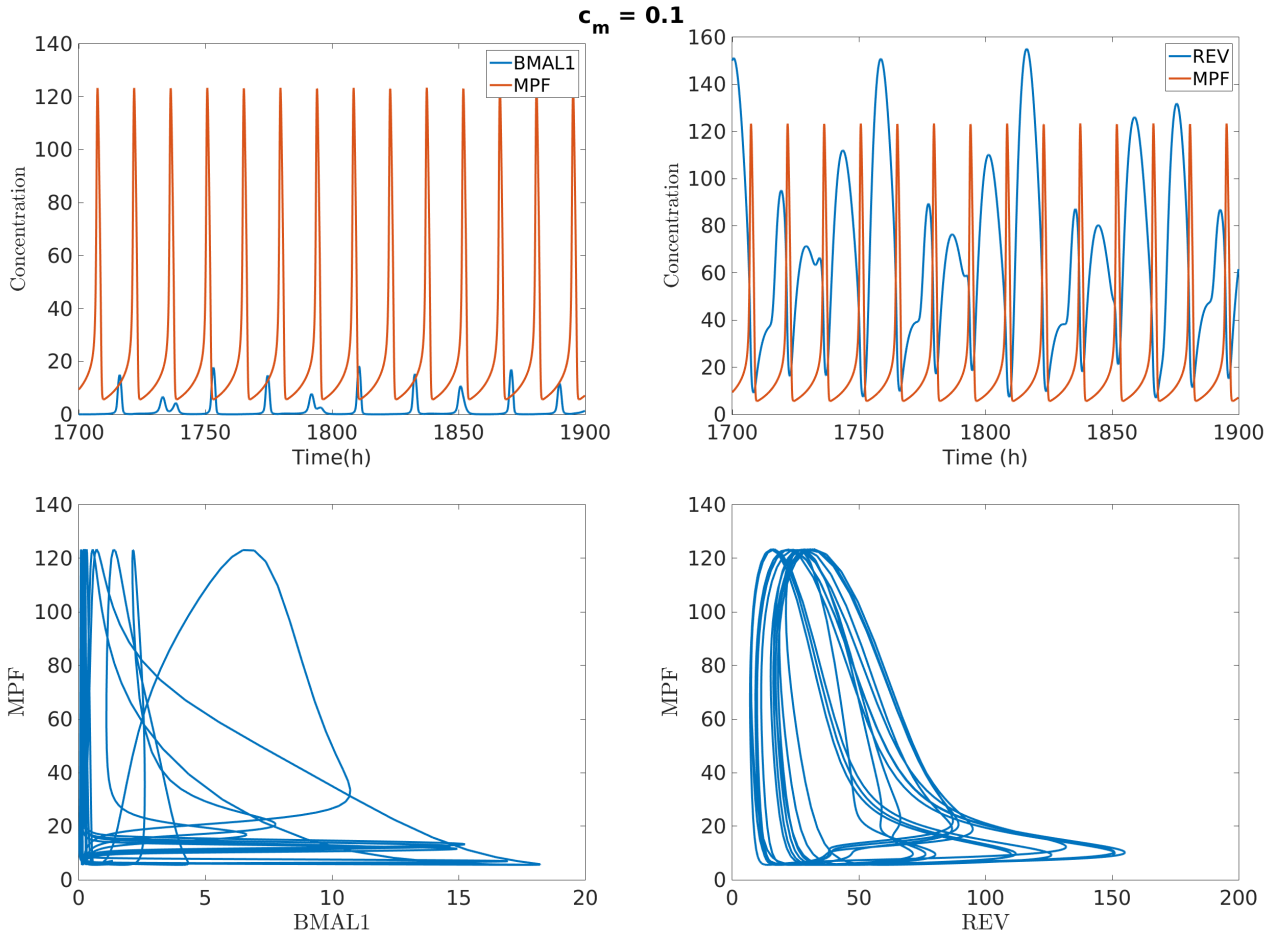

Figure F.3: **Oscillations and phase portraits of BMAL1, REV and MPF for a point outside of the *devil's staircase*.**
While keeping GF = 40, the cell cycle period is kept constant at 14,5 h in the unidirectional coupling. The coupling strength $c_m = 0.1$ results in a solution where the clock has a complex behavior.

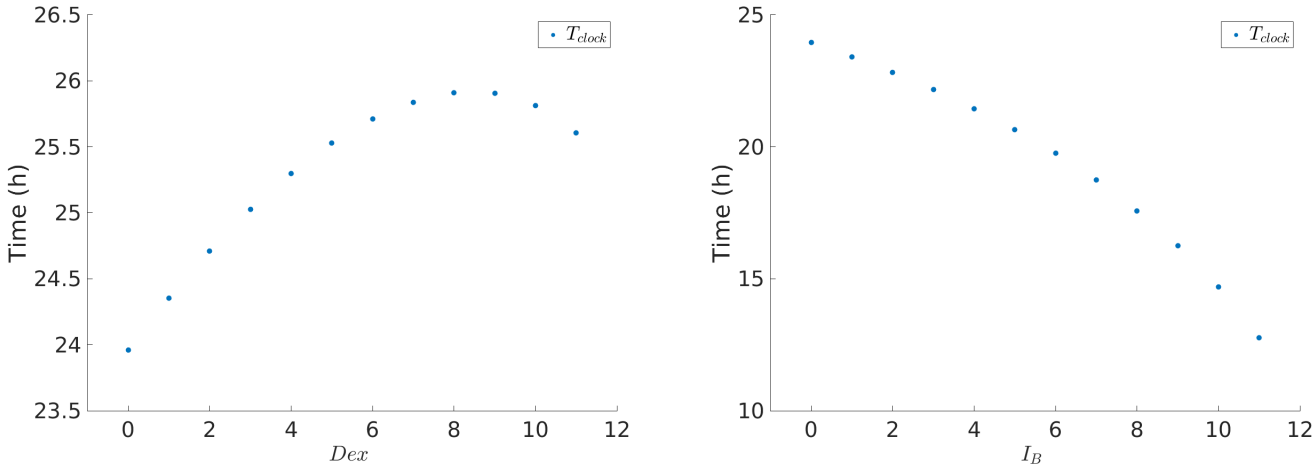

Figure F.4: **Variation of the intrinsic clock period with the Dex and I_B added inputs.** Dex and I_B are varied in the region of oscillation (from 0 to 11): Dex leads to a slower clock, while I_B accelerates the clock.

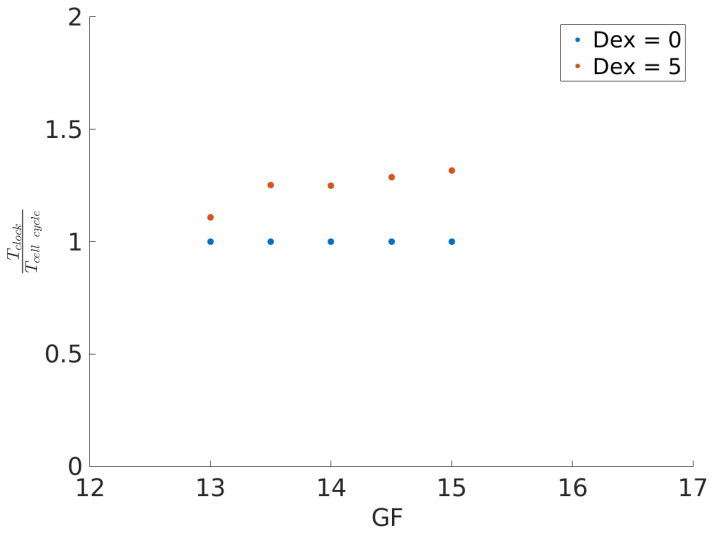

Figure F.5: **Input of Dex in the model coupled via BMAL1 repression of MPF.** With $c_b = 10$ values of $4 \leq GF \leq 15$ and Dex $= 0$ lock in 1:1 state. The introduction of Dex in this system promotes decoupling and a behavior similar to that of a smaller c_b value for a very limited region of GF ($13 \leq GF \leq 15$) .

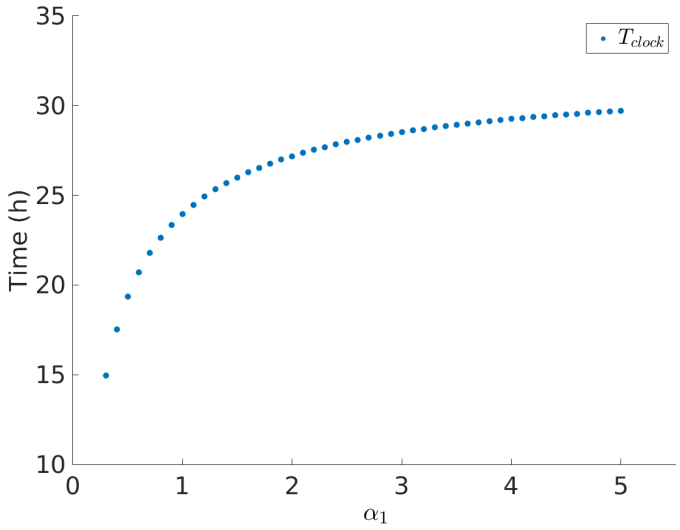

Figure F.6: **Evolution of clock period with parameter** α_1
In general the period of the clock increases with the value of α_1, tending towards saturation. Values of $\alpha_1 < 1$ are representative of the introduction of an R-box agonist in the system and values of $\alpha_1 > 1$ represent activity of R-box antagonistic drugs.

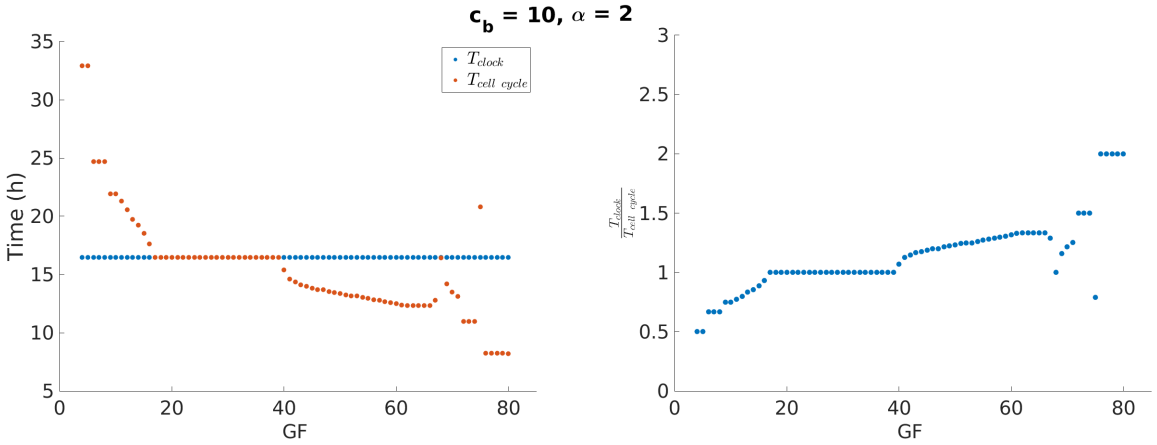

Figure F.7: **Evolution of the oscillators period and synchronization state with GF for** $\alpha = 2$ **in the unidirectional coupling via clock-controlled wee1 activation.**
By increasing γ_{rev} by a factor of 2, the clock is sped from 24 h to 16,5 h, leading to several different synchronization states between clock and cell cycle. This strategy is successfull in slowing down the cell cycle for small GF, where the 1:2 period entrainment occurs.

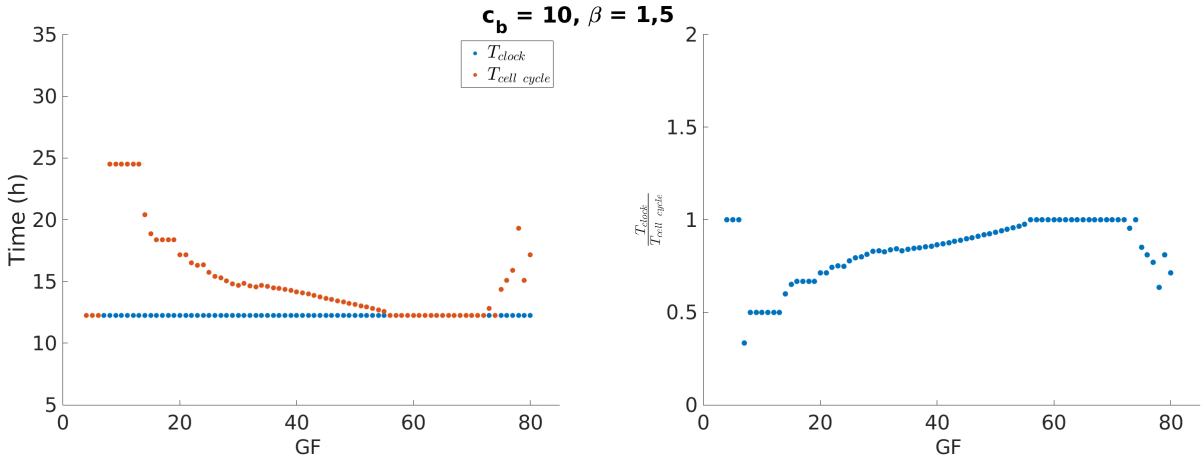

Figure F.8: **Evolution of the oscillators period and synchronization state with GF for $\beta = 1,5$ in the unidirectional coupling via clock-controlled wee1 activation.**
By increasing γ_{db} by a factor of 1,5, the clock is sped from 24 h to 12,4 h, leading to several different period-locked states between clock and cell cycle. The GF region for which the cell cycle is slower than the clock is very wide, however only in a small region the cell cycle period is higher than that of the intrinsic γ_{db} value (24 h with $\beta = 1$).

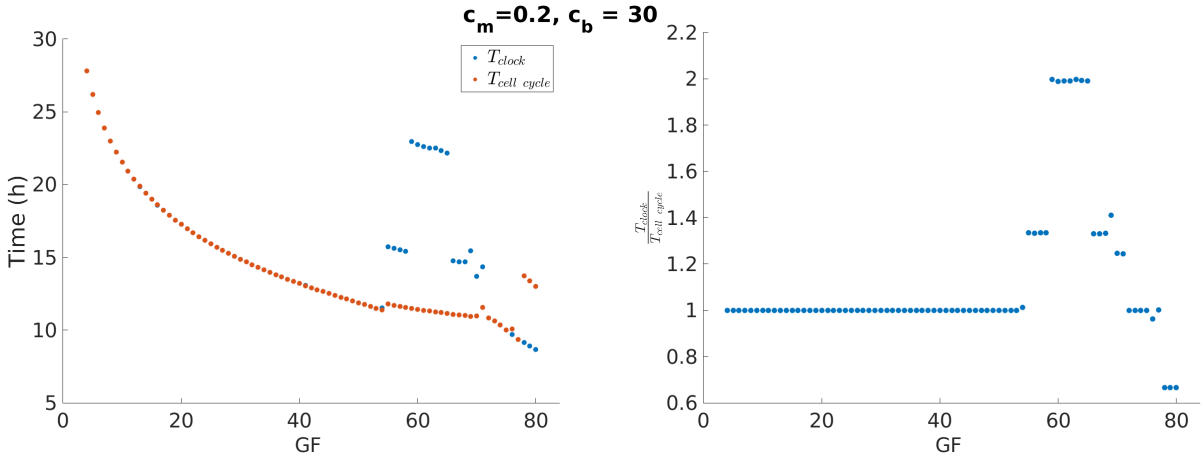

Figure F.9: **GF effect on the oscillators' period and synchronization state with bidirectional coupling via MPF-controlled REV degradation and BMAL1-induced wee1 expression.**
GF is a control parameter for the ratio of period-lock (r_T). With $c_m = 0.2$ and $c_b = 30$, for 4 $\leq$ GF $\leq$ 80 the system locks in 1:1 for the majority of GF values, for high GF other rational ratios appear constant by intervals.

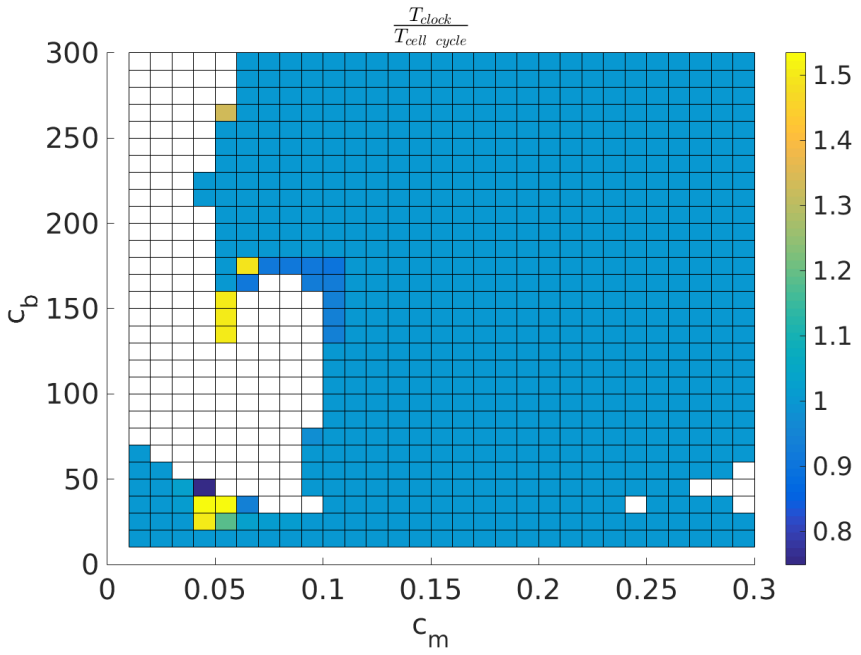

Figure F.10: **Period-lock for different values of c_b and c_m with GF = 5.** Varying c_b and c_m for fixed GF = 5 results in different period-lock ratios. In the white region there is no oscillation.

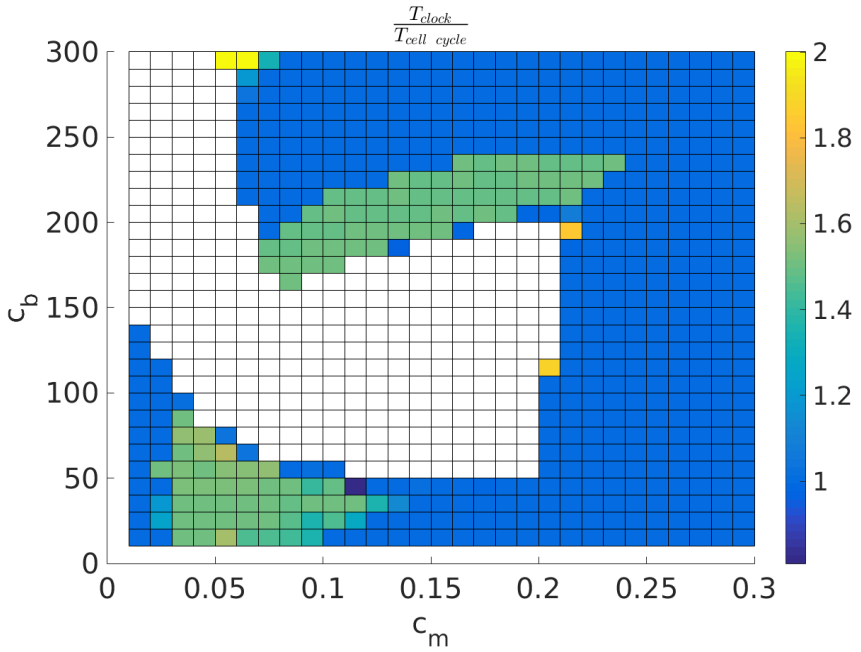

Figure F.11: **Period-lock for different values of c_b and c_m with GF = 10.** Varying c_b and c_m for fixed GF = 10 results in different period-lock ratios. In the white region there is no oscillation.

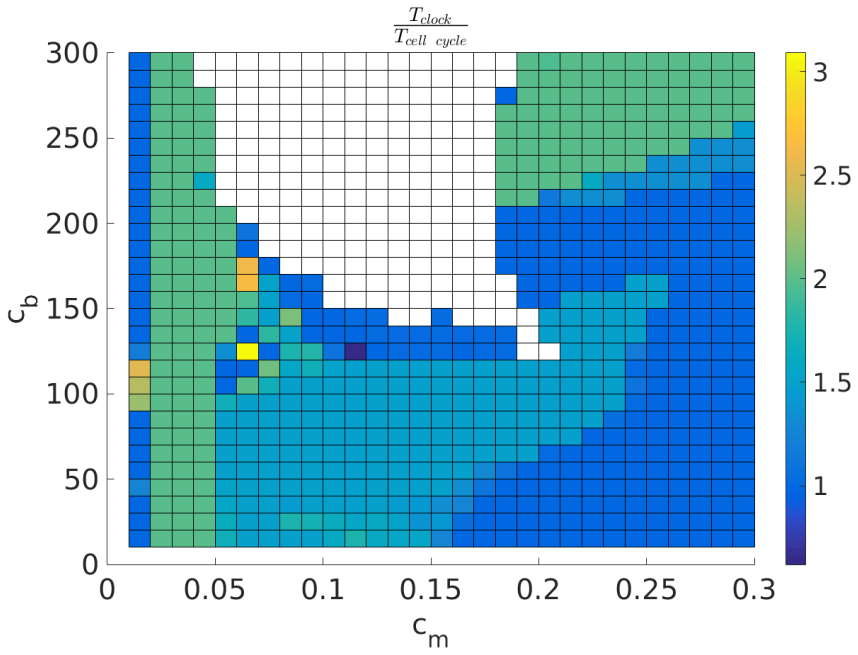

Figure F.12: **Period-lock for different values of c_b and c_m with GF = 30.** Varying c_b and c_m for fixed GF = 30 results in different period-lock ratios. In the white region there is no oscillation.

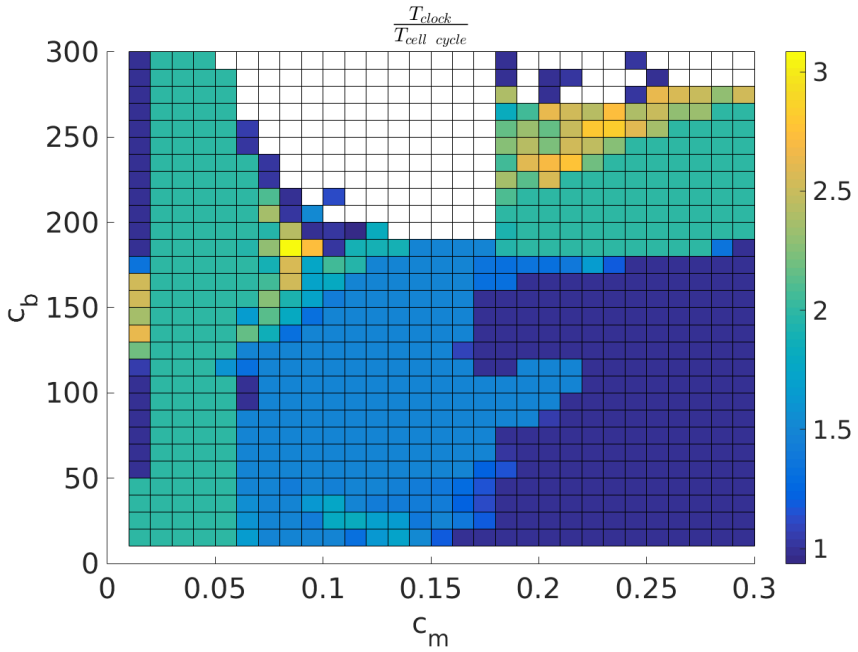

Figure F.13: **Period-lock for different values of c_b and c_m with GF = 40.** Varying c_b and c_m for fixed GF = 40 results in different period-lock ratios. In the white region there is no oscillation.

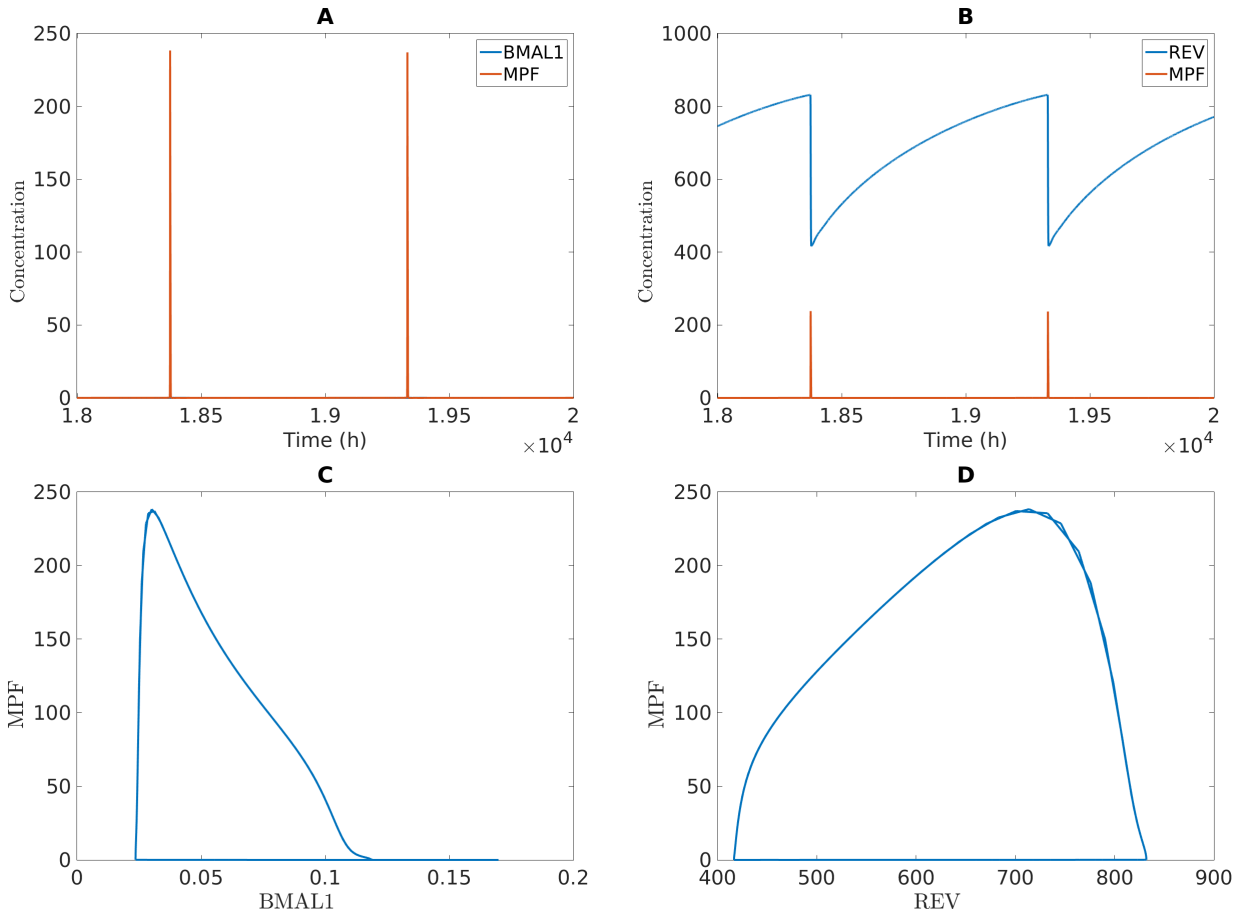

Figure F.14: **An oscillatory solution with a very long period in bidirectional coupling.** The solution for $c_m = 0.01$, $c_b = 70$ and GF=20 results in a very long period: $T_{clock} = T_{cellcycle} =$ 956 h; the system is in 1:1 period-lock.

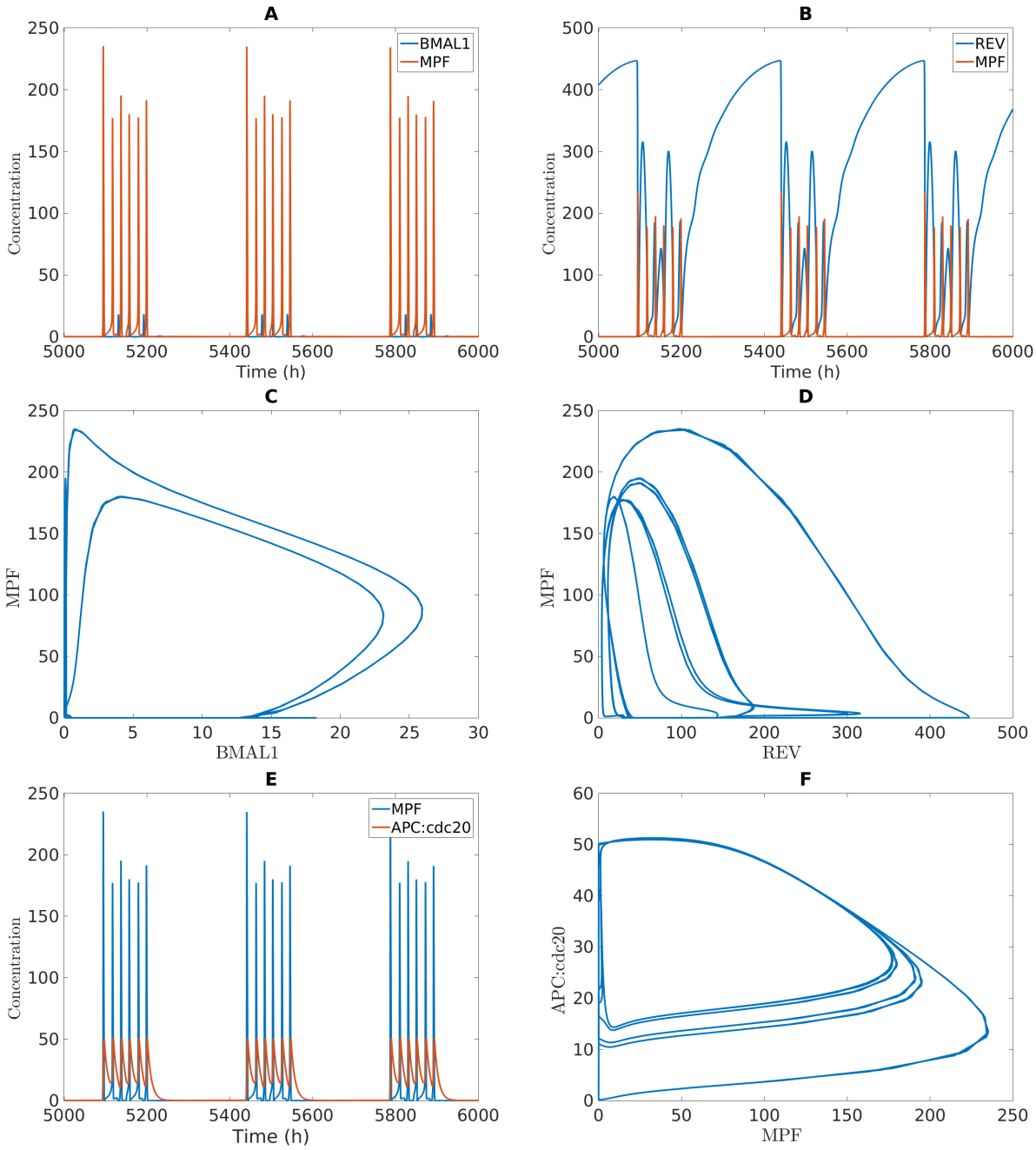

Figure F.15: **An oscillatory solution with complex behavior and a very long period in bidirectional coupling.**
The solution for $c_m = 0.1$, $c_b = 40$ and GF=10 results in a very long period with a complex behavior, where six peaks of MPF and APC:cdc20 occur every 347 h, interleaved by a long time interval where REV is up. $T_{clock} = T_{cellcycle} = 347$ h and in the region of MPF/BMAL1 peaks the two oscillators lock in 3:2 synchronization.

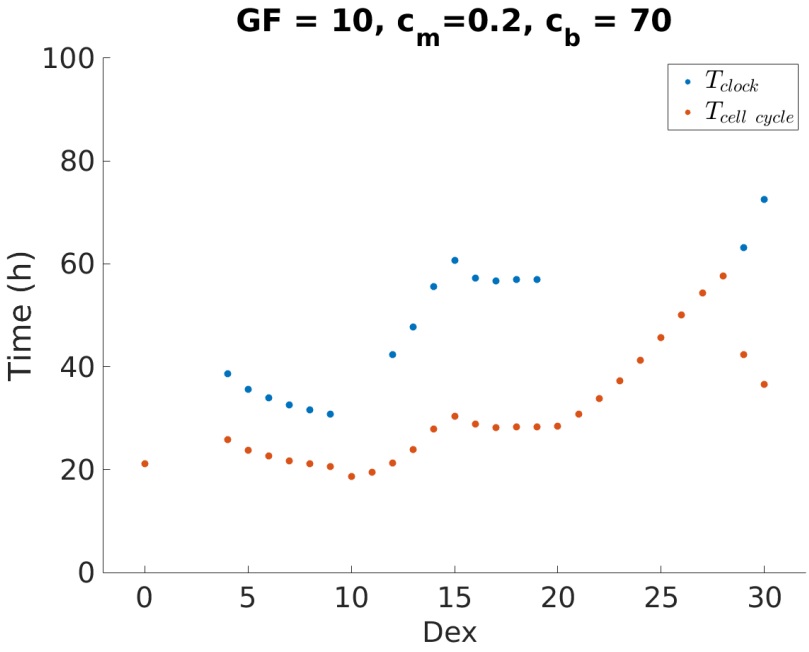

Figure F.16: **Variation of clock and cell cycle periods with Dex.**
When applying an increasing Dex input, the clock and cell cycle periods vary non-linearly: first with a region without oscillation then decreasing and then increasing again.

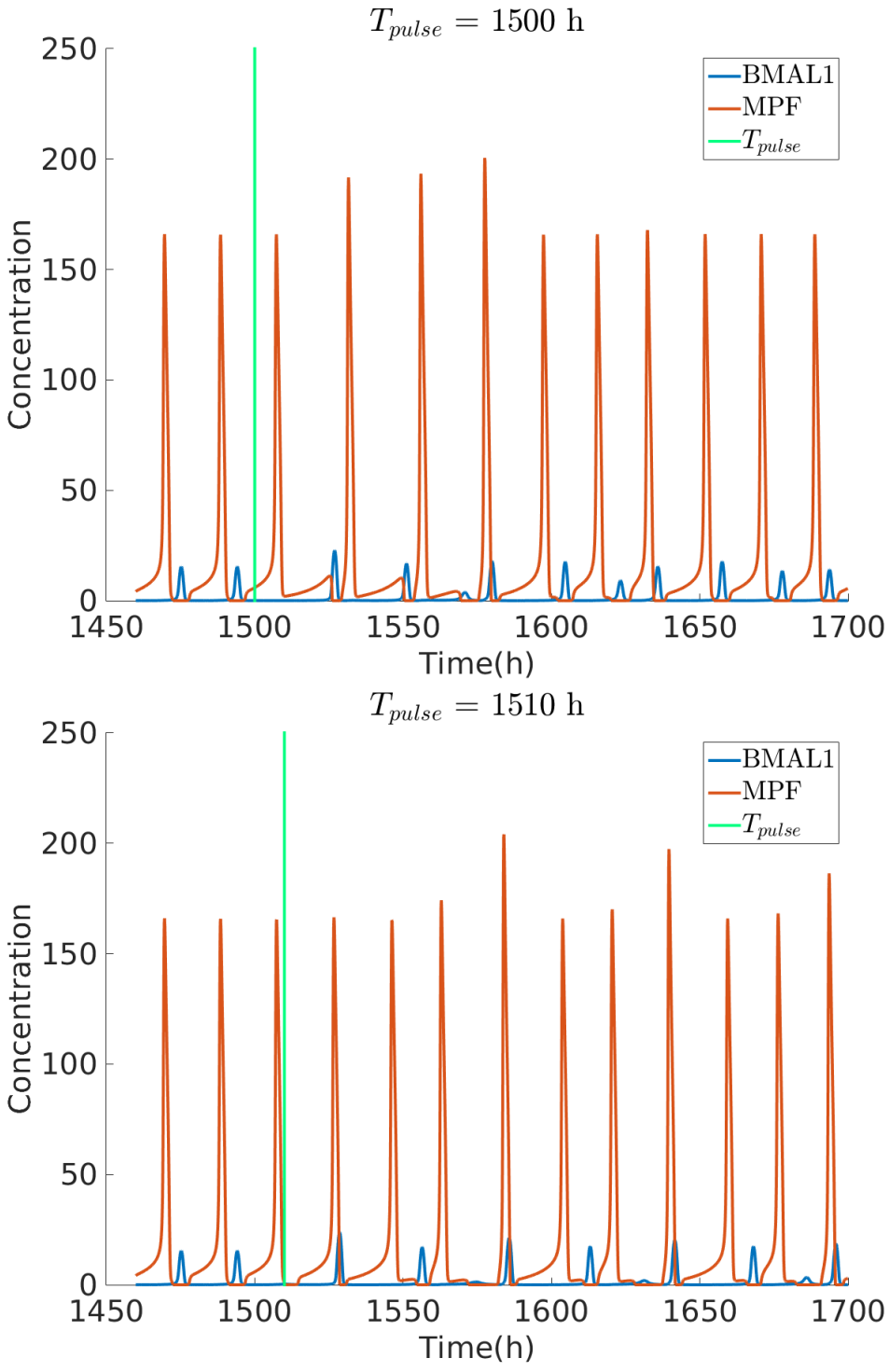

Figure F.17: **Time series of BMAL1 and MPF for T_{pulse} at the responsive and at the non-responsive region.**
Analyzing the three cycles following the pulse application (as was done in our computations of Fig. 4.24 and in experimental settings), there is approximately one peak of BMAL1 for each peak of MPF for T_{pulse} = 1500 h (T_{clock} = 24,3 h and $T_{cell\ cycle}$ = 24,4 h) and two peaks of BMAL1 for each three peaks of MPF for T_{pulse} = 1510 h (T_{clock} = 27,9 h and $T_{cell\ cycle}$ = 18,1h).

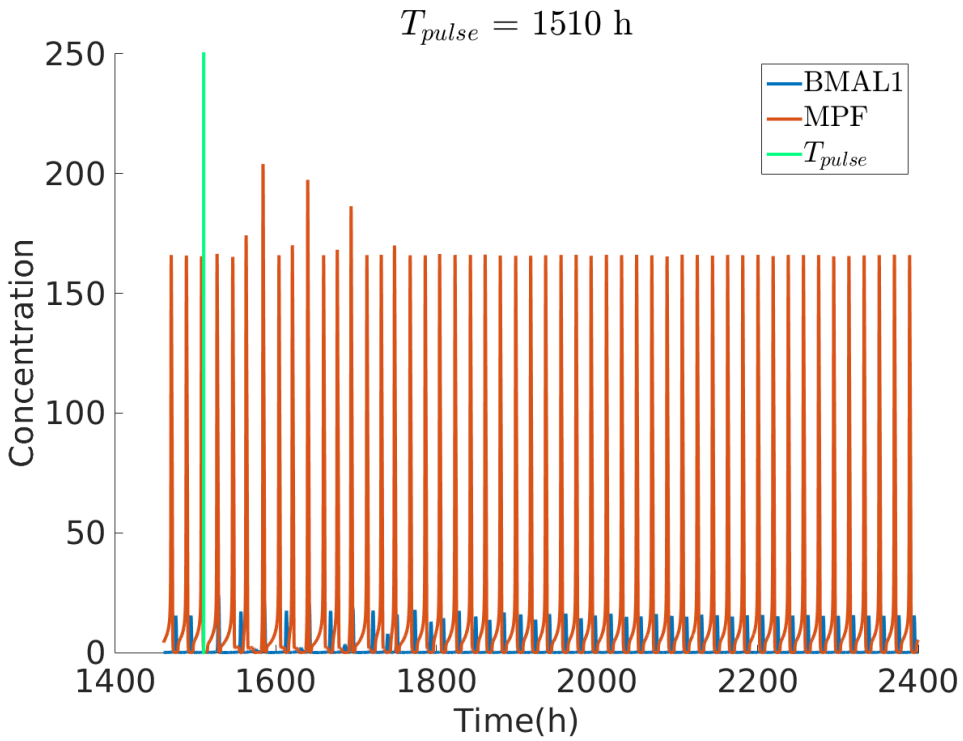

Figure F.18: **Time series of BMAL1 and MPF for T_{pulse} = 1510 h.** Same simulation as in the bottom panel of Fig. F.17 for a longer running time: the return to 1:1 synchronization can be seen.

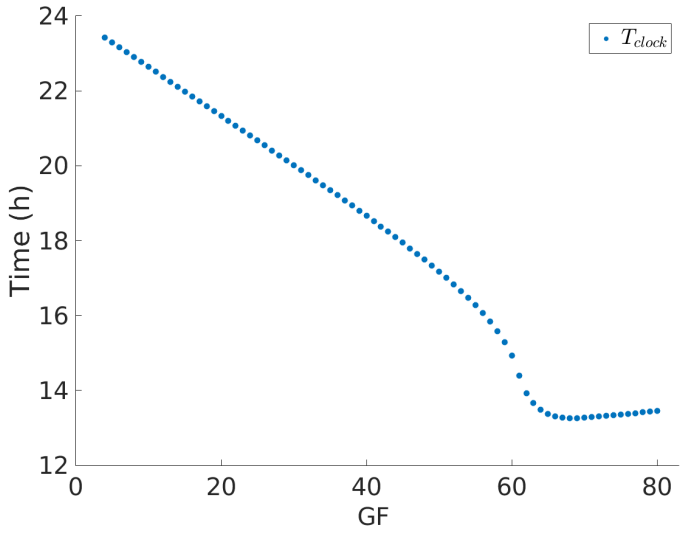

Figure F.19: **Clock period change with GF in the GF-controlled clock system.** As GF increases the period of the circadian clock decreases. Thus GF as a similar speeding up effect in the periods of both the clock and the cell cycle.

Bibliography

[1] Feillet C, Krusche P, Tamanini F, Janssens RC, Downey MJ, Martin P, Teboul M, Saito S, Lévi FA, Bretschneider T, van der Horst GT, Delaunay F, Rand DA. Phase locking and multiple oscillating attractors for the coupled mammalian clock and cell cycle. Proc Natl Acad Sci U S A. 2014 Jul 8;111(27):9828-33.

[2] ICycle Project . https://project.inria.fr/icycle/

[3] Purcell O, Savery NJ, Grierson CS, di Bernardo M. A comparative analysis of synthetic genetic oscillators. J R Soc Interface. 2010 Nov 6;7(52):1503-24.

[4] Almeida S, Chaves M, Delaunay F, Feillet C. A comprehensive reduced model of the mammalian cell cycle. IFAC-PapersOnLine 2017; 50(1):12617-22.

[5] Lodish H, Berk A, Zipursky SL, Matsudaira P, Baltimore D, Darnell J. Molecular Cell Biology. New York: W. H. Freeman; 2000.

[6] Ciliberto A, Lukács A, Tóth A, Tyson JJ, Novák B. Rewiring the exit from mitosis. Cell Cycle. 2005 Aug;4(8):1107-12.

[7] Perry JA, Kornbluth S. Cdc25 and Wee1: analogous opposites? Cell Div. 2007 May 4;2:12.

[8] Kramer ER, Scheuringer N, Podtelejnikov AV, Mann M, Peters JM. Mitotic regulation of the APC activator proteins CDC20 and CDH1. Mol Biol Cell. 2000 May;11(5):1555-69.

[9] Takahashi J. Transcriptional architecture of the mammalian circadian clock. Nat Rev Genet. 2017 Mar;18(3):164-179.

[10] Buhr E, Takahashi J. Molecular components of the mammalian circadian clock. Handb Exp Pharmacol. 2013; (217): 3–27.

[11] Preußner M, Heyd F. Post-transcriptional control of the mammalian circadian clock: implications for health and disease. Pflugers Arch. 2016 Jun;468(6):983-91.

[12] Gallego M, Virshup DM. Post-translational modifications regulate the ticking of the circadian clock. Nat Rev Mol Cell Biol. 2007 Feb; 8(2): 139-48.

[13] Leproult R, Holmbäck U, Van Cauter E. Circadian misalignment augments markers of insulin resistance and inflammation, independently of sleep loss. Diabetes. 2014 Jun;63(6):1860-9.

[14] Shostak A. Circadian Clock, Cell Division, and Cancer: From Molecules to Organism. Int J Mol Sci. 2017 Apr 20;18(4).

[15] Sulli G, Rommel A, Wang X, Kolar MJ, Puca F, Saghatelian A, Plikus MV, Verma IM, Panda S. Pharmacological activation of REV-ERBs is lethal in cancer and oncogene-induced senescence. Nature. 2018 Jan 18;553(7688):351-355.

[16] Brum MC, Filho FF, Schnorr CC, Bottega GB, Rodrigues TC. Shift work and its association with metabolic disorders. Diabetol Metab Syndr. 2015 May 17;7:45.

[17] West AC, Smith L, Ray DW, Loudon ASI, Brown TM, Bechtold DA. Misalignment with the external light environment drives metabolic and cardiac dysfunction. Nat Commun. 2017 Sep 12;8(1):417.

[18] Woller A, Duez H, Staels B, Lefranc M. A Mathematical Model of the Liver Circadian Clock Linking Feeding and Fasting Cycles to Clock Function. Cell Rep. 2016 Oct 18;17(4):1087-1097.

[19] Ozturk N, Ozturk D, Kavakli IH, Okyar A. Molecular Aspects of Circadian Pharmacology and Relevance for Cancer Chronotherapy. Int J Mol Sci. 2017 Oct 17;18(10).

[20] Feillet C, van der Horst GT, Levi F, Rand DA, Delaunay F. Coupling between the Circadian Clock and Cell Cycle Oscillators: Implication for Healthy Cells and Malignant Growth. Front Neurol. 2015 May 11;6:96.

[21] Matsuo T, Yamaguchi S, Mitsui S, Emi A, Shimoda F, Okamura H. Control mechanism of the circadian clock for timing of cell division in vivo. Science. 2003 Oct 10;302(5643):255-9.

[22] Gréchez-Cassiau A, Rayet B, Guillaumond F, Teboul M, Delaunay F. The circadian clock component BMAL1 is a critical regulator of p21WAF1/CIP1 expression and hepatocyte proliferation. J Biol Chem. 2008 Feb 22;283(8):4535-42.

[23] Pérez-Roger I, Solomon DL, Sewing A, Land H. Myc activation of cyclin E/Cdk2 kinase involves induction of cyclin E gene transcription and inhibition of p27(Kip1) binding to newly formed complexes. Oncogene. 1997 May 22;14(20):2373-81.

[24] Fu L, Pelicano H, Liu J, Huang P, Lee C. The circadian gene Period2 plays an important role in tumor suppression and DNA damage response in vivo. Cell. 2002 Oct 4;111(1):41-50.

[25] Zámborszky J, Hong CI, Csikász Nagy A. Computational analysis of mammalian cell division gated by a circadian clock: quantized cell cycles and cell size control. J Biol Rhythms. 2007 Dec;22(6):542-53.

[26] Gérard C, Goldbeter A. Entrainment of the Mammalian Cell Cycle by the Circadian Clock: Modeling Two Coupled Cellular Rhythms. PLoS Comput Biol. 2012 May;8(5):e1002516.

[27] Nagoshi E, Saini C, Bauer C, Laroche T, Naef F, Schibler U. Circadian gene expression in individual fibroblasts: cell-autonomous and self-sustained oscillators pass time to daughter cells. Cell. 2004 Nov 24;119(5):693-705.

[28] Traynard P, Feillet C, Soliman S, Delaunay F, Fages F. Model-based investigation of the circadian clock and cell cycle coupling in mouse embryonic fibroblasts: Prediction of RevErb-α up-regulation during mitosis. Biosystems. 2016 Nov;149:59-69.

[29] So AY, Bernal TU, Pillsbury ML, Yamamoto KR, Feldman BJ. Glucocorticoid regulation of the circadian clock modulates glucose homeostasis. Proc Natl Acad Sci U S A. 2009 Oct 13;106(41):17582-7.

[30] Bieler J, Cannavo R, Gustafson K, Gobet C, Gatfield D, Naef F. Robust synchronization of coupled circadian and cell cycle oscillators in single mammalian cells. Mol Syst Biol. 2014 Jul 15;10:739.

[31] Tyson JJ. Numerical analysis of a comprehensive model of M-phase control in Xenopus oocyte extracts and intact embryos. Proc Natl Acad Sci U S A. 1991 Aug 15;88(16):7328-32.

[32] Novak B, Tyson JJ. Numerical analysis of a comprehensive model of M-phase control in Xenopus oocyte extracts and intact embryos. J Cell Sci. 1993 Dec;106 (Pt 4):1153-68.

[33] Pomerening JR, Sontag ED, Ferrell JE Jr. Building a cell cycle oscillator: hysteresis and bistability in the activation of Cdc2. Nat Cell Biol. 2003 Apr;5(4):346-51.

[34] Qu Z, MacLellan WR, Weiss JN. Dynamics of the Cell Cycle: Checkpoints, Sizers, and Timers. Biophys J. 2003 Dec; 85(6): 3600–3611.

[35] Pomerening JR, Kim SY, Ferrell JE Jr. Systems-level dissection of the cell-cycle oscillator: bypassing positive feedback produces damped oscillations. Cell. 2005 Aug 26;122(4):565-78.

[36] Gérard C, Goldbeter A. Temporal self-organization of the cyclin/Cdk network driving the mammalian cell cycle. Proc Natl Acad Sci U S A. 2009 Dec 22;106(51):21643-8.

[37] Gérard C1, Goldbeter A. A skeleton model for the network of cyclin-dependent kinases driving the mammalian cell cycle. Interface Focus. 2011 Feb 6;1(1):24-35.

[38] Gérard C, Gonze D, Goldbeter A. Effect of positive feedback loops on the robustness of oscillations in the network of cyclin-dependent kinases driving the mammalian cell cycle. FEBS J. 2012 Sep;279(18):3411-31.

[39] Gérard C, Tyson JJ, Coudreuse D, Novák B. Cell Cycle Control by a Minimal Cdk Network. PLoS Comput Biol. 2015 Feb 6;11(2):e1004056.

[40] Goodwin B C. Oscillatory behavior in enzymatic control processes. Advances in Enzyme Regulation. 1965; 3: 425-437.

[41] Leloup JC, Goldbeter A. Toward a detailed computational model for the mammalian circadian clock. Proc Natl Acad Sci U S A. 2003 Jun 10;100(12):7051-6.

[42] Forger DB, Peskin CS. A detailed predictive model of the mammalian circadian clock. Proc Natl Acad Sci U S A. 2003 Dec 9;100(25):14806-11.

[43] Leloup JC, Goldbeter A. Modeling the mammalian circadian clock: sensitivity analysis and multiplicity of oscillatory mechanisms. J Theor Biol. 2004 Oct 21;230(4):541-62.

[44] Becker-Weimann S., Wolf J., Herzel H., Kramer A. Modeling Feedback Loops of the Mammalian Circadian Oscillator. Biophys J. 2004 Nov; 87(5): 3023–3034.

[45] Mirsky HP, Liu AC, Welsh DK, Kay SA, Doyle FJ 3rd. A model of the cell-autonomous mammalian circadian clock. Proc Natl Acad Sci U S A. 2009 Jul 7;106(27):11107-12.

[46] Relógio A, Westermark PO , Wallach T, Schellenberg K, Kramer A, Herzel H. Tuning the Mammalian Circadian Clock: Robust Synergy of Two Loops. PLoS Comput Biol. 2011 Dec; 7(12): e1002309.

[47] Comet JP, Bernot G, Das A, Diener F, Massot C, Cessieux A. Simplified Models for the Mammalian Circadian Clock. Procedia Computer Science. 2012; 11:127-138.

[48] Korenčič A, Bordyugov G, Košir R, Rozman D, Goličnik M, Herzel H. The Interplay of cis-Regulatory Elements Rules Circadian Rhythms in Mouse Liver. PLoS One. 2012;7(11):e46835.

[49] Jolley C, Ukai-Tadenuma M, Perrin D, Ueda H. A Mammalian Circadian Clock Model Incorporating Daytime Expression Elements. Biophys J. 2014 Sep; 107(6): 1462–1473.

[50] Podkolodnaya OA, Tverdokhleb NN, Podkolodnyy NL. Computational modeling of the cell-autonomous mammalian circadian oscillator. BMC Syst Biol. 2017 Feb; 11(Suppl 1):379.

[51] de Jong H. Modeling and simulation of genetic regulatory systems: A literature review. J Comput Biol. 2002;9(1):67-103.

[52] Segel LA. On the validity of the steady state assumption of enzyme kinetics. Bull Math Biol. 1988;50(6):579-93.

[53] J. Kuntz and D.A. Oyarzún and G.-B. Sta Model reduction of genetic-metabolic systems using timescale separation. Springer-Verlag, New York. 2014; System Theoretic Approaches to Systems and Synthetic Biology: 181-210.

[54] Perko L. Differential equations and dynamical systems. Springer-Verlag, New York. 1991.

[55] Bak P. The Devil's Staircase Physics Today. 1986 Dec;39(12):38.

[56] Zhao X, Hirota T, Han X, Cho H, Chong LW, Lamia K, Liu S, Atkins AR, Banayo E, Liddle C, Yu RT, Yates JR 3rd, Kay SA, Downes M, Evans RM. Circadian Amplitude Regulation via FBXW7-Targeted REV-ERBα Degradation. Cell. 2016 Jun 16;165(7):1644-1657.

[57] Sible JC, Tyson JJ. Mathematical Modeling as a Tool for Investigating Cell Cycle Control Networks. Methods. 2007 Feb;41(2):238-47.

[58] Sha W, Moore J, Chen K, Lassaletta AD, Yi CS, Tyson JJ, Sible JC. Hysteresis drives cell-cycle transitions in Xenopus laevis egg extracts. Proc Natl Acad Sci U S A. 2003 Feb 4;100(3):975-80.

[59] Yang Q, Ferrell JE Jr. The Cdk1-APC/C cell cycle oscillator circuit functions as a time-delayed, ultrasensitive switch. Nat Cell Biol. 2013 May;15(5):519-25.

[60] Tsai TY, Choi YS, Ma W, Pomerening JR, Tang C, Ferrell JE Jr. Robust, tunable biological oscillations from interlinked positive and negative feedback loops. Science. 2008 Jul 4;321(5885):126-9.

[61] Koike N, Yoo SH, Huang HC, Kumar V, Lee C, Kim TK, Takahashi J. Transcriptional Architecture and Chromatin Landscape of the Core Circadian Clock in Mammals. Science. 2012 Oct; 338(6105): 349–354.

[62] Zehring WA, Wheeler DA, Reddy P, Konopka RJ, Kyriacou CP, Rosbash M, Hall JC. P-element transformation with period locus DNA restores rhythmicity to mutant, arrhythmic Drosophila melanogaster. Cell. 1984 Dec;39(2 Pt 1):369-76.

[63] Bell-Pedersen D, Cassone VM, Earnest DJ, Golden SS, Hardin PE, Thomas TL, Zoran MJ. Circadian rhythms from multiple oscillators: lessons from diverse organisms. Nat Rev Genet. 2005 Jul;6(7):544-56.

[64] Yan J, Shi G, Zhang Z, Wu X, Liu Z, Xing L, Qu Z, Dong Z, Yang L, Xu Y. An intensity ratio of interlocking loops determines circadian period length. Nucleic Acids Res. 2014;42(16):10278-87.

[65] Ye R, Selby CP, Chiou YY, Ozkan-Dagliyan I, Gaddameedhi S, Sancar A. Dual modes of CLOCK:BMAL1 inhibition mediated by Cryptochrome and Period proteins in the mammalian circadian clock. Genes Dev. 2014 Sep; 28(18): 1989–1998.

[66] Smolen P D, Byrne, J H. Circadian Rhythm Models. Encyclopedia of Neuroscience. Elsevier Ltd. 2010; 957-963.

[67] Yamaguchi S, Mitsui S, Yan L, Yagita K, Miyake S, Okamura H. Role of DBP in the Circadian Oscillatory Mechanism. Mol Cell Biol. 2000 Jul; 20(13): 4773–4781.

[68] Lefta M, Wolff G, Esser KA. Circadian Rhythms, the Molecular Clock, and Skeletal Muscle. Curr Top Dev Biol. 2011;96:231-71.

[69] Ueda HR, Hayashi S, Chen W, Sano M, Machida M, Shigeyoshi Y, Iino M, Hashimoto S. System-level identification of transcriptional circuits underlying mammalian circadian clocks. Nat Genet. 2005 Feb;37(2):187-92.

[70] Yang F, Inoue I, Kumagai M, Takahashi S, Nakajima Y, Ikeda M. Real-time analysis of the circadian oscillation of the Rev-Erb β promoter. J Atheroscler Thromb. 2013;20(3):267-76.

[71] Yamamoto T, Nakahata Y, Soma H, Akashi M, Mamine T, Takumi T. Transcriptional oscillation of canonical clock genes in mouse peripheral tissues BMC Mol Biol. 2004 Oct; 5:18.

[72] Ukai-Tadenuma M, Yamada RG, Xu H, Ripperger JA, Liu AC, Ueda HR. Delay in feedback repression by cryptochrome 1 is required for circadian clock function. Cell. 2011 Jan 21;144(2):268-81.

[73] Bernot G, Comet J P, Richard A, Chaves M, Gouzé J L, Dayan F. Modeling and analysis of gene regulatory networks. In "Modeling in Computational Biology and Biomedicine", F. Cazals and P. Kornprobst Eds, Springer-Verlag Heidelberg (2013), pp. 47-80 .

[74] Crumbley C, Wang Y, Kojetin D J, P. Burris T P. Characterization of the Core Mammalian Clock Component, NPAS2, as a REV-ERBα/RORα Target Gene J Biol Chem. 2010 Nov; 285(46): 35386–92.

[75] Zamir I, Zhang J, Lazar M A. Stoichiometric and steric principles governing repression by nuclear hormone receptors. Genes Dev. 1997 Apr; 11(7):835-46.

[76] Everett L J, Lazar M A. Nuclear Receptor Rev-erbα: Up, Down, and All Around Trends Endocrinol Metab. 2014 Nov; 25(11): 586–592.

[77] Ko CH, Takahashi JS. Molecular components of the mammalian circadian clock. Hum Mol Genet. 2006 Oct 15;15.

[78] Yamajuku D, Shibata Y, Kitazawa M, Katakura T, Urata H, Kojima T, Takayasu S, Nakata O, Hashimoto S. Cellular DBP and E4BP4 proteins are critical for determining the period length of the circadian oscillator. FEBS Lett. 2011 Jul;585(14):2217-22.

[79] Gallego M, Eide EJ, Woolf MF, Virshup DM, Forger DB. An opposite role for tau in circadian rhythms revealed by mathematical modeling. Proc Natl Acad Sci U S A. 2006 Jul 11;103(28):10618-23.

[80] Ralph MR, Menaker M. A mutation of the circadian system in golden hamsters. Science. 1988 Sep 2;241(4870):1225-7.

[81] Meng QJ, Logunova L, Maywood ES, Gallego M, Lebiecki J, Brown TM, Sládek M, Semikhodskii AS, Glossop NRJ, Piggins HD, Chesham JE, Bechtold DA, Yoo SH, Takahashi JS, Virshup DM, Boot-Handford RP, Hastings MH, Loudon ASI. Setting clock speed in mammals: the CK1 epsilon tau mutation in mice accelerates circadian pacemakers by selectively destabilizing PERIOD proteins. Neuron. 2008 Apr 10;58(1):78-88.

[82] Loudon AS, Meng QJ, Maywood ES, Bechtold DA, Boot-Handford RP, Hastings MH. The biology of the circadian Ck1epsilon tau mutation in mice and Syrian hamsters: a tale of two species. Cold Spring Harb Symp Quant Biol. 2007;72:261-71.

[83] la Fleur SE, Kalsbeek A, Wortel J, Fekkes ML, Buijs RM. A daily rhythm in glucose tolerance: a role for the suprachiasmatic nucleus. Diabetes. 2001 Jun;50(6):1237-43.

[84] Oklejewicz M, Hut RA, Daan S, Loudon AS, Stirland AJ. Metabolic rate changes proportionally to circadian frequency in tau mutant Syrian hamsters. J Biol Rhythms. 1997 Oct;12(5):413-22.

[85] Trott AJ, Menet JS. Regulation of circadian clock transcriptional output by CLOCK:BMAL1. PLoS Genet. 2018 Jan 4;14(1):e1007156.

[86] Saini C, Morf J, Stratmann M, Gos P, Schibler U. Simulated body temperature rhythms reveal the phase-shifting behavior and plasticity of mammalian circadian oscillators. Genes Dev. 2012 Mar 15;26(6):567-80.

[87] Ramsey KM, Yoshino J, Brace CS, Abrassart D, Kobayashi Y, Marcheva B, Hong HK, Chong JL, Buhr ED, Lee C, Takahashi JS, Imai S, Bass J. Circadian Clock Feedback Cycle Through NAMPT-Mediated NAD+ Biosynthesis. Science. 2009 May 1;324(5927):651-4.

[88] Tang BL. Sirt1 and the Mitochondria. Molecules and Cells. 2016;39(2):87-95.

[89] Tamaru T, Hattori M, Honda K, Benjamin I, Ozawa T, Takamatsu K. Synchronization of circadian Per2 rhythms and HSF1-BMAL1:CLOCK interaction in mouse fibroblasts after short-term heat shock pulse. PLoS One. 2011;6(9):e24521.

[90] Reddy TE, Gertz J, Crawford GE, Garabedian MJ, Myers RM. The hypersensitive glucocorticoid response specifically regulates period 1 and expression of circadian genes. Mol Cell Biol. 2012 Sep;32(18):3756-67.

[91] Pendergast JS, Friday RC, Yamazaki S. Photic entrainment of Period mutant mice is predicted from their phase response curves. J Neurosci. 2010 Sep;30(36):12179-84.

[92] Heiland I, Bodenstein C, Hinze T, Weisheit O, Ebenhoeh O, Mittag M, Schuster S. Modeling temperature entrainment of circadian clocks using the Arrhenius equation and a

reconstructed model from Chlamydomonas reinhardtii. J Biol Phys. 2012 Jun;38(3):449-64.

[93] Gupta A, Hepp B, Khammash M. Noise Induces the Population-Level Entrainment of Incoherent, Uncoupled Intracellular Oscillators. Cell Syst. 2016 Dec 21;3(6):521-531.e13.

[94] Boulos Z, Macchi MM, Terman M. Twilights widen the range of photic entrainment in hamsters. J Biol Rhythms. 2002 Aug;17(4):353-63.

[95] Ishida A, Mutoh T, Ueyama T, Bando H, Masubuchi S, Nakahara D, Tsujimoto G, Okamura H. Light activates the adrenal gland: timing of gene expression and glucocorticoid release. Cell Metab. 2005 Nov; 2(5):297-307.

[96] Dang F, Sun X, Ma X, Wu R, Zhang D, Chen Y, Xu Q, Wu Y, Liu Y. Insulin post-transcriptionally modulates Bmal1 protein to affect the hepatic circadian clock. Nat Commun. 2016 Aug 31;7:12696.

[97] Zhou B, Zhang Y, Zhang F, Xia Y, Liu J, Huang R, Wang Y, Hu Y, Wu J, Dai C, Wang H, Tu Y, Peng X, Wang Y, Zhai Q. CLOCK/BMAL1 regulates circadian change of mouse hepatic insulin sensitivity by SIRT1. Hepatology. 2014 Jun;59(6):2196-206.

[98] Dyar KA, Ciciliot S, Wright LE, Biensø RS, Tagliazucchi GM, Patel VR, Forcato M, Paz MI, Gudiksen A, Solagna F, Albiero M, Moretti I, Eckel-Mahan KL, Baldi P5, Sassone-Corsi P, Rizzuto R, Bicciato S, Pilegaard H, Blaauw B, Schiaffino S. Muscle insulin sensitivity and glucose metabolism are controlled by the intrinsic muscle clock. Mol Metab. 2013 Oct 23;3(1):29-41.

[99] Zhang EE, Liu Y, Dentin R, Pongsawakul PY, Liu AC, Hirota T, Nusinow DA, Sun X, Landais S, Kodama Y, Brenner DA, Montminy M, Kay SA. Cryptochrome mediates circadian regulation of cAMP signaling and hepatic gluconeogenesis. Nat Med. 2010 Oct;16(10):1152-6.

[100] Woller A, Gonze D. Modeling clock-related metabolic syndrome due to conflicting light and food cues. Sci Rep. 2018 Sep 11;8(1):13641.

[101] Fan Y, Hida A, Anderson DA, Izumo M, Johnson CH. Cycling of CRYPTOCHROME proteins is not necessary for circadian-clock function in mammalian fibroblasts. Curr Biol. 2007 Jul 3;17(13):1091-100.

[102] Lee C, Etchegaray JP, Cagampang FR, Loudon AS, Reppert SM. Posttranslational mechanisms regulate the mammalian circadian clock. Cell. 2001 Dec 28;107(7):855-67.

[103] Gachon F, Olela FF, Schaad O, Descombes P, Schibler U. The circadian PAR-domain basic leucine zipper transcription factors DBP, TEF, and HLF modulate basal and inducible xenobiotic detoxification. Cell Metab. 2006 Jul;4(1):25-36.

[104] Chadwick DJ, Goode JA. Molecular Clocks and Light Signalling. Novartis Foundation: Symposium 253.

[105] Falvey E, Marcacci L, Schibler U. DNA-binding specificity of PAR and C/EBP leucine zipper proteins: a single amino acid substitution in the C/EBP DNA-binding domain confers PAR-like specificity to C/EBP. Biol Chem. 1996 Dec;377(12):797-809.

[106] Trautwein C, Rakemann T, Pietrangelo A, Plümpe J, Montosi G, Manns MP. Circadian C/EBP-beta/LAP controls down-regulation of albumin gene transcription during liver regeneration. J Biol Chem. 1996 Sep 6;271(36):22262-70.

[107] Ukai-Tadenuma M, Kasukawa T, Ueda HR. Proof-by-synthesis of the transcriptional logic of mammalian circadian clocks. Nat Cell Biol. 2008 Oct;10(10):1154-63.

[108] Preitner N, Damiola F, Lopez-Molina L, Zakany J, Duboule D, Albrecht U, Schibler U. The orphan nuclear receptor REV-ERBalpha controls circadian transcription within the positive limb of the mammalian circadian oscillator. Cell. 2002 Jul 26;110(2):251-60.

[109] Solt LA, Wang Y, Banerjee S, Hughes T, Kojetin DJ, Lundasen T, Shin Y, Liu J, Cameron MD, Noel R, Yoo SH, Takahashi JS, Butler AA, Kamenecka TM, Burris TP. Regulation of Circadian Behavior and Metabolism by Synthetic REV-ERB Agonists. Nature. 2012 Mar 29;485(7396):62-8

[110] Wallach T, Kramer A. Chemical chronobiology: Toward drugs manipulating time. FEBS Lett. 2015 Jun 22;589(14):1530-8.

[111] Hirota T, Lewis WG, Liu AC, Lee JW, Schultz PG, Kay SA. A chemical biology approach reveals period shortening of the mammalian circadian clock by specific inhibition of GSK-3β. Proc Natl Acad Sci U S A. 2008 Dec 30;105(52):20746-51.

[112] Yin L, Wang J, Klein PS, Lazar MA. Nuclear receptor Rev-erbα is a critical lithium-sensitive component of the circadian clock. Science. 2006 Feb 17;311(5763):1002-5.

[113] Roux J, Hafner M, Bandara S, Sims JJ, Hudson H, Chai D, Sorger PK. Fractional killing arises from cell-to-cell variability in overcoming a caspase activity threshold. Mol Syst Biol. 2015 May 7;11(5):803.

[114] Abel GA, Wochnik GM, Rüegg J, Rouyer A, Holsboer F, Rein T. Activity of the GR in G2 and Mitosis, Mol Endocrinol. 2002 Jun;16(6):1352-66.

[115] Caratti G, Iqbal M, Hunter L, Kim D, Wang P, Vonslow RM, Begley N, Tetley AJ, Woodburn JL, Pariollaud M, Maidstone R, Donaldson IJ, Zhang Z, Ince LM, Kitchen G, Baxter M, Poolman TM, Daniels DA, Stirling DR, Brocker C, Gonzalez F, Loudon AS, Bechtold DA, Rattray M, Matthews LC, Ray DW. REVERBa couples the circadian clock to hepatic glucocorticoid action. J Clin Invest. 2018 Oct 1;128(10):4454-4471.

[116] Fu L, Lee CC. The circadian clock: pacemaker and tumour suppressor. Nat Rev Cancer. 2003 May;3(5):350-61.

[117] Ye P, Hu Q, Liu H, Yan Y, D'ercole AJ. Cyclin D1-Cdk4 controls glucose metabolism independently of cell cycle progression. Nature. 2014 Jun 26;510(7506):547-51.

[118] Lee Y, Dominy JE, Choi YJ, Jurczak M, Tolliday N, Camporez JP, Chim H, Lim JH, Ruan HB, Yang X, Vazquez F, Sicinski P, Shulman GI, Puigserver P. beta-catenin mediates insulin-like growth factor-I actions to promote cyclin D1 mRNA expression, cell proliferation and survival in oligodendroglial cultures. Glia. 2010 Jul;58(9):1031-41.

[119] Kainrath S, Stadler M, Reichhart E, Distel M, Janovjak H. Green-light-induced inactivation of receptor signaling using cobalamin-binding domains. Angew Chem Int Ed Engl. 2017 Apr 10;56(16):4608-4611.

[120] Stanton BC, Siciliano V, Ghodasara A, Wroblewska L, Clancy K, Trefzer AC, Chesnut JD, Weiss R, Voigt CA. Systematic Transfer of Prokaryotic Sensors and Circuits to Mammalian Cells. ACS Synth Biol. 2014 Dec 19;3(12):880-91.

[121] Milias-Argeitis A, Summers S, Stewart-Ornstein J, Zuleta I, Pincus D, El-Samad H, Khammash M, Lygeros J. In silico feedback for in vivo regulation of a gene expression circuit. Nat Biotechnol. 2011 Nov 6;29(12):1114-6.

[122] Fernandez-Rodriguez J, Voigt CA. Post-translational control of genetic circuits using Potyvirus proteases. Nucleic Acids Res. 2016 Jul 27;44(13):6493-502.

[123] Potvin-Trottier L, Lord ND, Vinnicombe G, Paulsson J. Synchronous long-term oscillations in a synthetic gene circuit. Nature. 2016 Oct 27;538(7626):514-517.

[124] Engler C, Gruetzner R, Kandzia R, Marillonnet S. Golden gate shuffling: a one-pot DNA shuffling method based on type IIs restriction enzymes. PLoS One. 2009;4(5):e5553.

[125] Weber E, Engler C, Gruetzner R, Werner S, Marillonnet S. A modular cloning system for standardized assembly of multigene constructs. PLoS One. 2011 Feb 18;6(2):e16765.